IntechOpen

Symmetry (Group Theory) and Mathematical Treatment in Chemistry

Edited by Takashiro Akitsu

SYMMETRY (GROUP THEORY) AND MATHEMATICAL TREATMENT IN CHEMISTRY

Edited by **Takashiro Akitsu**

Symmetry (Group Theory) and Mathematical Treatment in Chemistry
http://dx.doi.org/10.5772/intechopen.68513
Edited by Takashiro Akitsu

Contributors

Zhen-Chuan Li, Kazimierz Stroz, Mazhar Ali, Elena Derunova, Amalia Stefaniu, Lucia Pintilie, Eduardo J. Delgado, Takao Satoh, Yasutaka Kitagawa, Toru Saito, Kizashi Yamaguchi, Eugene Mananga, Akil Hollington, Karen Registe, Takashiro Akitsu

Notice

Statements and opinions expressed in the chapters are these of the individual contributors and not necessarily those of the editors or publisher. No responsibility is accepted for the accuracy of information contained in the published chapters. The publisher assumes no responsibility for any damage or injury to persons or property arising out of the use of any materials, instructions, methods or ideas contained in the book.

First published in London, United Kingdom, 2018 by IntechOpen
eBook (PDF) Published by IntechOpen, 2019
IntechOpen is the global imprint of INTECHOPEN LIMITED, registered in England and Wales, registration number: 11086078, The Shard, 25th floor, 32 London Bridge Street
London, SE19SG – United Kingdom
Printed in Croatia

British Library Cataloguing-in-Publication Data
A catalogue record for this book is available from the British Library

Additional hard and PDF copies can be obtained from orders@intechopen.com

Symmetry (Group Theory) and Mathematical Treatment in Chemistry
Edited by Takashiro Akitsu

p. cm.

Print ISBN 978-1-78923-314-8

Online ISBN 978-1-78923-315-5

eBook (PDF) ISBN 978-1-83881-324-6

Meet the editor

Takashiro Akitsu (born in 1971), PhD, is a full-time professor in the Department of Chemistry, Faculty of Science Division II at Tokyo University of Science (2016–present). He completed his undergraduate school training (chemistry) from Osaka University, Japan (1995), and his graduate school training (physical and inorganic chemistry, especially coordination, crystal, and bioinorganic chemistry) from Osaka University, Japan (2000). He worked at Osaka, Keio, and Stanford Universities before his present position. Dr. Akitsu has published up to about 180 articles in peer-reviewed journals and has edited academic books at the international level. He has been a peer reviewer of many journals and acted as an organizing committee of several international conferences.

Contents

Preface XI

Chapter 1 **Introductory Chapter: Mathematical or Theoretical Treatments in Chemical Studies on Fire Materials 1**
Takashiro Akitsu

Chapter 2 **Treatment of Group Theory in Spectroscopy 7**
Eugene Stephane Mananga, Akil Hollington and Karen Registe

Chapter 3 **Group Theory from a Mathematical Viewpoint 19**
Takao Satoh

Chapter 4 **Symmetry of hR and Pseudo-hR Lattices 49**
Kazimierz Stróż

Chapter 5 **Linking Symmetry, Crystallography, Topology, and Fundamental Physics in Crystalline Solids 67**
Elena Derunova and Mazhar N. Ali

Chapter 6 **Thermodynamic Symmetry and Its Applications - Search for Beauty in Science 87**
Zhen-Chuan Li

Chapter 7 **Approximate Spin Projection for Broken-Symmetry Method and Its Application 121**
Yasutaka Kitagawa, Toru Saito and Kizashi Yamaguchi

Chapter 8 **A Computational Chemistry Approach for the Catalytic Cycle of AHAS 141**
Eduardo J. Delgado

Chapter 9 **Molecular Descriptors and Properties of Organic Molecules 161**
Amalia Stefaniu and Lucia Pintilie

Preface

As stated previously in the preface of many famous textbooks in this subject, group theory or discussion using symmetry or mathematical rules, may be a useful tool for chemists, though it sometimes seems to be difficult to study completely for young students of chemistry.

Symmetry pervades many forms of arts and science, and group theory provides a systematic way of thinking about symmetry. The mathematical concept of a group was invented in 1823 by Evariste Galois. Its applications in physical science developed rapidly during the twentieth century, and today, it is considered as an indispensable aid in many branches of physics and chemistry.

P. Jacob

For a contemporary chemist, group theory is not only a key element of the quantum mechanical methods of investigating the electronic structure of matter --- knowledge of symmetry and its group theoretical implications is also widely applied in analyzing the results of practically all spectroscopic techniques currently employed in organic and inorganic chemistry.

B. S. Tsukerblat

It aims to teach the use of symmetry arguments to the typical experimental chemist in a way that he will find meaningful and useful. Too brief or too superficial a tuition in the use of symmetry arguments in a waste of whatever time is devoted to it.

F. A. Cotton

Time is needed in order to assimilate the concepts of symmetry and to consolidate them into a working knowledge of the subject. It is hoped that this book will be helpful to all those meeting symmetry for the first time, whatever their specialization, and will prepare the reader for study of the current definitive text on symmetry, the International tables for crystallography, Volumes A and A1.

M. Ladd

The International Tables for Crystallography (ITC) have steadily grown into eight ponderous volumes, to become the true 'bible' of crystallographers. Of course, information about crystal symmetry is central to the ITC, but subjects such as the properties of radiations used in crystallography, the physical properties of crystals and the proper format for crystallographic software are also covered.

P. G. Radaelli

This book presents an introductory overview of mathematical treatments in chemistry with three main topics: basic group theory and symmetry in chemistry, examples of computational chemistry, and applications for solid-state physics. Moreover, this book also provides a comprehensive account on brief mathematical principle of group theory as well as materials scientific applications. This book will be beneficial for the graduate students, teachers, researchers, chemists, solid-state physicists and other professionals, who are interested in mathematics or group theory, and to expand their knowledge about symmetry in the field of inorganic chemistry, physical or quantum chemistry, organic or polymer chemistry, solid-state physics, etc.

This book comprises a total of nine chapters from multiple contributors around the world, including Chile, Egypt, Japan, Morocco, Pakistan, Poland, Romania, Russia, and the United States. I am grateful to all the contributors and leading experts for the submission of their stimulating and inclusive chapters in the preparation of the edited volume to bring the book on group theory and computational applications. I offer my special thanks and appreciation to IntechOpen publishing process managers for their encouragement and help in bringing out the book in the present form.

I express my heartfelt gratitude to Ms. Kristina Kardum et al. for their concern, efforts, and support in the task of publishing this volume.

Takashiro Akitsu
Department of Chemistry
Faculty of Science
Tokyo University of Science
Tokyo, Japan

Chapter 1

Introductory Chapter: Mathematical or Theoretical Treatments in Chemical Studies on Fire Materials

Takashiro Akitsu

Additional information is available at the end of the chapter

http://dx.doi.org/10.5772/intechopen.74202

1. Introduction

This book entitled *Symmetry (Group Theory) and Mathematical Treatment in Chemistry* deals with not only basic mathematics associated with linear algebra and group theory describing chemical symmetry about not only molecular shapes, molecular orbitals, and crystal structures but also spectroscopic discussion, DFT calculations or other computational treatments of several molecules or supramolecules, and symmetric structures of formula used in thermodynamics. In this way, this aspect may be one of the important approaches in chemical studies (along hierarchical structures group theory) [1] describing.

2. Results and discussion

Herein, as an example, a study on fire materials and possibility to apply these approaches is mentioned. The flame retardants prevent the burning of the material by either cutting the air supply or enhancing the requirements of oxygen. Some of the flame retardant used in the PVC or polymers can be classified as follows: (a) phosphorous compounds, (b) halogen compounds, (c) halogen phosphorous compounds, and (d) bicarbonates and inorganic oxides and borates. Some of the flame retardants may be broadly classified as halogen, and the aim of this example study is to prepare brominated (potential flame retardants) metal complexes to use as DSSC dyes, too. Crystal structure (space group $P2_1$) of a brominated complex (**Figure 1**) [2] is relative to crystal symmetry as condensed solid states or supramolecules. With the aid of DFT calculations [3], electronic states (UV-vis spectra) due to each transition between orbitals (of a certain irreducible representation) of the related complexes (**Figure 2**) could be estimated based on optimized molecular structures (coordination geometry is approximately $C2_v$). Of course, their

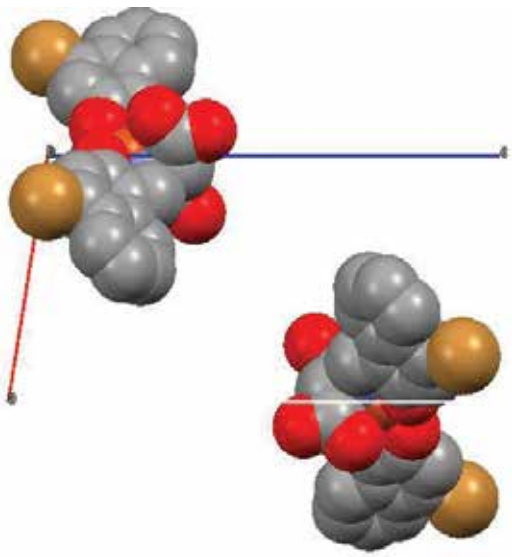

Figure 1. Crystal structure of a chiral complex.

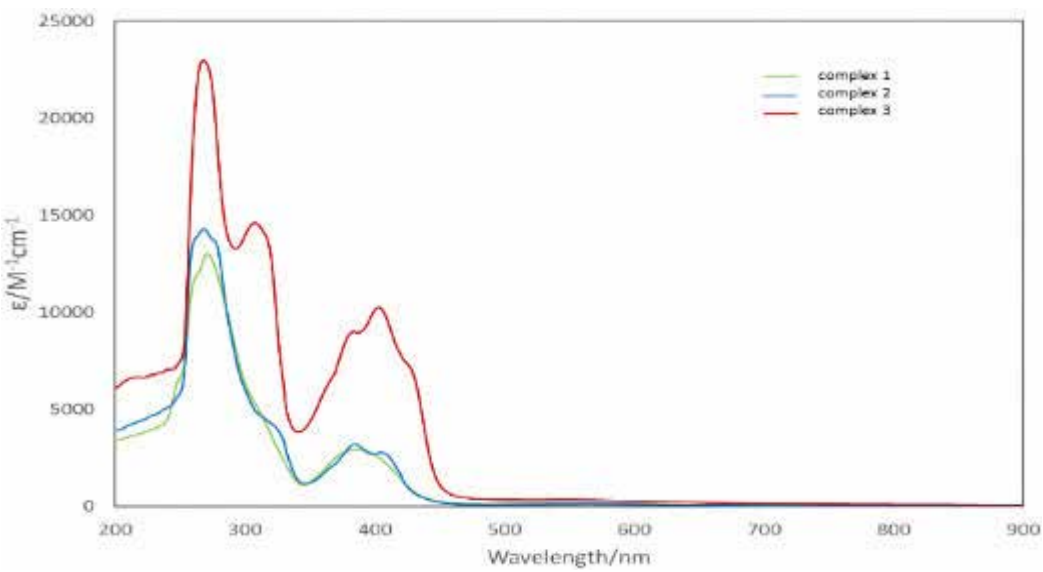

Figure 2. Electronic spectra.

vibrational (commonly infrared) spectra with normal modes (**Figure 3**) were relevant to molecular symmetry.

However, TG-DTA (**Figure 4**), a typical thermal analysis with "temperature" of crystalline complexes as well as hybrid materials dispersed in several types of polymer films was less

http://dx.doi.org/10.5772/intechopen.74202

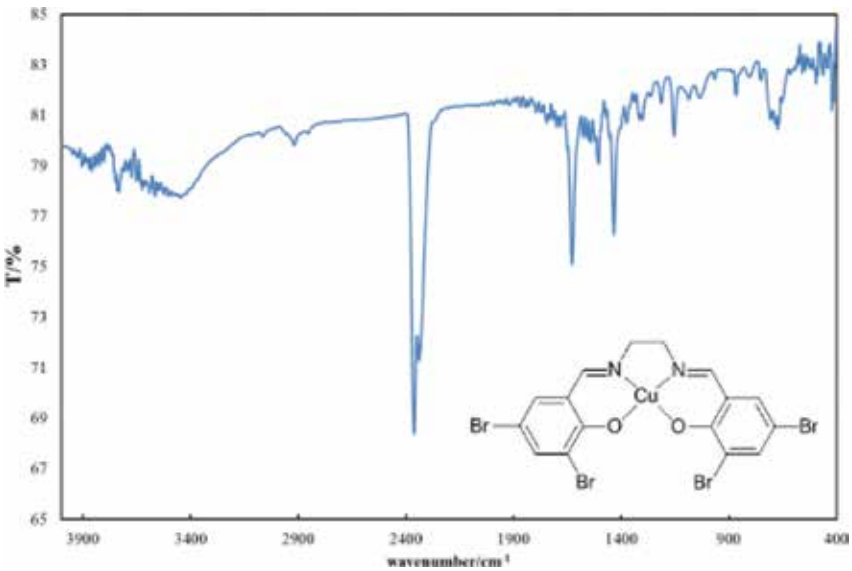

Figure 3. IR spectra (with structure).

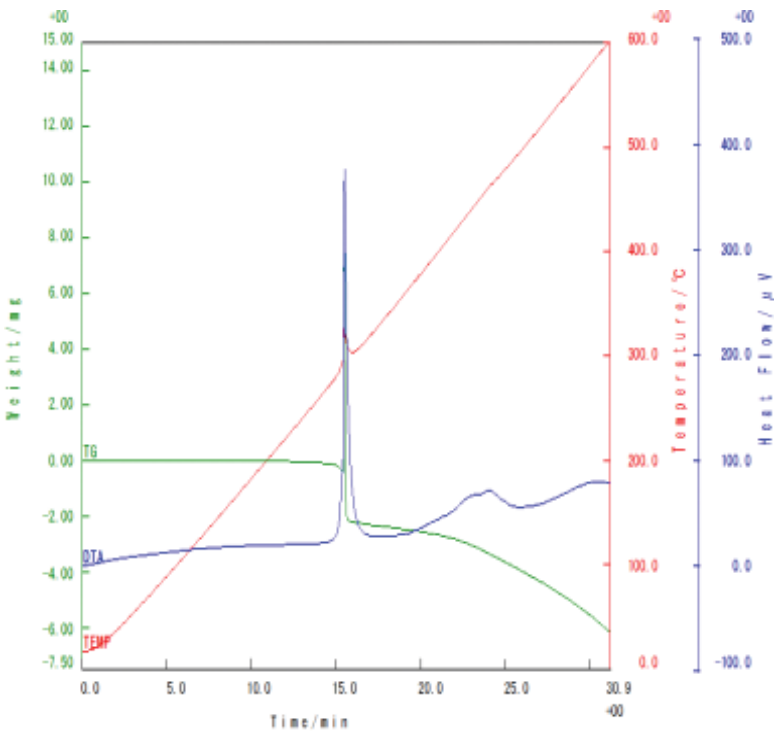

Figure 4. TG-DTA.

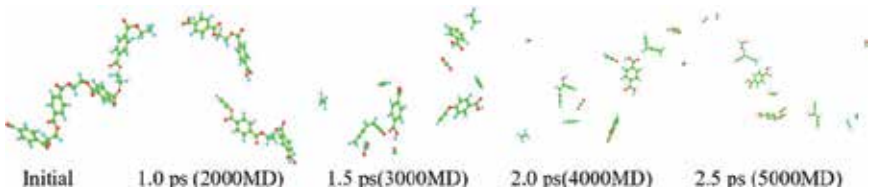

Figure 5. Thermolysis step of the quantity of PET polymer by the quantum molecular dynamics calculation.

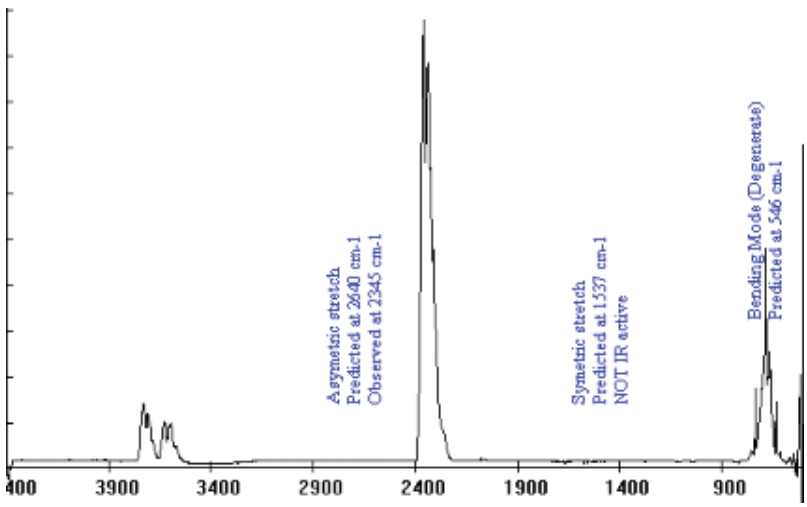

Figure 6. IR spectra of CO_2. The fundamental vibrations of molecules belonging to the $D_{\infty h}$ point group are similar in type to those of the nonsymmetrical linear molecules, but in this instance, they may also be symmetric (ν_s) or antisymmetric (ν_{as}) to the center of symmetry, and thus σ_g, σ_u, π_g, and π_u modes, two stretching and two bending (degenerate) vibrations. The ν_{as}(CO) mode and the degenerate δ(OCO) mode involve changes in the dipole moment during the vibration, and they are IR active. Thus, ν_{as} has been observed by IR as a very strong parallel-type band at 2349.3 cm^{-1}, while δ(OCO) appears as a strong perpendicular-type band at 667.3 cm^{-1}.

relevant to merely molecular symmetry. Furthermore, chemical reactions changing chemical species accompanying with "time" may be difficult to understand within the framework of symmetry. To discuss time-dependent chemical reaction, molecular dynamics may be a useful theoretical method of recently developed computations (**Figure 5**), while spectral detection of product gases (**Figure 6**) is sometimes possible to investigate closely rather than materials of solid states.

3. Conclusion

In this way, mathematical treatments of symmetry in chemistry can often lead to deep understanding, though it sometimes is not useless depending on conditions or phenomenon of targets. Similarly, theoretical computation should be carried out considering their limitation and frameworks (presupposition of theory).

Acknowledgements

The author thanks Mrs. Keita Takahashi, Marin Yamaguchi, Shinosuke Tanaka, Kazuya Takakura; Profs. Mutsumi Sugiyama, Masayuki Mizuno, Ken Matsuyama, Kazunaka Endo (Tokyo University of Science); and Prof. Tomonori Ida (Kanazawa University), Prof. Mauricio Alcolea Palafox (Universidad Complutense de Madrid), and Prof. Rakesh Kumar Soni (Chaudhary Charan Singh University) for providing examples of studies.

Author details

Takashiro Akitsu

Address all correspondence to: akitsu@rs.kagu.tus.ac.jp

Department of Chemistry, Faculty of Science, Tokyo University of Science, Tokyo, Japan

References

[1] Cotton FA. Chemical Applications of Group Theory. 3rd ed. Wiley-Interscience; 1990

[2] Takahashi K, Tanaka S, Yamaguchi M, Tsunoda Y, Akitsu T, Sugiyama M, Soni RK, Moon D. Dual purpose Br-containing Schiff base Cu(II) complexes for DSSC dyes and polymer flame retardants. Journal of the Korean Chemical Society. 2017;**61**:129-131

[3] Yamaguchi M, Takahashi K, Akitsu T. Molecular design through TD-DFT calculation of chiral salen Cu^{II} complexes toward NIR absorption for DSSC. Journal of the Indian Chemical Society. 2016;**93**:921-927

Chapter 2

Treatment of Group Theory in Spectroscopy

Eugene Stephane Mananga, Akil Hollington and Karen Registe

Additional information is available at the end of the chapter

http://dx.doi.org/10.5772/intechopen.75735

Abstract

The most important thing to consider when applying group theory is finding the molecule's point group or its particular symmetry operations. In order to identify a molecule's symmetry operations, one must first find the molecule's symmetry elements. In other words, the first stage in utilizing group theory with molecular properties is identifying a molecule's symmetry elements. For most beginners without experience this has proven to be most difficult because it requires the individual to visually identify the elements of symmetry in a 3D object. However, once this is overcome, applying group theory to forefront point groups and symmetry operations becomes second nature.

Keywords: group theory, symmetry operation, point group, spectroscopy, molecular energy levels

1. Introduction

Spectroscopy is defined as the scientific study of the many interactions between electromagnetic radiation and matter. Previously, spectroscopy came from the study of visible light that is dispersed with relation to its wavelength through a prism. As time progressed, the concept of spectroscopy was explored further and eventually included any interaction with energy derived from radiation that could be quantified and organized from its wavelength [1]. Max Planck's definition of blackbody radiation, Albert Einstein's view of the photoelectric effect, and Niels Bohr's understanding of atomic structure and spectra collectively come together to define spectroscopic studies and develop what is known as quantum. Spectroscopy is utilized constantly in both analytical and physical chemistry because unique spectra are found in atoms and molecules. Therefore, spectroscopy is utilized often to discover, define, and quantify information about the molecules and atoms. There are other fields that utilize spectroscopy as well such as

astronomy, for remote sensing on Earth [2]. Spectroscopy is a sufficiently broad field that many subdisciplines exist, each with numerous implementations of specific spectroscopic techniques. The various implementations and techniques can be classified in several ways. Spectroscopy is a very wide field that has multiple subcategories, each with its own application of techniques unique to spectroscopy. The various implementations and techniques can be classified in several ways. A few examples of the multitude of spectroscopy categories are scanning tunneling microscopy spectroscopy (with Gerd Binnig and Heinrich Rohrer, 1981), electron paramagnetic resonance (with Yevgeny Zavoisky, 1944), nuclear magnetic resonance (with Edward Mills Purcell and Felix Bloch, 1940s), microwave spectroscopy (with James Clerk Maxwell, 1864), and infrared spectroscopy (with Sir Frederick William Herschel, 1800). These are also the most significant developments over the past three centuries [3].

This book chapter presents the treatment of group theory in spectroscopy. Group theory is a powerful formal method for analyzing abstract and physical systems in which symmetry is present and has surprising importance in physics, especially quantum mechanics. Gauss developed group theory but did not publish parts of its mathematics. Therefore, Galois is generally considered to have been the first to develop the theory. Group theory was developed in the nineteenth century and found its first remarkable applications in physics in the twentieth century by Bethe (1929), Wigner (1931), and Kohlrausch (1935). "*It is often hard or even impossible to obtain a solution to the Schrödinger equation - however, a large part of qualitative results can be obtained by group theory. Almost all the rules of spectroscopy follow from the symmetry of a problem*", said Eugene Wigner (1931). Groups are very important in most fields, but especially in physics, because they serve to illustrate the symmetries that the laws of physics obey as well. Continuous symmetry of a physical system directly relates to a conservation law of the system, according to Noether's theorem. This is why many physicists become interested in group representations, especially of Lie groups, because they often point the way to the potential physical theories that may define them. The usages of these groups in physics include the standard model, gauge theory, the Lorentz group, and the Poincare group [3]. Group theory is used in other areas of science such as in chemistry and materials science where groups are used to classify crystal structures, regular polyhedra, and the symmetries of molecules. The assigned point groups can then be used to determine physical and spectroscopic properties and to construct molecular orbitals. Molecular symmetry is responsible for many physical and spectroscopic properties of compounds and provides relevant information about how chemical reactions occur.

The group theory has also been extensively utilized in many areas such as statistical mechanics, music, and harmonic analysis. In statistical mechanics, group theory can be used to resolve the incompleteness of the statistical interpretations of mechanics developed by Willard Gibbs, relating to the summing of an infinite number of probabilities to yield a meaningful solution. In music, the presence of the 12-periodicity in the circle of fifths yields applications of elementary group theory. In harmonic analysis, Haar measures, which are integrals invariant under the translation in a Lie group, are used for pattern recognition and other image processing techniques. Due to the various applications of group theory, it has proven to be one of the most powerful mathematical tools utilized in the field of spectroscopy and in quantum chemistry. It provides opportunities for individuals to adequately understand the molecule and make

informed inferences, which helps to break down complex theory and information. The most important understanding that this helps individuals to comprehend is that the set of operations associated with the symmetry elements of a molecule, collectively constitute a mathematical set called a group. What this serves to exemplify is that the application of mathematical theory can be applied when working with symmetry operations [4].

It is worth mentioning that the application of group theory in spectroscopy shed light on a molecule's symmetry that pertains to physical characteristics. This is effective when attempting to determine important physical data of a molecule. There are certain things that the symmetry of a molecule can help to deduce such as the energy levels that the orbitals will be at. Additionally, orbital symmetries in which unique transitions can occur between energy levels can also be determined. Bond order is also relatively easier to determine with tedious computation. The aforementioned examples place an emphasis on what makes group theory a very important tool [5].

2. Symmetry operations

Symmetry and group theory are intertwined in a multitude of ways. For instance, a symmetry group contains symmetry characteristics of common geometrical objects. The group contains the set of transformations that leave the object unchanged and the operation of combining two such transformations by performing one after the other. Lie groups are the symmetry groups used in the Standard Model of particle physics. Poincaré groups, which are also Lie groups, can express the physical symmetry underlying special relativity and point groups are also used to help understand symmetry phenomena in molecular chemistry [6].

2.1. Definition of a group

A group **G** is a finite or infinite set of elements together with a binary operation, that satisfy the four fundamental properties called the group axioms, namely, closure, associativity, identity, and invertibility [7].

2.1.1. Closure

For all elements A and B of the group G, we have

$$\mathbf{A}\,\mathbf{B}=\mathbf{C} \tag{1}$$

The result **C** is also an element of the group **G**.

2.1.2. Associativity

The combination rule must be associative, such that

$$\mathbf{A}\,(\mathbf{B}\,\mathbf{C})=(\mathbf{A}\,\mathbf{B})\,\mathbf{C} \tag{2}$$

2.1.3. Identity

There must be an element called the identity **I**, such that,

$$\mathbf{I\,R{=}R\,I{=}R} \tag{3}$$

This is true for all elements **R** of the group **G**.

2.1.4. Invertibility

Each element R must have an inverse R^{-1}, which is also a group element such that,

$$\mathbf{R\,R^{-1}{=}R^{-1}\,R{=}I} \tag{4}$$

A group is a "*monoid*" if each of its elements is invertible. Group theory is the study of groups. A group consisting of a fixed number of elements is known as a finite group, and the elements are defined as the group order of the group. A group may contain subgroups. The elements of a group that fall under group and inverse operations form a subgroup. Each subgroup is, in its turn, a group, and many known groups are, in fact, distinct subgroups of larger groups. The symmetric group $\mathbf{S_n}$ is a classic example of a finite group, while integers subjected to addition are a basic example of an infinite group. For continuous groups, one can consider the real numbers or the set of **n x n** invertible matrices [8]. The most well-known group is that of integers subjected to addition, though the theoretical formalization of the group axioms applies more widely if taken separately from the characteristics of any group and its governing operation. It allows entities with highly diverse mathematical origins in abstract algebra and beyond to be handled in a flexible way while retaining their essential structural aspects. The ubiquity of groups in numerous areas within and outside mathematics makes them a central organizing principle of contemporary mathematics [2]. The concept of a group arose from the study of polynomial equations, starting with Evariste Galois in the 1830s. After contributions from other fields such as number theory and geometry, the group notion was generalized and firmly established around 1870.

In group theory, the elements considered are symmetry operations. For a given molecular system described by the Hamiltonian $\boldsymbol{H}$, there is a set of symmetry operations $\boldsymbol{O_i}$, which commute with the Hamiltonian $\boldsymbol{H}$. $\boldsymbol{H}$ and $\boldsymbol{O_i}$ thus have a common set of Eigen functions, and the eigenvalues of $\boldsymbol{O_i}$ can be used as labels for the Eigen functions. This set of operations defines a symmetry group. In molecular physics and molecular spectroscopy, two types of groups are particularly important: the point groups and the permutation-inversion groups.

2.2. Point group operations and point group symmetry

Each molecule has a set of symmetry operations that describes the molecule's overall symmetry. This set of operations defines the point group of the molecule. Since all the elements of symmetry present in the molecule intersect at a common point, this point remains fixed under all symmetry operations of the molecule and is known as point symmetry groups. **Table 1** highlights the Common Point Groups and Symmetry Elements [9]. The point groups are utilized to define molecules that are considered to be rigid when observed through the

timescale of the particular spectroscopic experiment. Therefore, molecules that have a specific equilibrium configuration with no observable tunneling between two or more similar configurations can be used to define the point groups. There are five key symmetry operations for point groups. The first is the identity E, which leaves all coordinates unaltered. Next is the rotation C_n by an angle of $2\pi/n$ in the positive trigonometric sense. The symmetry axis with the greatest n value is chosen as the principal axis. If a molecule has a specific C_n axis with the greatest n value, then the molecule has a sustained dipole moment that lies along this axis. If a molecule has several C_n axes with the greatest n value, the molecule has no permanent dipole moment. The reflection through a plane is the next important key factor. These reflections are organized into two main categories. The first is a reflection through a horizontal plane, and the second the reflection through a vertical plane. Next on the list of key factors is the inversion, typically represented by (i), of all coordinates through the inversion center. Through this inversion, we discover the need for the next key factor for symmetry operation, which is the improper rotation, typically denoted as "S_n" or referred to as "*rotation-reflection*", which consists of a rotation by an angle of $2\pi/n$ around the z-axis, followed by a reflection through the plane perpendicular to the rotational axis. A molecule having an improper operation as symmetry operation is not able to be optically active and is subsequently labeled as achiral, as opposed to chiral. One example of symmetry is found within stereochemistry, more specifically, isomeric pairs of molecules called enantiomers. Enantiomers are mirror images of each

Point group	Symmetry elements	Simple description, chiral if applicable	Illustrative species
C_1	E	No symmetry, chiral	CFIBrH, Lysergic acid
C_8	E σ_h	Planar, no other symmetry	Thionyl chloride, hypochlorous acid
C_i	E_i	Inversion center	Anti 1,2-dichloro-1,2-dibromoethane
$C_\infty v$	E_2C_∞ σ_v	Linear	Hydrogen chloride, carbon monoxide
$D_{\infty h}$	E_2C_∞ $\infty\sigma_i$ *i* $2S_\infty$ ∞C_2	Linear with inversion center	Dihydrogen, azide anion, carbon dioxide
C_2	EC_2	"open book geometry," chiral	Hydrogen peroxide
C_3	EC_3	Propeller, chiral	Triphenylphosphine
C_{2h}	E C_2 *i* σ_h	Planar with inversion center	Trans-1,2- dichloroethylene
C_{3h}	$EC_3C_3^2$ σ_h $S_3S_3^5$	Propeller	Boric acid
C_{2v}	E C_2 σ_v(xz) σ_v'(yz)	Angular (H_2O) or see-saw (SF_4)	Water, sulfur tetrafluoride, sulfuryl fluoride
C_{3v}	$E_2C^3 3\sigma_v$	Trigonal pyramidal	Ammonia, phosphorus oxychloride
C_{4v}	$E_2C_4C_2 2\sigma_v$ $2\sigma_d$	Square pyramidal	Xenon oxytetrafluoride
T_d	$E_8C_3 3C_2 6S_4 6\sigma_d$	Tetrahedral	Methane, phosphorus pentoxide. Adamantine
O_h	E $8C_3$ $6C_2$ $6C_4$ $3C_2$ *i* $6S_4$ $8S_6$ $3\sigma_h$ $6\sigma_d$	Octahedral or cubic	Cubane, sulfur hexafluoride
I_h	E $12C_5$ $12C_5^2$ $20C_3$ $15C_2$ *i* $12S_{10}$ $12S_{10}^3$ $20S_6$ 15σ	Icosahedral	C_{60}, $B_{12}H_{12}^{2-}$

Table 1. Common point groups and symmetry elements.

other, but, when superimposed, the images are not identical. A consequence of this symmetrical relation is that they rotate the plane of polarized light passing through them in opposite directions. Molecules that fit this description are referred to as chiral. These aforementioned applications help to mitigate tedious research timescales and also place an emphasis on the symmetrical allocation to specific molecules and molecular geometry shapes.

2.3. Permutation-inversion operations and CNPI groups

The point groups are appropriated to describe rigid molecules. However, for floppy systems or when the transition between two states does not hold the same symmetry, another, more general definition is required. Longuet-Higgins and Hougen developed the complete nuclear permutation-inversion (CNPI) groups that rely on the fact that the symmetry operations leave the Hamiltonian unaltered. There are several symmetry operations of the CNPI groups. The first is the permuation (ij) of the coordinates of two identical nuclei. i and j denote the exchange of the nucleus i with the nucleus j [7]. The second is the cyclic permutation (ijk) of the coordinates of three identical nuclei i, j, and k. The nucleus i is replaced by the nucleus j, j by k, and k by i. We have all possible circular permutations of n identical nuclei. Next we have the inversion E^* of all coordinates of all particles through the center of the lab-fixed frame. We also have the permutation followed by an inversion $(ij)^* = E^* \cdot (ij)$ of all coordinates of all particles and the cyclic permutation followed by an inversion $(ijk)^*$ of all coordinates of all particles. Finally, we have all possible circular permutations followed by an inversion of all coordinates of n identical nuclei. The molecular Hamiltonian is left unchanged upon these operations because the permutation operations affect identical nuclei. The CNPI groups represent a more general description that can also be applied to rigid molecules. The point groups are commonly used in the case of rigid molecules. In the following, we will consider only rigid molecules and restrict ourselves to point group symmetry, but all concepts can be extended to the CNPI and MS groups [7]. The key to applying group theory is to be able to identify the point group of the molecule that describes the molecule's unique collection of symmetry operations. The symmetry elements of a molecule reveal the molecule's various symmetry operations. Thus, the initial step in applying group theory to molecular properties is to recognize the molecule's specific set of symmetry elements. The process of identifying a molecule's symmetry elements has proven difficult for beginners, as they must observe the elements of symmetry with the naked eye in a 3D object [4].

3. Applications of group theory in spectroscopy

Symmetry can help to solve many of the issues encountered in chemistry, and group theory is the primary tool that is utilized to identify symmetry. If we know how to determine the symmetry of small molecules, we can determine the symmetry of other targets. This is not only limited to the symmetry of molecules but also to the symmetries of local atoms, molecular orbitals, rotations, and vibrations of bonds. A typical example is the knowledge of the symmetries of molecular orbital wave functions allowing the identification of the nature and characteristics of the binding. Also, the particular methods associated with certain symmetries allow

us to decide if the transition is prohibited and to understand the bands observed in infrared or Raman spectrum. A *symmetry operation* to a molecule is an operation that leaves the physical proprieties of the molecule unchanged. This is equivalent to having the molecule unchanged before and after the symmetry operation is performed [5]. In other words, when we do a symmetry operation on a molecule, every point of the molecule will be in an equivalent position.

The application of group theory in spectroscopy intends to investigate the way in which symmetry considerations influence the interaction of light with matter. Group theory can be used to understand the molecular orbitals in a molecule and to determine the possible electronic states accessible by absorption of a photon. Another important function of group theory is the investigation of the light that excites different vibrational modes of a polyatomic molecule [10]. A photon of the appropriate energy is able to excite an electronic transition in an atom, subject to the following selection rules:

$$\Delta n = Integer \tag{5}$$

$$\Delta l = \pm 1 \tag{6}$$

$$\Delta L = 0, \pm 1 \tag{7}$$

$$\Delta S = 0 \tag{8}$$

$$\bigtriangleup J = 0, \pm 1; J = 0 \tag{9}$$

In general, different types of spectroscopic transitions obey different selection rules. The common transitions involve changing the electronic state of an atom and involve absorption of a photon in the UV or visible part of the electromagnetic spectrum. There are analogous electronic transitions in molecules, which we will consider here. The absorption of photons in the infrared region of the spectrum controls the vibrational excitation in molecules and the absorption of photons in the microwave region commands rotational excitation. Typically, each excitation executes its own selection rules, but the general methodology for establishing the selection rules is identical in all cases. The determination of the conditions under which the probability of transition is not zero is a simple process. Therefore, the first step in understanding the origins of selection rules is to learn how transition probabilities are computed, and this requires some quantum mechanics concepts [10]. Overall, group theory plays a very important role in spectroscopy, which we can see from various applications of group theory in spectroscopy such as infrared spectrum, Raman spectrum, electronic spectrum, and so on. Typically, the change in electronic energy is greater than in vibrational energy, which is also greater than in rotational energy. **Figure 1** illustrates the different energy levels in a molecule.

3.1. Electronic transitions in molecules

When an electron is excited from one electronic state to another, this is what is called an electronic transition. The selection rules for electronic transitions are governed by the transition moment integral. Due to the fact that the electrons are coupled between two vibrational states that are between two electronic states, it is important to consider both the electronic state

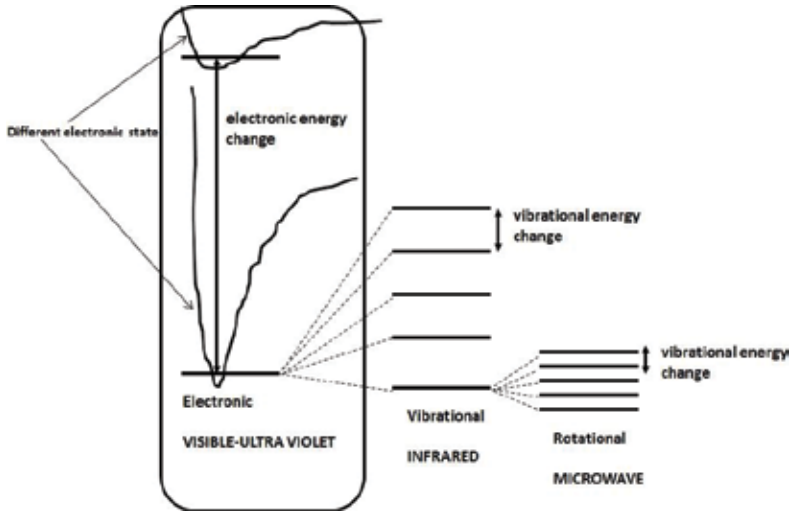

Figure 1. Molecular energy levels diagram.

symmetries and the vibration state symmetries. This modification of the transition moment integral produces the symmetry of the initial electronic and vibrational states called "***bra***" and the final electronic and vibrational states named "***ket.***"

This appears to be a modified version of the transition moment integral [5]. If we assume that we have a molecule in an initial state, we can determine which final states can be accessed by the absorption of a photon. So, we need to determine the symmetry of an electronic state. The symmetry of an electronic state is obtained by identifying any unpaired electrons and taking the direct product of the unrepresentative of the molecular orbitals in which they are detected. The total symmetric unrepresentative always holds the ground state of a closed-shell molecule in which all electrons are paired [10]. The determination of the unrepresentative electric dipole operator allows obtaining the electronic states accessible by absorption of photons. Light that is linearly polarized along the x, y, and z axes transforms in the same way as the functions x, y, and z in the appropriate character table. From the $\mathbf{C_{3v}}$ character table, we see that x- and y-polarized light transforms as **E**, while z-polarized light transforms as in the appropriate character table [10].

The excitation from one energy level to a higher energy level happens during the electronic transitions in a molecule. The change of energy associated with these transitions gives structural information of the molecule and determines many other molecular properties such as color. Planck's relation provides the relationship between the energy involved in the electronic transition and the frequency of radiation. Planck's equation is sometimes termed the Planck-Einstein:

$$E = h\gamma \tag{10}$$

where $h = 6.55 \times 10^{-34} J.s$ is a Planck constant. Electronic transitions in molecules occur between orbitals and they must cohere to angular momentum selection rules. **Figure 2** shows

possible *electronic* transitions of p, s, and *n* electrons. In the process of transition $\sigma \rightarrow \sigma^*$, electrons occupying a "HOMO" of a "sigma bond" can get excited to the "LUMO" of that bond. Similarly, in the process of transition $\pi \rightarrow \pi^*$, electrons from a "pi-bonding orbital" can get excited to the "antibonding-pi orbital" of that bond. Auxochromes with free electron pairs denoted as *n* have their own transitions. The following molecular electronic transitions exist:

3.2. Vibrational transitions in molecules

All molecules vibrate. While these vibrations can originate from several events, the most basic of these occurs when an electron is excited within the electronic state from one eigenstate to another. When an electron is excited from one eigenstate to another within the electronic state, there is a change in interatomic distance, which results in a vibration occurring. A vibration occurs when an electron remains within the electronic state but changes from one eigenstate to another. Just as in electronic transitions, the selection rules for Vibrational transitions are dictated by the transition moment integral. Light polarized along the x, y, and z axes of the molecule may be used to excite vibrations with the same symmetry as the x, y, and z functions listed in the character table. For example, in the $\mathbf{C_{2v}}$ point group, x-polarized light may be used to excite vibrations of $\mathbf{B_1}$ symmetry, y-polarized light to excite vibrations of $\mathbf{B_2}$ symmetry, and z-polarized light to excite vibrations of $\mathbf{A_1}$ symmetry. In $\mathbf{H_2O}$, we would use z-polarized light to excite the symmetric stretch and bending modes, and x-polarized light to excite the asymmetric stretch. Shining y-polarized light onto a molecule of $\mathbf{H_2O}$ would not excite any vibrational motion [10]. For instance, let us consider a simple case of a vibrating diatomic molecule where the restoring force is proportional to the displacement,

$$F = -kx. \tag{11}$$

The potential energy is

$$V = \frac{1}{2}kx^2 \tag{12}$$

and the allowed energy can be obtained from Schrodinger equation,

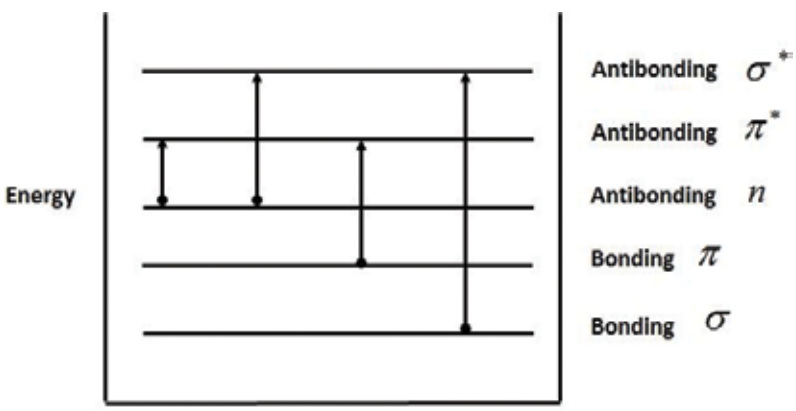

Figure 2. Absorbing species containing p, s, and n electrons.

$$E_v = \left(v + \frac{1}{2}\right)\hbar\omega \tag{13}$$

where

$$\omega = \left(\frac{k}{\mu}\right)^{1/2}, v = 0, 1, 2, 3, 4\ldots, \tag{14}$$

and

$$\mu = \frac{m_1 m_2}{m_1 + m_2}. \tag{15}$$

The vibrational terms of the molecule can therefore be given by

$$G_v = \left(v + \frac{1}{2}\right)\frac{1}{2\pi c}\left(\frac{k}{\mu}\right)^{1/2} \tag{16}$$

3.3. Raman scattering

Single photons often cannot reach vibrational modes in the molecule; however, it may still be possible to excite them. To achieve excitement, scientists often utilize Raman scattering, which is a two-photon process. These two photons utilized in Raman scattering might have different polarizations. The first photon sends the molecule into an intermediate state known as a virtual state, which is not a stationary state for the particular molecule. When considering the photon and the molecule as a system, a stationary state can be said to exist, but it exists only for a short period of time. Once the transition is over, a photon will be rapidly emitted back into the stable molecule. It is important to note that the photon may return different from its original state. The transition dipole for a particular Raman transition transforms as one of the Cartesian products. A Raman transition has the potential to excite Cartesian products if they are the product of a transformed vibrational mode. For example, modes that transform as x, y or z can be excited by a one-photon vibrational transition. Simple one-photon vibrational transitions can access all of the vibrational modes of water Raman transitions). The Cartesian products transform as follows in the $\mathbf{C_{2v}}$ point group. The stretch and the bending vibration of water are depictions of $\mathbf{A_1}$ symmetry. Consequently, Raman scattering processes involving two photons of identical polarization (x-, y- or z-polarized) can excite both. Conversely, an asymmetric stretch can be excited if one photon is x-polarized and the other is z-polarized.

As shown in **Figure 3**, Raman spectroscopy transition in resonance is the excitation from one particular electronic state to another state. The rules for selection are determined by the transition moment integral discussed in the electronic spectroscopy segment. Mechanically, Raman does produce a vibration similar to infrared, but selection protocols for Raman state that there must be a change in the polarization, which means that the volume occupied by the molecule must change [5]. The utilization of group theory to identify whether or not a transition is permitted can also be done using the transition moment integral presented in the electronic transition portion.

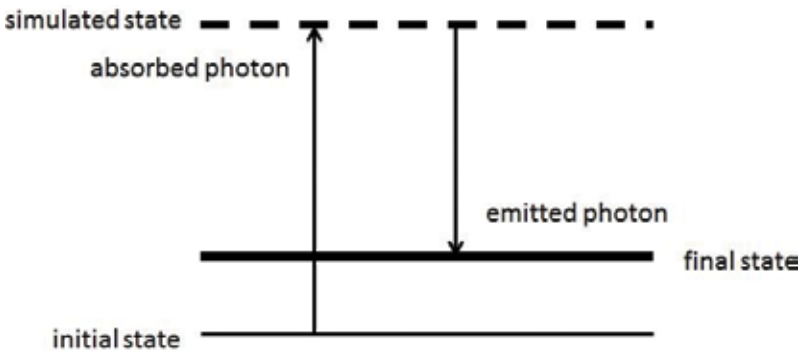

Figure 3. Raman scattering energy level diagram.

Acknowledgements

The authors thank the CUNY Office Assistant Oana Teodorescu for reading and for editing the manuscript. The first author acknowledges the support from the CUNY GRANT CCRG# 1517, the CUNY RESEARCH SCHOLAR PROGRAM-2017-2018 and THE NEXT BIIG THING INQUIRY GRANT 2017. He also acknowledges the mentee's student Francesca Serrano for helping in editing the manuscript. The contents of this chapter are solely the responsibility of the author and do not represent the official views of the NIH.

Author details

Eugene Stephane Mananga[1,2,3]*, Akil Hollington[3,4] and Karen Registe[5]

*Address all correspondence to: emananga@gradcenter.cuny.edu

1 Program Physics and Program Chemistry, Graduate Center, The City University of New York, New York, NY, USA

2 Department of Engineering, Physics, and Technology, BCC of CUNY, New York, USA

3 Department of Applied Physics, New York University, Brooklyn, NY, USA

4 Department of Chemistry, Syracuse University, Syracuse, NY, USA

5 Department of Mathematics, Lehman College, New York, USA

References

[1] Dixon JD. Problems in Group Theory. New York: Dover; 1973

[2] Horn K. Lecture note: "Introduction to Group Theory with Applications in Molecular and Solid State Physics". Fritz-Haber-Institut der Max-Planck-Gesellschaft

[3] Carmichael RD. Introduction to the Theory of Groups of Finite Order. New York: Dover; 1956

[4] Alperin JL, Bell RB. Groups and Representations. New York: Springer-Verlag; 1995

[5] Vallance C. Lecture note: "Molecular Symmetry, Group Theory, and Applications". University of Oxford

[6] Burrow M. Representation Theory of Finite Groups. New York: Dover; 1993

[7] Bunker PR, Jensen P. Molecular Symmetry and Spectroscopy. Ottawa: NRC Research Press; 1998

[8] Burnside W. Theory of Groups of Finite Order. 2nd ed. New York: Dover; 1955

[9] Arfken G. Introduction to Group Theory. In: §4.8 in Mathematical Methods for Physicists. 3rd ed. Orlando: Academic Press; 1985. pp. 237-276

[10] Lecture Note Physical Chemistry, PCV - Spectroscopy of atoms and molecules. ETHZ

Chapter 3

Group Theory from a Mathematical Viewpoint

Takao Satoh

Additional information is available at the end of the chapter

http://dx.doi.org/10.5772/intechopen.72131

Abstract

In this chapter, for the reader who does not major in mathematics but chemistry, we discuss general group theory from a mathematical viewpoint without proofs. The main purpose of the chapter is to reduce reader's difficulties for the abstract group theory and to get used to dealing with it. In order to do this, we exposit definitions and theorems of the field without rigorous and difficult arguments on the one hand and give lots of basic and fundamental examples for easy to understand on the other hand. Our final goal is to obtain well understandings about conjugacy classes, irreducible representations, and characters of groups with easy examples of finite groups. In particular, we give several character tables of finite groups of small order, including cyclic groups, dihedral groups, symmetric groups, and their direct product groups. In Section 8, we deal with directed graphs and their automorphism groups. It seems that some of ideas and techniques in this section are useful to consider the symmetries of molecules in chemistry.

Keywords: group theory, finite groups, conjugacy classes, representation theory, character tables, directed graphs, automorphisms of graphs

1. Introduction

To make a long story short, a group is a set equipped with certain binary operation, for example, the set of all integers with the addition and the set of all nth power roots of unity with the multiplication. One of the origins of the group theory goes back to the study of the solvability of algebraic equations by Galois in the nineteenth century. He focused on the permutations of the solutions of an equation and gave rise to a concept of permutation groups. On the other hand, in 1872 Felix Klein proposed that every geometry is characterized by its underlying transformation groups. Here the transformation group means the group that comes from certain symmetries of the space. By using group theory, he classified Euclidean geometry and non-Euclidean geometry. As is shown earlier, groups have been established as important research objects on the study of permutations and symmetries of a given object. The

group theory has achieved a good progress in modern mathematics and has various deep and sophisticated theories itself.

Today, the group theory has multiple facets and widespread applications in a broad range of science, including not only mathematics and physics but also chemistry. In chemistry, group theory is used to study the symmetries and the crystal structures of molecules. For each molecule, a certain group, which is called the point group, is defined by the symmetries on the molecule. The structure of this group reflects many physical and chemical properties, including the chirality and the spectroscopic property of the molecule. The group theory has become a standard and a powerful tool to study various properties of the molecule from a viewpoint of the molecular orbital theory, for example, the orbital hybridizations, the chemical bonding, the molecular vibration, and so on. In general, although each of modern mathematical theories is quite abstract and sophisticated to apply to the other sciences, the group theory has succeeded to achieve a good application by many authors, including Hans Bethe, Eugene Wigner, László Tisza, and Robert Mulliken. It seems that such expansions of mathematics to the other sciences are quite blessed facts for mathematicians.

Here we organize the contents of this chapter. First, we give mathematical notation and conventions which we use in this chapter. The reader is assumed to be familiar with elemental linear algebra and set theory. In Section 3, we review the definitions and some fundamental and important properties of groups. In particular, we show several methods to make new groups from known groups by considering subgroups and quotient groups. Then, we consider to classify known groups by using the concept of group isomorphism. In Section 4, we discuss and give many examples of finite groups, including symmetric groups, alternating groups, and dihedral groups. Then we give the classification theorem for finite abelian groups, which we can regard as an expansion of the Chinese remainder theorem. In Section 5, we consider to classify elements of groups by the conjugation and discuss the decomposition of a group into its conjugacy classes. In Section 6, we explain basic facts in representation theory of finite groups. In particular, we review representations of groups, irreducible representations, and characters. Finally, we give several examples of character tables of well-known finite groups. In Section 8, we consider finite-oriented graphs and their automorphisms. The automorphism group of a graph strongly reflects the symmetries of the graph. We remark that the reader can read this section without the knowledge of the facts in Sections 5 and 6.

2. Notation and conventions

In this section, we fix some notation and conventions and review some definitions in the set theory and the linear algebra:

$$\mathbf{N} := \text{the set of natural numbers} = \{1, 2, 3, \ldots\}$$

$$\mathbf{Z} := \text{the set of integers} = \{0, \pm 1, \pm 2, \pm 3, \ldots\}$$

$$\mathbf{Q} := \text{the set of rational numbers}$$

$$\mathbf{R} := \text{the set of real numbers}$$

$$\mathbf{C} := \text{the set of complex numbers} = \left\{ a + b\sqrt{-1} \,|\, a, b \in \mathbf{R} \right\}$$

- For any $a, b \in \mathbf{Z} \setminus \{0\}$, the greatest common divisor of a and b is denoted by $\gcd(a, b)$.
- For a set X, the cardinality of X is denoted by $|X|$. If X is a finite set, $|X|$ means the number of elements of X.
- For sets X and Y, the difference of sets X and Y is denoted by $X \setminus Y := \{x \mid x \in X, x \notin Y\}$.
- A map $f : X \to Y$ is surjective if for any $y \in Y$; there exists some $x \in X$ such that $f(x) = y$.
- A map $f : X \to Y$ is injective if $f(x) = f(x')$ for $x, x' \in X$; then $x = x'$.
- A map $f : X \to Y$ is bijective if f is surjective and injective. In other words, the bijective map is one-to-one correspondence between X and Y.
- Let K be $\mathbf{Q}$, $\mathbf{R}$ or $\mathbf{C}$. For K-vector spaces V and W, a map $f : V \to W$ is K-linear if f satisfies

$$f(\boldsymbol{x} + \boldsymbol{y}) = f(\boldsymbol{x}) + f(\boldsymbol{y}),$$
$$f(k\boldsymbol{x}) = kf(\boldsymbol{x})$$

for any $\boldsymbol{x}, \boldsymbol{y} \in V$ and $k \in K$.

- A linear map $f : V \to V$ is called a linear transformation on V.

3. General group theory

In this section, we review elemental and fundamental topics in group theory, based on the authors' book [1]. There are hundreds of textbooks for the group theory. Venture to say, if the reader wants to learn more from a viewpoint of symmetries, it seems to be better to see [2]. For high motivated readers, see [3, 4] for mathematical details.

3.1. Groups

Let G be a set. For any $\sigma, \tau \in G$, if there exists the unique element $\sigma \cdot \tau \in G$, which is called the **product** of σ and τ, such that the product satisfies the following three conditions, then the set G is called a **group**:

- **(Associativity)** For any $\sigma, \tau, \rho \in G$, $(\sigma \cdot \tau) \cdot \rho = \sigma \cdot (\tau \cdot \rho)$.
- **(Unit)** There exists some element $e \in G$ such that for any $\sigma \in G$,

$$e \cdot \sigma = \sigma \cdot e = \sigma.$$

We call the element e the **unit** of G. According to the mathematical convention, we write 1_G or simply 1, for the unit.

- **(Inverse element)** For any $\sigma \in G$, there exists some element $\sigma' \in G$ such that

$$\sigma \cdot \sigma' = \sigma' \cdot \sigma = e.$$

We call σ' the **inverse** element of σ and write σ^{-1}.

If the definition of the product is clear from the content, we often omit the symbol $\cdot$ and write $\sigma\tau$ instead of $\sigma \cdot \tau$ for simplicity. The product is a binary operator on G and is also called the **multiplication** of G.

Here we consider the following examples:

(E1) Each of the sets **Z**, **Q**, **R**, and **C** is a group with the usual addition. For the case **Z**, we see that the unit is 0 and for any $n \in \mathbf{Z}$, the inverse of n is $-n$. In general, if the product of a group G is additive, then G is called an **additive group**. We remark that **N** is not a group with the usual addition since any element does not have its inverse.

(E2) The set $\mathbf{R}^{\times} := \mathbf{R} \setminus \{0\}$ with the usual multiplication of real numbers forms a group. We see that the unit is 1 and for any $r \in \mathbf{R}^{\times}$, the inverse of r is $1/r$. We remark that **R** with the usual multiplication is not a group since 0 does not have its inverse. In general, if the product of a group G is multiplicative, then G is called a **multiplicative group**. Similarly, $\mathbf{Q}^{\times} := \mathbf{Q} \setminus \{0\}$ and $\mathbf{C}^{\times} := \mathbf{C} \setminus \{0\}$ are multiplicative groups.

(E3) For any $n \in \mathbf{N}$ $(n \geq 1)$, let $\mathcal{U}_n$ be the set of nth power roots of unity:

$$\mathcal{U}_n := \left\{ \exp\left(\frac{2k\pi\sqrt{-1}}{n}\right) \in \mathbf{C} \,\middle|\, 0 \leq k \leq n-1 \right\},$$

where

$$\exp\left(\frac{2k\pi\sqrt{-1}}{n}\right) := \cos\left(\frac{2k\pi}{n}\right) + \sqrt{-1}\sin\left(\frac{2k\pi}{n}\right).$$

Then $\mathcal{U}_n$ with the usual multiplication of **C** forms a group. Geometrically, $\mathcal{U}_n$ is the set of vertices of the regular n-gon on the unit circle in the complex plane **C**. For example, $\mathcal{U}_6$ consists of the following points for $\zeta = \exp\left(\frac{2\pi\sqrt{-1}}{6}\right)$ in **Figure 1**.

In general, for a group G, if G consists of finitely many elements, then G is called a **finite group**. The number of elements of a finite group G is called the **order** of G, denoted by $|G|$. If G is not a finite group, then G is called an **infinite group**. The group $\mathcal{U}_n$ is a finite group of order n, and the groups discussed in (E1) and (E2) are infinite groups.

(E4) Let K be **Q**, **R**, or **C**. We denote by $\mathrm{M}(2, K)$ the set of 2×2 matrices with all entries in K:

$$\mathrm{M}(2, K) := \left\{ \begin{pmatrix} a & b \\ c & d \end{pmatrix} \,\middle|\, a, b, c, d \in K \right\}.$$

Furthermore, we denote by $\mathrm{GL}(2, K)$ the set of elements of $\mathrm{M}(2, K)$ whose determinant is not equal to zero:

$$\mathrm{GL}(2, K) := \{A \in \mathrm{M}(2, K) \mid \det A \neq 0\}.$$

Then $\mathrm{M}(2, K)$ with the usual addition of matrices forms an additive group. The unit of $\mathrm{M}(2, K)$ is zero matrix, and for any $A = (a_{ij}) \in \mathrm{M}(2, K)$, its inverse is $-A := (-a_{ij})$. Since $\mathrm{GL}(2, K)$ does not

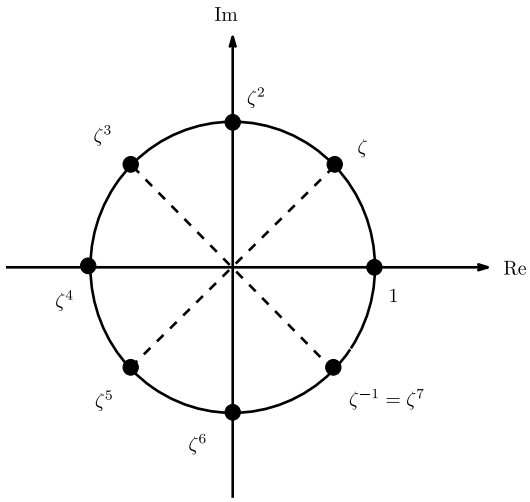

Figure 1. The sixth roots of unity.

have the zero matrix, the set $\mathrm{GL}(2,K)$ is not an additive group. On the other hand, the set $\mathrm{GL}(2,K)$ with the usual multiplication of matrices forms a multiplicative group. The unit of $\mathrm{GL}(2,K)$ is the unit matrix E_2, and for any $A = (a_{ij}) \in \mathrm{GL}(2,K)$, its inverse is the inverse matrix A^{-1} as follows:

$$E_2 := \begin{pmatrix} 1 & 0 \\ 0 & 1 \end{pmatrix}, \quad A^{-1} = \frac{1}{\det A} \begin{pmatrix} a_{22} & -a_{12} \\ -a_{21} & a_{11} \end{pmatrix}.$$

The group $\mathrm{GL}(2,K)$ is called the **general linear group** of degree 2. Similarly, we can consider the general linear group $\mathrm{GL}(n,K)$ of degree n for any $n \in \mathbf{N}$.

Both $\mathrm{M}(2,K)$ and $\mathrm{GL}(2,K)$ are infinite groups. But the most significant difference between them is the commutativity of the products. Although we see $A + B = B + A$ in $\mathrm{M}(2,K)$ for any $A, B \in \mathrm{M}(2,K)$, the equation $AB = BA$ does not hold in $\mathrm{GL}(2,K)$ in general. For example, if $A = \begin{pmatrix} 1 & 1 \\ 0 & 1 \end{pmatrix}$ and $B = \begin{pmatrix} 1 & 0 \\ 1 & 1 \end{pmatrix}$, then we see

$$AB = \begin{pmatrix} 2 & 1 \\ 1 & 1 \end{pmatrix}, \quad BA = \begin{pmatrix} 1 & 1 \\ 1 & 2 \end{pmatrix}.$$

For a group G, if $\sigma\tau = \tau\sigma$ holds for any $\sigma, \tau \in G$, then G is called an **abelian group**. The group $\mathrm{GL}(2,K)$ is a non-abelian group, and all the groups as mentioned before except for $\mathrm{GL}(2,K)$ are abelian groups.

3.2. Subgroups

Since group theory is an abstract itself, it had better for beginners to have sufficiently enough examples to understand it. In order to make further examples, we consider several methods to make new groups from known groups. The first one is a subgroup.

Let G be a group. If a nonempty subset H of G satisfies the following two conditions, then H is called a **subgroup** of G:

- For any $\sigma, \tau \in H$, $\sigma\tau \in H$.
- For any $\sigma \in H$, $\sigma^{-1} \in H$.

We can consider H itself is a group by restricting the product of G to H. For any group G, the one point subset $\{1_G\}$ is a subgroup of G. We call this subgroup the **trivial subgroup** of G. Let us consider some other examples:

(E5) The additive group $\mathbf{Z}$ is a subgroup of $\mathbf{Q}$, $\mathbf{R}$, and $\mathbf{Z}$. For any $n \in \mathbf{Z}$, the subset

$$n\mathbf{Z} := \{0, \pm n, \pm 2n, \ldots\} \subset \mathbf{Z}$$

of $\mathbf{Z}$ consisting of multiples of n is a subgroup of $\mathbf{Z}$. Since $0\mathbf{Z} = \{0\}$ is the trivial subgroup, and since $n\mathbf{Z} = (-n)\mathbf{Z}$, we usually consider the case $n \in \mathbf{N}$.

(E6) Consider the group $\mathcal{U}_6$ consisting of 6th power roots of unity. Then we can consider $\mathcal{U}_2$ and $\mathcal{U}_3$ are subgroups of $\mathcal{U}_6$.

(E7) Let K be $\mathbf{Q}$, $\mathbf{R}$, or $\mathbf{C}$. The subset

$$\mathrm{SL}(2, K) := \{A \in \mathrm{GL}(2, K) \mid \det A = 1\} \subset \mathrm{GL}(2, K)$$

of $\mathrm{GL}(2, K)$ consisting of matrices whose determinants are equal to one is a subgroup of $\mathrm{GL}(2, K)$. We call $\mathrm{SL}(2, K)$ the **special linear group** of degree 2.

In general, we can construct a subgroup from a subset of a group. Let S be a subset of a group G. Then the subset

$$\langle S \rangle := \left\{ s_1^{e_1} s_2^{e_2} \cdots s_m^{e_m} \mid m \in \mathbf{Z}_{\geq 0}, s_i \in S, e_i = \pm 1 \right\}$$

of G consisting of elements which are written as a product of some elements in S, and their inverses are a subgroup of G. Remark that if $m = 0$, the product $s_1^{e_1} \cdots s_m^{e_m}$ means 1_G and that for any $\sigma = s_1^{e_1} s_2^{e_2} \cdots s_m^{e_m} \in \langle S \rangle$, its inverse is given by $\sigma^{-1} = s_m^{-e_m} s_{m-1}^{-e_{m-1}} \cdots s_1^{-e_1}$. We call $\langle S \rangle$ the subgroup of G **generated by** S. The elements of S are called **generators** of the subgroup $\langle S \rangle$. Here we give some examples:

(E8) The additive group $\mathbf{Z}$ is generated by 1. For any $n \geq 1$, the group $\mathcal{U}_n$ of nth power roots of unity is generated by $\zeta = \exp\left(2\pi\sqrt{-1}/n\right)$. In general, a group generated by a single element is called a **cyclic group**. Thus, $\mathbf{Z}$ is an infinite cyclic group, and $\mathcal{U}_n$ is a finite cyclic group. Remark that -1 and $\zeta^{-1} = \exp\left(-2\pi\sqrt{-1}/n\right)$ are also generators of $\mathbf{Z}$ and $\mathcal{U}_n$, respectively.

(E9) It is known that the additive groups $\mathbf{Q}$, $\mathbf{R}$, and $\mathbf{C}$ and the multiplicative groups $\mathrm{GL}(2, K)$ and $\mathrm{SL}(2, K)$ for $K = \mathbf{Q}, \mathbf{R}, \mathbf{C}$ are not finitely generated group.

Next, we consider a relation between the orders of a finite group and its subgroup. Let G be a group and H a subgroup of G. For any $\sigma \in G$, the subset

$$\sigma H := \{\sigma\tau \in G \mid \tau \in H\}$$

is called a left coset of H in G. We can see that $\sigma H = \tau H$ if and only if there exists some $h \in H$ such that $\sigma = \tau h$.

(E10) In the additive group $\mathbf{Z}$, for any $n \in \mathbf{N}$, consider the subgroup $n\mathbf{Z}$. Then, since the product of $\mathbf{Z}$ is written additively, a left coset of $n\mathbf{Z}$ is given by

$$\sigma + n\mathbf{Z} = \{\sigma + n\tau \mid \tau \in \mathbf{Z}\}$$

for an element $\sigma \in \mathbf{Z}$. On the other hand, if we take the remainder r of the division of σ by n, then we see $\sigma + n\mathbf{Z} = r + n\mathbf{Z}$. Hence all left cosets of $n\mathbf{Z}$ in $\mathbf{Z}$ are given by

$$n\mathbf{Z},\ 1 + n\mathbf{Z},\quad (n-1) + n\mathbf{Z}.$$

For simplicity, we write $[r]_n$ for $r + n\mathbf{Z}$.

(E11) Consider the finite cyclic group $\mathcal{U}_6$ and its subgroup $\mathcal{U}_2 = \{\pm 1\}$ of order 2. Set $\zeta := \exp\left(2\pi\sqrt{-1}/6\right)$. Then we can see that

$$\zeta\mathcal{U}_2 = \{\pm\zeta\} = \left\{\zeta, \zeta^4\right\} = \zeta^4\mathcal{U}_2, \quad \zeta^2\mathcal{U}_2 = \zeta^5\mathcal{U}_2, \quad \zeta^3\mathcal{U}_2 = \mathcal{U}_2.$$

Hence there exist three left cosets of $\mathcal{U}_2$.

In example (E11), we can see that the order of $\mathcal{U}_2$ times the number of left cosets of $\mathcal{U}_2$ is equal to six, which is the order of $\mathcal{U}_6$. This is no coincidence. In general, for a finite group G and a subgroup H of G, the number of left cosets of H is called the **index** of H in G and is denoted by $[G : H]$. Then we have the following:

Theorem 3.1 (Lagrange). *As the above notation C, we have* $|G| = |H|[G : H]$. *Namely, the order of any subgroup of a finite group G is a divisor of* $|G|$.

As a corollary, we obtain the following:

Corollary 3.2. *If G is a finite group of prime order, then G is a cyclic group.*

3.3. Quotient groups

For a group G and its subgroup H, the set of left cosets of H is denoted by

$$G/H := \{\sigma H \mid \sigma \in G\}.$$

In general, this set does not have a natural group structure. Here we consider a condition to make it a group.

Let N be a subgroup of G. If $\sigma n \sigma^{-1} \in N$ for any $n \in N$ and any $\sigma \in G$, then N is called a **normal subgroup** of G. If G is abelian group, any subgroup of G is a normal subgroup. For a normal

subgroup N of G, we define the product on G/N by using that on G. Namely, for any $\sigma N, \tau N \in G/N$, define

$$\sigma N \cdot \tau N := (\sigma\tau)N.$$

Then this definition is well defined, and G/N with this product forms a group. The unit is $1_G N = N$, and for any $\sigma N \in G/N$, its inverse is given by $(\sigma N)^{-1} = \sigma^{-1} N$. We call G/N the **quotient group** of G by N.

(E12) The most important example for quotient groups is

$$\mathbf{Z}/n\mathbf{Z} = \{[0]_n, [1]_n, \ldots, [n-1]_n\}$$

for $n \in \mathbf{N}$. For any $a, b \in \mathbf{Z}$, we have

$$[a]_n + [b]_n = [a+b]_n, \quad -[a]_n = [-a]_n.$$

For example, in the group $\mathbf{Z}/6\mathbf{Z}$, we have

$$[1]_6 + [3]_6 = [4]_6, \quad [2]_6 + [7]_6 = [9]_6 = [3]_6, \quad -[4]_6 = [-4]_6 = [2]_6.$$

For any $0 \le r \le n-1$, since we see

$$[r]_n = [1]_n + [1]_n + \cdots + [1]_n \in \mathbf{Z}/n\mathbf{Z},$$

the group $\mathbf{Z}/n\mathbf{Z}$ is a cyclic group of order n generated by $[1]_n$.

3.4. Homomorphisms and isomorphisms

As mentioned above, we have many examples of groups. Here, we consider relations between groups and examine which ones are essentially of the same type of groups. To say more technically, we classify groups by using isomorphisms.

Let G and H be groups. If a map $f : G \to H$ satisfies

$$f(\sigma\tau) = f(\sigma)f(\tau) \quad \text{for any } \sigma, \tau \in G,$$

then f is called a **homomorphism**. A bijective homomorphism $f : G \to H$ is called an **isomorphism**. Namely, an isomorphism is a map such that it is one-to-one correspondence between the groups and that it preserves the products of the groups. If G and H are isomorphic, we write $G \cong H$.

(E13) Set

$$\mathbf{R}_{>0} := \{x \in \mathbf{R} \mid x > 0\},$$

and consider it as a multiplicative subgroup of $\mathbf{R}^\times$. The exponent map $\exp : \mathbf{R} \to \mathbf{R}_{>0}$ is an isomorphism from the additive group $\mathbf{R}$ to $\mathbf{R}_{>0}$.

(E14) Let K be $\mathbf{Q}$, $\mathbf{R}$, or $\mathbf{C}$. Then the determinant map $\det \mathrm{GL}(2,K) \to K^\times$ is a homomorphism. It is, however, not an isomorphism since f is not injective. For example, $\det E_2 = \det(-E_2) = 1$.

On the other hand, $\mathrm{SL}(2,K)$ is a normal subgroup of $\mathrm{GL}(2,K)$. For any $\sigma, \tau \in \mathrm{GL}(2,K)$, we can see that

$$\sigma\mathrm{SL}(2,K) = \tau\mathrm{SL}(2,K) \Leftrightarrow \det\sigma = \det\tau.$$

Define the map $f : \mathrm{GL}(2,K)/\mathrm{SL}(2,K) \to K^\times$ by

$$\sigma\mathrm{SL}(2,K) \mapsto \det\sigma.$$

Then f is an isomorphism. Indeed f is injective. For any $x \in K^\times$, if we consider the element $\sigma := \begin{pmatrix} x & 0 \\ 0 & 1 \end{pmatrix} \in \mathrm{GL}(2,K)$, we have $f(\sigma\mathrm{SL}(2,K)) = x$. Hence f is surjective. Moreover, we have

$$\begin{aligned} f((\sigma\mathrm{SL}(2,K))(\tau\mathrm{SL}(2,K))) &= f((\sigma\tau)\mathrm{SL}(2,K)) = \det(\sigma\tau) \\ &= (\det\sigma)(\det\tau) = f(\sigma\mathrm{SL}(2,K))f(\tau\mathrm{SL}(2,K)). \end{aligned}$$

(E15) For any $n \in \mathbf{N}$, define the map $f : \mathbf{Z}/n\mathbf{Z} \to \mathcal{U}_n$ by $[k]_n \mapsto \exp\left(2k\pi\sqrt{-1}/n\right)$. Then f is an isomorphism since f is bijective, and

$$\begin{aligned} f([k]_n + [l]_n) &= f([k+l]_n) = \exp\left(2(k+l)\pi\sqrt{-1}/n\right) \\ &= \exp\left(2k\pi\sqrt{-1}/n\right)\exp\left(2l\pi\sqrt{-1}/n\right) = f([k]_n)f([l]_n). \end{aligned}$$

Let G and H be isomorphic groups. Then, even if G and H are different as a set, they have the same structure as a group. This means that if one is abelian, finite or finitely generated, then so is the other, respectively. In other words, for example, an abelian group is never isomorphic to a non-abelian group and so on.

4. Finite groups

In this section, we give some examples of important finite groups.

4.1. Symmetric groups

For any $n \in \mathbf{N}$, set $X := \{1, 2, \ldots, n\}$. A bijective map $\sigma : X \to X$ is called a permutation on X. A permutation σ is denoted by

$$\sigma = \begin{pmatrix} 1 & 2 & \cdots & n \\ \sigma(1) & \sigma(2) & \cdots & \sigma(n) \end{pmatrix}.$$

Remark that this is not a matrix. We can omit a letter i $(1 \le i \le n)$ if the letter i is fixed. For example, for $n = 4$:

$$\begin{pmatrix} 1 & 2 & 3 & 4 \\ 3 & 2 & 4 & 1 \end{pmatrix} = \begin{pmatrix} 1 & 3 & 4 \\ 3 & 4 & 1 \end{pmatrix}$$

We call the permutation

$$\varepsilon := \begin{pmatrix} 1 & 2 & \cdots & n \\ 1 & 2 & \cdots & n \end{pmatrix}$$

the **identity permutation**.

Let $\mathfrak{S}_n$ be the set of permutations on X. For any $\sigma, \tau \in \mathfrak{S}_n$, define the product of σ and τ to be the composition $\sigma \circ \tau$ as a map. Then the set $\mathfrak{S}_n$ with this product forms a group. We call it the **symmetric group** of degree n. The unit is the identity permutation, and for any $\sigma \in \mathfrak{S}_n$, its inverse is given by

$$\sigma^{-1} = \begin{pmatrix} \sigma(1) & \sigma(2) & \cdots & \sigma(n) \\ 1 & 2 & \cdots & n \end{pmatrix}.$$

The symmetric group $\mathfrak{S}_n$ is a finite group of order $n!$.

Since $\mathfrak{S}_1$ is the trivial group, and

$$\mathfrak{S}_2 = \left\{ \varepsilon, \begin{pmatrix} 1 & 2 \\ 2 & 1 \end{pmatrix} \right\},$$

we see that $\mathfrak{S}_n$ is abelian if $n \leq 2$. For $n = 3$, we have

$$\mathfrak{S}_3 = \left\{ \varepsilon, \begin{pmatrix} 1 & 2 \\ 2 & 1 \end{pmatrix}, \begin{pmatrix} 1 & 3 \\ 3 & 1 \end{pmatrix}, \begin{pmatrix} 2 & 3 \\ 3 & 2 \end{pmatrix}, \begin{pmatrix} 1 & 2 & 3 \\ 2 & 3 & 1 \end{pmatrix}, \begin{pmatrix} 1 & 2 & 3 \\ 3 & 1 & 2 \end{pmatrix} \right\},$$

and

$$\begin{pmatrix} 1 & 2 \\ 2 & 1 \end{pmatrix} \begin{pmatrix} 2 & 3 \\ 3 & 2 \end{pmatrix} = \begin{pmatrix} 1 & 2 & 3 \\ 2 & 3 & 1 \end{pmatrix} \neq \begin{pmatrix} 1 & 2 & 3 \\ 3 & 1 & 2 \end{pmatrix} = \begin{pmatrix} 2 & 3 \\ 3 & 2 \end{pmatrix} \begin{pmatrix} 1 & 2 \\ 2 & 1 \end{pmatrix}.$$

Hence, $\mathfrak{S}_3$ is non-abelian. Similarly, for any $n \geq 3$, $\mathfrak{S}_n$ is non-abelian.

Here we consider another description of permutations. For distinct letters $a_1, \ldots, a_m \in X$, the permutation

$$\begin{pmatrix} a_1 & a_2 & \cdots & a_{m-1} & a_m \\ a_2 & a_3 & \cdots & a_m & a_1 \end{pmatrix}$$

is denoted by $(a_1, a_2, \cdots, a_m)$ and is called a **cyclic permutation** of length m. We call a cyclic permutation of length 2 a **transposition**. Namely, any transposition is of type

$$(i, j) = \begin{pmatrix} i & j \\ j & i \end{pmatrix}.$$

A cyclic permutation of length 1 is nothing but the identity permutation:

$$(1) = (2) = \cdots = (n) = \varepsilon.$$

In general, a permutation cannot be written as a single cyclic permutation but a product of some cyclic permutations which do not have a common letter. For example, consider

$$\sigma = \begin{pmatrix} 1 & 2 & 3 & 4 & 5 \\ 3 & 5 & 4 & 1 & 2 \end{pmatrix}.$$

Then we see

$$\sigma : 1 \mapsto 3 \mapsto 4 \mapsto 1, \quad 2 \mapsto 5 \mapsto 2,$$

and hence

$$\sigma = (1,3,4)(2,5) = (2,5)(1,3,4).$$

Remark that two cyclic permutations which do not have a common letter are commutative. For any cyclic permutation $(a_1, a_2, \cdots, a_m)$, we have

$$(a_1, a_2, \cdots, a_m) = (a_1, a_2)(a_2, a_3)\cdots(a_{m-1}, a_m).$$

By using the above facts, we see

Theorem 4.1. *Every permutation can be written as a product of transpositions.*

An expression of a permutation as a product of transpositions is not unique. For example,

$$(1,3,2) = (1,2)(1,3) = (1,3)(2,3).$$

However, we have

Theorem 4.2. *For any permutation σ, consider expressions of σ as a product of transpositions. Then the parity of the number of transpositions is invariant.*

For a permutation σ, if σ is written as a product of even (resp. odd) numbers of transpositions, then σ is called **even permutation** (resp. **odd permutation**). For example, the cyclic permutation $(a_1, a_2, \cdots, a_m)$ is even (resp. odd) permutation if m is odd (resp. even).

4.2. Alternating groups

In this subsection, we consider important normal subgroups of the symmetric groups. Let $\mathfrak{A}_n$ be the set of even permutations of $\mathfrak{S}_n$. For any $\sigma \in \mathfrak{A}_n$, if we write σ as a product of transpositions, $\sigma = \tau_1 \cdots \tau_k$, then we see

$$\sigma^{-1} = \tau_k \tau_{k-1} \cdots \tau_1 \in \mathfrak{A}_n.$$

Clearly, if $\sigma, \tau \in \mathfrak{A}_n$, then $\sigma\tau \in \mathfrak{A}_n$. Thus, the subset $\mathfrak{A}_n$ is a subgroup of $\mathfrak{S}_n$. We call $\mathfrak{A}_n$ the **alternating group** of degree n. It is easily seen that $\mathfrak{A}_n$ is a normal subgroup of $\mathfrak{S}_n$. For example, for $n = 3$ and 4, we have

$$\mathfrak{A}_3 = \{\varepsilon, (1,2,3), (1,3,2)\},$$
$$\mathfrak{A}_4 = \{\varepsilon, (1,2,3), (1,3,2), (1,2,4), (1,4,2), (1,3,4), (1,4,3), (2,3,4), (2,4,3), (1,2)(3,4), (1,3)(2,4), (1,4)(2,3)\}.$$

For any $\sigma \in \mathfrak{S}_n$, we have

$$\sigma\mathfrak{A}_n = \begin{cases} (1,2)\mathfrak{A}_n, & \text{if } \sigma \text{ is odd permutation,} \\ \mathfrak{A}_n, & \text{if } \sigma \text{ is even permutation.} \end{cases}$$

Hence $[\mathfrak{S}_n : \mathfrak{A}_n] = 2$. Therefore, from Lagrange's theorem, we see that $\mathfrak{A}_n$ is a finite group of order $n!/2$.

4.3. Dihedral groups

For any $n \in \mathbf{N}$ $(n \geq 3)$, consider a regular polygon V_n with n sides, and fix it. A map $\sigma : V_n \to V_n$ is called a congruent transformation on V_n if σ preserves the distance between any two points in V_n. Namely, σ is considered as a symmetry on V_n. Set

$$D_n := \{\sigma : V_n \to V_n \mid \sigma \text{ is a congruent transformation}\}.$$

For any $\sigma, \tau \in D_n$, define the product of σ and τ to be the composition $\sigma \circ \tau$ as a map. Then the set D_n with this product forms a group. We call it the **dihedral group** of degree n. The unit is the identity transformation.

Each congruent transformation on V_n is determined by the correspondence between vertices of V_n. Indeed, attach the number $1, 2, \ldots, n$ to vertices of V_n in counterclockwise direction. For any $\sigma \in D_n$, if $\sigma(1) = i$, then the vertices $2, 3, \ldots, n$ are mapped to $i+1, i+2, \ldots, n, 1, 2, \ldots i-1$, respectively, Cor mapped to $i-1, i-2, \ldots, 1, n, n-1, \ldots, i+1$, respectively. If we express this by using the notation for permutations, we have

$$\sigma = \begin{pmatrix} 1 & 2 & \cdots & n-1 & n \\ i & i+1 & \cdots & i-2 & i-1 \end{pmatrix} \text{ or } \begin{pmatrix} 1 & 2 & \cdots & n-1 & n \\ i & i-1 & \cdots & i+2 & i+1 \end{pmatrix}.$$

The former case is a rotation, and the latter case is the composition of a rotation and a reflection. For $n = 3$, see **Figure 2**. Thus the dihedral group D_n is a finite group of order $2n$ and is naturally considered as a subgroup of $\mathfrak{S}_n$. For $n = 3$, since D_3 is a subgroup of $\mathfrak{S}_3$, and since both groups are of order 6, we see that $D_3 = \mathfrak{S}_3$.

Let $\sigma \in D_n$ be the rotation of V_n with angle $\frac{2\pi}{n}$ in the counterclockwise direction and $\tau \in D_n$ be the reflection of V_n which fixes the vertex 1. Namely,

$$\sigma = \begin{pmatrix} 1 & 2 & \cdots & n-1 & n \\ 2 & 3 & \cdots & n & 1 \end{pmatrix}, \quad \tau = \begin{pmatrix} 1 & 2 & \cdots & n-1 & n \\ 1 & n & \cdots & 3 & 2 \end{pmatrix}.$$

http://dx.doi.org/10.5772/intechopen.72131

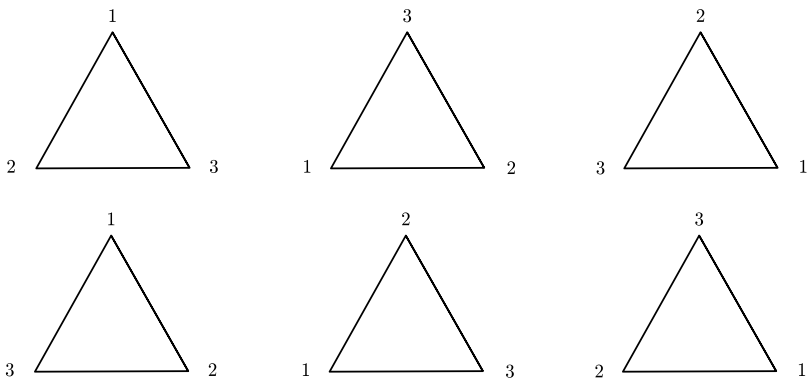

Figure 2. The transformations of the regular triangle.

Then the reflection of V_n which fixes the vertex i is written as $\sigma^{i-1}\tau\sigma^{-(i-1)}$. Hence D_n is generated by σ and τ. Moreover, we have

$$D_n = \{1, \sigma, \sigma^2, \ldots, \sigma^{n-1}, \tau, \sigma\tau, \sigma^2\tau, \ldots, \sigma^{n-1}\tau\}.$$

4.4. The structure theorem for finite abelian groups

In this subsection, we give a complete classification of finite abelian groups up to isomorphism. To begin with, we review the direct product of groups.

Let G and H be groups. Consider the direct product set

$$G \times H := \{(g,h) \mid g \in G,\ h \in H\},$$

and define the product of elements $(g,h), (g',h') \in G \times H$ to be

$$(g,h) \cdot (g',h') := (gg', hh').$$

Then $G \times H$ with this product forms a group. The unit is $(1_G, 1_H)$, and for any $(g,h) \in G \times H$, its inverse is given by $(g^{-1}, h^{-1}) \in G \times H$. We call the group $G \times H$ the **direct product group** of G and H. Similarly, for finitely many groups $G_1, G_2, \ldots, G_n$, we can define its direct product group $G_1 \times \cdots \times G_n$. For each $1 \leq i \leq n$, if G_i is a finite group of order m_i, then $G_1 \times \cdots \times G_n$ is a finite group of order $m_1 m_2 \cdots m_n$. The following theorem is famous in elementary number theory.

Theorem 4.3 (Chinese remainder theorem). *For any $m, n \in \mathbf{N}$ such that $\gcd(m,n) = 1$. Then we have*

$$\mathbf{Z}/mn\mathbf{Z} \cong \mathbf{Z}/m\mathbf{Z} \times \mathbf{Z}/n\mathbf{Z}.$$

An isomorphism $f : \mathbf{Z}/mn\mathbf{Z} \to \mathbf{Z}/m\mathbf{Z} \times \mathbf{Z}/n\mathbf{Z}$ is given by

$$[x]_{mn} \mapsto \left([x]_m, [x]_n\right).$$

(E16) Consider the case $m = 2$ and $n = 3$. Each element $[x]_6$ of $\mathbf{Z}/6\mathbf{Z}$ is mapped to the following element by the above isomorphism f:

$$[1]_6 \mapsto ([1]_2, [1]_3), \quad [2]_6 \mapsto ([2]_2, [2]_3) = ([0]_2, [2]_3), \quad [3]_6 \mapsto ([3]_2, [3]_3) = ([1]_2, [0]_3),$$
$$[4]_6, \mapsto ([4]_2, \ [4]_3) \ = ([0]_2, [1]_3), \quad [5]_6 \mapsto ([5]_2, [5]_3) = ([1]_2, [2]_3), \quad [0]_6 \mapsto ([0]_2, [0]_3).$$

(E17) If $\gcd(m, n) \neq 1$, the theorem does not hold. For example, consider the case of $m = n = 2$. Any element $x \in \mathbf{Z}/2\mathbf{Z} \times \mathbf{Z}/2\mathbf{Z}$ satisfies that $x + x$ is equal to zero. On the other hand, for the element $y := [1]_4 \in \mathbf{Z}/4\mathbf{Z}$, $y + y$ is not equal to zero. Hence the group structures of $\mathbf{Z}/2\mathbf{Z} \times \mathbf{Z}/2\mathbf{Z}$ and $\mathbf{Z}/4\mathbf{Z}$ are different.

Now, we show one of the most important theorems in finite group theory.

Theorem 4.4 (structure theorem for finite abelian groups). *Let G be a nontrivial finite abelian group. Then G is isomorphic to a direct product of finite cyclic groups of prime power order*:

$$G \cong \mathbf{Z}/p_1^{e_1}\mathbf{Z} \times \cdots \times \mathbf{Z}/p_r^{e_r}\mathbf{Z}.$$

The tuple $\left(p_1^{e_1}, p_2^{e_2}, \ldots, p_r^{e_r}\right)$ is uniquely determined by G, up to the order of the factors.

(E18) The list of finite abelian groups of order 72 up to isomorphism is given by

$$\mathbf{Z}/9\mathbf{Z} \times \mathbf{Z}/8\mathbf{Z}, \quad \mathbf{Z}/9\mathbf{Z} \times \mathbf{Z}/4\mathbf{Z} \times \mathbf{Z}/2\mathbf{Z}, \quad \mathbf{Z}/9\mathbf{Z} \times \mathbf{Z}/2\mathbf{Z} \times \mathbf{Z}/2\mathbf{Z} \times \mathbf{Z}/2\mathbf{Z},$$
$$\mathbf{Z}/3\mathbf{Z} \times \mathbf{Z}/3\mathbf{Z} \times \mathbf{Z}/8\mathbf{Z}, \quad \mathbf{Z}/3\mathbf{Z} \times \mathbf{Z}/3\mathbf{Z} \times \mathbf{Z}/4\mathbf{Z} \times \mathbf{Z}/2\mathbf{Z},$$
$$\mathbf{Z}/3\mathbf{Z} \times \mathbf{Z}/3\mathbf{Z} \times \mathbf{Z}/2\mathbf{Z} \times \mathbf{Z}/2\mathbf{Z} \times \mathbf{Z}/2\mathbf{Z}.$$

5. Conjugacy classes

In this section, we consider the classification of elements of a group by using the conjugation. The results of this section are used in Section 6.

Let G a group. For elements $x, y \in G$, if there exists some $g \in G$ such that $x = gyg^{-1}$; then we say that x is **conjugate** to y and write $x \sim y$. This is an equivalence relation on G. Namely, for any $x \in G$, we have $x \sim x$ by observing $x = 1_G x 1_G^{-1}$. If $x \sim y$, then $x = gyg^{-1}$ for some $g \in G$. Thus $y = g^{-1}x\left(g^{-1}\right)^{-1}$, and hence $y \sim x$. If $x \sim y$ and $y \sim z$, then $x = gyg^{-1}$ and $y = hzh^{-1}$ for some $g, h \in G$. Thus $x = (gh)z(gh)^{-1}$, and hence $x \sim z$. For any $x \in G$, the set

$$C(x) := \{y \in G \mid y \sim x\}$$

is called the **conjugacy class** of x in G. If G is abelian group, for any $x \in G$, there exists no element conjugate to x except for x, and hence $C(x) = \{x\}$. Here we give a few examples.

(E19) (Dihedral groups) For $n \geq 3$, the conjugacy classes of D_n are as follows:

1. If n is even:

$$\{1\}, \{\sigma, \sigma^{-1}\}, \{\sigma^2, \sigma^{-2}\}, \ldots, \left\{\sigma^{\frac{n-2}{2}}, \sigma^{\frac{2-n}{2}}\right\}, \{\sigma^{\frac{n}{2}}\},$$
$$\{\tau, \sigma^2\tau, \ldots, \sigma^{n-2}\tau\}, \{\sigma\tau, \sigma^3\tau, \ldots, \sigma^{n-1}\tau\}.$$

2. If n is odd:

$$\{1\}, \{\sigma, \sigma^{-1}\}, \{\sigma^2, \sigma^{-2}\}, \ldots, \left\{\sigma^{\frac{n-1}{2}}, \sigma^{\frac{1-n}{2}}\right\},$$
$$\{\tau, \sigma\tau, \ldots, \sigma^{n-1}\tau\}.$$

Indeed, for the case where n is even, we can see the above from the following observation. For any $x \in D_n$, since

$$x\sigma^i x^{-1} = \begin{cases} \sigma^j\sigma^i\sigma^{-j} = \sigma^i, & \text{if } x = \sigma^j, \\ \sigma^j\tau\sigma^i\tau\sigma^{-j} = \sigma^{-i}, & \text{if } x = \sigma^j\tau, \end{cases}$$

the conjugates of σ^i are $\sigma^{\pm i}$. On the other hand, for any $x \in D_n$, since

$$x\sigma^i\tau x^{-1} = \begin{cases} \sigma^j\sigma^i\tau\sigma^{-j} = \sigma^{i+2j}\tau, & \text{if } x = \sigma^j, \\ \sigma^j\tau\sigma^i\tau\tau\sigma^{-j} = \sigma^{i+2(j-i)}\tau, & \text{if } x = \sigma^j\tau, \end{cases}$$

the conjugates of $\sigma^i\tau$ are $\sigma^k\tau$ for any k such that $k \equiv i \pmod 2$. These facts induce Part (1).

(E20) (Symmetric groups) For any $\sigma \in \mathfrak{S}_n$, we can write σ as a product of cyclic permutations which do not have a common letter, like

$$\sigma = (a_1 \cdots a_k)(b_1 \cdots b_l) \cdots (c_1 \cdots c_m).$$

Furthermore, we may assume $k \geq l \geq \cdots \geq m$ since the cyclic permutations appeared in the right hand side are commutative. Then we call $(k, l, \ldots, m)$ is the **cycle type** of σ.

Theorem 5.1. *Elements $\sigma, \sigma' \in \mathfrak{S}_n$ are conjugate if and only if the cycle types of σ and σ' are equal.*

For example, conjugacy classes of $\mathfrak{S}_4$ are given by

Cycle type	**Conjugacy class**
$(1,1,1,1)$	$\{1_{\mathfrak{S}_4}\}$
$(2,1,1)$	$\{(1,2),(1,3),(1,4),(2,3),(2,4),(3,4)\}$
$(2,2)$	$\{(1,2)(3,4),(1,3)(2,4),(1,4)(2,3)\}$
$(3,1)$	$\{(1,2,3),(1,2,4),(1,3,2),(1,3,4),(1,4,2),(1,4,3),(2,3,4),(2,4,3)\}$
(4)	$\{(1,2,3,4),(1,2,4,3),(1,3,2,4),(1,3,4,2),(1,4,2,3),(1,4,3,2)\}$

In the above examples, we verify that the number of elements of any conjugacy class is a divisor of the order of the group. In general, we have

Theorem 5.2. *Let G be a finite group. For any $x \in G$, $|C(x)|$ is a divisor of $|G|$.*

6. Representation theory of finite groups

In this section, we give a brief introduction to representation theory of finite groups. There are also hundreds of textbooks for the representation theory. One of the most famous and standard textbooks is [5]. For high motivated readers, see [6–8] for mathematical details.

6.1. Representations

In this subsection, we assume that G is a finite group. Let V be a finite-dimensional $\mathbf{C}$-vector space. Consider the following situation. For any $\sigma \in G$ and any $\mathbf{v} \in V$, there exists a unique element $\sigma \cdot \mathbf{v} \in V$ such that

1. $\sigma \cdot (\boldsymbol{v} + \boldsymbol{w}) = \sigma \cdot \boldsymbol{v} + \sigma \cdot \boldsymbol{w}$,

2. $\sigma \cdot (\alpha \boldsymbol{v}) = \alpha(\sigma \cdot \boldsymbol{v})$,

3. $\sigma \cdot (\tau \cdot \boldsymbol{v}) = (\sigma\tau) \cdot \boldsymbol{v}$,

4. $1_G \cdot \boldsymbol{v} = \boldsymbol{v}$

for any $\sigma, \tau \in G$, $\alpha \in \mathbf{C}$ and $\boldsymbol{v}, \boldsymbol{w} \in V$. Then we say that G **acts** on V and V is called a G**-vector space**.

The conditions (1) and (2) mean that for any $\sigma \in G$, the map $\rho(\sigma) : V \to V$ defined by $\mathbf{v} \mapsto \sigma \cdot \mathbf{v}$ is a linear transformation on V. Furthermore, from the conditions (3) and (4), we see that for any $\sigma \in G$, the linear transformation $\rho\left(\sigma^{-1}\right)$ is the inverse linear transformation of $\rho(\sigma)$. Namely, each $\rho(\sigma)$ is a bijective. Set

$$\mathrm{GL}(V) := \{f : V \to V \mid f \text{ is abijective linear transformation}\},$$

and consider it as a group with the product given by the composition of maps. Then we obtain the group homomorphism $\rho : G \to \mathrm{GL}(V)$ by $\sigma \mapsto \rho(\sigma)$. In general, for a finite group G and for a finite-dimensional $\mathbf{C}$-vector space V, a homomorphism $\rho : G \to \mathrm{GL}(V)$ is called a **representation** of G. Then V is a G-vector space by the action of G on V given by

$$\sigma \cdot \boldsymbol{v} := (\rho(\sigma))(\mathbf{v})$$

for any $\sigma \in G$ and $\boldsymbol{v} \in V$. The dimension $\dim_{\mathbf{C}} V$ of V as a $\mathbf{C}$-vector space is called the **degree** of the representation ρ. Observe the following examples:

(E21) For any finite group G, and any $\mathbf{C}$-vector space V, we can consider the trivial action of G on V by $\sigma \cdot \boldsymbol{v} := \boldsymbol{v}$ for any $\sigma \in G$ and $\boldsymbol{v} \in V$. Namely, we can consider the homomorphism $\mathbf{triv} : G \to \mathrm{GL}(V)$ by assigning σ to the identity map on V for any $\sigma \in G$. This is called the **trivial representation** of G.

(E22) For any $n \in \mathbf{N}$, consider the cyclic group $\mathcal{U}_n$ and the action of $\mathcal{U}_n$ on $\mathbf{C}$ given by the usual multiplication $\exp\left(2k\pi\sqrt{-1}/n\right) \cdot z := \exp\left(2k\pi\sqrt{-1}/n\right)z$ of the complex numbers for any $k \in \mathbf{Z}$ and $z \in \mathbf{C}$. The action of $\exp\left(2k\pi\sqrt{-1}/n\right)$ on $\mathbf{C}$ is the rotation on $\mathbf{C}$ in the counterclockwise direction centered at the origin with angle $(2k\pi)/n$. If we take $1 \in \mathbf{C}$ as a basis of the $\mathbf{C}$-vector space $\mathbf{C}$, we can identify $\mathrm{GL}(\mathbf{C})$ with the general linear group $\mathrm{GL}(1, \mathbf{C}) = \mathbf{C}^\times$ by considering the matrix representation. Under this identification, the corresponding representation $\rho : \mathcal{U}_n \to \mathrm{GL}(\mathbf{C}) = \mathbf{C}^\times$ is given by the natural inclusion map $\mathcal{U}_n \acute{} \mathbf{C}^\times$.

(E23) Consider the symmetric group $\mathfrak{S}_3$ and the numerical vector space $\mathbf{C}^3$. The group $\mathfrak{S}_3$ naturally acts on $\mathbf{C}^3$ by the permutation of the components given by

$$\sigma \cdot \begin{pmatrix} x_1 \\ x_2 \\ x_3 \end{pmatrix} := \begin{pmatrix} x_{\sigma^{-1}(1)} \\ x_{\sigma^{-1}(2)} \\ x_{\sigma^{-1}(3)} \end{pmatrix}.$$

If we take the standard basis $\boldsymbol{e}_1, \boldsymbol{e}_2, \boldsymbol{e}_3$ as a basis of $\mathbf{C}^3$, we can identify $\mathrm{GL}\left(\mathbf{C}^3\right)$ with the general linear group $\mathrm{GL}(3, \mathbf{C})$ by considering the matrix representation. Under this identification, the corresponding representation $\rho : \mathfrak{S}_3 \to \mathrm{GL}\left(\mathbf{C}^3\right) = \mathrm{GL}(3, \mathbf{C})$ is given by $\sigma \mapsto \left(\boldsymbol{e}_{\sigma(1)}\boldsymbol{e}_{\sigma(2)}\boldsymbol{e}_{\sigma(3)}\right)$. Similarly, we can obtain the representation $\rho : \mathfrak{S}_n \to \mathrm{GL}(\mathbf{C}^n) = \mathrm{GL}(n, \mathbf{C})$ that is given by

$$\sigma \mapsto \left(\boldsymbol{e}_{\sigma(1)}\boldsymbol{e}_{\sigma(2)}\cdots\boldsymbol{e}_{\sigma(n)}\right).$$

This is called the **permutation representation** of $\mathfrak{S}_n$.

Next we consider subrepresentations of a representation. Let $\rho : G \to \mathrm{GL}(V)$ a representation. If there exists a subspace W of V such that

$$\sigma \cdot \boldsymbol{w} \in W \ (\Leftrightarrow (\rho(\sigma))(\boldsymbol{w}) \in W)$$

for any $\sigma \in G$ and $\boldsymbol{w} \in W$, then W is called a G**-subspace** of V. For any $\sigma \in G$, the restriction $\rho(\sigma)|_W : W \to W$ of $\rho(\sigma)$ is a bijective linear transformation on W, and we obtain the representation $\rho|_W : G \to \mathrm{GL}(W)$ given by $\sigma \mapsto \rho(\sigma)|_W$. It is called a **subrepresentation** of ρ.

(E24) Consider the permutation representation $\rho : \mathfrak{S}_3 \to \mathrm{GL}\left(\mathbf{C}^3\right) = \mathrm{GL}(3, \mathbf{C})$ as in (E23). Let us consider subspaces

$$W_1 := \left\{ \begin{pmatrix} x \\ x \\ x \end{pmatrix} \;\middle|\; x \in \mathbf{C} \right\},\ W_2 := \left\{ \begin{pmatrix} x \\ y \\ z \end{pmatrix} \;\middle|\; x, y, z \in \mathbf{C},\ x + y + z = 0 \right\}$$

of $\mathbf{C}^3$. It is easily seen that these are $\mathfrak{S}_3$-subspaces and the subrepresentation $\rho|_{W_1}$ is the trivial representation. Geometrically, W_1 and W_2 in $\mathbf{C}^3$ are drawn in **Figure 3**. In a precise sense, if we naturally consider $\mathbf{R}^3$ as a subset of $\mathbf{C}^3$, then **Figure 3** shows $W_1 \cap \mathbf{R}^3$ and $W_2 \cap \mathbf{R}^3$ in $\mathbf{R}^3$.

For a G-vector space V, if there exist G-subspaces W_1 and W_2 of V such that any element $\mathbf{v} \in V$ can be **uniquely** written as

$$\boldsymbol{v} = \boldsymbol{w}_1 + \boldsymbol{w}_2 \ (\boldsymbol{w}_1 \in W_1, \boldsymbol{w}_2 \in W_2),$$

then V is called the **direct sum** of W_1 and W_2 and is written as $V = W_1 \oplus W_2$. Similarly, we can define the direct sum of G-subspaces $W_1, W_2, \ldots, W_m$ for any $m \geq 3$. Let ρ, $\rho|_{W_1}$, and $\rho|_{W_2}$ be the correspondent representations of G to V, W_1, and W_2, respectively. We also say that the representation ρ is the direct sum of $\rho|_{W_1}$ and $\rho|_{W_2}$.

(E25) As the notation in (E24), V is the direct sum of W_1 and W_2. Indeed, for the standard basis $\boldsymbol{e}_1, \boldsymbol{e}_2, \boldsymbol{e}_3$ of V, we see that $\boldsymbol{e}_1 + \boldsymbol{e}_2 + \boldsymbol{e}_3$ and $\boldsymbol{e}_1 - \boldsymbol{e}_2, \boldsymbol{e}_1 - \boldsymbol{e}_3$ are bases of W_1 and W_2, respectively. Thus, for any $\boldsymbol{x} = x_1\boldsymbol{e}_1 + x_2\boldsymbol{e}_2 + x_3\boldsymbol{e}_3 \in \mathbf{C}^3$, we can rewrite

$$\boldsymbol{x} = \frac{x_1 + x_2 + x_3}{3}(\boldsymbol{e}_1 + \boldsymbol{e}_2 + \boldsymbol{e}_3) + \frac{x_1 - 2x_2 + x_3}{3}(\boldsymbol{e}_1 - \boldsymbol{e}_2) + \frac{x_1 + x_2 - 2x_3}{3}(\boldsymbol{e}_1 - \boldsymbol{e}_3).$$

Furthermore, we verify that this expression is unique by direct calculations.

In general, we have

Theorem 6.1 (Maschke). *Let $\rho : G \to \mathrm{GL}(V)$ a representation and W a G-subspace of V. Then there exists a G-subspace W' such that $V = W \oplus W'$.*

6.2. Irreducible representations

In subsection 4.4, we have discussed the classification of finite abelian groups by using the concept of group isomorphisms. Here we consider the classification of finite-dimensional representations of finite groups by using irreducible representations and equivalence relations among representations.

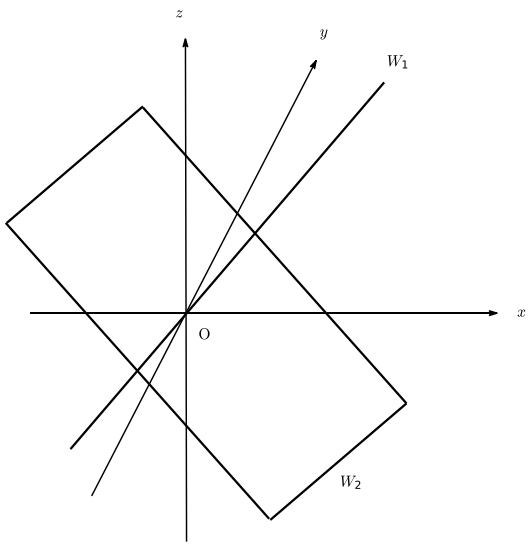

Figure 3. The subspaces W_1 and W_2 in $\mathbf{C}^3$.

Let G be a finite group and $\rho : G \to \mathrm{GL}(V)$ its representation. The trivial subspaces $\{\mathbf{0}\}$ and V are G-subspaces of V. If V has no G subspace other than these, V is called the **irreducible G-space**, and ρ is called the **irreducible representation** of G.

(E26) Any one-dimensional representation is trivial. For example, the representation $\rho : \mathcal{U}_n \to \mathrm{GL}(\mathbf{C}) = \mathbf{C}^\times$ in (E23) is irreducible. Let us consider the other example. For any $\sigma \in \mathfrak{S}_n$, set

$$\mathrm{sgn}\,(\sigma) := \begin{cases} 1 & \text{if} \quad \sigma \text{ is even permutation,} \\ -1 & \text{if} \quad \sigma \text{ is odd permutation.} \end{cases}$$

Then we can easily see that the map $\mathrm{sgn} : \mathfrak{S}_n \to \mathbf{C}^\times = \mathrm{GL}(\mathbf{C})$ is a homomorphism and, hence, is a representation of $\mathfrak{S}_n$. This irreducible representation is called the **signature representation** of $\mathfrak{S}_n$.

(E27) As the notation in (E24), $\rho|_{W_1}$ is irreducible since it is one-dimensional. The representation $\rho|_{W_2}$ is also irreducible. Indeed, if W_2 is not irreducible, there exists a one-dimensional G-subspace W in W_2 since W_2 is a 2-dimensional G-vector space. Take $\boldsymbol{w} \in W$ ($\boldsymbol{w} \neq \mathbf{0}$). Then $\boldsymbol{w}$ is an eigenvector of $\rho|_{W_2}(\sigma)$ for any $\sigma \in \mathfrak{S}_3$. However, we can see that there is no such vector in W_2 by direct calculations.

By observing (E25), (E26), and (E27), we see that $\mathbf{C}^3$ is a direct sum of the irreducible G-subspaces W_1 and W_2. In general, by using Maschke's theorem above, we obtain.

Theorem 6.2. *For any representation $\rho : G \to \mathrm{GL}(V)$ of a finite group G, the G-vector space V can be written as a direct sum of some irreducible G-subspaces. Namely, ρ can be written as sum of some irreducible representations of G.*

Remark that the expression of a direct sum of irreducible representations is not unique in general. For example, let $\rho : G \to \mathrm{GL}(\mathbf{C}^2)$ be the trivial representation. Then for the standard basis $\boldsymbol{e}_1, \boldsymbol{e}_2$ of $\mathbf{C}^2$, we have

$$\mathbf{C}^2 = \mathbf{C}\boldsymbol{e}_1 \oplus \mathbf{C}\boldsymbol{e}_2 = \mathbf{C}\boldsymbol{e}_1 \oplus \mathbf{C}(\boldsymbol{e}_1 + \boldsymbol{e}_2) = \mathbf{C}\boldsymbol{e}_1 \oplus \mathbf{C}(\boldsymbol{e}_1 + 2\boldsymbol{e}_2) = \cdots.$$

In order to do the classification of representations, we consider the equivalency of representations. Let $\rho_1 : G \to \mathrm{GL}(V_1)$ and $\rho_2 : G \to \mathrm{GL}(V_2)$ be representations of G. If there exists a bijective linear map $\iota : V_1 \to V_2$ such that

$$\iota(\sigma \cdot \boldsymbol{v}) = \sigma \cdot \iota(\boldsymbol{v}), \quad \sigma \in G, \boldsymbol{v} \in V_1,$$

then we say that V_1 is isomorphic to V_2 as a G-vector space and write $V_1 \cong V_2$. We also say that ρ_1 is equivalent to ρ_2 and write $\rho_1 \sim \rho_2$.

(E28) For any group G. let **unit** : $G \to \mathrm{GL}(\mathbf{C}) = \mathbf{C}^\times$ be the trivial representation of G. Then any trivial representation $\rho : G \to \mathrm{GL}(V)$ is equivalent to **unit**. The representation **unit** is called the **unit representation** of G.

The following theorem is one of the most important theorems in representation theory of finite groups.

Theorem 6.3. *Let G be a finite group.*

1. *The number of irreducible representations of G up to equivalent is finite. Furthermore, it is equal to the number of the conjugacy classes of G.*
2. *For any representation $\rho : G \to \mathrm{GL}(V)$, ρ is equivalent to a direct sum of some irreducible representations*:

   $V \cong W_1 \oplus W_2 \oplus \cdots \oplus W_m$.

   Furthermore, the tuple of the components is uniquely determined by G, up to the order.

6.3. Characters

In this subsection, for a given representation, we give a method to determine whether it is irreducible or not by using characters. Let $\rho : G \to \mathrm{GL}(V)$ be a representation. Take a basis $\boldsymbol{v}_1, \ldots, \boldsymbol{v}_n$ of V, and fix it. By using this basis, we can consider $\rho(\sigma)$ as an $(n \times n)$-matrix $A_\sigma = \left(a_{ij}\right)$, which is the matrix representation of $\rho(\sigma)$. Then set

$$\chi_\rho(\sigma) := \mathrm{Tr}(A_\sigma) = a_{11} + a_{22} + \cdots + a_{nn} \in \mathbf{C}$$

for any $\sigma \in G$. Remark that this definition is well defined since it does not depend on the choice of a basis of V. Indeed, if $\boldsymbol{w}_1, \ldots, \boldsymbol{w}_n$ is another basis of V, the matrix representation of $\rho(\sigma)$ with respect to this basis is given by $P^{-1}A_\sigma P$ for a some regular matrix P. Hence $\mathrm{Tr}\left(P^{-1}A_\sigma P\right) = \mathrm{Tr}(A_\sigma)$. We call the map $\chi_\rho : G \to \mathbf{C}$ the **character** of ρ. Remark that for elements $\sigma, \tau \in G$, if $\sigma \sim \tau$, then $\rho(\sigma) \sim \rho(\tau)$ in $\mathrm{GL}(V)$. Thus, $\chi_\rho(\sigma) = \chi_\rho(\tau)$. Namely, χ_ρ is constant on each of the conjugacy classes of G.

(E29) Consider the example (E25). Let $\rho : \mathfrak{S}_3 \to \mathrm{GL}\left(\mathbf{C}^3\right)$ be the permutation representation of $\mathfrak{S}_3$. The conjugacy classes of $\mathfrak{S}_3$ are as follows:

Cycle type	Conjugacy class
$(1,1,1)$	$\{1_{\mathfrak{S}_3}\}$
$(2,1)$	$\{(1,2),(1,3),(2,3)\}$
(3)	$\{(1,2,3),(1,3,2)\}$

Hence, in order to calculate the values of the character χ_ρ of ρ, it suffices to calculate its values on $1_{\mathfrak{S}_3}$, $(1,2)$, and $(1,2,3)$. If we take the standard basis $\boldsymbol{e}_1, \boldsymbol{e}_2, \boldsymbol{e}_3$ of $\mathbf{C}^3$, we have $\rho(\sigma) = \left(\boldsymbol{e}_{\sigma(1)}\, \boldsymbol{e}_{\sigma(2)}\, \boldsymbol{e}_{\sigma(3)}\right)$, and hence

$$\chi_\rho(1_{\mathfrak{S}_3}) = 3, \quad \chi_\rho((1,2)) = 1, \quad \chi_\rho((1,2,3)) = 0.$$

In general, as in (E29), for a representation $\rho : G \to \mathrm{GL}(V)$, $\chi_\rho(1_G)$ is the degree of the representation, which is equal to $\dim_{\mathbf{C}}(V)$.

Now, we define the inner product of characters. For complex functions $\varphi, \psi : G \to \mathbf{C}$ on G, set

$$\langle \varphi, \psi \rangle = \frac{1}{|G|} \sum_{\sigma \in G} \varphi(\sigma)\overline{\psi(\sigma)}$$

where $\overline{z}$ means the complex conjugation of $z \in \mathbf{C}$. We call it the inner product of ϕ and ψ. The following theorems are quite important and useful from the viewpoint to find and to calculate all of the irreducible representations.

Theorem 6.4.

1. (*Orthogonality*) *Let* $\rho_i : G \to \mathrm{GL}(V_i)$ $(i = 1, 2)$ *be irreducible representations. Then*

$$\left\langle \chi_{\rho_1}, \chi_{\rho_2} \right\rangle = \begin{cases} 1 & \text{if} \quad \rho_1 \sim \rho_2, \\ 0 & \text{if} \quad \rho_1 / \sim \rho_2. \end{cases}$$

2. For a representation $\rho : G \to \mathrm{GL}(V)$,

$$\rho \ \textit{is irreducible} \Leftrightarrow \left\langle \chi_\rho, \chi_\rho \right\rangle = 1.$$

σ	$\mathbf{1}_{\mathfrak{S}_3}$	$(\mathbf{1},\mathbf{2})$	$(\mathbf{1},\mathbf{3})$	$(\mathbf{2},\mathbf{3})$	$(\mathbf{1},\mathbf{2},\mathbf{3})$	$(\mathbf{1},\mathbf{3},\mathbf{2})$
$\chi_{\mathbf{unit}}(\sigma)$	1	1	1	1	1	1
$\chi_{\mathrm{sgn}}(\sigma)$	1	−1	−1	−1	1	1
$\chi_{\rho\|_{W_2}}(\sigma)$	2	0	0	0	−1	−1

(E30) We have the three irreducible representations of $\mathfrak{S}_3$. By direct calculations, we obtain the following list:

Hence we see that in each of cases, we have $\left\langle \chi_\rho, \chi_\rho \right\rangle = 1$.

By Theorem 6.3, we see that for any representation $\rho : G \to \mathrm{GL}(V)$, V can be written as

$$V \cong W_1^{\oplus m_1} \oplus W_2^{\oplus m_2} \oplus \cdots \oplus W_k^{\oplus m_k}$$

where each W_i is an irreducible G-vector space and W_i is not isomorphic to W_j as a G-vector space if $i \neq j$. For each $1 \leq i \leq k$, the number m_i is called the **multiplicity** of W_i in V.

Theorem 6.5. *As the notation above, let* ρ_i *be the irreducible representation of* G *correspond to the* G*-vector space* W_i*. Then we have*

1. $\chi_\rho = m_1\chi_{\rho_1} + \cdots + m_k\chi_{\rho_k}$.

2. $\left\langle \chi_\rho, \chi_{\rho_i} \right\rangle = m_i$.

Namely, each of the multiplicity of the irreducible G*-vector spaces in* V *is calculated by the inner product of the characters*

3. $|G| = \sum_{i=1}^{k} \chi_{\rho_i}(1)^2$.

Namely, the sum of the squares of the degrees of the irreducible representations is equal to the order of G.

From the above theorems, we verify that if we want to know all irreducible representations of G, it suffices to calculate its characters. The list of all values of all characters is called the **character table** of G. Finally, we give a few examples of the character tables of finite groups.

(E31) Observe (E30). Since we have

$$\chi_{\mathbf{unit}}(1)^2 + \chi_{\mathrm{sgn}}(1)^2 + \chi_{\rho|_{W_2}}(1)^2 = 4 + 1 + 1 = 6 = |\mathfrak{S}_3|,$$

it turns out that **unit**, sgn , and $\rho|_{W_2}$ are all irreducible representations of $\mathfrak{S}_3$ up to equivalence. Hence the list in (E30) is the character table of $\mathfrak{S}_3$.

(E32) Consider the cyclic group $\mathcal{U}_n$. Since $\mathcal{U}_n$ is abelian, any conjugacy class consists of a single element, and there exist n conjugacy classes. Hence there exist n distinct irreducible representations. Now, for any $0 \le l \le n-1$, define the map $\rho_l : \mathcal{U}_n \to \mathrm{GL}(\mathbf{C}) = \mathbf{C}^\times$ by

$$\zeta^k \mapsto \zeta^{kl} \quad (0 \le k \le n-1)$$

where $\zeta = \exp\left(2\pi\sqrt{-1}/n\right)$. Then we obtain

σ	$\mathbf{1}_{\mathcal{U}_n}$	ζ	ζ^2	...	ζ^{n-1}
$\chi_{\rho_0}(\sigma)$	1	1	1	1	1
$\chi_{\rho_1}(\sigma)$	1	ζ	ζ^2	...	ζ^{n-1}
$\vdots$					$\vdots$
$\chi_{\rho_{n-1}}(\sigma)$	1	ζ^{n-1}	ζ^{n-2}	...	ζ

Hence we see that $\rho_0, \rho_1, \ldots, \rho_{n-1}$ are nonequivalent one-dimensional representations, and hence the above list is the character table of $\mathcal{U}_n$. In general, all irreducible representations of an abelian group are of degree 1.

(E33) (Dihedral groups) For $n \ge 3$, consider the dihedral groups D_n. First, for any $a, b = \pm 1$, there exist the four one-dimensional representations $\varepsilon_{a,b} : D_n \to \mathbf{C}^\times$ defined by

$$\varepsilon_{a,b}(x) = \begin{cases} (-1)^{ak} & \text{if} \quad x = \sigma^k, \\ (-1)^{ak+b} & \text{if} \quad x = \sigma^k\tau. \end{cases}$$

These maps are characterized by the images of σ and τ, which are $(-1)^a$ and $(-1)^b$, respectively. Next, for any $1 \le l \le n-1$, we can consider the two-dimensional representations $\rho_l : D_n \to \mathrm{GL}(2, \mathbf{C})$ given by

$$\rho_l(x) = \begin{cases} \begin{pmatrix} \cos 2kl\pi/n & -\sin 2kl\pi/n \\ \sin 2kl\pi/n & \cos 2kl\pi/n \end{pmatrix} & \text{if} \quad x = \sigma^k, \\ \begin{pmatrix} \cos 2kl\pi/n & -\sin 2kl\pi/n \\ \sin 2kl\pi/n & \cos 2kl\pi/n \end{pmatrix} \begin{pmatrix} 0 & 1 \\ 1 & 0 \end{pmatrix} & \text{if} \quad x = \sigma^k\tau. \end{cases}$$

i. The case where n is even. For any $1 \leq l \leq \frac{n-2}{2}$, since we can see $\left\langle \chi_{\rho_l}, \chi_{\rho_l} \right\rangle = 1$ by direct calculation, ρ_ls are irreducible representations of D_n. Since we have

$$\begin{aligned} \chi_{\varepsilon_{1,1}}(1)^2 + \quad & \chi_{\varepsilon_{1,-1}}(1)^2 + \chi_{\varepsilon_{-1,1}}(1)^2 + \chi_{\varepsilon_{-1,-1}}(1)^2 \\ & + \chi_{\rho_1}(1)^2 + \cdots + \chi_{\rho_{\frac{n-2}{2}}}(1)^2 = 2n = |D_n|, \end{aligned}$$

it turns out that $\varepsilon_{a,b}$ and ρ_l for $a, b = \pm 1$ and $1 \leq l \leq \frac{n-2}{2}$ are all irreducible representations of D_n up to equivalence. The character table of D_4 is give as follows:

x	$\{\mathbf{1}_{D_4}\}$	$\{\sigma, \sigma^3$	$\{\sigma^2\}$	$\{\sigma\tau, \sigma^3\tau\}$	$\{\tau, \sigma^2\tau\}$
$\chi_{\varepsilon_{1,1}}(x)$	1	1	1	1	1
$\chi_{\varepsilon_{1,-1}}(x)$	1	1	1	−1	−1
$\chi_{\varepsilon_{-1,1}}(x)$	1	−1	1	−1	1
$\chi_{\varepsilon_{-1,-1}}(x)$	1	−1	1	1	−1
$\chi_{\rho_1}(\sigma)$	2	0	−2	0	0

ii. The case where n is odd. Similarly, we can see that $\varepsilon_{1,b}$ and ρ_l for $b = \pm 1$ and $1 \leq l \leq \frac{n-1}{2}$ are all irreducible representations of D_n up to equivalence. The character table of D_5 is give as follows:

x	$\{\mathbf{1}_{D_5}\}$	$\{\sigma, \sigma^4\}$	$\{\sigma^2, \sigma^3\}$	$\{\tau, \sigma\tau, \ldots, \sigma^4\tau\}$
$\chi_{\varepsilon_{1,1}}(x)$	1	1	1	1
$\chi_{\varepsilon_{1,-1}}(x)$	1	1	1	−1
$\chi_{\rho_1}(\sigma)$	2	$2\cos 2\pi/5$	$2\cos 4\pi/5$	0
$\chi_{\rho_2}(\sigma)$	2	$2\cos 4\pi/5$	$2\cos 2\pi/5$	0

7. Direct products

In chemistry, groups appear in symmetries of molecules. The structures of some of them are given by direct products of finite groups. Here we consider direct product groups and its irreducible representations.

Let G and H be finite groups. Set

$$G \times H := \{(g,h) \mid g \in G,\ h \in H\},$$

and define the product on $G \times H$ by

$$(g,h) \cdot (g',h') := (gg',hh').$$

Then $G \times H$ with this product forms a group. This is called the **direct product group** of G and H. The unit is $(1_G, 1_H)$, and the inverse of (g,h) is $\left(g^{-1}, h^{-1}\right)$. If G and H are finite groups, then it is clear that $|G \times H| = |G||H|$. For conjugacy classes C and C' of G and H, respectively, the direct product set $C \times C'$ is a conjugacy class of $G \times H$, and any conjugacy class of $G \times H$ is obtained by this way.

In order to construct irreducible representations of $G \times H$, we consider tensor products of vector spaces. For G-vector space V and H-vector space W, let F be the vector space with basis $\{(\boldsymbol{v},\boldsymbol{w}) \mid \boldsymbol{v} \in V,\ \ \boldsymbol{w} \in W\}$ and R the subspace of F generated by

$$\begin{aligned}
&(\boldsymbol{v}_1 + \boldsymbol{v}_2, \boldsymbol{w}) - (\boldsymbol{v}_1, \boldsymbol{w}) - (\boldsymbol{v}_2, \boldsymbol{w}),\\
&(\boldsymbol{v}, \boldsymbol{w}_1 + \boldsymbol{w}_2) - (\boldsymbol{v}, \boldsymbol{w}_1) - (\boldsymbol{v}, \boldsymbol{w}_2),\\
&(\alpha\boldsymbol{v}, \boldsymbol{w}) - \alpha(\boldsymbol{v}, \boldsymbol{w}),\ \ (\boldsymbol{v}, \alpha\boldsymbol{w}) - \alpha(\boldsymbol{v}, \boldsymbol{w}),
\end{aligned}$$

for any $\boldsymbol{v}, \boldsymbol{v}_1, \boldsymbol{v}_2 \in V$, $\boldsymbol{w}, \boldsymbol{w}_1, \boldsymbol{w}_2 \in W$, and $\alpha \in \mathbf{C}$. The quotient vector space F/R is called the **tensor product** of V and W and is denoted by $V \otimes W$. The coset class of $(\boldsymbol{v},\boldsymbol{w})$ is denoted by $\boldsymbol{v} \otimes \boldsymbol{w}$. If $\boldsymbol{v}_1, \ldots, \boldsymbol{v}_m$ and $\boldsymbol{w}_1, \ldots, \boldsymbol{w}_n$ are bases of V and W, respectively, then elements $\boldsymbol{v}_i \otimes \boldsymbol{w}_j$ $(1 \le i \le m$ and $1 \le j \le n)$ form a basis of $V \otimes W$. Hence $\dim(V \otimes W) = (\dim V)(\dim W)$.

For any $g \in G$ and $h \in H$, we can define the action of $G \times H$ on $V \otimes W$ by

$$(g,h) \cdot \sum_{i=1}^{m}\sum_{j=1}^{n} \alpha_{ij}\boldsymbol{v}_i \otimes \boldsymbol{w}_j := \sum_{i=1}^{m}\sum_{j=1}^{n} \alpha_{ij}(g\boldsymbol{v}_i) \otimes \left(h\boldsymbol{w}_j\right),$$

and hence, $V \otimes W$ is a $G \times H$-vector space. For the representations $\rho : G \to \mathrm{GL}(V)$ and $\rho' : G \to \mathrm{GL}(W)$ corresponding to the G-vector spaces V and W, respectively, we denote by $\rho \otimes \rho' : G \to \mathrm{GL}(V \otimes W)$ the representation corresponding to the $(G \times H)$-vector space $V \otimes W$. Then we have

Theorem 7.1. *(1) As the notation above, if ρ and ρ' are irreducible, so is $\rho \otimes \rho'$.*

(2) If $\rho_1, \ldots, \rho_k$ (resp. $\rho'_1, \ldots, \rho'_l$) are all irreducible representations of G (resp. H) up to equivalence, then $\rho_i \otimes \rho_{j'}$ $(1 \le i \le m$ and $1 \le j \le n)$ are all irreducible representations of $G \times H$ up to equivalence.

(E34) For $V = \mathbf{C}$ and $W = \mathbf{C}$, the tensor product $V \otimes W$ of V and W is a one-dimensional $\mathbf{C}$-vector space with basis $1 \otimes 1$. Thus, we have a bijective linear map $V \otimes W \to \mathbf{C}$ given by

$$a(1 \otimes 1) \mapsto a.$$

In general, we identify $\mathbf{C} \otimes \mathbf{C}$ with $\mathbf{C}$ through this map.

Let us consider the direct product $\mathcal{U}_2 \times \mathcal{U}_3$. Under the identification $\mathbf{C} \otimes \mathbf{C} = \mathbf{C}$, the character table is given as follows:

σ	$\{(\mathbf{1},\mathbf{1})\}$	$\{(\mathbf{1},\zeta)\}$	$\{(\mathbf{1},\zeta^{\mathbf{2}})\}$	$\{(-\mathbf{1},\mathbf{1})\}$	$\{(-\mathbf{1},\zeta)\}$	$\{(-\mathbf{1},\zeta^{\mathbf{2}})\}$
$\chi_{\rho_0\otimes\rho_0}(\sigma)$	1	1	1	1	1	1
$\chi_{\rho_0\otimes\rho_1}(\sigma)$	1	ζ	ζ^2	1	ζ	ζ^2
$\chi_{\rho_0\otimes\rho_2}(\sigma)$	1	ζ^2	ζ	1	ζ^2	ζ
$\chi_{\rho_1\otimes\rho_0}(\sigma)$	1	1	1	-1	-1	-1
$\chi_{\rho_1\otimes\rho_1}(\sigma)$	1	ζ	ζ^2	-1	$-\zeta$	$-\zeta^2$
$\chi_{\rho_1\otimes\rho_2}(\sigma)$	1	ζ^2	ζ	-1	$-\zeta^2$	$-\zeta$

where $\zeta = \exp 2\pi\sqrt{-1}/3$.

(E35) Consider the direct product $\mathcal{U}_2 \times \mathfrak{S}_3$. Its character table is given as follows:

σ	$\{(\mathbf{1},\mathbf{1}_{\mathfrak{S}_3})\}$	$\{(\mathbf{1},(i,j))\}$	$\{(\mathbf{1},(i,j,k))\}$	$\{(-\mathbf{1},\mathbf{1}_{\mathfrak{S}_3})\}$	$\{(-\mathbf{1},(i,j))\}$	$\{(-\mathbf{1},(i,j,k))\}$
$\chi_{\rho_0\otimes\mathbf{unit}}(\sigma)$	1	1	1	1	1	1
$\chi_{\rho_0\otimes\,\mathrm{sgn}}(\sigma)$	1	-1	1	1	-1	1
$\chi_{\rho_0\otimes\rho\vert_{W_2}}(\sigma)$	2	0	-1	2	0	-1
$\chi_{\rho_1\otimes\mathbf{unit}}(\sigma)$	1	1	1	-1	-1	-1
$\chi_{\rho_1\otimes\,\mathrm{sgn}}(\sigma)$	1	-1	1	-1	1	-1
$\chi_{\rho_1\otimes\rho\vert_{W_2}}(\sigma)$	2	0	-1	-2	0	1

8. Graphs and their automorphisms

In this section, we consider directed graphs and their automorphism groups. Here we do not assume for the reader to know the facts in Sections 5 and 6.

8.1. Graphs

According to literatures, there are several different definitions of a graph. Briefly Ca **directed graph** Γ consists of **vertices** and **oriented edges** whose endpoints are vertices. (For details for the definition of graphs, see page 14 of [9].) For an oriented edge e, we denote by $i(e)$ and $t(e)$ the **initial vertex** and the **terminal vertex** of e. Each oriented edge e has the **inverse edge** $\overline{e}$ such that $\overline{e} \neq e$ and $\overline{\overline{e}} = e$. It is clear that $i(\overline{e}) = t(e)$ and $t(\overline{e}) = i(e)$. An oriented edge e such that $i(e) = t(e)$ is called a **loop**. For any $v, w \in V(\Gamma)$, we assume that there may exist more than one oriented edge whose initial vertex is v and terminal vertex w. If this is the case, we say that Γ has multiple oriented edges.

(E36) A directed graph is easy to understand if it is drawn by a picture. See **Figure 4**. The vertices v, w, x, y, z are depicted by small circles. The oriented edges a, b, c, d, e, f, g, h are

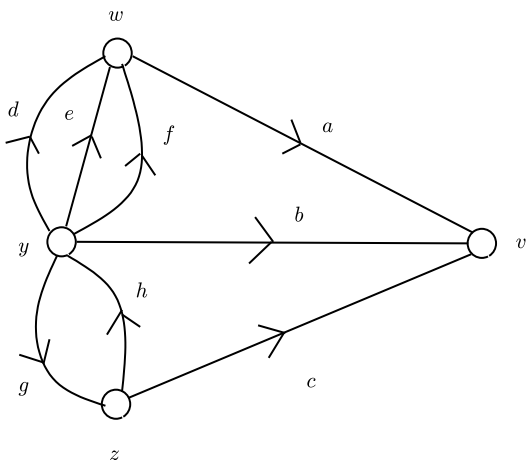

Figure 4. An example of a graph.

depicted by arrows from the initial vertex to the terminal vertex, and their inverse edges are omitted for simplicity.

We denote by $V(\Gamma)$ and $E(\Gamma)$ the sets of the vertices and the oriented edges of Γ, respectively. If both $V(\Gamma)$ and $E(\Gamma)$ are finite set, we call Γ a finite graph. Here, we consider only finite graphs. Remark that $|E(\Gamma)|$ is always even since $E(\Gamma)$ is written as $\{e_1, \bar{e}_1, \ldots, e_m, \bar{e}_m\}$. For any $v, w \in V(\Gamma)$, if there exists a successive sequence of oriented edges such that the initial vertex of the first edge is v and the terminal vertex of the last edge w, then the graph is called a **connected graph**. For example, see **Figure 5**. In the following, we assume that all graphs are connected.

8.2. Automorphisms of graphs

Let Γ and Γ' be graphs. A morphism of directed graphs from Γ to Γ' is a map

$$\sigma : V(\Gamma) \cup E(\Gamma) \to V(\Gamma') \cup E(\Gamma')$$

which maps vertices to vertices and edges to edges, such that

$$\sigma(i(e)) = i(\sigma(e)),\ \sigma(t(e)) = t(\sigma(e)),\ \sigma(\bar{e}) = \overline{\sigma(e)}$$

for any $e \in E(\Gamma)$. Namely, σ maps the initial vertex, the terminal vertex, and the inverse edge of an oriented edge to those of the corresponding oriented edge, respectively. For simplicity, we write $\sigma : \Gamma \to \Gamma'$. If σ is bijective, then it is called an **isomorphism**. An isomorphism from Γ to Γ is called an **automorphism** of Γ. Let $\mathrm{Aut}(\Gamma)$ be the set of all automorphisms of Γ. Then $\mathrm{Aut}(\Gamma)$ with the composition of maps forms a group. We call it the **automorphism group** of Γ. Let us consider a few easy examples of $\mathrm{Aut}(\Gamma)$.

(E37) See **Figure 6**. The graph Γ_1 consists of one vertex v and two oriented edges e and $\bar{e}$. Hence all morphisms from Γ_1 to Γ_1 are automorphisms since if $\sigma : \Gamma \to \Gamma$ is a morphism, then $\sigma(v) = v$, and $\sigma(e) = e$ or $\sigma(e) = \bar{e}$. If $\sigma(e) = e$, then $\sigma(\bar{e}) = \bar{e}$ as a consequence, and hence σ is the identity map on Γ. If $\sigma(e) = \bar{e}$, then $\sigma(\bar{e}) = e$ as a consequence, and hence σ is the

http://dx.doi.org/10.5772/intechopen.72131

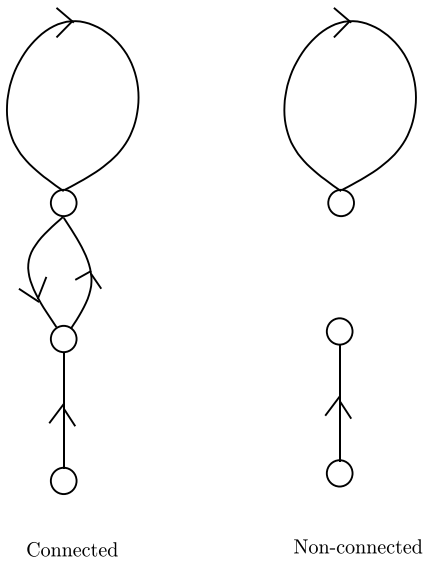

Figure 5. Examples of a connected and a non-connected graph.

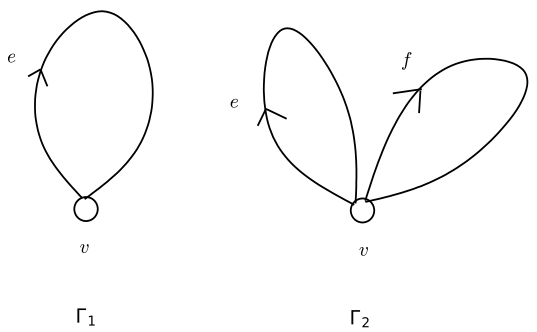

Figure 6. Graphs which have one vertex.

orientation-reversing automorphism on Γ. Thus, $\mathrm{Aut}(\Gamma_1) = \{\sigma_1, \sigma_2\} \cong \mathbf{Z}/2\mathbf{Z}$ where $\sigma_1(e) = e$ and $\sigma_2(e) = \overline{e}$.

On the other hand, the graph Γ_2 consists of one vertex v and four oriented edges $e, \overline{e}, f$, and $\overline{f}$. It is easily seen that there are eight possible automorphisms on Γ_2. Namely, all of them map v to v, and the correspondences of edges are given by

$$\sigma_1 : (e,f) \mapsto (e,f),\ \sigma_2 : (e,f) \mapsto (\overline{e},f),\ \sigma_3 : (e,f) \mapsto \left(e,\overline{f}\right),\ \sigma_4 : (e,f) \mapsto \left(\overline{e},\overline{f}\right),$$
$$\sigma_5 : (e,f) \mapsto (f,e),\ \sigma_6 : (e,f) \mapsto \left(\overline{f},e\right),\ \sigma_7 : (e,f) \mapsto (f,\overline{e}),\ \sigma_8 : (e,f) \mapsto \left(\overline{f},\overline{e}\right).$$

Hence $\mathrm{Aut}(\Gamma_2) = \{\sigma_1, \ldots, \sigma_8\}$. It turns out that σ_2, σ_3, and σ_5 are generators of $\mathrm{Aut}(\Gamma_2)$. In (E41), we study the structure of $\mathrm{Aut}(\Gamma_2)$ more.

Next, in order to describe the group structure of $\mathrm{Aut}(\Gamma)$ more simply, we consider semidirect products of groups. For high motivated readers, see [10] for details and more examples. The

semidirect product groups are kinds of generalizations of direct product groups. Let G be a group, K a subgroup of G, and H a normal subgroup of G. Furthermore, if we have

$$G = \{hk | h \in H,\ k \in K\},\ H \cap K = \{1_G\},$$

then we call G the semidirect product group of H and K and denote it by $G = H \rtimes K$.

(E38) Recall the dihedral group $D_n = \{1, \sigma, \sigma^2, \ldots, \sigma^{n-1}, \tau, \sigma\tau, \sigma^2\tau, \ldots, \sigma^{n-1}\tau\}$. Set $H := \{1, \sigma, \sigma^2, \ldots, \sigma^{n-1}\}$ and $K := \{1, \tau\}$. Then we can see that the subset H is a normal subgroup of D_n, $H \cap K = \{1\}$, and $D_n = \{hk | h \in H,\ k \in K\}$. Thus $D_n = H \rtimes K$.

Remark that for any $g \in G$, we can write $g = hk$ for some $h \in H$ and $k \in K$ and that this expression is unique. Namely, if $g = hk = h'k'$ for $h, h' \in H$ and $k, k' \in K$, then we have $(h')^{-1}h = k'k^{-1} \in H \cap K$. Hence $(h')^{-1}h = k'k^{-1} = 1_G$, and hence $h = h'$ and $k = k'$. Therefore, if $|G| < \infty$, we see that $|G| = |H||K|$. We also remark that if $hk = kh$ for any $h \in H$ and $k \in K$, then G is isomorphic to the direct product group of H and K, namely, $G \cong H \times K$. Thus, the semidirect product is a generalization of the direct product.

Now, let Γ be a graph. For any $v, w \in V(\Gamma)$, we number the oriented edges of Γ with v as initial vertex and w as terminal vertex. Then every oriented edge e can be uniquely represented as $e = (v, w, k)$. In particular, we can arrange the numbering such that $\overline{e} = (w, v, k)$ for any $e = (v, w, k) \in E(\Gamma)$.

(E39) See **Figure 7**. We can arrange a numbering of the oriented edges as

$$e = (v, w, 1), \overline{e} = (w, v, 1), f = (v, w, 2), \overline{f} = (w, v, 2), g = (v, w, 3), \overline{g} = (w, v, 3),$$
$$h = (w, w, 1), \overline{h} = (w, w, 2).$$

Let T be the subgroup of $\mathrm{Aut}(\Gamma)$ consisting of automorphisms that fix all vertices pointwise:

$$T := \{t \in \mathrm{Aut}(\Gamma) \,|\, t(v) = v,\ v \in V(\Gamma)\}.$$

Let M be the subgroup of $\mathrm{Aut}(\Gamma)$ consisting of automorphisms that fix the numberings of edges:

$$M := \{m \in \mathrm{Aut}(\Gamma) \ \mid\ m(v, w, k) = (v', w', k) \text{ for any } v, w \in V \text{ and any number } k\}.$$

Then we have $\mathrm{Aut}(\Gamma) = T \rtimes M$

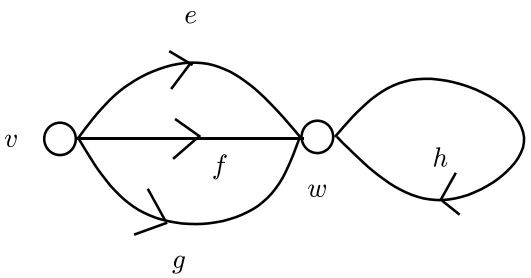

Figure 7. An example of a graph.

(E40) Recall the graph Γ_1 in (E37). Since every automorphism fixes the vertex v, we see that $\mathrm{Aut}(\Gamma_1) = T$ and $M = \{1\}$. Similarly, if a graph Γ has only one vertex, then $\mathrm{Aut}(\Gamma) = T$.

(E41) Recall the graph Γ_2 in (E37). We have $\mathrm{Aut}(\Gamma_2) = T$ and $M = \{1\}$. Set $H := \langle \sigma_2, \sigma_3 \rangle$ and $K := \langle \sigma_5 \rangle$. Then it is seen that $H \cong \mathbf{Z}/2\mathbf{Z} \times \mathbf{Z}/2\mathbf{Z}$, $K \cong \mathbf{Z}/2\mathbf{Z}$, and $\mathrm{Aut}(\Gamma_2) \cong H \rtimes K$.

(E42) Consider the directed graph Γ depicted as the regular n-gon. Then we see that $T = \{1\}$ since if an automorphism fixes all vertices then it must fix all edges. Thus, $\mathrm{Aut}(\Gamma) = M$. Furthermore, we can see that $M \cong D_n = \langle \sigma, \tau \rangle$ where σ is the $2\pi/n$-angled rotation and τ is the reflection.

(E43) Consider the directed graph Γ in **Figure 8**. We arrange a numbering of the oriented edges as

$$e = (w, v, 1),\ \overline{e} = (v, w, 1),\ f = (w, v, 2),\ \overline{f} = (v, w, 2),\ g = (w, v, 3),\ \overline{g} = (v, w, 3).$$

The subgroup T consists of automorphisms which permute the oriented edges e, f, g, and hence $T \cong \mathfrak{S}_3$. On the other hand, the subgroup Q consists of two automorphisms given by the identity map and

$$\sigma : (v, w) \mapsto (w, v),\ (e, f, g) \mapsto \left(\overline{e}, \overline{f}, \overline{g}\right),$$

and hence $Q \cong \mathbf{Z}/2\mathbf{Z}$. Therefore $\mathrm{Aut}(\Gamma) \cong \mathfrak{S}_3 \rtimes \mathbf{Z}/2\mathbf{Z}$.

The readers are strongly encouraged to consider further examples by oneself. It makes their understandings better and deeper.

As a remark, we mention the irreducible representations of a semidirect product group. As mentioned in Section 7, the irreducible representations of a direct product group $G \times H$ can be calculated with those of G and H. The situation for semidirect products groups, however, is much more complicated. In general, in order to study the irreducible representations of semidirect product groups, we require some arguments in advanced algebra.

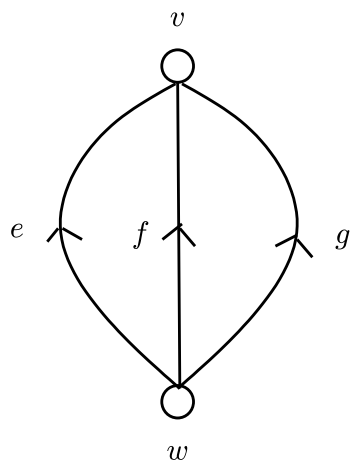

Figure 8. An example of a graph.

Acknowledgements

The author would like to thank Professor Takashiro Akitsu, who is a chemist of our faculty, for introducing to him this work and many useful comments. He considers it a privilege since this is the first interaction across disciplines as a mathematician. He also would like to thank Professor Naoko Kunugi, who is a mathematician majoring in the representation theory of finite groups, for her useful comments about references of the field.

A part of this work was done when the author stayed at the University of Bonn in 2017. He would like to express his sincere gratitude to the Mathematical Institute of the University of Bonn for its hospitality and to Tokyo University of Science for its financial supports.

Author details

Takao Satoh

Address all correspondence to: takao@rs.tus.ac.jp

Department of Mathematics, Faculty of Science Division II, Tokyo University of Science, Tokyo, Japan

References

[1] Satoh T. Sylow's Theorem. Spotlight Series 1. Kindaikagakusya; 2015. 168p. (Japanese)

[2] Armstrong MA. Groups and Symmetry. Undergraduate Texts in Mathematics. Springer-Verlag; 1988. 186p

[3] Rotman JJ. An Introduction to the Theory of Groups. 4th ed. Graduate Texts in Mathematics 148. Springer-Verlag; 1995. 513p

[4] Suzuki M. Group Theory I. Grundlehren der Mathematischen Wissenschaften 247. Springer-Verlag; 1982. 434p

[5] Serre JP. Linear Representations of Finite Groups. Graduate Texts in Mathematics 42. Springer-Verlag; 1977. 170p

[6] James G, Liebeck M. Representations and Characters of Groups. Cambridge University Press: Cambridge Mathematical Textbooks; 1993. 419p

[7] Alperin JL, Bell RB. Groups and Representations. Graduate Texts in Mathematics 162. Springer-Verlag; 1995. 194p

[8] Curtis CW, Reiner I. Representation theory of finite groups and associative algebras. AMS Chelsea Publishing; 2006. 689p

[9] Chiswell I. Introduction to Λ-Trees. World Scientific; 2001. 315p

[10] Brady T. The integral cohomology of $\mathrm{Out}_+(F_3)$. Journal of Pure and Applied Algebra. 1993;**87**:123-167

Chapter 4

Symmetry of *hR* and Pseudo-*hR* Lattices

Kazimierz Stróż

Additional information is available at the end of the chapter

http://dx.doi.org/10.5772/intechopen.72314

Abstract

Matrix methods for metric symmetry determination are fast, efficient, reliable, and, in contrast to reduction techniques, allow to establish simply all possible pseudo-symmetries in the vicinity of higher symmetry borders. It is shown that distances to borders may be characterized by one or a few monoaxial deformations measured by parameter ε, which corresponds to the relative change in the interplanar distance. The scope of this chapter is limited to a careful analysis of rhombohedral or monoclinic deformations occurring in *hR* lattices.

Keywords: semi-reduced lattices, lattice symmetry, Bravais type border, lattice deformation

1. Introduction

Chemical species are structurally classified by symmetry. The preliminary classification takes into account only translational properties, the *lattice* of a crystal structure. But identical lattices may be described by an infinite number of different unit cells (a,b,c, α,β,γ or corresponding metric tensor G) and thus it is important to select finally the reference cell called the *Bravais* cell, which symmetry reflects the lattice symmetry. While the derivation of unit cell parameters from good X-ray diffraction data is generally straightforward, the problem of symmetry-standardization is challenging [1], especially in the presence of random errors, pseudo-symmetry caused by the vicinity of Bravais type boundaries, textures, etc. Stable algorithms should recognize admittable symmetry and pseudo-symmetry(-tries) and calculate the distance(s) from the experimental unit-cell data to the Bravais lattice(s) subspace. Conceptually, a similar problem arises in the determination of distances between pairs of unit cells for database searching. A concise review of commonly used lengths (metrics) and its application to protein database search [2] showed that there is still room for improvements to characterize better the lattice on the symmetry borders. Advances in X-ray

diffraction techniques as well as improvements in data analyzing procedures allow to conclude that some of the previously obtained results may be based on pseudo-symmetry rather than on true symmetry (typical dilemma: *hR* or *mC*?). Some new diffraction data suggest, for example, that generally accepted trigonal crystal structures α-Cr_2O_3, α-Fe_2O_3, and $CaCO_3$ show monoclinic distortions [3, 4]. In consequence, the importance of border problems has a growing-up tendency.

Classifications of unique lattice representatives obtained by the *Niggli reduction* or *Delaunay reduction* are commonly used techniques to assign the Bravais symmetry to a given lattice. Another approach, called the *matrix method*, directly derives isometric transformations from the lattices by *B*-matrices, which transform a lattice onto itself [1, 5, 6], or by the space distribution of orthogonalities [7], or by filtering predefined set *V* of 480 potential symmetry matrices [8, 9]. The latter technique is applicable to a wide class of semi-reduced lattice descriptions, additionally forced by a geometric interpretation of symmetry operations. The following advantages seem to be apparent: (i) the filtering process is extremely simple, (ii) semi-reduced lattices after a small deformation are generally still semi-reduced, (iii) symmetry axes and planes are automatically indexed, (iv) a lattice deformation, which retains the given symmetry, is easily deduced. The property (iv) can be utilized as a 'distortion index', a new measure of the distance between symmetrical lattices. The aim of this chapter is to carefully look at the border problems frequently occurring in *hR* lattices (*hR-cF*, *hR-cP*, *hR-cI*, *hR-mC*), but in the less-known *semi-reduced* lattice representations. Two appended real-life examples explain deeper the proposed technique and its possibilities.

2. Semi-reduced lattice descriptions

The concept of a semi-reduced lattice description (s.r.d.) has been given elsewhere [9]. The emphasis on the crystallographic features of lattices was obtained by shifting the focus (i) from the analysis of a lattice metric to the analysis of symmetry matrices [6], (ii) from the geometric interpretation of isometric transformation based on invariant subspaces to the orthogonality concept [7] extended to splitting indices [8], (iii) and from predefined cell transformations to transformations derivable via geometric information [6, 7]. It was shown that both corresponding arithmetic and geometric holohedries share the space distribution of symmetry elements and thus simplify the crystallographic description of structural phase transitions, especially those observed with the use of powder diffraction. Moreover, the completeness of s.r.d. types revealed a combinatorial structure of *V* (see below).

The main result of introduced semi-reduced lattice representations consists in the extension of the famous characterization of Bravais lattices according to their metrical, algebraic, and geometric properties onto a wide class of primitive, less restrictive lattices (including Niggli-reduced, Buerger-reduced, nearly Buerger-reduced, and a substantial part of Delaunay-reduced). While the *geometric* operations in Bravais lattices map the basis vectors onto themselves, the *arithmetic* operators in s.r.d. transform the basis vectors into cell vectors (basis vectors, face or space diagonals) and are represented by matrices from the set *V* of 480 matrices with the determinant 1 and elements {0, ±1} of the matrix powers. A lattice is in s.r.d. if the

absolute values of off-diagonal elements in both metric tensors G and G^{-1} are smaller than the corresponding two diagonal elements sharing the same column and sharing the same row. The experimental s.r.d. metric G must be unchanged (with some relaxation) by the symmetry operation from V, thus by simple filtering:

$$G' = V^{T} GV, V \in V \text{ and } (a, b, c, \alpha, \beta, \gamma) \rightarrow G \sim G' \rightarrow (a', b', c', \alpha', \beta', \gamma') \quad (1)$$

and the subsequent geometric interpretation of the filtered matrices leads to mathematically stable and rich information on the individual transformation bringing the lattice into coincidence with itself (known as an *isometry* or a *symmetry operation*) and deviations from the exact match:

$$\Delta a/a\,\%, \Delta b/b\,\%, \Delta c/c\,\%, \Delta\alpha^{\circ}, \Delta\beta^{\circ}, \Delta\gamma^{\circ}, \delta^{\circ}, \quad (2)$$

where $\Delta a/a\%$ denotes $(a'\text{-}a)/a\cdot 100[\%]$, $\Delta\alpha^{\circ} = \alpha'\text{-}\alpha[^{\circ}]$ and δ° is Le Page parameter [7]. For exact isometric transformation, all such discrepancy parameters should be zero (or very close to zero).

It is obvious that symmetry operations fulfill the closure, associative, identity, and inverse axioms and form a group: an *arithmetic holohedry* or in other words a *lattice group*. The set V of all possible transformations in s.r.d. is covered by the arithmetic holohedries of 39 highest symmetry lattices (**Table 1**).

In the s.r.d. approach, the primitive-to-Bravais transformations are not stored, but dynamically constructed, based on the geometric interpretation of symmetry matrices. Unfortunately, the classical symbol of a point or space symmetry operation bears information on an operation type and a 1D subspace (or 2D in the case of symmetry planes) of points invariant under this operation [10], but the information on the complement orthogonal subspace, invariant as a whole, is lost. In the developed *splitting* or *dual* symbol introduced in [8], orientation of

Lattice	Metric	Lattice	Metric	Lattice	Metric	Lattice	Metric
hP_1	2,2,1,0,0,−1	hP_4	2,2,1,0,0,1	cF_7	2,2,2,0,−1,−1	cI_7	4,3,3,1,2,2
hP_2	2,1,2,0,−1,0	hP_5	2,1,2,0,1,0	cF_8	2,2,2,1,1,0	cI_8	3,3,4,−2,−2,1
hP_3	1,2,2,−1,0,0	hP_6	1,2,2,1,0,0	cF_9	2,2,2,1,0,1	cI_9	3,4,3,−2,1,−2
cP_0	1,1,1,0,0,0			cF_{10}	2,2,2,0,1,1	cI_{10}	4,3,3,1,−2,−2
cF_1	2,2,2,1,1,1	cI_1	3,3,3,−1,−1,−1	cF_{11}	2,2,2,1,−1,0	cI_{11}	3,3,4,−2,2,−1
cF_2	2,2,2,−1,−1,1	cI_2	3,3,3,1,1,−1	cF_{12}	2,2,2,1,0,−1	cI_{12}	3,4,3,−2,−1,2
cF_3	2,2,2,−1,1,−1	cI_3	3,3,3,1,−1,1	cF_{13}	2,2,2,0,1,−1	cI_{13}	4,3,3,−1,−2,2
cF_4	2,2,2,1,−1,−1	cI_4	3,3,3,−1,1,1	cF_{14}	2,2,2,−1,1,0	cI_{14}	3,3,4,2,−2,−1
cF_5	2,2,2,−1,−1,0	cI_5	3,3,4,2,2,1	cF_{15}	2,2,2,−1,0,1	cI_{15}	3,4,3,2,−1,−2
cF_6	2,2,2,−1,0,−1	cI_6	3,4,3,2,1,2	cF_{16}	2,2,2,0,−1,1	cI_{16}	4,3,3,−1,2,−2

Metrics corresponding to lattice descriptions cI_5–cI_{16} determine non-Buerger cells.

Table 1. Complete set M of metrical tensors of highest-symmetry lattices referred to semi-reduced bases [8].

both subspaces is given by specifying direction [*uvw*] orthogonal to the family of planes (*hkl*). The centering in the [*uvw*] direction as well as the crystallographic orthogonality between a lattice direction and a lattice plane, hidden in the symmetry matrix, is enclosed in this new geometric symbol $n^{+(-)}$ [*uvw*](*hkl*). Some properties of [*uvw*](*hkl*) are mathematically obvious; splitting indices specify the same vector, or more strictly, a pair of parallel directions in direct and reciprocal spaces. Others, like calculations of the interplanar distance $d_{(hkl)}$, the distance between lattice points $l_{[uvw]}$, deriving Le Page angle δ [7] between [*uvw*] and (*hkl*), or even using indices to predict deformations, which retain a given cyclic group, need additionally *G* data. In a lattice given by *G*, the uniaxial deformation along symmetry [*uvw*] direction

$$G' = G + \varepsilon \begin{pmatrix} hh & hk & hl \\ kh & kk & kl \\ lh & lk & ll \end{pmatrix} \tag{3}$$

modifies only 1D subspace and in consequence retains the symmetry axis in [*uvw*] direction and also axes orthogonal to this direction, if any. Other symmetries will be broken.

3. Rhombohedral lattices in s.r.d.

It is difficult to classify or compare lattices that drastically change their class-dependent descriptions as a result of small deformations, structural phase transitions, or experimental errors. Such discontinuities in the Niggli-reduced space can be overcome by a deep mathematical treatment like in [11] or by applying a less restrictive method of Bravais cell assignment: Niggli reduction → Delaunay reduction → s.r.d. A wide class of lattices, including a trigonal and three cubic lattices, is considered here as 'rhombohedral' lattices. The actual form of a cell has no meaning, but a given lattice can be represented by a rhombohedron with equal sides $a = b = c$ and angles $\alpha = \beta = \gamma$. The symmetry does not depend on the scale, so we can assume that all sides are equal to 1 and thus the class is one-parametric with the rhombohedral angle α, $0° < \alpha < 120°$. Symmetry matrices of 'rhombohedral' lattices cover *V* nearly completely (excluding 6 hexagonal groups). As mentioned earlier, every symmetry matrix describes an isometric transformation of basis vectors into cell vectors. Neglecting the vector sense, there are 13 cell vectors grouped in the rhombohedral case into four triads <001>, <011>, <01–1>, <1–1-1 > of directions related by threefold axis along [111]. Triad <01–1 > corresponds to twofold axes. Moreover, lattice vector [111] is orthogonal to coplanar vectors <01–1>, which interaxial angle is 60°. Thus, symmetry matrices of *hR* lattice in the Bravais description ($a = b = c$, $\alpha = \beta = \gamma < 120°$) are characterized by dual symbols: 3^+[111](111), 3^-[111](111), 2[01–1](01–1), 2[1–10](1–10), 2[−101](−101) and this geometric property is exposed in the hexagonal description with $c/a = l_{[111]}/l_{<01-1>}$. Metrical relationships between lengths of cell vectors as functions of α are drawn in **Figure 1**.

The angle $\alpha = 90°$ and a cubic shape can be considered as the central point of the sketch. Both left and right parts separated by 90° are connected by the lattice inversion. Other characteristic points (i.e., intersection of curves) are collected in **Table 2**.

Information contained in both **Figure 1** and **Table 2** explains discontinuities in descrip tions of rhombohedral lattices. Descriptions of Niggli- or Buerger-reduced lattices must be changed during crossing characteristic angles 60° and 109.47°, since they are based on the shortest

http://dx.doi.org/10.5772/intechopen.72314

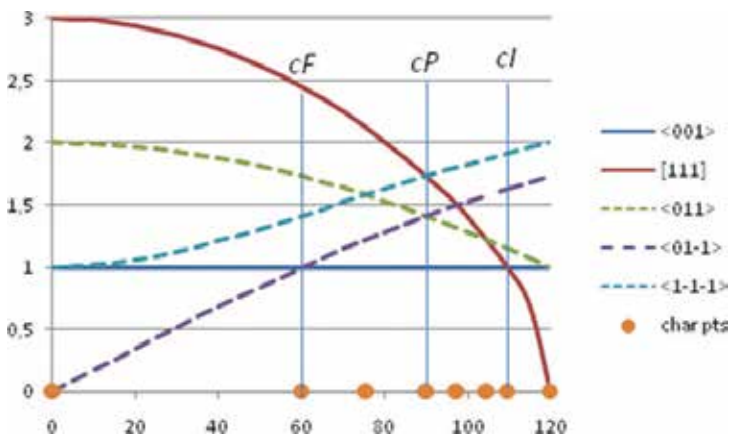

Figure 1. Lengths of cell vectors as a function of rhombohedral angle. Intersections of curves define characteristic points (*e.g.*, higher symmetry lattices: *cF*, *cP*, and *cI*).

No.	cos(α)	α[°]	Description
1	1	0	1D
2	1/2	60	cF
3	1/4	75.5225	c/a = √(3)
4	0	90	cP
5	−1/8	97.1808	c/a = √(3/3)
6	−1/4	104.4775	c/a = √(3/5)
7	−1/3	109.4712	cI
8	−1/2	120	2D

Lattice *cP* (point 4) maximally extended along [111] reduces 3D space to the 1D (point 1); maximal compression leads to 2D space (point 8). Intermediate points (2, 7) correspond to centered lattices: *cF*, *cI*. Other intersections (points 5 and 6) have no influence on symmetry.

Table 2. Characteristic points (intersections of curves) in **Figure 1**.

non-coplanar lattice vectors. Similarly, Bravais descriptions should reflect the increased symmetry for these angles (directions <001> reveal extra twofold and threefold symmetry). In sharp contrast to the above lattice representations, no drastic changes is necessary in semi-reduced descriptions of rhombohedral lattices, without losing relation with Bravais standardization.

4. Distance to the higher symmetry border: ε concept

In crystallography, it is crucial to standardize lattice descriptions and to assign one from the fourteen 3D Bravais types differentiated by symmetry. The process is straightforward for good quality data and faraway from the Bravais borders but in opposite cases, especially in

the presence of unavoidable experimental errors, the solution cannot be unique. Usable distances should be defined to rank positive candidates. Most considerations about the calculation of such distances are devoted to the Niggli reduction, for example, see [11] and references contained therein; only some discuss the Buerger reduction [1, 7].

The geometric properties of matrices that transform an s.r.d. lattice into itself are utilized in the presented approach to the greatest degree, which form the *geometric image* of the filtered transformation. Each isometric or pseudo-isometric action on the current lattice is estimated by three metrical and four angular parameters (2) and oriented in the lattice space by dual indices [*uvw*] (*hkl*). Deviations are controlled by two thresholds: metrical *tol1* and angular *tol2*. The *maxdev* (that is maximal value of all unsigned deviations for all isometric transformations grouped in the lattice symmetry) was selected as an introductory concept of similarity between the probe cell and a cell with given symmetry. For exact symmetry, *maxdev* should be zero (or very close to zero). In the vicinity of symmetry borders, high values of *tol1* and *tol2* (*e.g.*, 5) reveal higher pseudo- (in another words 'approximate') symmetry—with greater *maxdev* values and standard group-subgroup relations (**Table 3**). For reasonable thresholds, the number of filtered matrices cannot exceed 24.

The filtering of symmetry matrices near cubic borders results in a rather big number (7 × 24) of quantitative data. As **Table 3** shows, deviations are interrelated, not random. A maximal unsigned deviation well reflects this situation. Moreover, strict *hR* symmetry including 2 isometries denoted geometrically as $3^{+(-)}[-1-13](001)$ and pseudo-*cF* symmetry suggest that all deviations can be explained by a rhombohedral deformation. According to (3), the uniaxial deformation along direction [−1–13] orthogonal to planes (001) modifies metric *G*:

$$G' = \begin{pmatrix} 2 & 1 & 1 \\ 1 & 2 & 1 \\ 1 & 1 & 2.1 \end{pmatrix} + \varepsilon \begin{pmatrix} 0 & 0 & 0 \\ 0 & 0 & 0 \\ 0 & 0 & 1 \end{pmatrix}.$$

It is clear from **Table 1** that *G*′ with *cF* symmetry should be cF_1 = (2, 2, 2, 1, 1, 1). The above symmetric matrix equation can be rewritten in a vector form:

$$(2, 2, 2, 1, 1, 1) = (2, 2, 2.1, 1, 1, 1) + \varepsilon(0, 0, 1, 0, 0, 0)$$

with the solution $\varepsilon = -0.1$. As a result, distance ε between *hR* and *cF* cells is −0.1. This new concept is more informative in comparison with *maxdev* parameter; the deformation type is explicitly given by $\varepsilon \cdot (hkl)$ and can be converted into $\Delta d_{(hkl)}/d_{(hkl)}$), shortly $\Delta d/d$, and related with diffraction line shifts in *XRD* patterns. The ε distances depend not only on a rhombohedral angle but also on the lattice scale, and thus for practical purposes, the $\Delta d/d$ distance is more appropriate, since it can be compared with experimental $\Delta d/d$ resolution. The interplanar distance may be calculated from the following formula:

$$d_{(hkl)} = 1/[(hkl) \cdot G \cdot (hkl)^{\mathrm{T}})^{1/2} \quad (4)$$

The sign of ε or Δd is also important; it informs on which side of the higher symmetry border the analyzed lattice is located.

For rhombohedral lattices, two kinds of ε distances to the border (based on rhombohedral or monoclinic deformations) are generally analyzed. In more complicated cases, like cubic lattices

Δa/a%	Δb/b%	Δc/c%	Δα°	Δβ°	Δγ°	δ°	Operation
0.00	0.00	0.00	0.00	0.00	0.00	0.00	1[]()
0.00	0.00	0.00	0.00	0.00	0.00	0.00	2[010](121)
0.00	0.00	0.00	0.00	0.00	0.00	0.00	2[1–10](1–10)
0.00	0.00	0.00	0.00	0.00	0.00	0.00	2[100](211)
0.00	0.00	0.00	0.00	0.00	0.00	0.00	3 + [−1–13](001)
0.00	0.00	0.00	0.00	0.00	0.00	0.00	3-[−1–13](001)
0.00	2.47	−2.41	0.00	−0.79	0.79	1.95	2[01–1](01–1)
2.47	2.47	0.00	−2.38	−2.38	−1.59	1.95	2[001](112)
2.47	0.00	−2.41	−0.79	0.00	0.79	1.95	2[−101](−1–1)
0.00	2.47	−2.41	0.00	−0.79	0.79	1.95	2[−111](011)
2.47	0.00	−2.41	−0.79	0.00	0.79	1.95	2[1–11](101)
2.47	2.47	0.00	−2.38	−2.38	−1.59	1.95	2[11–1](110)
0.00	2.47	−2.41	0.00	−0.79	0.79	1.30	3 + [111](111)
2.47	0.00	−2.41	−0.79	0.00	0.79	1.30	3-[111](111)
0.00	2.47	−2.41	0.00	−0.79	0.79	1.30	3+ [3-1-1](100)
2.47	2.47	0.00	−2.38	−2.38	−1.59	1.30	3-[3-1-1](100)
2.47	2.47	0.00	−2.38	−2.38	−1.59	1.30	3 + [−13–1](010)
2.47	0.00	−2.41	−0.79	0.00	0.79	1.30	3-[−13–1](010)
2.47	0.00	−2.41	−0.79	0.00	0.79	1.95	4 + [−111](011)
2.47	2.47	0.00	−2.38	−2.38	−1.59	1.95	4-[−111](011)
2.47	2.47	0.00	−2.38	−2.38	−1.59	1.95	4 + (1–11](101)
0.00	2.47	−2.41	0.00	−0.79	0.79	1.95	4-[1-11](101)
2.47	0.00	−2.41	−0.79	0.00	0.79	1.95	4+ [11-1](110)
0.00	2.47	−2.41	0.00	−0.79	0.79	1.95	4-[11-1](110)

Items with zero deviations define true *hR* symmetry (*a*,*b*,*c* = 1.41421, *α*,*β*,*γ* = 60.7941°) with *maxdev* = 0, while all 24 operations correspond to pseudo-*cF* symmetry (*a*,*b*,*c* = 2.025, *α*,*β*,*γ* = 91.3976°) with *maxdev* = 2.47.

Table 3. Geometric images (7 discrepancy parameters + geometric description) of filtered matrices for the lattice *G* = (2, 2, 2.1, 1, 1, 1) and illustration of *maxdev* distances.

modified by simultaneous rhombohedral and tetragonal distortions, few ε distances can be derived. Calculations are also possible in the presence of experimental errors, if they are smaller than distortions.

The concept of a quantitative measure between the probe cell and cells with higher symmetry based on monoaxial deformations is thus outlined, but for practical applications this idea should be thoroughly investigated in s.r.d. This study provides analyses and two real-life examples limited to rhombohedral lattices.

5. Distances between *hR* and cubic lattices

In the case being considered, the semi-reduced *hR* lattice should be viewed as a rhombohedrally distorted *cF*, *cI*, or *cP* pseudo-lattice with exact *hR* symmetry. It is also assumed that every equivalent description is equally distanced from a cubic lattice, and thus only one representation of a lattice is necessary to properly derive such distance. This assumption validity may be carefully checked by creating all semi-reduced variants of *hR* lattices in the neighborhood of cubic lattices.

5.1. *hR-cF* border

Let us have *hR* lattice in a standard description (a,b,c = 1,449,138; α,β,γ = 58,41,186°). It is obviously relatively close to *cF* lattice. The analysis of pseudo-symmetry outlined in Section 4 reveals that the distance ε to the higher symmetry is equal to −0.1. An opposite deformation of 16 *cF* descriptions in **Table 1** according to 4 threefold axes allows to generate all 64 semi-reduced *hR* variants of the given lattice and thus relations in **Table 4** '*hR* metric' + 'deformation' = *cF* are obvious. But, as verified by computer tests, the same deformations can be extracted also from the geometric images of pseudo-symmetry without any relation to the predefined *cF* metrics.

The interpretation of 4 × 16 items in **Table 4** is very easy due to the fact that Miller indices of planes perpendicular to the unique threefold axis are given explicitly in the deformation symbols. In the considered situation, the operation on *G* vectors is as follows: $G_{cF} = G_{\mathbf{hR}} - 0.1\cdot(hh, kk, ll, kl, hl, hk)$. For example, the last three items give:

(2.1, 2, 2.1, 0, −1.1, 1) - 0.1·(−1·-1, 0·0, 1·1, 1·0, 1·-1, −1·0) = (2, 2, 2, 0, −1, 1)

(2, 2.1, 2, 0. -1, 1) - 0.1·(0·0, 1·1, 0·0, 0·1, 0·0, 0·1) = (2, 2, 2, 0, −1, 1)

(2, 2, 2.1, 0, −1, 1) - 0.1·(0·0, 0·0, 1·1, 1·0, 1·0, 0·1) = (2, 2, 2, 0, −1, 1)

Assigning the symmetry group to the final ***G*** metric or comparing it with **Table 1** reveals *cF* symmetry in cF_{16} description. In consequence, distance ε from *hR*(a,b,c = 1.449138; α,β,γ = 58.41186°) to *cF*(a,b,c = 2; α,β,γ = 90°) is equal to −0.1 and does not depend on the actual description. The original *d* spacing along threefold axis is changed from 1.1972 (*hR* lattice) to 1.1577 (*cF* lattice) and $\Delta d/d$ = −0.0355. Such values characterize not only each item in **Table 4** but also all *hR* lattices with rhombohedral angle 58.41186°. Since ε corresponds with the rational part of *G* components in **Table 4**, similar tables of equivalent descriptions of *hR* (other ε) can be simply constructed. For example, the modification of rational parts from 0.1 to −0.01 will result in obtaining new *hR* lattice (a,b,c = 1.410674; α,β,γ = 60.1661°) with a shorter ε distance to *cF* border equal to 0.01.

5.2. *hR-cI* border

The *hR* lattice close to *cI* border seems to be less populated. The metrical relationships between the length of cell vectors look more complicated in comparison with *cF* neighborhood (**Figure 1**), but the analysis of pseudo-symmetries is similar. The same distance ε = −0.1 gives *hR* lattice with the rhombohedral angle 106.8773°. All semi-reduced descriptions together with deformations needed in order to obtain higher *cI* symmetry are compiled in **Table 5**.

***hR* metric**						**deformation**	***hR* metric**						**deformation**
2.1	2.1	2.1	1.1	1.1	1.1	−0.1·(111)	2.1	2.1	2	1	0	1.1	−0.1·(110)
2	2	2.1	1	1	1	−0.1·(001)	2	2.1	2.1	1.1	0	1	−0.1·(011)
2	2.1	2	1	1	1	−0.1·(010)	2	2	2.1	1	0	1	−0.1·(001)
2.1	2	2	1	1	1	−0.1·(100)	2.1	2	2	1	0	1	−0.1·(100)
2.1	2.1	2.1	−1	−1	1.1	−0.1·(−1–11)	2.1	2.1	2	0	1	1.1	−0.1·(110)
2	2	2.1	−1	−1	1	−0.1·(001)	2.1	2	2.1	0	1.1	1	−0.1·(101)
2	2.1	2	−1	−1	1	−0.1·(010)	2	2.1	2	0	1	1	−0.1·(010)
2.1	2	2	−1	−1	1	−0.1·(100)	2	2	2.1	0	1	1	−0.1·(001)
2.1	2.1	2.1	−1	1.1	−1	−0.1·(1–1 − 1)	2	2.1	2.1	1.1	-1	0	−0.1·(011)
2	2	2.1	−1	1	−1	−0.1·(001)	2.1	2	2.1	1	−1.1	0	−0.1·(−101)
2	2.1	2	−1	1	−1	−0.1·(010)	2	2.1	2	1	−1	0	−0.1·(010)
2.1	2	2	−1	1	−1	−0.1·(100)	2.1	2	2	1	−1	0	−0.1·(100)
2.1	2.1	2.1	1.1	−1	−1	−0.1·(−11–1)	2	2.1	2.1	1.1	0	−1	−0.1·(011)
2	2	2.1	1	−1	−1	−0.1·(001)	2.1	2.1	2	1	0	−1.1	−0.1·(1–10)
2	2.1	2	1	−1	−1	−0.1·(100)	2.1	2	2	1	0	−1	−0.1·(100)
2.1	2	2	1	−1	−1	−0.1·(010)	2	2	2.1	1	0	−1	−0.1·(001)
2	2.1	2.1	−1	−1	0	−0.1·(01–1)	2.1	2	2.1	0	1.1	−1	−0.1·(101)
2.1	2	2.1	−1	−1	0	−0.1·(−101)	2.1	2.1	2	0	1	−1.1	−0.1·(1–10)
2	2.1	2	−1	−1	0	−0.1·(010)	2	2.1	2	0	1	−1	−0.1·(010)
2.1	2	2	−1	−1	0	−0.1·(100)	2	2	2.1	0	1	−1	−0.1·(001)
2	2.1	2.1	−1	0	−1	−0.1·(01–1)	2.1	2	2.1	−1	1.1	0	−0.1·(101)
2.1	2.1	2	−1	0	−1	−0.1·(1–10)	2	2.1	2.1	−1.1	1	0	−0.1·(01–1)
2.1	2	2	−1	0	−1	−0.1·(001)	2	2.1	2	−1	1	0	−0.1·(010)
2	2	2.1	−1	0	−1	−0.1·(100)	2.1	2	2	−1	1	0	−0.1·(100)
2.1	2.1	2	0	−1	−1	−0.1·(1–10)	2.1	2.1	2	−1	0	1.1	−0.1·(110)
2.1	2	2.1	0	−1	−1	−0.1·(−101)	2	2.1	2.1	−1.1	0	1	−0.1·(01–1)
2	2.1	2	0	−1	−1	−0.1·(010)	2.1	2	2	−1	0	1	−0.1·(100)
2	2	2.1	0	−1	−1	−0.1·(001)	2	2	2.1	−1	0	1	−0.1·(001)
2	2.1	2.1	1.1	1	0	−0.1·(011)	2.1	2.1	2	0	−1	1.1	−0.1·(110)
2.1	2	2.1	1	1.1	0	−0.1·(101)	2.1	2	2.1	0	−1.1	1	−0.1·(−101)
2.1	2	2	1	1	0	−0.1·(100)	2	2.1	2	0	−1	1	−0.1·(010)
2	2.1	2	1	1	0	−0.1·(010)	2	2	2.1	0	−1	1	−0.1·(001)

The illustration of *hR* lattice is represented by semi-reduced descriptions. Every four descriptions are close to one of the *cF* lattice variants given in **Table 1**, what is easily seen by rejecting a rational part in metric elements. The distance to the border *hR* – *cF* is −0.1, or −0.035514356 given in $\Delta d/d$ units, where *d* is an interplanar distance between a family of planes perpendicular to the threefold axis.

Table 4. Sixty-four semi-reduced descriptions of the same *hR* lattice (*a*,*b*,*c* = 1,449,138; α,β,γ = 58,41,186°) and its rhombohedral deformations to the *cF* lattice (*a*,*b*,*c* = 2; α,β,γ = 90°).

hR metric						deformation	hR metric						deformation
3.1	3.1	3.1	−1	−1	−1	−0.1·(111)	3.1	4.4	3.9	−2.6	1.3	−2.2	−0.1·(1–23)
3.1	3.9	3.1	−1	−1	−1	−0.1·(−13–1)	3.1	4.4	3.1	−1.8	0.9	−2.2	−0.1·(−121)
3.1	3.1	3.9	−1	−1	−1	−0.1·(−1–13)	3.1	4.4	3.1	−2.2	0.9	−1.8	−0.1·(12–1)
3.9	3.1	3.1	−1	−1	−1	−0.1·(3–1-1)	3.9	4.4	3.1	−2.2	1.3	−2.6	−0.1·(3–21)
3.1	3.1	3.1	0.9	0.9	−1	−0.1·(−1–11)	4.4	3.9	3.1	1.3	−2.2	−2.6	−0.1·(−231)
3.1	3.1	3.9	1.3	1.3	−1	−0.1·(113)	4.4	3.1	3.9	1.3	−2.6	−2.2	−0.1·(−213)
3.1	3.9	3.1	1.3	0.9	−1	−0.1·(−131)	4.4	3.1	3.1	0.9	−2.2	−1.8	−0.1·(21–1)
3.9	3.1	3.1	0.9	1.3	−1	−0.1·(3–11)	4.4	3.1	3.1	0.9	−1.8	−2.2	−0.1·(2–11)
3.1	3.1	3.1	0.9	−1	0.9	−0.1·(−11–1)	3.1	3.1	4.4	−1.8	2.2	−0.9	−0.1·(112)
3.1	3.1	3.9	1.3	−1	0.9	−0.1·(−113)	3.1	3.1	4.4	−2.2	1.8	−0.9	−0.1·(−1–12)
3.1	3.9	3.1	1.3	−1	1.3	−0.1·(131)	3.1	3.9	4.4	−2.6	2.2	−1.3	−0.1·(−13–2)
3.9	3.1	3.1	0.9	−1	1.3	−0.1·(31–1)	3.9	3.1	4.4	−2.2	2.6	−1.3	−0.1·(3–12)
3.1	3.1	3.1	−1	0.9	0.9	−0.1·(1–1-1)	3.1	4.4	3.9	−2.6	−1.3	2.2	−0.1·(−1–23)
3.1	3.1	3.9	−1	1.3	0.9	−0.1·(1–13)	3.1	4.4	3.1	−1.8	−0.9	2.2	−0.1·(121)
3.1	3.9	3.1	−1	0.9	1.3	−0.1·(13–1)	3.1	4.4	3.1	−2.2	−0.9	1.8	−0.1·(1–21)
3.9	3.1	3.1	−1	1.3	1.3	−0.1·(311)	3.9	4.4	3.1	−2.2	−1.3	2.6	−0.1·(32–1)
3.1	3.1	4.4	2.2	1.8	0.9	−0.1·(−112)	4.4	3.1	3.9	−1.3	−2.6	2.2	−0.1·(−2–13)
3.1	3.9	4.4	2.6	2.2	1.3	−0.1·(132)	4.4	3.9	3.1	−1.3	−2.2	2.6	−0.1·(23–1)
3.1	3.1	4.4	1.8	2.2	0.9	−0.1·(−11–2)	4.4	3.1	3.1	−0.9	−1.8	2.2	−0.1·(211)
3.9	3.1	4.4	2.2	2.6	1.3	−0.1·(312)	4.4	3.1	3.1	−0.9	−2.2	1.8	−0.1·(2–1-1)
3.1	4.4	3.9	2.6	1.3	2.2	−0.1·(123)	3.1	3.9	4.4	2.6	−2.2	−1.3	−0.1·(−132)
3.1	4.4	3.1	2.2	0.9	1.8	−0.1·(1–2-1)	3.1	3.1	4.4	1.8	−2.2	−0.9	−0.1·(11–2)
3.1	4.4	3.1	1.8	0.9	2.2	−0.1·(12–1)	3.1	3.1	4.4	2.2	−1.8	−0.9	−0.1·(112)
3.9	4.4	3.1	2.2	1.3	2.6	−0.1·(321)	3.9	3.1	4.4	2.2	−2.6	−1.3	−0.1·(3–1-2)
4.4	3.1	3.9	1.3	2.6	2.2	−0.1·(213)	3.1	4.4	3.1	1.8	−0.9	−2.2	−0.1·(−12–1)
4.4	3.1	3.1	0.9	2.2	1.8	−0.1·(2–11)	3.1	4.4	3.9	2.6	−1.3	−2.2	−0.1·(−123)
4.4	3.1	3.1	0.9	1.8	2.2	−0.1·(−2–11)	3.1	4.4	3.1	2.2	−0.9	−1.8	−0.1·(121)
4.4	3.9	3.1	1.3	2.2	2.6	−0.1·(231)	3.9	4.4	3.1	2.2	−1.3	−2.6	−0.1·(3–2-1)
3.1	3.1	4.4	−2	−2	0.9	−0.1·(−112)	4.4	3.1	3.9	−1.3	2.6	−2.2	−0.1·(2–13)
3.1	3.9	4.4	−3	−2	1.3	−0.1·(13–2)	4.4	3.9	3.1	−1.3	2.2	−2.6	−0.1·(−23–1)
3.1	3.1	4.4	−2	−2	0.9	−0.1·(−112)	4.4	3.1	3.1	−0.9	1.8	−2.2	−0.1·(−211)
3.9	3.1	4.4	−2	−3	1.3	−0.1·(31–2)	4.4	3.1	3.1	−0.9	2.2	−1.8	−0.1·(211)

The illustration of *hR* lattice is represented by semi-reduced descriptions. The distance to the border *hR* – *cI* is −0.1, which corresponds to −0.123 given in $\Delta d/d$ units.

Table 5. Sixty-four semi-reduced descriptions of *hR* lattice (a,b,c = 1.7607; α,β,γ = 106.8773°) and its deformations to the *cI* lattice (a,b,c = 2; α,β,γ = 90°).

The last three lines give:

(4.4, 3.9, 3.1, −1.3, 2.2, −2.6) − 0.1·(−2·−2, 3·3, −1·−1, −1·3, −1·−2, −2·3) = (4, 3, 3, −1, 2, −2)
(4.4, 3.1, 3.1, −0.9, 1.8, −2.2) − 0.1·(−2·−2, 1·1, 1·1, 1·1, 1·−2, −2·1) = (4, 3, 3, −1, 2, −2)
(4.4, 3.1, 3.1, −0.9, 2.2, −1.8) − 0.1·(2·2, 1·1, 1·1, 1·1, 1·2, 2·1) = (4, 3, 3, −1, 2, −2)

The assigning of a symmetry group to a modified metric or comparing it with **Table 1** reveals *cI* symmetry in cI_{16} description. As a result, the distance from *hR* lattice (*a*,*b*,*c* = 1.760682; α,β,γ = 106.8773°) to *cI* lattice (*a*,*b*,*c* = 2; α,β,γ = 90°) is equal to −0.1 ($\Delta d/d$ = −0.123) and as expected does not depend on the selected description. Theoretical descriptions of other *hR* lattices may be easily obtained: for example, by lowering ε 10 times (4, 3, 3, −1, 2, −2) + 0.01·(2·2, 1·1, 1·1, 1·1, 1·2, 2·1) = (4.04, 3.01, 3.01, −0.99, 2.02; −1.98), which corresponds to the Bravais description: (*a*,*b*,*c* = 1.734935; α,β,γ = 109.2022°), ε = −0.01 and $\Delta d/d$ = −0.01467.

The presence of random errors complicates the derivation of ε and $\Delta d/d$. If *G* approximately describes *hR* lattice, the distances to the borders will be also approximate. Assuming that *G* = (4.41, 3.08, 3.12, −0.98, 2.23, −1.9) a threefold pseudo-symmetry axis can be found parallel to the [110] direction, which is nearly orthogonal to (211) planes. Least squares "best solution" of following equation

(4.41, 3.08, 3.12, −0,98, 2,23, −1.9) + ε·(2·2, 1·1, 1·1, 1·2, 2·1) = (4, 3, 3, −1, 2, −2)

gives ε = −0,093, which can be considered as a rather interesting result.

5.3. *hR*-*cP* border

To all cells contained in **Tables 4, 5** exact *hR* and approximate *cF* or *cI* symmetries are easily assigned by filtering *V* set only. No additional process of cell manipulation is necessary. But it is not true near *hR* – *cP* border: the exact *hR* symmetry can be recognized, but pseudo *cP* symmetry generally not. This discontinuity on the *hR*– *cP* border is caused by the fact that there is a unique semi-reduced description of *cP* lattice, namely, cP_0 (metric = 1,1,1,0,0,0). Any additional description of this lattice is not semi-reduced and its symmetry group contains symmetry matrices outside the considered *V* set. We are interested in finding such descriptions, which contain at least one *hR* subgroup in *V*. The problem, attacked from the *cF* and *cI* sides, leads to results included in **Table 6**.

Symbol	*cP* metric						Symbol	*cP* metric					
cP_1	1	1	2	−1	0	0	cP_{49}	1	1	2	−1	0	0
cP_2	1	1	2	0	−1	0	cP_{50}	1	1	2	0	−1	0
cP_3	1	1	2	0	1	0	cP_{51}	1	1	2	0	1	0
cP_4	1	1	2	1	0	0	cP_{52}	1	1	2	1	0	0
cP_5	1	2	1	−1	0	0	cP_{53}	1	2	1	−1	0	0
cP_6	1	2	1	1	0	0	cP_{54}	1	2	1	0	0	−1
cP_7	1	2	1	0	0	−1	cP_{55}	1	2	1	0	0	1
cP_8	1	2	1	0	0	1	cP_{56}	1	2	1	1	0	0
cP_9	2	1	1	0	1	0	cP_{57}	2	1	1	0	−1	0
cP_{10}	2	1	1	0	0	1	cP_{58}	2	1	1	0	0	−1
cP_{11}	2	1	1	0	0	−1	cP_{59}	2	1	1	0	0	1
cP_{12}	2	1	1	0	−1	0	cP_{60}	2	1	1	0	1	0
cP_{13}	1	2	2	1	1	1	cP_{61}	1	1	3	−1	−1	0
cP_{14}	1	2	2	−1	−1	1	cP_{62}	1	1	3	−1	1	0
cP_{15}	1	2	2	−1	1	−1	cP_{63}	1	1	3	1	−1	0

Symbol	*cP* metric						Symbol	*cP* metric					
cP_{16}	1	2	2	1	−1	−1	cP_{64}	1	1	3	1	1	0
cP_{17}	1	2	2	−1	−1	0	cP_{65}	1	3	1	−1	0	−1
cP_{18}	1	2	2	−1	0	−1	cP_{66}	1	3	1	−1	0	1
cP_{19}	1	2	2	1	1	0	cP_{67}	1	3	1	1	0	−1
cP_{20}	1	2	2	1	0	1	cP_{68}	1	3	1	1	0	1
cP_{21}	1	2	2	1	−1	0	cP_{69}	3	1	1	0	−1	−1
cP_{22}	1	2	2	1	0	−1	cP_{70}	3	1	1	0	−1	1
cP_{23}	1	2	2	−1	1	0	cP_{71}	3	1	1	0	1	−1
cP_{24}	1	2	2	−1	0	1	cP_{72}	3	1	1	0	1	1
cP_{25}	2	1	2	1	1	1	cP_{73}	2	1	3	−1	−2	1
cP_{26}	2	1	2	−1	−1	1	cP_{74}	2	1	3	−1	2	−1
cP_{27}	2	1	2	−1	1	−1	cP_{75}	2	1	3	1	−2	−1
cP_{28}	2	1	2	1	−1	−1	cP_{76}	2	1	3	1	2	1
cP_{29}	2	1	2	−1	−1	0	cP_{77}	2	3	1	−1	−1	2
cP_{30}	2	1	2	0	−1	−1	cP_{78}	2	3	1	−1	1	−2
cP_{31}	2	1	2	1	1	0	cP_{79}	2	3	1	1	−1	−2
cP_{32}	2	1	2	0	1	1	cP_{80}	2	3	1	1	1	2
cP_{33}	2	1	2	1	−1	0	cP_{81}	3	1	2	−1	−2	1
cP_{34}	2	1	2	0	1	−1	cP_{82}	3	1	2	−1	2	−1
cP_{35}	2	1	2	−1	1	0	cP_{83}	3	1	2	1	−2	−1
cP_{36}	2	1	2	0	−1	1	cP_{84}	3	1	2	1	2	1
cP_{37}	2	2	1	1	1	1	cP_{85}	1	2	3	−2	−1	1
cP_{38}	2	2	1	−1	−1	1	cP_{86}	1	2	3	−2	1	−1
cP_{39}	2	2	1	−1	1	−1	cP_{87}	1	2	3	2	−1	−1
cP_{40}	2	2	1	1	−1	−1	cP_{88}	1	2	3	2	1	1
cP_{41}	2	2	1	−1	0	−1	cP_{89}	1	3	2	−2	−1	1
cP_{42}	2	2	1	0	−1	−1	cP_{90}	1	3	2	2	−1	−1
cP_{43}	2	2	1	1	0	1	cP_{91}	1	3	2	2	1	1
cP_{44}	2	2	1	0	1	1	cP_{92}	1	3	2	−2	1	−1
cP_{45}	2	2	1	1	0	−1	cP_{93}	3	2	1	−1	−1	2
cP_{46}	2	2	1	0	1	−1	cP_{94}	3	2	1	−1	1	−2
cP_{47}	2	2	1	−1	0	1	cP_{95}	3	2	1	1	−1	−2
cP_{48}	2	2	1	0	0	1	cP_{96}	3	2	1	1	1	2

Small rhombohedral deformations change descriptions in the table into semi-reduced forms of hR lattices. Positive deformations allow to continuously transform cP into cF (cP1 – cP48→cF1 – cF16). Similarly, negative deformations transform cP into cI (cP49 – cP96→cF1 – cF16). Twelve metrics (cP1 – cP12 and cP49 – cP60) coincide. The cP0 case links all primitive and centered cubic lattices by rhombohedral deformations.

Table 6. Non-semi-reduced descriptions of *cP* lattices close to semi-reduced *hR*.

For all *cP* descriptions in **Table 6**, the filtering of *V* fails in obtaining a complete set of symmetry matrices and assigning *cP* Bravais type, but in all cases the matrices comprise at least one complete *hR* group, indicated geometrically by symbols of threefold axes with corresponding directions and Miller indices. Rhombohedral deformations based on obtained (*hkl*)'s and assumed $\varepsilon > 0$ transform cP_1-cP_{48} into 60 semi-reduced variants of some *hR* lattice. Together with 4 variants arising from cP_0 (1,1,1,0,0,0), the total number is again 64. All are equi-distanced from the *cP* lattice. Similar analysis leads to 64 semi-reduced *hR* descriptions obtained from cP_{49}-cP_{96} and cP_0 by rhombohedral distortion with $\varepsilon < 0$.

In the neighborhood of cubic symmetry, the semi-reduced *hR* lattices reveal distorted rhombohedral *cF*, *cI*, or *cP* pseudo-symmetries and exact *hR* symmetry. The distortion can be extracted from the lattice metric using the geometric information from the 'strict' threefold axis. The distance to the border given by ε or $\Delta d/d$ value does not depend on the lattice description (64 semi-reduced variants). Such distance corresponds to the angular differences: α-60°, α-90°, α-109.47° for a conventional description of *hR* lattice.

6. Distances between *hR* and monoclinic lattices: composed deformations

As mentioned earlier, the symmetry axis splits orthogonally 3D lattice into union of 1D lattice and 2D lattice and is stable during uniaxial deformation in 1D direction. But a twofold axis is less restrictive in comparison with higher order axes, and in this case 2D lattice can also be modified. This complicates the modeling of *mC*–*hR* border and the calculation of distance from *mC* to *hR* lattices. The modeling is simplified if the *hR* lattice description is restricted to the conventional form ($a = b = c$, $\alpha = \beta = \gamma < 120°$). The geometric interpretation of symmetry is characterized by dual symbols: 3^+[111](111), 3^-[111](111), 2[01–1](01–1), 2[1–10](1–10), 2[−101](−101). The dot product [*uvw*]·(*hkl*) is 2 for all twofold axes, which means that deformation ε (*hkl*), where (*hkl*) = (01–1), (1–10), (−101), transforms an *hR* lattice to the centered monoclinic, for example, *mC*. Other ε deformations are also possible. For a twofold axis in [*uvw*] direction, any deformation ε (*hkl*), where [*uvw*]·(*hkl*) = 0, retains the given twofold symmetry. Moreover, small deformations are additive and their (*hkl*)-type can be recognized by geometric images (**Table 7**).

Δa/a [%]	Δb/b [%]	Δc/c [%]	Δα [°]	Δβ [°]	Δγ [°]	δ [°]	Operation
Deformation 0.001·(01–1) →*mC* (1, 1.0320, 1.7143, 90°, 123.2094°, 90°)							
0.0000	0.0000	0.0000	0.0000	0.0000	0.0000	0.0000	2[01–1](01–1)
0.0500	−0.0500	0.0000	−0.0800	0.0800	0.0000	0.0934	2[1–10](1–10)
0.0500	0.0000	−0.0500	−0.0800	0.0000	0.0800	0.0934	2[−101](−101)
0.0500	0.0000	−0.0500	−0.0800	0.0000	0.0800	0.0000	3 + [111](111)
0.0500	−0.0500	0.0000	−0.0800	0.0800	0.0000	0.0000	3-[111](111)
Deformation 0.001·(011) →*mC* (1, 1.0301, 1.7155, 90°, 123.1840°, 90°)							
0.0000	0.0000	0.0000	0.0000	0.0000	0.0000	0.0000	2[01–1](01–1)
0.0500	−0.0500	0.0000	0.0496	−0.0496	0.0000	0.0556	2[1–10](1–10)

Δa/a [%]	Δb/b [%]	Δc/c [%]	Δα [°]	Δβ [°]	Δγ [°]	δ [°]	Operation
0.0500	0.0000	−0.0500	0.0496	0.0000	−0.0496	0.0556	2[−101](−101)
0.0500	0.0000	−0.0500	0.0496	0.0000	−0.0496	0.0532	3 + [111](111)
0.0500	−0.0500	0.0000	0.0496	−0.0496	0.0000	0.0532	3-[111](111)
Deformation 0.001·(01–1) + 0.001·(011) →*mC* (1, 1.0320, 1.7155, 90°, 123.1840°, 90°)							
0.0000	0.0000	0.0000	0.0000	0.0000	0.0000	0.0000	2[01–1](01–1)
0.1000	−0.0999	0.0000	−0.0304	0.0304	0.0000	0.0774	2[1–10](1–10)
0.1000	0.0000	−0.0999	−0.0304	0.0000	0.0304	0.0774	2[−101](−101)
0.1000	0.0000	−0.0999	−0.0304	0.0000	0.0304	0.0532	3 + [111](111)
0.1000	−0.0999	0.0000	−0.0304	0.0304	0.0000	0.0532	3-[111](111)

Geometric images of monoclinic simple deformations 0.001·(01–1), 0.001·(011) and composed deformation 0.001·(01–1) + 0.001·(011) = 0.002·(010). Resulting monoclinic lattice parameters are given explicitly.

Table 7. Examples of the border *hR*-*mC* models for *hR* lattice (*a*,*b*,*c* = 1, *α*,*β*,*γ* = 62°).

The ε-deformations are additive by the definition, but this feature is also valid for geometric images (excluding *δ*) in the vicinity of a border, as was exemplified in **Table 7**. This feature means that more complicated images can be decomposed and explained by a few ε-deformations, at least in theory. In this situation, the goal is to obtain *maxdev* ≈ 0 by uniaxial deformations of a probe cell, where deformation types (*hkl*)'s can be predicted from the geometric images. The introductory application of such analysis is shown in the following two real-life examples.

7. The distances for phospolipase A_2

For a comparative study of different distances between a probe cell and the items in protein database (PDB), McGill and others [2] used unit cells of phospolipase A_2 discussed in [12], which concluded that items 1g2x, 1u4j, and 1fe5 describe the same structure. Study, among other interesting conclusions, showed a similarity only between 1g2x and 1u4j cells for all applied distances. This result is also confirmed by analysis based on *ε* distances (**Table 8**).

1g2x	80.949	80.572	57.098	90°	90.35°	90°	C
1u4j	80.36	80.36	99.44	90°	90°	120°	R
1fe5	57.98	57.98	57.98	92.02°	92.02°	92,02°	P
1g2x	3260.18	3261.15	3261.15	15.22	14.12	14.12	original
	ε = −1.04·(011) +0.07·(01–1)			deformation: monoclinic			
	3260.18	3260.18	3260.18	14.12	14.12	14.12	hR
	ε = −14.12·(111)			deformation: rhombohedral			
	3246.06	3246.06	3246.06	0.00	0.00	0.00	cP

1u4j	3251.28	3251.28	3251.28	22.41	22.41	22.41	original
	ε = −22,41·(111)			deformation: rhombohedral			
	3228.87	3228.87	3228.87	0.00	0.00	0.00	cP
1fe5	3361.68	3361.68	3361.68	−118.49	−118.49	−118.49	original
	ε = 118,49·(111)			deformation: rhombohedral			
	3480.17	3480.17	3480.17	0.00	0.00	0.00	cP

Upper lines give standard Bravais descriptions for three items. Corresponding three parts compare original metric tensors, ε distances to higher symmetry borders, and metric tensors of these borders for each item.

Table 8. Original cell data for PDB items (1g2x, 1u4j, 1fe5) and ε distances to higher symmetry borders.

The monoclinic deformation of 1g2x cell is very small. Rhombohedral distances ε to the cubic border are similar for 1g2x and 1u4j, but drastically different in comparison with that in 1fe5. Moreover, the different sign suggests that if one agrees that all three items describe the same structure it must also allow the possibility that the true symmetry is cubic. It is also visible that this method is sensitive for much smaller (then analyzed) deviations from the symmetry borders.

8. *hR-mC* dilemma in α-Cr_2O_3, α-Fe_2O_3, $CaCO_3$

The crystal structures of $BiFeO_3$, as well as of α-Cr_2O_3, α-Fe_2O_3, $CaCO_3$ are usually described as trigonal, but there are motivations that come from systematic (*hkl*) peak broadening and anisotropic microstrains, indicating monoclinic deformations, to assume that an average metric structure reveals monoclinic, that is, broken symmetry. [3, 4] Such broadening is systematic and increases with the crushing polycrystalline powders in a planetary mill and thus, at least in theory, can modify symmetry. High-resolution synchrotron radiation powder diffractions and Rietveld refinement were used in [3, 4] to obtain precise cell parameters. Values of agreement factors obtained with the Rietveld refinement of the trigonal and monoclinic models were very similar. The authors concluded that the lowering of symmetry should result in splitting some diffraction lines, which was not observed.

Let us look at the published data obtained for the monoclinic model [3, 4]. Cell parameters were recalculated to the primitive form, which was not Niggli. The strict symmetry had geometric description 2 [1–10](1–10). Therefore, it was assumed that composite deformation ε_1(1–10) + ε_2(110) brings these monoclinic cells to the rhombohedral ones. The $BiFeO_3$ cell data were not available but all the data for α-Cr_2O_3, α-Fe_2O_3, $CaCO_3$ and different milling times reveal similar values $\varepsilon_1 = \varepsilon_2 \approx -0.004$. Values do not depend on the milling time, even if systematically broadened peaks are shown. Deviations from *hR* borders in the form of $\Delta d/d \approx -0.0004$ mean that it is practically not possible to observe the line splitting. A strict and systematic relationship $\varepsilon_1 = \varepsilon_2$ seems to be nonphysical, rather a result of the monoclinic constrains in Rietveld refinements. Despite the high precision of synchrotron powder diffraction, a monoclinic lattice deformation was not metrically determined.

9. Summary

Generally, border problems cannot be overlooked in s.r.d. Small, but not negligible, values of discrepancy parameters indicate the border problem and give some measure to the higher symmetry border. Deviations in isometric actions on the investigated cell can be explained by monoaxial deformations measured by parameter ε or by $\Delta d/d$, which is more informative for powder diffraction investigations.

Moreover, ε is not dependent on the choice of lattice representation in s.r.d. It was explicitly shown in **Tables 4** and **5**. These data can be also used for testing other definitions of distances, because 64 items describe the same rhombohedral lattice (distances between items should be zero and between each item and the cubic *cF* and *cI* lattices should be fixed).The situation is more complicated in the vicinity of *cP* border. Pseudo-*cP* symmetry cannot be recognized for most s.r.d representations of *hR* lattices, since they are similar to non-semi-reduced *cP* descriptions listed in **Table 6**. But there is still a possibility to select such *hR* description, which is simultaneously Niggli-reduced, and to find the distance to cP_0.

The concept is outlined and tested for *hR* lattices, but for wider applications other lattice types (especially cubic) should be investigated.

Author details

Kazimierz Stróż

Address all correspondence to: kazimierz.stroz@us.edu.pl

Faculty of Computer Science and Material Sciences, University of Silesia, Katowice, Poland

References

[1] Maciček J, Yordanov A. BLAF – A robust program for tracking out admittable Bravais lattice(s) from the experimental unit-cell data. Journal of Applied Crystallography. 1992;**25**:73-80

[2] McGill KJ, Asadi M, Karkasheva MT, Andrews LC, Bernstein HJ. The geometry of Niggli reduction: SAUC – Search of alternative unit cells. Journal of Applied Crystallography. 2014;**47**:360-364

[3] Stękiel M, Przeniosło R, Sosnowska I, Fitch A, Jasiński JB, Lussier JA, Bieringer M. Lack of a threefold rotation axis in α -Fe_2O_3 and α -Cr_2O_3 crystals. Acta Crystallographica. 2015;**B71**:203-208

[4] Przeniosło R, Fabrykiewicz P, Sosnowska I. Monoclinic deformation of calcite crystals at ambient conditions. Physica B. 2016;**496**:49-56

[5] Himes VL, Mighell AD. A matrix method for lattice symmetry determination. Acta Crystallographica. 1982;**A38**:748-749

[6] Himes VL, Mighell AD. A matrix approach to symmetry. Acta Crystallographica. 1987;**A43**: 375-384

[7] Le Page Y. The derivation of the axes of the conventional unit cell from the dimensions of the Buerger-reduced cell. Journal of Applied Crystallography. 1982;**15**:255-259

[8] Stróż K. Space of symmetry matrices with elements 0, ±1 and complete geometric description; its properties and application. Acta Crystallographica. 2011;**A67**:421-429

[9] Stróż K. Symmetry of semi-reduced lattices. Acta Crystallographica. 2015;**A71**:268-278

[10] Stróż K. A systematic approach to the derivation of standard orientation-location parts of symmetry-operation symbols. Acta Crystallographica. 2007;**A63**:447-454

[11] Andrews CL, Bernstein HJ. The geometry of Niggli reduction: BGAOL – Embedding Niggli reduction and analysic of boundaries. Journal of Applied Crystallography. 2014;**47**:346-359

[12] Le Trong I, Stenkamp RE. An alternate description of two crystal structures of phospholipase A_2 from *Bungarus caeruleus*. Acta Crystallographica. 2007;**D63**:548-549

Chapter 5

Linking Symmetry, Crystallography, Topology, and Fundamental Physics in Crystalline Solids

Elena Derunova and Mazhar N. Ali

Additional information is available at the end of the chapter

http://dx.doi.org/10.5772/intechopen.74175

Abstract

In this chapter, we briefly introduce the evolution of symmetry as a mathematical concept applied to physical systems and lay the mathematical groundwork for discussion of topological physics. We explain how topological phases, like the Berry phase, can be obtained from a gauge symmetry of a quantum system. Also, we introduce numerical tools (e.g., Chern numbers, Wilson loops) for topological analysis of chemical solids based on the crystal structure and corresponding electronic structure.

Keywords: topological physics, topological quantum chemistry, Weyl semimetals, Dirac semimetals, Hall effects, Berry phase, Berry curvature

1. Introduction

This past century saw a dramatic advancement of our understanding of the physical world driven by the dethronement of classical physics by the combined discoveries of relativistic and quantum mechanics. From those revelations, and the subsequent intensive fundamental investigations, a new age of unprecedented rapid technological progress was ushered in. These physical theories were heavily inspired by differential geometry and linear algebra, like in the case of reinterpreting gravitation as a curvature of space or in the case of reimagining objects as both particles and waves. Today, another evolution in our understanding of physics is underway, this time inspired by the ideas of topology and symmetry. While the application of these concepts is slowly beginning to extend to all branches of science, the recent ramifications of their adaptation to crystal structures, electronic structures, and electronic properties have been profound. So much so, the 2016 Nobel Prize in Physics was awarded to Duncan Haldane, J. Michael Kosterlitz, and David J. Thouless for theoretical discoveries in topological phase

transitions and topological phases of matter. Ranging from superconductivity, superfluidity, quantized Hall effects and now to new quasiparticles, the ideas of topology and symmetry are revealing new, unexpected properties and states of matter.

The evolution of physical theories matches well with the evolution of symmetry as a mathematical concept. At first, symmetry was considered just as a transformation of space which conserves certain qualities. However, mathematicians later realized that all such transformations can form a group which can be a characterization of the quality. Crystallographic groups were born from this understanding of symmetry. Conserved, in this case, are the relative positions of atoms in space because the only allowed transformations are linear transforms (rotations and translations, i.e., Galilean transformations), which saves distances between points in space. Such an approach was enough for the dominant idea, at the time, of linear space and was consistent with Newton's classical mechanics. After Einstein's revolution, however, it turned out that distances between points are not necessarily conserved in real life. Since particles in crystals can move with velocities close to the speed of light, modern transport theory in crystals cannot ignore relativistic effects, requiring an expanded conceptualization of symmetry.

This issue was mitigated in quantum mechanics with the idea of nonhomogeneous space. The main equations there are written not for a vector in space but for a wave function, i.e., one does not have to deal with a real space of points but with a Hilbert space of possible transformations of all points in the space. Used in this way, the properties of the space itself are less important than the properties of the transformations. This transformation of space can include real numbers as well as complex numbers. Since complex numbers cannot be measured and observed, physicists consider the square of the wave function at some point as a probability to detect a particle at that point. Since the idea of a fixed position in space is not valid anymore, a new understanding of symmetry is required. Previously, symmetry transformations affected points in space; however, in quantum mechanics, the transforming object is a function, and symmetry operations are actually maps between functions a.k.a. an operator. In general, an operator is not required to have an expression, but for certain special functions, an action of the operator can be expressed as simply as, for example, a multiplication by a number. This number is called an eigenvalue, and this function is called eigenfunction (also often referred to as eigenvector or eigenstate). Both are characteristic of the operator. In the case where the eigenvalue is one (or is a strictly unitary operator), the operator will, of course, not change the eigenfunction. So if the wave function is an eigenfunction of the corresponding unitary operator of a transformation, the wave function can be considered to have a symmetry based on the transformation. In practice, the determination of eigenvalues is not typically such a trivial task, especially when the operator does not have an expression. However for linearly bounded operators in a Hilbert space, there is always a representation via the scalar product. Due to the Riesz representation theorem, any linearly bounded operator can be represented as a scalar product with another function. Note that here the scalar product is not the same as the usual product of numbers. For quantum mechanical operators, it can be written using integral notation, which is part of why physicists consider these kinds of operators as observable. Another important note to remember is that a wave function in quantum mechanics is also a map to complex space. As mentioned earlier, a symmetry operator's eigenvalue should be 1,

http://dx.doi.org/10.5772/intechopen.74175

but the complex plane has two ways to achieve this: a unit in the real part which is, of course, 1 and also a unit in the imaginary part which is i. Thus the symmetry operator can be unitary or anti-unitary, respectively. Since the wave function is the solution of Schrodinger equation, the symmetry operator must also commute with the Hamiltonian of the system (this ensures that the operator acting on the wave function returns an eigenfunction of the Hamiltonian). In this way, a symmetry group of the wave function can be generalized to a group of operators, which have eigenvalues with an absolute value equal to one. This group is called a gauge group, and this symmetry causes topological phases of the wave function, which will be explained in this chapter.

2. Preliminaries

In order to use a consistent description, we first formulate basic mathematical definitions. The set $G = \{g_1, g_2, \ldots, g_n\}$ with the operation denoted by " $\cdot$ " is called a "group" if the following conditions hold:

- Every element $g = g_i \cdot g_j$ belongs to G.
- There exist unique unitary element $e \in G$ such that $e \cdot g = g \cdot e = g, \forall g \in G$.
- For every element $g \in G$, there exist inverse element g^{-1} such that $g^{-1} \cdot g = g \cdot g^{-1} = e$.
- We can combine elements of G in pair in any order $\left(g_i \cdot g_j\right) \cdot g_k = g_i \cdot \left(g_j \cdot g_k\right)$.

If in addition, if the order of the operation does not matter, i.e., $g_i \cdot g_j = g_j \cdot g_i$, the group is called commutative or abelian, otherwise it is called non-commutative or non-abelian.

If we have the commutative group V with the operation "+", we also can multiply every element $x \in V$ by a number, either real or complex, in the following way:

- $1x = x, \forall x \in V$,
- $(a+b)x = ax + bx, \forall a, b - \ numbers, \ \forall x \in V$,
- $a(x+y) = ax + ay, \forall a - \ number, \ \forall x, y \in V$.

In this case, V is called a vector space (real or complex, respectively), and any element $x \in V$ is called a vector. The mapping $A : V \to V$ which sets the relationship between elements of the space V is called an operator. If the operator A satisfies the following properties,

$$A(cx) = cA(x), \quad A(x+y) = A(x) + A(y), \ \forall c - number, \ \forall x, y \in V, \tag{1}$$

then it is called a linear operator, or linear transformation, of the space V. The linear transformation between two different vector spaces V_1, V_2 is defined in the same way. A set of invertible linear transformations form a group with operation $A_1 \circ A_2$, which is the composition of the operators, and this group is called a general linear group on V and denoted by $GL(V)$.

If a physical system is described by some vector v, then a map defining the relationship between a real number and that vector is called a functional. Note that since we can only add vectors and multiply them by a number, the functionals $f : V \to \mathbb{R}$ which are useful for physical applications are the linear transformations, called linear functionals. The space of all such linear functionals on V is called a dual space and is denoted by V^*. Note that without the multiplication of two vectors in V, we cannot define analogues of polynomial functions on V. To obtain nonlinear functionals on V, we will define the multiplication of two vectors that give a number as a result. This makes functionals acting on V similar to the functions acting on the space of real numbers $\mathbb{R}$. The multiplication denoted by "$< x, y >$" is called the scalar product and satisfies the following conditions (assuming that V is a complex vector space and $\overline{x}$ is the complex conjugation):

- $< x, y >= \overline{< y, x >}, \forall x, y \in V,$
- $< x, x > \geq 0$, *and* $< x, x >= 0 \leftrightarrow x = 0, \quad \forall x \in V,$
- $< a(x + y), z >= a < x, z > + a < y, z >, \forall a \in \mathbb{C}, \quad \forall x, y, z \in V.$

The vector space with the scalar product is called a Hilbert space. The two vectors x and y are called orthogonal if $< x, y >= 0$. The $\sqrt{< x, x >} \equiv \|x\|$ is called the norm of the vector x, and it returns magnitude of the vector x, like the length of a vector in real space. Usually Hilbert spaces consist of functions; therefore, elements of Hilbert spaces are denoted simply by Greek letters.

The maximal set of vectors $\{\varphi_i\}_{all\ \ i}$ in a Hilbert space such that

$$\sum_i a_i < \varphi_i, \varphi_j >= 0 \leftrightarrow a_i = 0, \quad \forall i, \tag{2}$$

is called a basis. If the following conditions also hold:

$$\|\varphi_i\| = 1, \ < \varphi_i, \varphi_j >= \delta_{ij}, \quad \forall i, j, \tag{3}$$

then it is called an orthonormal basis. In this case, any vector $\psi \in V$ can be decomposed into the sum

$$\psi = \sum_i a_i \cdot \varphi_i, \tag{4}$$

where a_i are numbers. If the number of basis vectors is finite, e.g., n, then ψ can be written just as a vector $(a_1, a_2 \ldots, a_n)$. Note that space V can have different bases and ψ can be represented as vectors in different ways. The operator on V in this case can be written just as an $n \times n$ matrix.

In general, the symmetry of the physical system described by the vectors from V should make a group G composed of operators on V which are not necessarily linear. Of course it is easier to deal with linear operators; therefore, we introduce the concept of a representation of the group. The representation of the group $G = \{g_1, g_2, \ldots, g_n\}$ with the operation "$\cdot$" on the vector space V is the mapping $p : G \to GL(V)$, which preserves the group operation "$\cdot$" in the following way:

$$p(g_1 \cdot g_2) = p(g_1) \circ p(g_2). \tag{5}$$

For example, the spatial symmetries of a crystal belong to a subgroup of group $GL(\mathbb{R}^3)$, but the symmetries of quantum objects are usually represented as a subgroup of $GL(\mathbb{C}^n)$. The relationships between those representations give rise to many interesting properties of crystals.

3. Spacial symmetries

Assume we have a point $x \in \mathbb{R}^3$ and we have a group $G_x = \{g_1, g_2, \ldots, g_m\}$, where g_i is a linear transformation of space that leaves x fixed. The group G_x is called a point group. Now if we act on the point x by translating by a lattice vector R:

$$T_R(x) = x + R, \quad x \in \mathbb{R}^3, \tag{6}$$

we obtain the set of points:

$$O_{T_R}(x) = \{y \in \mathbb{R}^3 : y = gx, \quad \forall g \in T_R\}, \tag{7}$$

which is called the orbit of the action of the group of translations T_R on the element x.

If then we act by every element g_i on the point $y \in O_{T_R}$, we obtain a crystal lattice, i.e., the set of points in space that remain unchanged under the action of the group $G = G_x \times T_R$. In this case, G is called a symmorphic space group. It means the quotient space

$$R \setminus T_R = \{x \in \mathbb{R}^3 : y = gx, \forall g \in T_R, \forall y \in \mathbb{R}^3\} \tag{8}$$

has a point, x, with site group symmetry that is isomorphic to the original point group G_x [1].

Otherwise, if the lattice is invariant under the action of the group of linear transformations of a space that cannot be decomposed into $G = G_x \times T_R$ at least for one point x inside the unit cell, G is called nonsymmorphic. In this case, some operations of the group G are not separable into a combination of rotation and translation by lattice vectors, i.e., they should be complex operations like glide or skew operations. Examples of nonsymmorphic symmetry are shown in **Figure 1**. The converse, in general, is not true, because some particular combinations of glides or screws can leave one point inside unit cell fixed.

Any linear transformation L of $\mathbb{R}^3$ can be expressed in the following form:

$$L = Ax + b, \forall x \in \mathbb{R}^3, \tag{9}$$

where A is 3×3 matrix and b is a vector in $\mathbb{R}^3$. All 3×3 matrices with a nonzero determinant and the multiplication operation form a group $GL(\mathbb{R}^3)$. The matrix A should have a determinant of 1 or -1, where 1 corresponds to proper rotations and -1 corresponds to improper

Figure 1. Symmorphic and nonsymmorphic symmetry.

rotations or reflections. All such matrices form a subgroup of $GL(\mathbb{R}^3)$, which is called an orthogonal group and is denoted by $O(\mathbb{R}^3)$. Thus, the point group G_x is a subgroup of the group $O(\mathbb{R}^3)$ [2].

4. Quantum observables

Now consider a function $\psi(x) : \mathbb{R}^3 \to \mathbb{C}$ that sets a correspondence between every point $\mathbb{R}^3$ and point $\mathbb{C}$. This function is called a wave function and represents a state of quantum system, like an electronic state in a crystal.

We can also define the sum and product of such functions and use multiplication by a number to represent interaction of the particles with each other or external forces:

$$(\psi + \phi)(x) = \psi(x) + \phi(x); \quad (\alpha\psi)(x) = \alpha \cdot \psi(x), \forall x \in \mathbb{R}^3, \alpha \in \mathbb{C} \tag{10}$$

$$(\psi\phi)(x) \equiv < \psi(x), \phi(x) > = \int_{\mathbb{R}^3} \psi(x)\overline{\phi(x)}dx. \tag{11}$$

The space of all such functions and operations is called $L_2(\mathbb{R}^3, \mathbb{C})$. The product is a scalar product, and thus, $L_2(\mathbb{R}^3, \mathbb{C})$ is a Hilbert space.

When an observation of a physical state is carried out, it sets a correspondence between the wave function and a real number, i.e., the observation is a linear bounded functional $f : L_2(\mathbb{R}^3, \mathbb{C}) \to \mathbb{R}$. Thus, any observable property of particles should be an operator $A : L_2{}^*(\mathbb{R}^3, \mathbb{C}) \to L_2{}^*(\mathbb{R}^3, \mathbb{C})$. Luckily, Hilbert space is self-dual, i.e., $L_2{}^*(\mathbb{R}^3, \mathbb{C}) = L_2(\mathbb{R}^3, \mathbb{C})$, and thus, A is acting on $L_2(\mathbb{R}^3, \mathbb{C})$. In this case, due to the Riesz representation theorem [3], A can be represented as scalar product $A(\psi(x)) =< a(x), \psi(x) >$. Thus any element of $L_2(\mathbb{R}^3, \mathbb{C})$ can be considered as a wave function and also as a functional; to distinguish this, the so-called "bra-ket" language is used—the wave functions are called "ket" vectors and denoted by $|\psi(x) > \in L_2(\mathbb{R}^3, \mathbb{C})$, while the functionals are called "bra" vectors and denoted by $< \psi(x)| \in L_2{}^*(\mathbb{R}^3, \mathbb{C})$—the scalar in this case is denoted by $< \psi(x)|\psi(x) >$, and the action of an operator A is denoted by $< \psi(x)|A|\psi(x) >$. Schematically the relationship between these spaces is shown in **Figure 2**.

http://dx.doi.org/10.5772/intechopen.74175

For some functions the actions of the operator can be written as multiplication by the number

$$A(\varphi) = \lambda\varphi, \quad \lambda \in \mathbb{C}. \tag{12}$$

The number λ is called the eigenvalue, and the function $\varphi(x)$ is called the eigenfunction or eigenvector. All operators considered in quantum mechanics are assumed to be Hermitian, meaning the operator has real eigenvalues and the set of its eigenfunctions $\{\varphi_i\}_i$ form an orthogonal basis [4]. Assume the operator has finite number of eigenvalues; in this case, the action of the operator on the function from the subspace spanned by eigenfunctions is expressed by the following matrix:

$$A = \begin{pmatrix} \lambda_1 & 0 & \dots & 0 \\ 0 & \lambda_2 & \dots & 0 \\ \dots & \dots & \dots & \dots \\ 0 & 0 & \dots & \lambda_n \end{pmatrix}. \tag{13}$$

One of the most important operators in quantum mechanics is the momentum operator $i\hbar\frac{d}{dt'}$ which is particularly used when analyzing a material's electronic structure or electronic energy vs. momentum map. Its eigenfunctions $\varphi_n(x)$ are called eigenstates and denoted by $|n>$. Thus, we can decompose the wave function as $\psi(x) = \sum_n c_n\varphi_n(x) = \sum_n c_n|n>$. The eigenvalues form a matrix which is called the Hamiltonian of the quantum system, and they correspond to the measured energy of the system.

If we also add the normalization condition $\|\psi(x)\| = 1$, we can consider $\psi(x)$ as a probabilistic measure. That means the functional

$$< \psi(x)|x|\psi(x) >= \int_{\mathbb{R}^3} \psi(x)x\overline{\psi(x)}dx \tag{14}$$

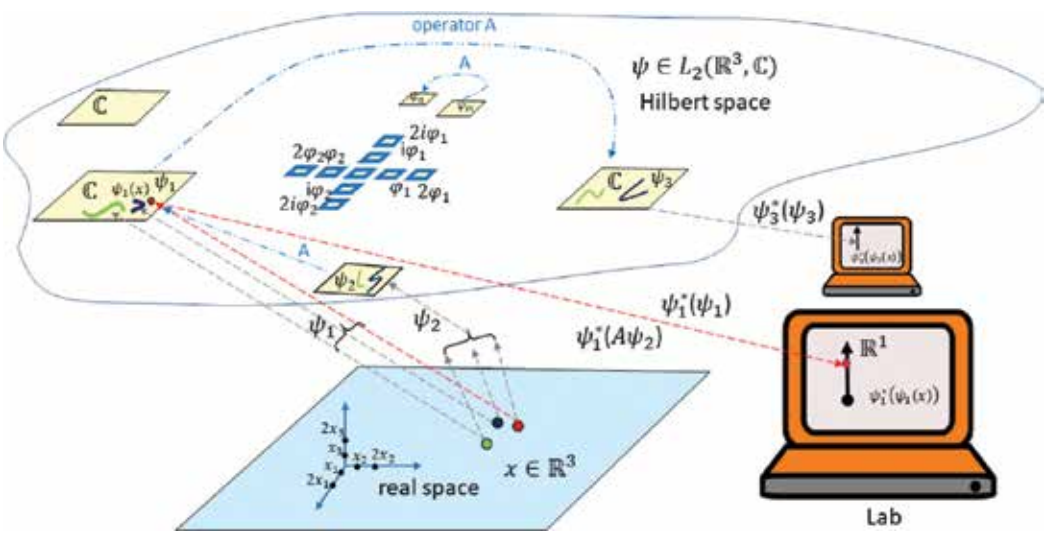

Figure 2. Different spaces used in quantum mechanics.

defines a probability to observe the particle in the position x. The $|\psi|^2$ in this case defines a probability density [4]. As we can see from **Figure 3**, different symmetries between real and imaginary parts of the wave function define different types of symmetries of the probability density.

Consider now all possible transformations of the function which preserve it as an eigenfunction of the Hamiltonian with the same eigenvalue. For the eigenfunction φ_n, the Hamiltonian acts just as multiplication by the function $\lambda_n\varphi_n$, i.e.,

$$H\varphi_n = <\lambda_n\varphi_n, \varphi_n> = \lambda_n < \varphi_n, \varphi_n> = \lambda_n\|\varphi_n\|^2 \tag{15}$$

Thus such a transformation should not change $\|\varphi_n\|^2$; if one wave function can be obtained from another via such a transformation, those wave functions are not distinguishable through observation. This group is called a gauge group and represents the symmetry group of the wave function [4]. Since

$$\forall a \in \mathbb{C}, \quad \|a\varphi_n(x)\|^2 = a\bar{a} \cdot \|\varphi_n(x)\|^2 = |a|^2 \cdot \|\varphi_n(x)\|^2, \tag{16}$$

multiplication by complex numbers with $|a| = 1$ forms the group of such transformations. These numbers lie on a unit circle in the complex plane, and the group of multiplications by such numbers is called $U(1)$ or the group of unitary transformations of the complex plane. The complex number $a = |a|(\cos(\alpha) + i \cdot \sin(\alpha))$ can be represented as an exponential function in the following way:

$$a = |a|e^{i\alpha} \tag{17}$$

$$|a| = 1 \rightarrow a = e^{i\alpha}. \tag{18}$$

Thus the action of the U (1) gauge is just a multiplication by the function $e^{i\alpha}$. If we represent the complex plane as a stereographic projection of Riemann sphere, we can illustrate U (1) action as rotation of the sphere. Schematically, it is shown in **Figure 4**.

If the wave function corresponds to a fermion, according to the Pauli principle, only two fermions with opposite sign spins can occupy the same energy state. So it is convenient to

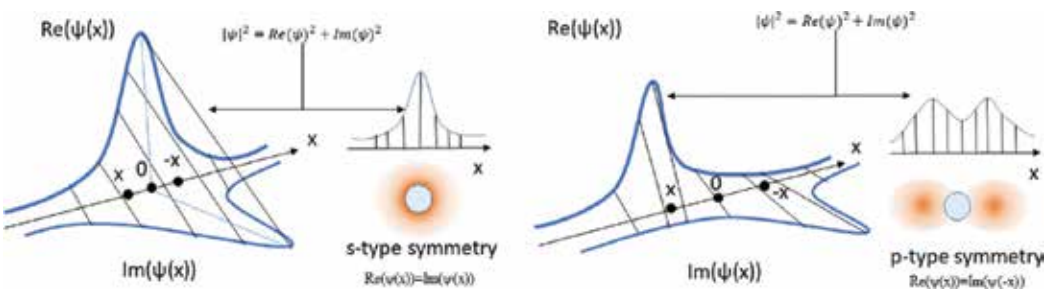

Figure 3. Symmetry of the wave function.

http://dx.doi.org/10.5772/intechopen.74175

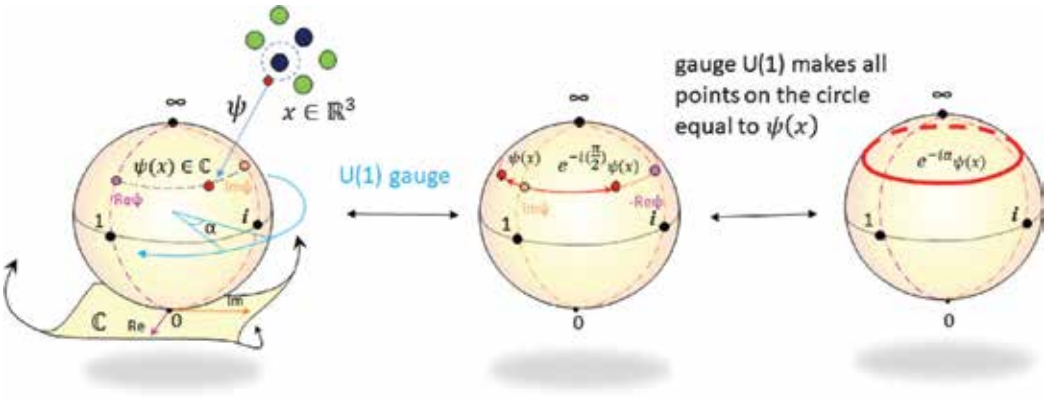

Figure 4. Action of the U (1) gauge on complex space.

consider $\psi(x)$ as having two components $\psi = \left(\psi_{up}, \psi_{down}\right)$, i.e., ψ is acting to $\mathbb{C}^2$. In this case the transformation of the vector $\left(\psi_{up}, \psi_{down}\right)$ in the two-dimensional complex space $\mathbb{C}^2$ is described by a 2×2 complex matrix A. For the same reasons as above, this matrix should be unitary, i.e., $AA^{+} = I$ (where A^{+} is a Hermitian conjugated matrix). All such matrices form a group U (2). The eigenvalues of such matrices lie on the unit circle that implies any matrix A from U (2) can be represented in the following form:

$$A = \begin{pmatrix} e^{i\alpha_1} & 0 \\ 0 & e^{i\alpha_2} \end{pmatrix} \tag{19}$$

$$A\psi = \begin{pmatrix} e^{i\alpha_1} & 0 \\ 0 & e^{i\alpha_2} \end{pmatrix} \begin{pmatrix} \psi_{up} \\ \psi_{down} \end{pmatrix} = \begin{pmatrix} e^{i\alpha_1}\psi_{up} \\ e^{i\alpha_2}\psi_{down} \end{pmatrix}. \tag{20}$$

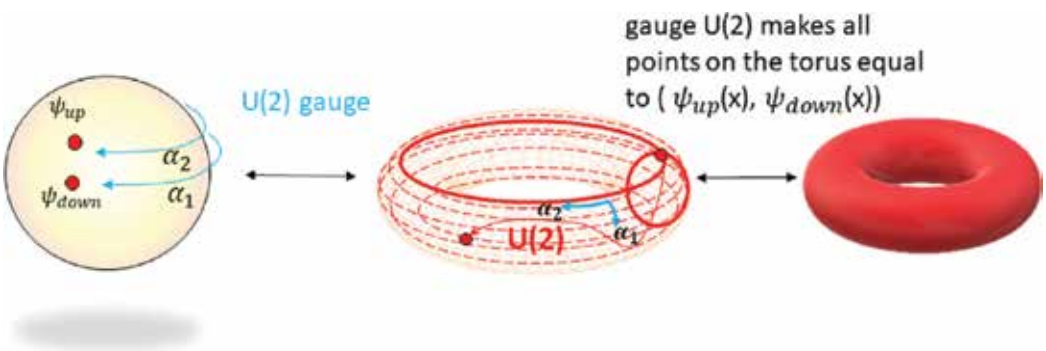

Figure 5. Action of the U (2) gauge on complex space.

Thus, if we represent $\left(\psi_{up}, \psi_{down}\right)$ as two different points on the Riemann sphere, then the action U (2) is a simultaneous rotation of the point ψ_{up}, by angle α_1 and the point ψ_{down}, by angle α_2. After the full circle rotation, we arrive at the initial point making the space of parameters (α_1, α_2) a torus. This is shown schematically in **Figure 5**.

5. Geometrical phases of the Bloch states

The dynamics of the $\psi(x)$, i.e., changing $\psi(x)$ in time, is defined by the time-dependent Schrödinger equation:

$$i\hbar \frac{\partial \psi(t,x)}{\partial t} = H\psi(t,x), \tag{21}$$

where H is the Hamiltonian and consists of all possible physical interactions (ideally) that the particle can be involved in. The wave function can be determined by solving this equation. The solution of the Eq. (21) for the eigenstates of the Hamiltonian can be written in the following form:

$$\varphi_n(t,x) = e^{-\frac{i}{\hbar}\int_0^t dt' \lambda_n(t')} \varphi_n(0,x), \tag{22}$$

For a free electron, H consists only of the kinetic energy term $-\frac{\hbar^2}{2m}\nabla^2$. Its eigenfunctions are well known as s, p, d, f, etc. (the atomic orbitals). If the electron is moving in crystal, an external periodic potential, formed by ion cores, and the average potential of all of the other electrons must be included. In this case, due to the Bloch theorem [5], the eigenfunctions of the Hamiltonian can be written as

$$\varphi_k^n(0,x) = \varphi_k^n(x) = e^{ikx} u_k^n(x), \quad u_k^n(x+R) = u_k^n(x). \tag{23}$$

The value $\hbar k$ is called the crystal momentum and is associated with an electron in the lattice. If the lattice consists of N atoms and every atom has n electrons, the full lattice Hamiltonian is the $Nn \times Nn$ matrix for the Nn electron system. Working with such high dimensional objects is not convenient. Therefore, the wave functions are categorized into bands $\left\{\varphi_n^k\right\}_{k=1..N}$ according to the local symmetry of the wave function (like shown previously in **Figure 3**), which is described by quantum numbers of the atom. After Fourier transformation, φ_n becomes a function represented in a new basis of functions which depend on crystal momentum (schematically, it is shown in **Figure 6**). This makes up the energy versus momentum band structure that is a more convenient representation of the full lattice Hamiltonian, compared with matrix notation. The band in reciprocal space, however, is not really a function; it consists of discrete points and is neither smooth nor continuous. However this band structure contains all information about the original function $\psi(x)$. Roughly speaking, the band is made up of the coordinates of the function $\varphi_n(x)$ in the basis of harmonics $\left\{e^{i\frac{2\pi n}{l}x}\right\}_{n=1..N}$ (eigenfunctions of the translation operator [6]) where N is the number of unit cells and l is the lattice parameter.

http://dx.doi.org/10.5772/intechopen.74175

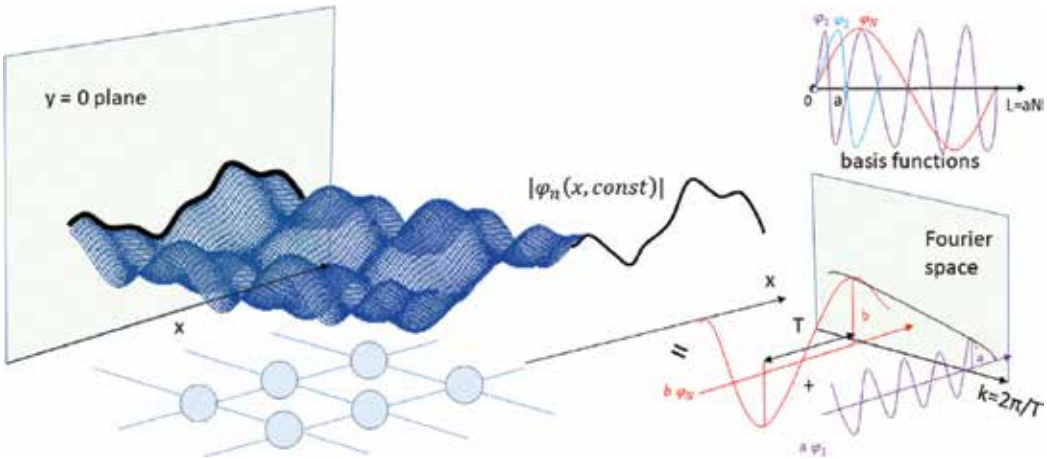

Figure 6. Representation of a function in the Fourier space.

According to the quantum adiabatic theorem during the time evolution, the system remains in the eigenstates $\varphi_n(0,x) = |n(0)>$ up to phase factor or in other words $|n(0)>= e^{-i\alpha_n}|n(t)>$. If we consider k as a parameter changing in time then

$$\frac{d\varphi(k(t),x)}{dt} = e^{ikx}\left(ixu_k(x)\frac{dk}{dt} + \partial_k u_k(x)\frac{dk}{dt}\right) \tag{24}$$

that gives rise to an additional phase factor to the solution of Schrodinger equation [7]:

$$\varphi_n(t,x) = e^{i\gamma_n} e^{-\frac{i}{\hbar}\int_0^t dt' \lambda_n(k(t'))} |n(k(t))>, \tag{25}$$

$$\gamma_n = i \int\limits_{path\ C} dk < n(k)|\frac{\partial}{\partial k}|n(k)> . \tag{26}$$

If the path C is closed, then $\gamma_n(t)$ is called the Berry phase. The expression

$$A_n(k) = i < n(k)|\frac{\partial}{\partial k}|n(k)> \tag{27}$$

is called the Berry connection, and it is the vector field over all reciprocal space. We also can define a curl of this vector field which is called the Berry curvature:

$$\Omega^n_{i,j}(k) = \frac{\partial}{\partial k_i}A^n_j(k) - \frac{\partial}{\partial k_j}A^n_i(k) \tag{28}$$

Origin of the Berry curvature in the reciprocal space is schematically demonstrated in **Figure 7**.

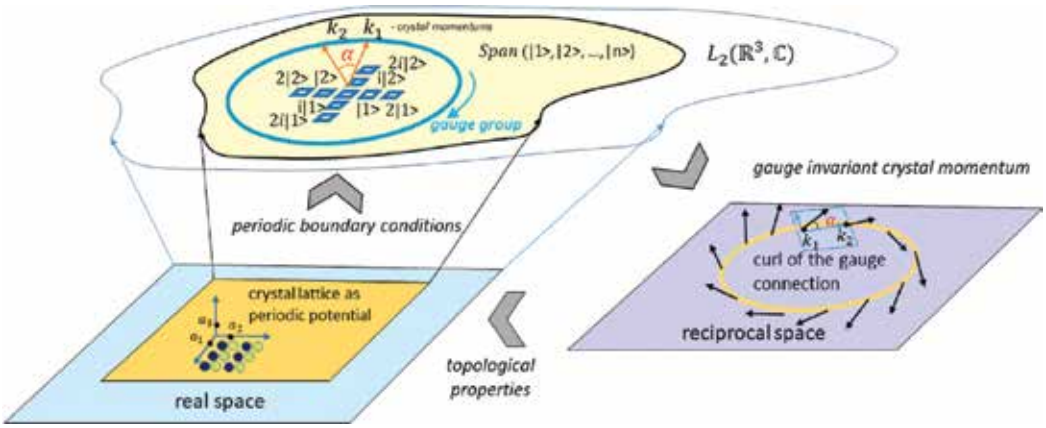

Figure 7. Berry curvature in the reciprocal space.

The Berry curvature is involved in the semiclassical equation of motion of the particle [8]:

$$\frac{dx_i}{dt} = \frac{\partial \lambda_n(k)}{\hbar \cdot \partial k^i} - \frac{dk_j}{dt} \cdot \Omega^n_{i,j}(k), \tag{29}$$

which makes the Berry curvature fundamental to various Hall effects, i.e., quantum (integer and fractional) Hall effects (QHE), the quantum anomalous Hall effect (QAHE), and the quantum spin Hall effect (QSHE) [9–11]. The QAHE is where an anomalously large current is generated orthogonal to the applied electric field without application of an external magnetic field. The QSHE is where a spin current is generated orthogonal to the applied electric field also without application of an external magnetic field.

Notice that if we change direction of time $t = -t$, we change the route from counterclockwise to clockwise in the path integrals. If time reversal symmetry is broken and the clockwise integral is *not* equal to the counterclockwise integral, it requires the Berry connection to have a nonzero curl, i.e., nonzero Berry curvature.

If time reversal symmetry is not broken, the Berry curvature still can be nonzero due to spacial symmetries. In this case, analysis can be done using topological indices resulting from the band structure.

6. Gauge action on the reciprocal space

First consider a one-dimensional case. As it was shown before, the U (1) gauge action can be represented as multiplication by the factor $e^{i\alpha}$. For an electron in a crystal, it has the following form:

$$e^{i\alpha}\varphi(x) = e^{i\alpha}e^{ikx}u_k(x) = e^{i(kx+\alpha)}u_k(x). \tag{30}$$

http://dx.doi.org/10.5772/intechopen.74175

Thus the action of the gauge can be considered as an additional phase factor or shift by α in reciprocal space. So the gauge allows the change of parameter k in time, and all geometrical phases described above can be considered a result of the gauge symmetry. Schematically this is shown in **Figure 8**.

The gauge symmetry is the conservation of the eigenvalues and eigenstates of the momentum operator. The eigenstates of the momentum operator in a crystal are assumed to also be eigenstates of the operator of translation by a lattice vector. Orthogonality of the eigenstates implies that bands in the band structure should not intersect, i.e., not have identical E and k values. If two bands intersect that means that the corresponding eigenstates $|n>, |n+1>$ are not orthogonal and the corresponding matrix representing the action of the Hamiltonian has off-diagonal terms. This is contradictory to the Hermitian rules of the Hamiltonian, i.e., its eigenstates should be orthogonal. This can happen when the eigenstates of the translation operator are not a suitable set of functions to form a basis. But how can this occur?

The Hamiltonian for electrons in the crystal lattice is usually constructed from a tight-binding model and the linear combination of the atomic orbitals (LCAO) [12]. Since the crystal Hamiltonian has the following form:

$$H = -\frac{\hbar^2}{2m}\nabla^2 + (terms\ \ representing\ \ interactions), \tag{31}$$

it is reasonable to assume that eigenstates of the electrons in the lattice do not differ strongly from the eigenstates of the free electron Hamiltonian $-\frac{\hbar^2}{2}\nabla^2$ which are s, p, d, f, etc. orbitals. Thus we can represent the full lattice Hamiltonian as linear combinations of atomic orbitals according to the space group symmetry, which is the basic logic of *molecular* orbital theory. If the space group is nonsymmorphic, then there is also translation by a fraction of a lattice vector that generates additional eigenstates that, in combination with other symmetries, give rise to degeneracies in the band structure.

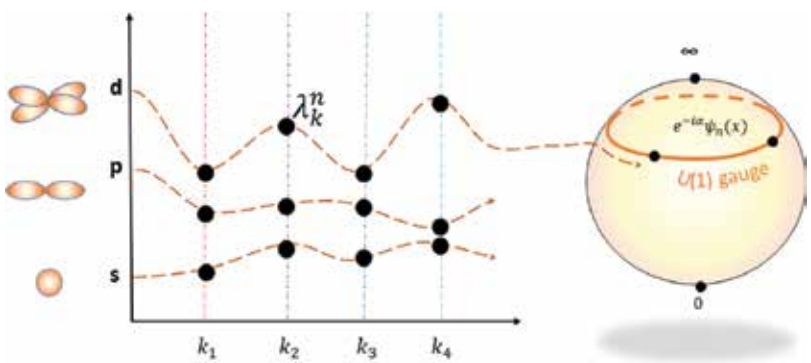

Figure 8. Gauge connection on the band structure.

To understand this we can introduce Wannier functions as bases for representation of the eigenstates of the Hamiltonian, instead of eigenstates of a translation operator, as basis. The Wannier functions can be obtained from the Bloch eigenstates in the following way [13]:

$$\phi_R^n(x) = \frac{V}{2\pi^3} \int_{BZ} dk e^{-ikR} \psi_k^n(x), \tag{32}$$

where V is the real space primitive cell volume. The Wannier functions essentially let one transform the band structure back from reciprocal space to real space, allowing relatively easy application of symmetry and the calculation of real space properties like the quantum spin Hall effect.

Now let us consider higher dimensions. The 1D band structure is the cross section of a higher-dimensional picture. In this case the anti-crossing point can remain a point in higher dimensions but may also be a line or even surface in a 3D space as illustrated below. While for the 2D case, we can still plot a 2D band structure and distinguish points from a line just visually, in 3D it becomes quite complicated. The typical procedure is to project full 3D band structure on various surfaces and analyze the series of projections. Schematically, this is shown in **Figure 9**. A degenerate point in the band structure, which remains a point on the Fermi surface, is called Dirac point or in spinful case Weyl point. An example of the calculated Dirac point of $HgTe$ [14] and the measured Dirac point (via ARPES) of Sb_2Te_3 [15] is shown in **Figure 10**.

There are ways to avoid degeneracy, however. If we consider the spinful case with U (2) gauge and include a spin orbit coupling (SOC) term in the Hamiltonian, the two degenerate states become one connected state in terms of the two-component wave function. In this case, the Dirac point becomes a source of Berry curvature and thus gives nontrivial spin-dependent transport properties like the anomalous and spin Hall effect.

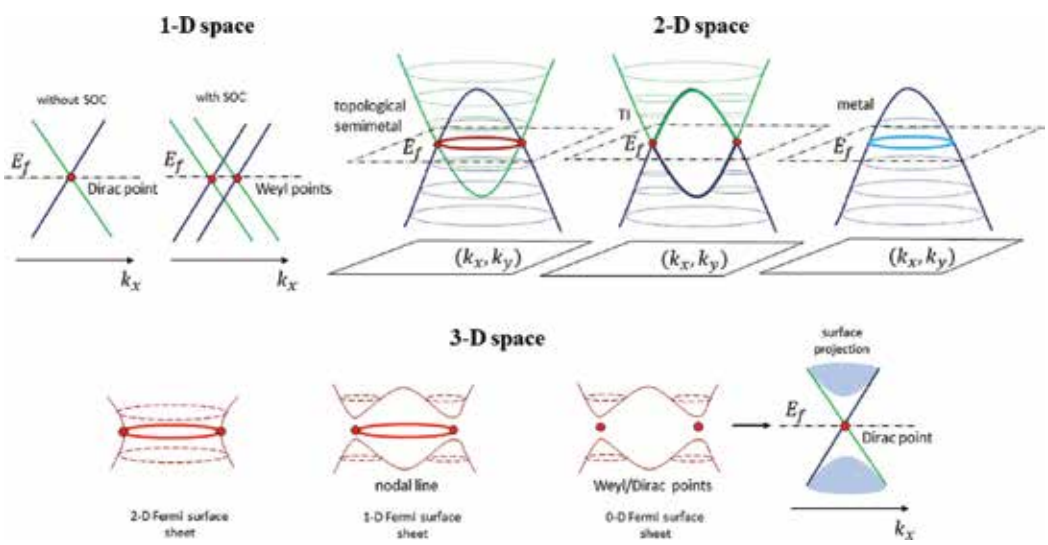

Figure 9. Degenerate manifolds in the band structure.

http://dx.doi.org/10.5772/intechopen.74175

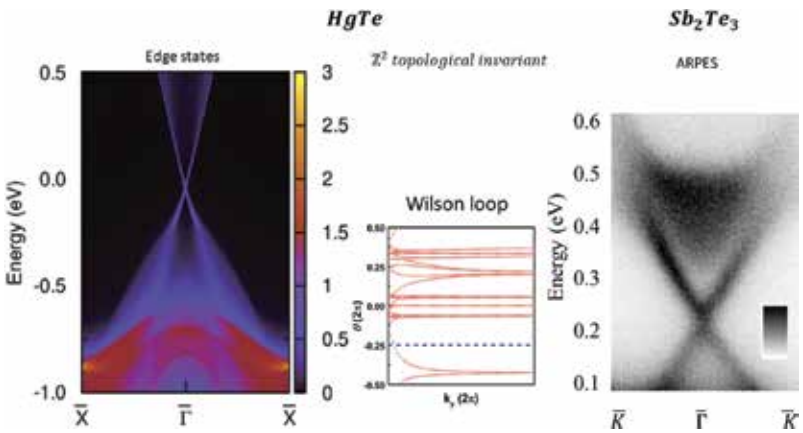

Figure 10. Numerical and experimental observation of Dirac cone [16].

Another way to do anti-crossing analysis is to use topological indices. This numerical method is the basis for the algorithmic analysis of space group symmetry and their possibilities of yielding varying topologically nontrivial band structures.

7. Topological indices

It turns out that existence of Hall conductance can be checked directly from the band structure and that it is an internal property of the bands. The indicator that physicists use to identify this topological property of the band structure is called the Chern number, which is the integral of the Berry curvature of the band over the entire Brillouin zone:

$$C_{ij}^{n} = \frac{1}{2\pi} \int_{BZ} \Omega_{i,j}^{n}(k) d_{k_i} d_{k_j} \tag{33}$$

In this case, the Hall conductance of the n^{th} band is proportional to the Chern number, quantized in units of $\frac{e^2}{\hbar}$ and can be calculated by the formula:

$$\sigma_{ij}^{n} = \frac{e^2}{\hbar} \cdot C_{ij}^{n} \tag{34}$$

The Chern number is a very powerful tool; it can be used not only for calculation of the Hall conductance but also to indicate a surface state. For example, the Chern number described above is the "first" Chern number, and this nonzero number indicates surface conductance for a 2D bulk insulator. For a 3D bulk insulator, higher Chern numbers can be used to indicate surface states [16].

Another way to obtain a topological index is using the Wilson loop [17]:

$$W(l) = e^{\int_l A(k)dl} \tag{35}$$

where l is a loop in k-space and $A_{ij}(k) =< u_{i,k}, \nabla_k u_{j,k} >$ is a Berry-Wilczek-Zee connection. Note for this connection we need at least a two-band system, like $\left(\psi_{up}, \psi_{down}\right)$. The Wilson loop describes a parallel transport of the gauge field along the closed loop.

Mathematically, a path between two points k_1, k_2 in k-space can be parametrized by an argument t in the following way—$k_t = tk_1 + (1-t)k_2, t \in [0,1]$—when loop $k_1 = k_2$. The Wilson loop shows how the gauge varies with crystal momentum along a closed path in k-space; the final gauge phase should be the same as initial. For example, the parameter space of the U (1) gauge is a circle; thus, moving along a loop in k-space the gauge phase can be either unchanged or equal to an integer number of full circles ($2\pi n$). We can consider also the class of equivalent loops: loops that give one circle of phase, two circles, etc. These classes of equivalent loops form a group, called a fundamental group [18]. As it was shown before, the parameter space of the U (2) gauge is a torus. The torus has two types of loops: one which shrinks into a point and one which does not. This is known as fundamental group of the torus. The Wilson loop distinguishes those cases and yields a $\mathbb{Z}^2$ topological classification. In **Figure 10**, an example of a calculated Wilson loop for the Se_2Te_3 is shown. The connection between red dashed lines indicated an index of 1 in the $\mathbb{Z}^2$ topological classification.

The gauge transformation is a transformation that preserves the eigenfunction, and the crystal eigenfunction is represented as a band in electronic structures. In the LCAO approach, bands

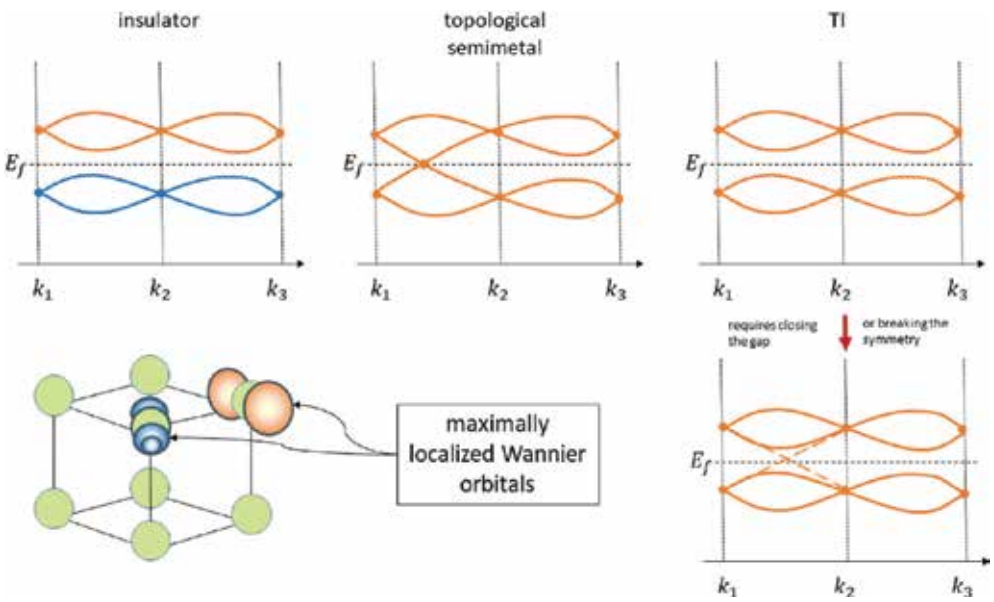

Figure 11. Connectivity of bands.

in the electronic structure can be considered also as representations of the spacial symmetry of corresponding orbitals and space group symmetry operations. Recently, a monumental and soon-to-be defining work of this field was carried out where topological analysis and classification were done for all 230 crystallographic space groups that describe all possible arrangements of atoms in space [19]. In their work, Bradlyn et al. use the fact that bands can form a connected group of bands in the band structure corresponding to Wannier functions centered at maximal Wyckoff positions. If the Fermi level occurs inside such a set of bands, the compound should be topological. If the real compound's set of bands is connected but filled by only a fraction of the number of electrons required to fully occupy the set of bands, the compound is a symmetry enforced semimetal. If such set of bands should be connected but in the real compound's band structure, the set splits into a gapped state with the Fermi level inside the gap, the compound must be a topological insulator, and the bands become connected though surface states. Schematically, this is shown in **Figure 11**.

8. Conclusion

We began this chapter by asserting that evolutions in our understanding of the physical universe have been driven by the reimagining of physical theories with different mathematical concepts and that we are currently undergoing another such evolution inspired by ideas from topology and symmetry. Starting from basic mathematical and physical concepts, we constructed the ideas of eigenfunctions, eigenstates, gauge transformations, and how symmetries affect/define them. We then showed how electrons (and their wave functions) in crystals can be understood in this manner. Finally, the power of this type of understanding was illustrated by the classification of topological phases of matter with Bradlyn's effort being the pinnacle of the body of work in the field over the last decade. Such a general work outlining the possibilities for topological phases as a matter of symmetry group will drastically change how chemists and physicists search for new topological materials; they will now be able to definitively start from a set of known possible topological outcomes, given a space group, and adjust the Fermi level using chemical/physical control to realize the type of topological state desired.

The time is arriving for topological physics to reach technological application. To this end, researchers are attempting to take advantage of the intrinsic quantum anomalous and quantum spin Hall effects (QSHE) both of which have their basis in Berry curvature which, as described earlier, can be understood from a symmetry perspective. The QSHE in particular has immediate applications to the field of spintronics, which requires large spin currents for switching the states of devices. Since anti-crossings can be sources of Berry curvature and since large Berry curvature can result in a large spin Hall effect, it follows that topological materials (which commonly have demanded or gapped anti-crossings) will be ideal candidates for spin Hall materials.

In the last 10 years, materials scientists have realized topological insulators, Dirac semimetals, Weyl semimetals, Dirac/Weyl line nodes, and compounds with three, six, and eightfold degenerate fermions Na_3Bi, Cd_3As_2 [20], $ZrSiS$ [21], WTe_2 [22], Bi_2Te_3 [23], $LuPtBi$, $YPtBi$ [24], and Ta_3Sb [25]. However almost all of this work has been done on nonmagnetic systems; the inclusion of magnetism is difficult in current density function theory calculations. For accurate

electronic structure calculations, magnetic ordering needs to be experimentally determined and verified because competing magnetically ordered states can be energetically similar. Soon, Bradlyn's type of analysis will be expanded for the 1651 magnetic space groups in three dimensions, which opens an even larger and more diverse world of possible compounds with ever more interesting properties to explore.

Author details

Elena Derunova and Mazhar N. Ali*

*Address all correspondence to: maz@berkeley.edu

Max Planck Institute for Microstructure Physics, Halle, Germany

References

[1] Fedorov E. A. S. for X-ray, and E. Diffraction. Symmetry of Crystals. American Crystallographic Association: ACA monograph; 1971

[2] Cotton F. Chemical Applications of Group Theory. India: Wiley; 2008

[3] Reed M, Simon B. I: Functional Analysis. Methods of Modern Mathematical Physics: Elsevier Science; 1981

[4] Bohm A, Loewe M. Quantum Mechanics: Foundations and Applications. Springer Study Edition. New York: Springer; 1993

[5] Kittel C. Introduction to Solid State Physics. Wiley; 2004

[6] Ashcroft N, Mermin N. Solid State Physics. HRW international editions, Holt, Rinehart and Winston, 1976

[7] D Xiao, M-C Chang, Q Niu. Berry phase effects on electronic properties. Reviews of Modern Physics. 2010;**82**:1959 (2007, Jul 2010)

[8] Haldane FDM. Berry curvature on the fermi surface: Anomalous hall effect as a topological fermi-liquid property. Physical Review Letters. November 2004;**93**:206602

[9] Sinova J, Valenzuela SO, Wunderlich J, Back C, Jungwirth T. Spin Hall effects. Reviews of Modern Physics. Oct. 2015;**87**:1213-1260

[10] Sinova J, Culcer D, Niu Q, Sinitsyn NA, Jungwirth T, MacDonald AH. Universal intrinsic spin hall effect. Physical Review Letters. March 2004;**92**:126603

[11] Gradhand M, Fedorov DV, Pientka F, Zahn P, Mertig I, Györffy BL. First-principle calculations of the Berry curvature of Bloch states for charge and spin transport of electrons. Journal of Physics: Condensed Matter. May 2012;**24**:213202

[12] Hoffmann R. Solids and Surfaces: A Chemist's View Of Bonding In Extended Structures. VCH Publishers; 1988

[13] Marzari N, Mostofi AA, Yates JR, Souza I, Vanderbilt D. Maximally localized Wannier functions: Theory and applications. Reviews of Modern Physics. October 2012;**84**:1419-1475

[14] Li J, He C, Meng L, Xiao H, Tang C, Wei X, Kim J, Kioussis N, Malcolm Stocks G, Zhong J. Two-dimensional topological insulators with tunable band gaps: Single-layer HgTe and HgSe. Scientific Reports. September 2015;**5**:14115

[15] Johannsen JC, Autès G, Crepaldi A, Moser S, Casarin B, Cilento F, Zacchigna M, Berger H, Magrez A, Bugnon P, Avila J, Asensio MC, Parmigiani F, Yazyev OV, Grioni M. Engineering the topological surface states in the $(Sb_2)_m - sb_2te_3$ (m = 0-3) superlattice series. Physical Review B. 2015;**91**(20):201101

[16] Bernevig B, Hughes T. Topological Insulators And Topological Superconductors. Princeton University Press; 2013

[17] Alexandradinata A, Wang Z, Bernevig BA. Topological insulators from group cohomology. Physical Review X. 2016;**6**:021008

[18] Tom Dieck T. Algebraic Topology. EMS Textbooks in Mathematics. Corrected 2nd printing edition. Zurich: European Mathematical Society; 2010. OCLC: 711865106

[19] Bradlyn B, Elcoro L, Cano J, Vergniory MG, Wang Z, Felser C, Aroyo MI, Bernevig BA. Topological quantum chemistry. Nature. July 2017;**547**:298

[20] Jenkins GS, Lane C, Barbiellini B, Sushkov AB, Carey RL, Liu F, Krizan JW, Kushwaha SK, Gibson Q, Chang T-R, Jeng H-T, Lin H, Cava RJ, Bansil A, Drew HD. Three-dimensional dirac cone carrier dynamics in na3Bi and cd_3as_2. Physical Review B. August 2016;**94**: 085121

[21] Schoop LM, Ali MN, Straßer C, Topp A, Varykhalov A, Marchenko D, Duppel V, Parkin SSP, Lotsch BV, Ast CR. Dirac cone protected by non-symmorphic symmetry and three-dimensional Dirac line node in ZrSiS. Nature Communications. May 2016;**7**:11696

[22] Ali MN, Xiong J, Flynn S, Tao J, Gibson QD, Schoop LM, Liang T, Haldolaarachchige N, Hirschberger M, Ong NP, Cava RJ. Large, nonsaturating magnetoresistance in WTe2. Nature. September 2014;**514**:205

[23] Barua S, Rajeev KP, Gupta AK. Evidence for topological surface states in metallic single crystals of bi 2 te 3. Journal of Physics: Condensed Matter. 2015;**27**(1):015601

[24] Yang H, Yu J, Parkin SSP, Felser C, Liu C-X, Yan B. Prediction of triple point fermions in simple half-heusler topological insulators. Physical Review Letters. September 2017;**119**: 136401

[25] Bradlyn B, Cano J, Wang Z, Vergniory M, Felser C, Cava R, Bernevig BA. Beyond dirac and weyl fermions: Unconventional quasiparticles in conventional crystals. Science. 2016; **353**(6299):aaf5037

Chapter 6

Thermodynamic Symmetry and Its Applications - Search for Beauty in Science

Zhen-Chuan Li

Additional information is available at the end of the chapter

http://dx.doi.org/10.5772/intechopen.72839

"A theory is the more impressive the greater the simplicity of its premises are, the more different kinds of things it relates, and the more extended is its area of applicability. Therefore the deep impression that classical thermodynamics made upon me. It is the only physical theory of universal content concerning which I am convinced that, within the framework of applicability of its basic concepts, it will never be overthrown."

(Albert Einstein, 1946)

Abstract

A variety of thermodynamic variables are properly arranged at vertices of an extended concentric multi-polyhedron diagram based on their physical meanings. A symmetric function with "patterned self-similarity" is precisely be defined as the function, which is unchanged not only in function form but also in variable's nature and neighbor relationship under symmetric operations. Thermodynamic symmetry roots in the symmetric reversible Legendre transforms of the potentials. The specific thermodynamic symmetries revealed by the diagram are only one C_3 symmetry about the $U \sim \Phi$ diagonal direction and C_4 and σ symmetries on three U-containing squares. Based on the equivalence principle of symmetry, numerous equations of the 12 families can concisely be depicted by overlapping 12 specifically created rigid, movable graphic patterns on fixed {1, 0, 0} diagrams through σ and/or C_4 symmetric operations. Any desired partial derivatives can be derived in terms of several available quantities by a foolproof graphic method. It is the symmetry that made possible to build up the diagram as a model like the Periodic Table of the Elements to exhibit an integration of the entire structure of the thermodynamic variables into a coherent and complete exposition of thermodynamics and to facilitate the subject significantly.

Keywords: thermodynamic symmetry, thermodynamics, symmetry, graphic method, Legendre transforms, polyhedrons, physical chemistry, chemical physics

1. Introduction

An interpretation of thermodynamics being a science of symmetry was proposed by Herbert Callen [1, 2]. While an integration of the entire structure into a coherent and complete exposition of thermodynamics was not undertaken, since it would require repetition of an elaborate formalism with which the reader presumably is familiar. Such an abstract conceptual interpretation has not widely been recognized.

Symmetry generally conveys two primary meanings: beauty and "patterned self-similarity." A symmetric function with "patterned self-similarity" can precisely be defined as the function, which is unchanged not only in function form but also in variable's nature and relationship under symmetric operations. Many works, such as an important class of thermodynamic equations being resolved by "standard form" into families [3, 4] and expressed by geometric diagrams (square [5], cub octahedron [6], concentric multi-circle [7], cube [8], and Venn diagram [9]), have revealed symmetry existing in thermodynamics, a keen sense of which is helpful to every one of the subject.

You might wonder about a series of following questions: Why does symmetry exist in thermodynamics? What are specific thermodynamic symmetries? How can we apply the specific symmetries for different purposes? What are significant results of its applications? In this chapter, you will gradually find out answers of all questions above.

2. Configuration of 3D diagram

2.1. Thermodynamic variables

From a mathematical point of view, thermodynamic properties behave like multi-variable functions and can usually be differentiated and integrated. A variety of thermodynamic variables can be classified into natural variables, thermodynamic potentials, and all of the thermodynamic properties of a system, which can be found by taking partial derivatives of a thermodynamic potential of the system with respect to its natural variables if the thermodynamic potential can be determined as a function of its natural variables.

2.1.1. Natural variables and thermodynamic potentials

A thermodynamic potential is a scalar function used to represent the thermodynamic state of a system. One main thermodynamic potential, which has a physical interpretation, is the internal energy, U. The variables that are held constant in this process are termed the natural variables of that potential.

For a single component one phase system, the number of natural variables (independent variables to describe the extensive state) of the system is three. A set of three natural variables for the internal energy are entropy (S), volume (V), and particle number (N), and they are all extensive variables. The integration (Euler's equation) of the fundamental equation for internal energy, $dU = TdS - PdV + \mu dN$, at constant values of the intensive variables [temperature (T), pressure (P), and chemical potential (μ)] yields

$$U(S,V,N) = TS - PV + \mu N \tag{1}$$

Since S and V are often inconvenient natural variables from an experimental point of view, the Legendre transforms are used to define further thermodynamic potentials. Each Legendre transform is a linear change in variables in which one or more products of conjugate variables are subtracted from the internal energy to define a new thermodynamic potential.

2.1.2. Complete set of the thermodynamic potentials

A complete set of Legendre transforms initially from the internal energy $U(S, V, N)$ for the system is shown below [10]. There are no generally accepted symbols for all of the eight thermodynamic potentials, and so a suggestion published in [8] is utilized here.

$$H(S,P,N) = U(S,V,N) - (-P\cdot V) = TS + \mu N \tag{2}$$

$$A(T,V,N) = U(S,V,N) - (T\cdot S) = -PV + \mu N \tag{3}$$

$$\psi(S,V,\mu) = U(S,V,N) - (\mu\cdot N) = TS - PV \tag{4}$$

$$G(T,P,N) = U(S,V,N) - (-P\cdot V) - (T)\cdot S) = \mu N \tag{5}$$

$$\Omega\ (T,V,\mu) = U(S,V,N) - (T\cdot S) - (\mu\cdot N) = -PV \tag{6}$$

$$\chi(S,P,\mu) = U(S,V,N) - (-P\cdot V) - (\mu\cdot N) = TS \tag{7}$$

$$\Phi(T,P,\mu) = U(S,V,N) - (T\cdot S) - (-P\cdot V) - (\mu\cdot N) = 0 \tag{8}$$

2.1.3. Thermodynamic properties

The thermodynamic properties can be expressed in terms of the derivatives of the potentials with respect to their natural variables. These equations are known as equations of state, since they specify the properties of the thermodynamic state.

First-order partial derivative variables:

$$T = \left(\frac{\partial U}{\partial S}\right)_{VN} = \left(\frac{\partial H}{\partial S}\right)_{PN} = \left(\frac{\partial \psi}{\partial S}\right)_{V\mu} = \left(\frac{\partial \chi}{\partial S}\right)_{P\mu} \tag{9}$$

$$-P = \left(\frac{\partial U}{\partial V}\right)_{SN} = \left(\frac{\partial A}{\partial V}\right)_{TN} = \left(\frac{\partial \Omega}{\partial V}\right)_{T\mu} = \left(\frac{\partial \psi}{\partial V}\right)_{S\mu} \tag{10}$$

$$\mu = \left(\frac{\partial U}{\partial N}\right)_{SV} = \left(\frac{\partial H}{\partial N}\right)_{SP} = \left(\frac{\partial A}{\partial N}\right)_{TV} = \left(\frac{\partial G}{\partial N}\right)_{TP} \tag{11}$$

$$-S = \left(\frac{\partial G}{\partial T}\right)_{PN} = \left(\frac{\partial A}{\partial T}\right)_{VN} = \left(\frac{\partial \Omega}{\partial T}\right)_{V\mu} \tag{12}$$

$$V = \left(\frac{\partial G}{\partial P}\right)_{TN} = \left(\frac{\partial H}{\partial P}\right)_{SN} = \left(\frac{\partial \chi}{\partial P}\right)_{S\mu} \tag{13}$$

$$-N = \left(\frac{\partial \Omega}{\partial \mu}\right)_{TV} = \left(\frac{\partial \chi}{\partial \mu}\right)_{SP} = \left(\frac{\partial \psi}{\partial \mu}\right)_{SV} \tag{14}$$

Each first-order partial derivative of a potential is associated (or conjugated) with its corresponding independent (or natural) variable of the potential to comprise a pair of conjugate variables. Above six symbols of the first-order partial derivatives are almost the same as the symbols of the six natural variables, except for three of them ($-S$, $-P$, and $-N$) holding a negative sign ($-$). The negative sign in front of those three variables indicates that they physically seek a maximum, rather than a minimum, during spontaneous changes and equilibriums. The six different symbols of the variables can make three intensive versus extensive conjugate variable pairs ($T \sim S$, $P \sim V$, and $\mu \sim N$), within three products of the conjugate variable pairs ($T \cdot S$, $P \cdot V$, and $\mu \cdot N$) have the same units as the potentials (U, H, A, ψ, G, Ω, χ, and Φ), and they also significantly comprise three opposite sign conjugate variable pairs ($T \sim -S$, $-P \sim V$, and $\mu \sim -N$) if the negative sign ($-$) in front of those three variables ($-S$, $-P$, and $-N$) must be taken into account for an essential necessity explained later.

Second-order partial derivative variables:

C_P (isobaric thermal capacity) and C_V (isochoric thermal capacity)

$$C_{PN} = \left(\frac{\partial H}{\partial T}\right)_{PN} = T\left(\frac{\partial S}{\partial T}\right)_{PN} = -T\left(\frac{\partial^2 G}{\partial T^2}\right)_{PN} = C_P \tag{15}$$

$$C_{VN} = \left(\frac{\partial U}{\partial T}\right)_{VN} = T\left(\frac{\partial S}{\partial T}\right)_{VN} = -T\left(\frac{\partial^2 A}{\partial T^2}\right)_{VN} = C_V \tag{16}$$

Other partial derivative variables:

$$\text{The isobaric expansion coefficient: } \alpha = \frac{1}{V}\left(\frac{\partial V}{\partial T}\right)_P \tag{17}$$

$$\text{The isothermal compressibility: } \kappa_T = -\frac{1}{V}\left(\frac{\partial V}{\partial P}\right)_T \tag{18}$$

etc.

http://dx.doi.org/10.5772/intechopen.72839

2.1.4. A 3D diagram of the thermodynamic variables

A variety of thermodynamic variables including three conjugate pairs of natural variables, eight thermodynamic potentials, and six first-order partial derivatives can properly be arranged in a concentric multi-polyhedron diagram (**Figure 1**) based on their physical meanings as follows:

1. The natural variables: Three conjugate (intensive ∼ extensive) pairs of natural variables, i.e., temperature (T) ∼ entropy (S), pressure (P) ∼ volume (V), and chemical potential (μ) ∼ particle number (N), are arranged at vertices of a small octahedron with the Cartesian coordinates: $T[1,0,0] \sim S[-1,0,0]$, $P[0,-1,0] \sim V[0,1,0]$, and $\mu[0,0,1] \sim N[0,0,-1]$.

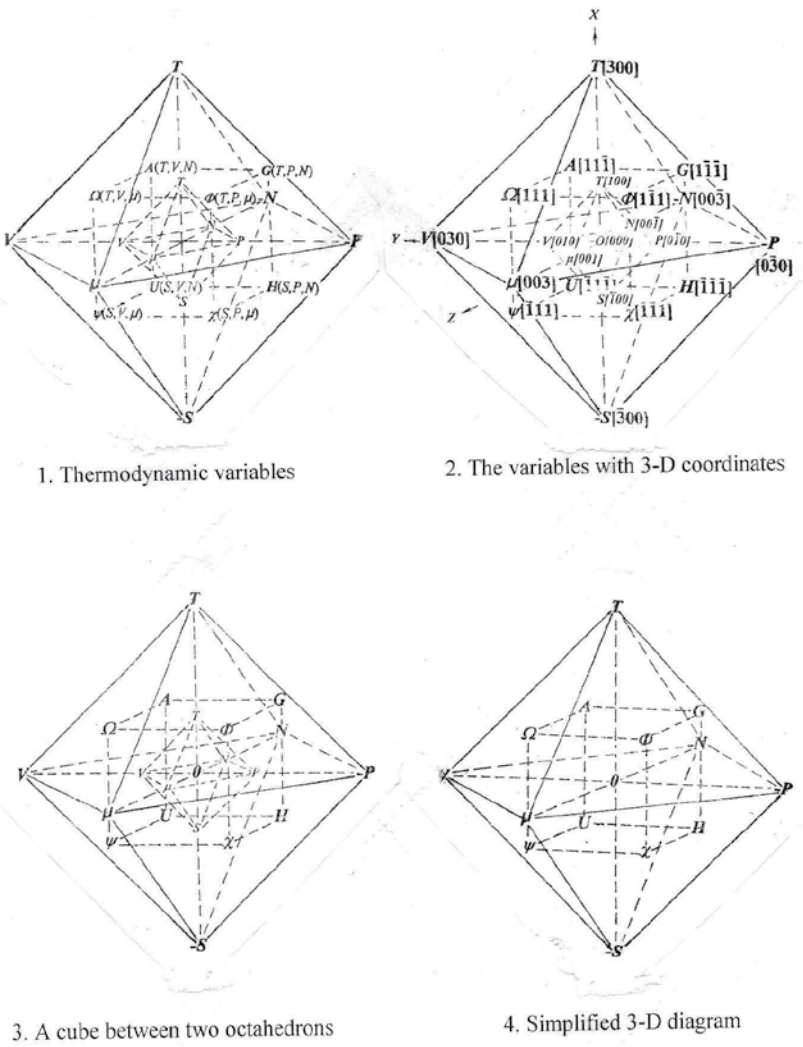

Figure 1. 3D concentric multi-polyhedron diagram.

2. The thermodynamic potentials: In order to exhibit a close relationship between each thermodynamic potential and its three correlated natural valuables, let four pairs of thermodynamic potentials {internal energy $U(S, V, N) \sim \Phi(T, P, \mu)$, enthalpy $H(S, P, N) \sim$ grand canonical potential Ω (T, V, μ), Gibbs free energy $G(T, P, N) \sim \psi(S, V, \mu)$, and Helmholtz free energy $A(T, V, N) \sim \chi(S, P, \mu)$} be located at the opposite ends of four diagonals of a cube with the Cartesian coordinates: $U[-1, 1, -1] \sim \Phi[1, -1, 1]$, $H[-1,-1,-1] \sim \Omega$ [1, 1, 1], $G[1, -1, -1] \sim \psi[-1, 1, 1]$, and $A[1, 1, -1] \sim \chi[-1, -1, 1]$.
3. The first-order partial derivatives: Let the six first-order partial derivatives (T, $-S$, $-P$, V, μ, and $-N$) similarly be located at vertices of a large octahedron with the Cartesian coordinates: $T[3,0,0]$, $-S[-3,0,0]$, $-P[0,-3,0]$, $V[0,3,0]$, $\mu[0,0,3]$, and $-N[0,0,-3]$.

2.2. Variable's neighbor relationship in the diagram

2.2.1. To simplify the diagram

Different categories of the variables are located at different polyhedrons, whereas symbols of the variables at two octahedrons are almost same except for $-S$, $-P$, and $-N$. Therefore, it is possible for us to simplify two octahedrons into the large one (**Figure 1**)(4) if the negative sign ("−") in front of those variables ($-S$, $-P$, and $-N$) could be taken into account by a specific way, which will be described later.

2.2.2. Variable's neighbor relationship

Relations between any two variables can be visually determined by their neighbor relationship in the diagram. Neighbors can be classified as first, second, and third ones based on distances between them. Correlated or conjugate relation between two variables can easily be determined by the neighbor relationship. A pair of conjugate variables are always located at opposite ends of a diagonal of the polyhedron, for example, $T \sim -S$, $-P \sim V$, $\mu \sim -N$, or $U \sim \Phi$. The correlated relation between each potential and its natural variables is always the closest (first) neighbor relationship shown in the diagram.

3. Thermodynamic symmetry

3.1. Symmetry roots in the Legendre transforms

3.1.1. The Legendre transforms

Each Legendre transform (*ELT* or *E*) is a leaner conversion between a pair of multiple variable functions [$M = m(x, y, w)$ and $F = f(x, y, z)$], which is associated with a transform from one to another between a pair of conjugate variables (w and z) [11].

The Legendre transform (E: $F \rightarrow M$ and z → w) is defined as:

$$m(x, y, w) = f(x, y, z) - w \cdot z \tag{19}$$

where the two functions (M and F) and a product term (w · z) of the two conjugate variables (w and z) have same units.

Every Legendre transform (E) has its own reverse Legendre transform (RLT or R: $M \rightarrow F$ and $w \rightarrow z$). The reverse Legendre transform (R) is therefore written as:

$$f(x, y, z) = m(x, y, w) + z \cdot w \tag{20}$$

E and R are reversible each other. Reversible Legendre transforms are associated with a pair of the conjugate variables (w and z), a pair of the functions [$M = m(x, y, w)$ and $F = f(x, y, z)$, or $M = m(w)$ and $F = f(z)$, or M and F], and a pair of the reversible conversions (E and R). The reversible Legendre transforms can be written as ($E \leftrightarrow R$), where a double arrow symbol ($\leftrightarrow$) stands for "reversible". There are ($M \leftrightarrow F$) and ($w \leftrightarrow z$) in the reversible ($E \leftrightarrow R$).

3.1.2. Symmetry of the Legendre transforms

3.1.2.1. The Legendre transforms with a pair of same sign conjugate variables

It can be seen by comparing Eq. (19) with Eq. (20) that although they are basically same, but not exactly same since there is a slight difference in an opposite sign (negative or positive) in front of the product term of the two conjugate variables ($w \cdot z$) in the reversible ($E \leftrightarrow R$) under a pair of the same sign conjugate variables (w and z). Therefore, the reversible ($E \leftrightarrow R$), without a general formula, are asymmetric if the two conjugate variables (w and z) have same sign.

3.1.2.2. The Legendre transforms with a pair of opposite sign conjugate variables

Although the reversible ($E \leftrightarrow R$) are asymmetric under a pair of the same sign conjugate variables (w and z), however, if the negative sign ($-$) in front of the product term can be taken into account by a pair of opposite sign conjugate variables (z and $-w$ or $-z$ and w), and if the negative sign ($-$) in front of either negative conjugate variable ($-w$ or $-z$) can be controlled by a pair of opposite conjugate variable treatments (either canceling or keeping the negative sign), which are symbolized as [ ] and { }, respectively, the asymmetric reversible ($E \leftrightarrow R$) is able to become symmetric reversible Legendre transforms ($E^* \leftrightarrow R^*$), where an asterisk symbol (*) stands for symmetric. In other words, the asymmetric ($E \leftrightarrow R$) can become symmetric ($E^* \leftrightarrow R^*$) under two required conditions: a pair of the opposite sign conjugate variables (z and $-w$ or $-z$ and w) and a pair of the opposite conjugate variable treatments ([ ] and { }) are involved in the symmetric ($E^* \leftrightarrow R^*$).

3.1.2.3. A general formula for the symmetric reversible Legendre transforms

The general formula for the symmetric ($E^* \leftrightarrow R^*$) must be generalized from the two reversible equations, Eqs. (19) and (20). It can be seen in their common writing order, from left to right, that the two equations commonly consist of two kinds of symbols: one kind of a series of

conventional mathematical symbols, which are an equal sign (=) located between the two functions, an uncertain changeable sign (− or +) located between a pair the functions and the product term, and a product sign (·) located between the two opposite sign conjugate variables, respectively, and another kind of a series of symbols associated with given information, which are a pair of the reversible functions (*M* and *F*) and a pair of the involved opposite sign conjugate variables. The given information symbols can be called as first, second, third, and fourth one in the writing order from left to right, respectively.

If we use a pair of square symbols (□ and □) symbolizing a pair of the known functions (*M* and *F*), and a pair of different symbols ([ ] and { }) symbolizing a pair of the opposite treatments (canceling and keeping), and put an empty space for the uncertain (or unknown) sign (− or +) located between the functions and the product term, the general formula may be created for the symmetric ($E^* \leftrightarrow R^*$) to be

$$\text{either } \square = \square \quad [\ ] \cdot \{\ \} \text{ or } \square = \square \quad \{\ \} \cdot [\ ] \tag{21}$$

It can be seen in Eq. (21) that the two different possible orders of the opposite treatments, [ ] · { } and { }· [ ], would make the general formula uncertain, not unique. The general formula for the symmetric ($E^* \leftrightarrow R^*$) must be unique.

3.1.2.4. The order of the opposite treatments on a pair of the opposite sign conjugate variables

It is found out during my thinking about above problem that only one of two possible opposite signs (either positive or negative) could be bestowed on each conjugate variable to make sense, whereas another opposite sign makes no sense, and similarly that only one of two possible treatment orders (either [ ] · { } or { } · [ ]) can make sense, whereas another opposite order makes no sense. Therefore, a unique opposite treatment order can be determined only by checking against the well-known basic conclusions and formulas in the subject.

After a series of serious checks against some well-known basic conclusions and formulas in thermodynamics, such as the entropy (*S*) seeks for a maximum, rather than a minimum, during any spontaneous processes and equilibriums, the first-order partial derivative of the potentials (*G*, *A*, and Ω) with respect to their natural variable of temperature (*T*) equals $-S$ in Eq. (12), rather than *S* (no sign means positive), if the negative sign is bestowed only on those three conjugate natural variables (*S*, *P*, and *N*), respectively, rather than oppositely on *T*, *V*, and μ, then a set of the three opposite sign conjugate natural variable pairs ($T \sim -S$, $-P \sim V$, and $\mu \sim -N$) will exactly be same as those six first-order partial derivatives of the potentials in Eqs. (9)–(14) and so on, then it is found out that the right unique order of the two opposite treatments in the general formula must be [ ] · { }, rather than { }· [ ]; therefore, the general formula for the symmetric ($E^* \leftrightarrow R^*$) must be symbolized as:

$$\square = \square \quad [\ ] \cdot \{\ \} \tag{22}$$

rather than □ = □ { } · [ ], since Eq. (22) makes sense.

3.1.2.5. A general procedure for using the symbolized general formula

If we knew a pair of the two opposite sign conjugate variables (either $-w$ and z or w and $-z$), a pair of the two associated functions (M and F), and a direction of the Legendre transform (either $F \rightarrow M$ or $M \rightarrow F$), thus we would be able to find out the unknown (uncertain) sign of the product term (either $w \cdot z$ or $z \cdot w$) in Eq. (22) for the symmetric ($E^* \leftrightarrow R^*$). The general procedure of a created specific method comprises the following four steps, here take a given Legendre transform ($U \rightarrow H$) as an example.

Step 1: Obtain information about a pair of given potentials {$U(-S, V, -N)$ and $H(-S, -P, -N)$} and a pair of associated opposite sign conjugate natural variables (V and $-P$) as well as the conversion direction ($\rightarrow$) involved in the given conversion ($U \rightarrow H$);

Step 2: Use the first square symbol (□) in Eq. (22) to select the converted (ended) potential $H(-S, -P, -N)$, the second square symbol (□) to select the converting (starting) potential $U(-S, V, -N)$, the third canceling symbol [ ] to cancel any negative sign of the conjugate variable ($-P$) of the potential $H(-S, -P, -N)$ located in the first place, and the fourth keeping symbol { } to keep any negative sign of the conjugate variable (V) of the potential $U(-S, V, -N)$ located in the second place, respectively;

Step 3: Find out an unknown sign of the product term between the two pairs of the symbols in the general formula, the unknown sign is found out to be positive (+), in this case, since no sign in front of the conjugate variable (V), which is associated with the potential $U(-S, V, -N)$ located in the second place, is kept by the keeping symbol { };

Step 4: Write down a series of results of both the known and the unknown obtained above in the writing order of the general formula from left to right, and double check it for sure as below:

$$H(-S, -P, -N) = U(-S, V, -N) + P \cdot V \tag{23}$$

3.1.3. Symmetry of the thermodynamic potentials

The Legendre transforms are used to define thermodynamic potentials from one to another, thus the exchangeable (reversible) potentials are symmetric when a pair of opposite sign conjugate variables ($T \sim -S$, $V \sim -P$ or $\mu \sim -N$) are treated under a pair of opposite ways (canceling [ ] or keeping { }). Based on the general procedure of the specific method described above, we can write down the reversible Legendre transforms for any pair of the closest neighbor potentials.

For example, take V and $-P$ as a pair of the opposite sign conjugate natural variables, which are exactly same as a pair of the first-order partial derivatives, and exchange the two conjugate natural variables ($V \leftrightarrow -P$), thus four parallel potential pairs like ($U \leftrightarrow H$), ($A \leftrightarrow G$), ($\Omega \leftrightarrow \Phi$), and ($\psi \leftrightarrow \chi$), shown in **Figure 1**, will mirror-symmetrically be exchanged in each pair, respectively. Some symmetric exchangeable equations in ($U \leftrightarrow H$) and ($A \leftrightarrow G$) can be written down on the spot as follows:

$$U \to H : H(-S,-P,-N) = U(-S,V,-N)\,?\,[-P]\cdot\{V\} = U(-S,V,-N) + P\cdot V \quad (2)$$

$$H \to U : U(-S,V,-N) = H(-S,-P,-N)\,?\,[V]\cdot\{-P\} = H(-S,-P,-N) - V\cdot P \quad (1)$$

$$A \to G : G(T,-P,-N) = A(T,V,-N)\,?\,[-P]\cdot\{V\} = A(T,V,-N) + P\cdot V \quad (5)$$

$$G \to A : A(T,V,-N) = G(T,-P,-N)\,?\,[V]\cdot\{-P\} = G(T,-P,-N) - V\cdot P \quad (3)$$

Similarly, take $-S$ and T as a pair of the opposite sign conjugate natural variables, which are also exactly same as a pair of the first-order partial derivatives, and exchange the two conjugate natural variables ($-S \leftrightarrow T$), thus four parallel potential pairs like ($U \leftrightarrow A$), ($H \leftrightarrow G$), ($\psi \leftrightarrow \Omega$), and ($\chi \leftrightarrow \Phi$) shown in **Figure 1** will mirror-symmetrically be exchanged in each pair, respectively. Some symmetric exchangeable equations in ($U \leftrightarrow A$) and ($H \leftrightarrow G$) can be written down on the spot as follows:

$$U \to A : A(T,V,-N) = U(-S,V,-N)\,?\,[T]\cdot\{-S\} = U(-S,V,-N) - T\cdot S \quad (3)$$

$$A \to U : U(-S,V,-N) = A(T,V,-N)\,?\,[-S]\cdot\{T\} = A(T,V,-N) + S\cdot T \quad (1)$$

$$H \to G : G(T,-P,-N) = H(-S,-P,-N)\,?\,[T]\cdot\{-S\} = H(-S,P,-N) - T\cdot S \quad (5)$$

$$G \to H : H(-S,-P,-N) = G(T,-P,-N)\,?\,[-S]\cdot\{T\} = G(T,-P,-N) + S\cdot T \quad (2)$$

It is found out by checking above equations against **Figure 1** that the symbolized general formula [Eq. (22)] works very well and makes sense, that specific symmetries involved in the symmetric reversible conversions of the potentials {F^*, (+/−)z) ↔ M^*, (−/+)w} are mirror symmetry (σ) with respect to a mirror and fourfold rotating symmetry (C_4) about an axis and that each mirror is always perpendicular to a linking segment of the two opposite sign conjugate variables, and each rotating axis is the linking segments of a pair of opposite sign conjugate variables.

3.1.4. Symmetry of the thermodynamic properties

The thermodynamic properties can be expressed in terms of the derivatives of the potentials with respect to their natural variables. Therefore, many thermodynamic equations (properties) are symmetric too. For example, it can be seen that following four rewritten Maxwell equations

$$\left(\frac{\partial V}{\partial T}\right)_{PN} = -\left(\frac{\partial S}{\partial P}\right)_{TN} or \left(\frac{\partial (V)}{\partial T}\right)_{PN} = \left(\frac{\partial (-S)}{\partial P}\right)_{TN} \quad (24)$$

$$\left(\frac{\partial T}{\partial P}\right)_{SN} = \left(\frac{\partial V}{\partial S}\right)_{PN} or \left(\frac{\partial (T)}{\partial P}\right)_{SN} = \left(\frac{\partial (V)}{\partial S}\right)_{PN} \quad (25)$$

$$-\left(\frac{\partial P}{\partial S}\right)_{VN} = \left(\frac{\partial T}{\partial V}\right)_{SN} or \left(\frac{\partial (-P)}{\partial S}\right)_{VN} = \left(\frac{\partial (T)}{\partial V}\right)_{SN} \quad (26)$$

$$\left(\frac{\partial S}{\partial V}\right)_{TN} = \left(\frac{\partial P}{\partial T}\right)_{VN} or \left(\frac{\partial (-S)}{\partial V}\right)_{TN} = \left(\frac{\partial (-P)}{\partial T}\right)_{VN} \quad (27)$$

http://dx.doi.org/10.5772/intechopen.72839

display mirror symmetry (σ) with respect to both sides of each equation and fourfold rotation symmetry (C_4) about the conjugate pair of μ and $-N$ in **Figure 1**.

3.2. Koenig's results and geometric explanations

There are not generally accepted symbols for all thermodynamic potentials. In Koenig's paper, Callen's transformed symbols [2, 4], which are also recommended by IUPAC [10], were used; whereas, in this chapter, Pate's symbols [8] are used. In order to conveniently discuss Koenig's results, a comparison of these symbols is shown in **Figure 2**, where another kind of symbols

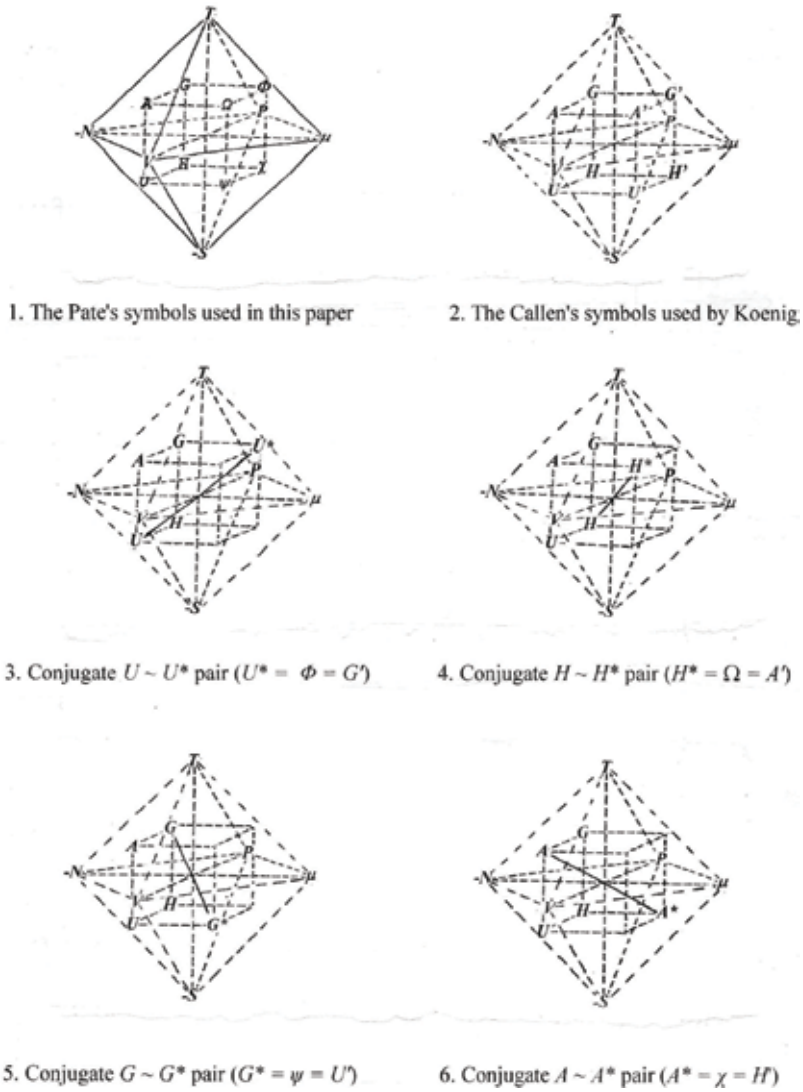

Figure 2. Comparison of the symbols for thermodynamic potentials.

(conjugate ones) is also introduced. The relations among three different kinds of the symbols for four transformed potentials are as follows:

$$U' = \psi = G^*;\ H' = \chi = A^*;\ G' = \Phi = U^*;\ A' = \Omega = H^*.$$

where symbols with a prime (′) stand for Callen's transformed ones (**Figure 2**(2)) and symbols with an asterisk (*) stand for conjugate ones (**Figure 2**(3–6)).

Koenig pointed out that an important class of thermodynamic equations being resolved by "standard form" into families [3, 4], and the equations of greatest physical interest belong to

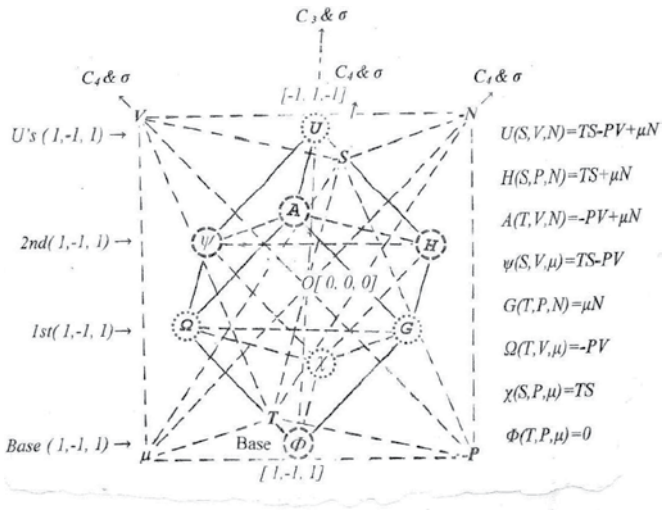

1. The special conjugate $U \sim \Phi$ pair pivoted at $\Phi(T, P, \mu) = 0$

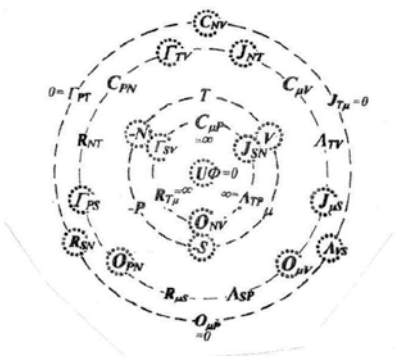

2. The (1, -1, 1) projection diagram

Figure 3. Thermodynamic symmetry: One C_3 symmetry about the [1, −1, 1] ($U \sim \Phi$ diagonal) direction and C_4 and σ symmetries on three U-containing squares.

http://dx.doi.org/10.5772/intechopen.72839

families having 48, 24, 12, or 8 members. The remaining possibilities for the number of members per family are 6, 4, 3, and 1. Also, he gave one example of each kind:

1. 48 members $(\partial U/\partial V)_{T,N} = T(\partial P/\partial T)_{V,N} - P$

2. 24 members: $(\partial T/\partial V)_{S,N} = -(\partial P/\partial S)_{V,N}$

3. 12 members: $A = U - TS$

4. 8 members: $dU = TdS - PdV + \mu dN$

5. 6 members: $U - A + G - H = 0$

6. 4 members: $U - G' = TS - PV + \mu N$

7. 3 members: $U + A + G + H - H' - G' - A' - U' = 4\mu N$

8. 1 member: $U - A + G - H + H' - G' + A' - U' = 0$

He evaluated the value of his results being less in the technique, which supplies for generating formulas, than in its revelation of the symmetry of the equations of thermodynamics, a keen sense of which is helpful to every one of the subject.

It can be geometrically explained and verified by a well-oriented cub octahedron diagram (**Figure 3**) that his most results are true, however, that the example of the four member family should be sum (plus or addition) of U and G', rather than difference (minus or subtraction) between them, that the example of the one member family could be difference (minus or subtraction) between U and G', rather than $U - A + G - H + H' - G' + A' - U' = 0$, and that the revealed symmetry in thermodynamics is not perfect as the geometric symmetry of the cub octahedron is since the zero potential (Φ) damages the cube symmetry.

3.3. Thermodynamic symmetry

The thermodynamic symmetry revealed and verified by above geometric analysis in **Figure 3** exhibits only one C_3 (threefold rotation) symmetry about the [1, −1, 1] ($U \sim \Phi$ diagonal) direction and C_4 (fourfold rotation) and σ (mirror) symmetries on three U-containing squares, where the square including U, H, G, and A is the most important and useful one.

4. Extension

Koenig extended the square [5] to the octahedron [4], developed his results described above, and also raised a question at the end of his paper: Can the octahedron be extended to higher cases? Answer of the question is positive. Based on the equivalence principle of symmetry (reproducibility and predictability) [12], if we knew a sample member of any family, we would be able to know all other members of the family through symmetric operations. So, we can use the verified symmetry to extend the diagram to deal with the second-order partial derivative variables.

4.1. To develop novel C_P type variables and build up an extended 26-face polyhedron

4.1.1. C_P (isobaric thermal capacity) and C_V (isochoric thermal capacity)

Both *Cp* and C_V are second-order partial derivatives of the Gibbs free energy, $G(T, P, N)$ and the Helmholtz free energy, $A(T, V, N)$, respectively (see Eqs. (15) and (16)), thus they should be arranged at two proper locations outside of the large octahedron, where they close to their correlated variables, i.e., C_{PN} to G, T, P, and N, and C_{VN} to A, T, V, and N, respectively. Their Cartesian coordinates are C_{PN} [3.62, −1.50, −1.50] and C_{VN} [3.62, 1.50, −1.50].

4.1.2. Other members of the C_P's family

When N = constant, similarly other members of C_P's family can be defined symmetrically as follows:

$$R_{TN}[h,-k,-h] = \left(\frac{\partial A}{\partial P}\right)_{TN} = -P\left(\frac{\partial V}{\partial P}\right)_{TN} = -P\left(\frac{\partial^2 G}{\partial P^2}\right)_{TN} \tag{28}$$

$$R_{SN}[-h,-k,-h] = \left(\frac{\partial U}{\partial P}\right)_{SN} = -P\left(\frac{\partial V}{\partial P}\right)_{SN} = -P\left(\frac{\partial^2 H}{\partial P^2}\right)_{SN} \tag{29}$$

$$O_{PN}[-k,-h,-h] = \left(\frac{\partial G}{\partial S}\right)_{PN} = -S\left(\frac{\partial T}{\partial S}\right)_{PN} = -S\left(\frac{\partial^2 H}{\partial S^2}\right)_{PN} \tag{30}$$

$$O_{VN}[-k,h,-h] = \left(\frac{\partial A}{\partial S}\right)_{VN} = -S\left(\frac{\partial T}{\partial S}\right)_{VN} = -S\left(\frac{\partial^2 U}{\partial S^2}\right)_{VN} \tag{31}$$

$$J_{SN}[-h,k,-h] = \left(\frac{\partial H}{\partial V}\right)_{SN} = V\left(\frac{\partial P}{\partial V}\right)_{SN} = -V\left(\frac{\partial^2 U}{\partial V^2}\right)_{SN} \tag{32}$$

$$J_{TN}[h,k,-h] = \left(\frac{\partial G}{\partial V}\right)_{TN} = V\left(\frac{\partial P}{\partial V}\right)_{TN} = -V\left(\frac{\partial^2 A}{\partial V^2}\right)_{TN} \tag{33}$$

and others.

4.1.3. An extended polyhedron

Total 24 members of the C_P's family can be constructed as an extended 26-face polyhedron (rhombicuboctahedron) shown in **Figure 4**. The Cartesian coordinates for 24 vertices of the concentric rhombicuboctahedron are all permutations of <*h*, *h*, *k*>, where h equals one and half unit (h = 1.50), and k is larger than h by $(1 + \sqrt{2})$ times (k = 3.62).

Physically, such a scheme shown in **Figure 4** to arrange the four categories of thermodynamic variables at four kinds of the vertices of the extended concentric multi-polyhedron corresponds to Ehrenfest's scheme to classify phase transitions.

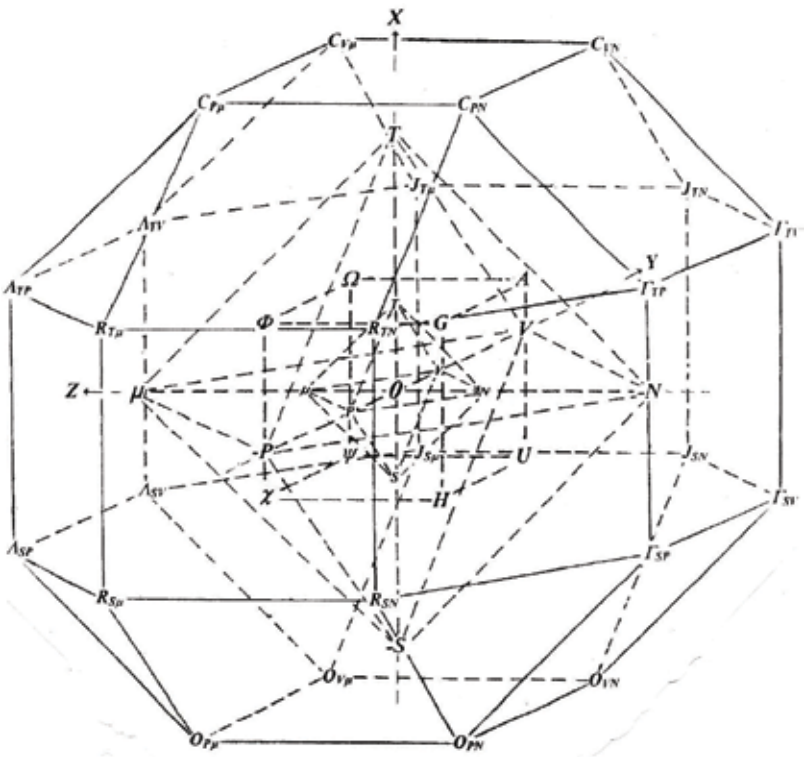

Figure 4. An extended concentric multi-polyhedron diagram in thermodynamics.

4.2. To develop relations for C_P's family

4.2.1. The closest neighbor relation between C_P and C_V

A closest neighbor relation between C_P and C_V is well known as

$$C_V = C_P - \frac{\alpha^2 VT}{\kappa_T}$$

The relation could also be expressed in terms of the natural variables (T, S, P, V, μ, and N) as

$$C_{PN}(T, -P, -N) \rightarrow C_{VN}(T, V, -N) : C_{VN} = C_{PN} + \left(\frac{\partial V}{\partial T}\right)_{PN} \bullet T \bullet \left(\frac{\partial(-P)}{\partial T}\right)_{VN} \tag{34}$$

$$C_{VN}(T, V, -N) \rightarrow C_{PN}(T, -P, -N) : C_{PN} = C_{VN} + \left(\frac{\partial P}{\partial T}\right)_{VN} \bullet T \bullet \left(\frac{\partial(V)}{\partial T}\right)_{PN} \tag{35}$$

Similarly, the closest neighbor relations for other pairs of the C_P type variables could be

$$R_{SN}(-S, -P, -N) \rightarrow R_{TN}(T, -P, -N) : R_{TN} = R_{SN} + \left(\frac{\partial T}{\partial P}\right)_{SN} \bullet P \bullet \left(\frac{\partial(-S)}{\partial P}\right)_{TN} \tag{36}$$

$$R_{TN}(T, -P, -N) \rightarrow R_{SN}(-S, -P, -N) : R_{SN} = R_{TN} + \left(\frac{\partial S}{\partial P}\right)_{TN} \bullet P \bullet \left(\frac{\partial (T)}{\partial P}\right)_{SN} \tag{37}$$

$$O_{VN}(-S, V, -N) \rightarrow O_{PN}(-S, -P, -N) : O_{PN} = O_{VN} + \left(\frac{\partial P}{\partial S}\right)_{VN} \bullet S \bullet \left(\frac{\partial (V)}{\partial S}\right)_{PN} \tag{38}$$

$$O_{PN}(-S, -P, -N) \rightarrow O_{VN}(-S, V, -N) : O_{VN} = O_{PN} + \left(\frac{\partial V}{\partial S}\right)_{PN} \bullet S \bullet \left(\frac{\partial (-P)}{\partial S}\right)_{VN} \tag{39}$$

$$J_{SN}(-S, V, -N) \rightarrow J_{TN}(T, V, -N) : J_{TN} = J_{SN} + \left(\frac{\partial T}{\partial V}\right)_{SN} \bullet V \bullet \left(\frac{\partial (-S)}{\partial V}\right)_{TN} \tag{40}$$

$$J_{TN}(T, V, -N) \rightarrow J_{SN}(-S, V, -N) : J_{SN} = J_{TN} + \left(\frac{\partial S}{\partial V}\right)_{TN} \bullet V \bullet \left(\frac{\partial (T)}{\partial V}\right)_{SN} \tag{41}$$

These symmetric reversible linear conversions between the two closest C_P type variables are similar to the symmetric reversible Legendre transforms between two closest potentials. Because all of them are resulted from the reversible conversions between a pair of the opposite sign conjugate variables ($T \leftrightarrow -S$ or $-P \leftrightarrow V$).

4.2.2. The parallel relations

It is easily found that following relations are true:

$$C_P \bullet O_P = T \bullet (-S) = -T\,S \tag{42}$$

$$C_V \bullet O_V = T \bullet (-S) = -T\,S \tag{43}$$

$$J_T \bullet R_T = V \bullet (-\boldsymbol{P}) = -P\,V \tag{44}$$

$$J_S \bullet R_S = V \bullet (-\boldsymbol{P}) = -P\,V \tag{45}$$

They can be called the parallel relations, as shown in the diagram.

4.2.3. The cross relations

It can also be found that following relations are true:

$$C_V \bullet R_T = C_P \bullet R_S \tag{46}$$

$$R_T \bullet O_P = R_S \bullet O_V \tag{47}$$

$$O_P \bullet J_S = O_V \bullet J_T \tag{48}$$

$$C_V \bullet J_S = C_P \bullet J_T \tag{49}$$

They can be called the cross relations, as shown in the diagram.

http://dx.doi.org/10.5772/intechopen.72839

5. Applications

5.1. To distinguish and identify partial derivatives

Different partial derivatives can visually be distinguished and identified by variable neighbor relationship in the diagram (**Figure 5**).

5.1.1. "Maxwell equations"-like partial derivatives

Any partial derivative, $(\partial X/\partial Y)_Z$, can be expressed by a ratio of other two partial derivatives, $(\partial X/\partial Y)_Z = \{-(\partial Z/\partial Y)_X/(\partial Z/\partial X)_Y\}$, based on Euler's chain relation $(\partial X/\partial Y)_Z \bullet (\partial Y/\partial Z)_X \bullet$

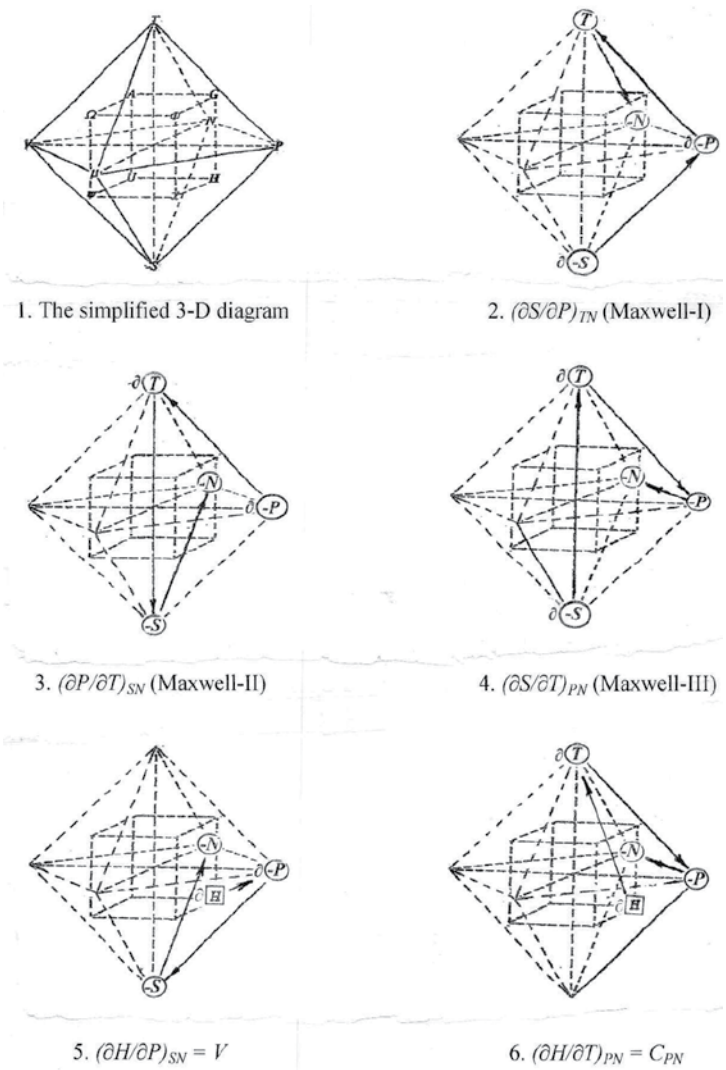

Figure 5. Different variable neighbor relationships.

$(\partial Z/\partial X)_Y = -1$, where three partial derivatives look like same in their forms and variable's categories, but different each other from their variable neighbor relationship in thermodynamics (**Figure 5**-2–4). For an example, $(\partial P/\partial T)_{SN} = \{-(\partial S/\partial T)_{PN}/ (\partial S/\partial P)_{TN}\}$, all of them look as same as the Maxwell partial derivatives, but they are different. It is quite difficult to determine, which one is a real Maxwell partial derivative or not by their forms and variables only.

The partial derivative $(\partial S/\partial P)_{TN}$, which is involved in one of the Maxwell equations $(\partial(S)/\partial P)_{TN} = -(\partial V/\partial T)_{PN}$ [Eq. (24)], can be called a Maxwell-I partial derivative. It stands for a partial derivative of the function S, $S = S(P,T,N)$, with respect to one of S's first neighbor variables, P, while holding S's two order-mixed (second and first) neighbor variables, T and N, constant (**Figure 5**-2). The partial derivative $(\partial P/\partial T)_{SN}$ can be called Maxwell-II or inverted Maxwell-I partial derivative. It stands for a partial derivative of the function P, $P = P(T,S,N)$, with respect to one of P's first neighbor variables, T, while holding P's other two first neighbor variables, S and N, constant (**Figure 5**-3). The partial derivative $(\partial S/\partial T)_{PN}$, which can be called Maxwell-III partial derivative, stands for a partial derivative of the function S, $S = S(T,P,N)$, with respect to S's second neighbor (or conjugate) variable, T, while holding S's two first neighbor variables, P and N, constant (**Figure 5**-4). Therefore, Maxwell like partial derivatives can be visually distinguished by the variable neighbor relationship in the diagram and identified (or classified) into three different families: Maxwell-I, -II, and -III partial derivatives.

5.1.2. $(\partial H/\partial P)_{SN}$ and $(\partial H/\partial T)_{PN}$

Two partial derivatives $(\partial H/\partial P)_{SN}$ and $(\partial H/\partial T)_{PN}$ look like same in their forms and variable's categories but totally different each other from their physical meanings: $(\partial H/\partial P)_{SN} = V$ (volume) and $(\partial H/\partial T)_{PN} = C_P$ (isobaric heat capacity). Such a difference between them can also visually be distinguished by their different variable neighbor relations shown in **Figure 5**-5 and 6. The partial derivative $(\partial H/\partial P)_{SN}$ stands for a partial derivative of the enthalpy H, $H = H(P, S, N)$, with respect to one of H's first neighbor (or natural) variables, P, while holding H's other two first neighbor variables, S and N, constant, whereas another partial derivative, $(\partial H/\partial T)_{PN,}$ stands for a partial derivative of the enthalpy H, $H = H(T, P, N)$ with respect to one of H's second neighbor variables, T, while holding H's two first neighbor variables, P and N, constant.

It should be emphasized here after the above analysis that the general formula of a family regarding to a group of similar partial derivatives must be unchanged not only in form but also in variable's nature and neighbor relationship under symmetric operations, conversely, that those similar partial derivatives, which display same form and variable's category without same variable's neighbor relationship, are not classified into a same family since they do not have a general formula, and that any difference in the variable's neighbor relationship can certainly be distinguished by the diagram.

5.2. Predict novel members of families

5.2.1. The Gibbs-Helmholtz equation's family

When we discuss temperature dependence of the Gibbs free energy, the famous Gibbs-Helmholtz equation is satisfied as:

$$\left(\frac{\partial(G/T)}{\partial T}\right)_{PN} = -\frac{H}{T^2} \quad \text{or} \quad \left(\frac{\partial\left(\frac{G}{T}\right)}{\partial\left(\frac{1}{T}\right)}\right)_{PN} = H \tag{50}$$

It can be predicted by the σ and C_4 symmetries, then justified by conventional derivation that following other members of the family are true:

$$\left(\frac{\partial\left(\frac{G}{T}\right)}{\partial\left(\frac{1}{T}\right)}\right)_{PN} = H = \left(\frac{\partial\left(\frac{U}{V}\right)}{\partial\left(\frac{1}{V}\right)}\right)_{SN} \tag{51}$$

and

$$\left(\frac{\partial\left(\frac{A}{T}\right)}{\partial\left(\frac{1}{T}\right)}\right)_{VN} = U = \left(\frac{\partial\left(\frac{H}{P}\right)}{\partial\left(\frac{1}{P}\right)}\right)_{SN} \tag{52}$$

5.2.2. The Jacobian equations

The Jacobian method is useful and entirely foolproof [13, 14]. If we could combine it with this method, it would be more helpful for anyone of the subject.

The Jacobian of two functions (f and g) with respect to two independent variables (x and y) is defined by

$$J(f,g) = \frac{\partial(f,g)}{\partial(x,y)} = \begin{pmatrix} (\partial f/\partial x)_y & (\partial g/\partial x)_y \\ (\partial f/\partial y)_x & (\partial g/\partial y)_x \end{pmatrix} \tag{53}$$

If the functions (f and g) or the variables (x and y) are interchanged, then sign is changed, and if one function and one variable are identical, the Jacobian reduces to a single partial derivative. For example, if $g = y$, then

$$J(f,y) = \frac{\partial(f,y)}{\partial(x,y)} = -\frac{\partial(y,f)}{\partial(x,y)} = \frac{\partial(y,f)}{\partial(y,x)} = \left(\frac{\partial f}{\partial x}\right)_y \tag{54}$$

If the functions (f and g) and the variables (x and y) are functions of a new set of variables (w and z), then

$$J(f,g) = \frac{\partial(f,g)}{\partial(x,y)} = \frac{\partial(f,g)/\partial(w,z)}{\partial(x,y)/\partial(w,z)} = \frac{\partial(f,g)}{\partial(w,z)} \bullet \frac{\partial(w,z)}{\partial(x,y)} \tag{55}$$

In practice, it is convenient to take T and P as the independent variables since they are readily controlled experimentally. Based on Eq. (55), that is equivalent to $J(T, P) = 1$, since $J(T,P) = \frac{\partial(T,P)}{\partial(T,P)} = 1$. Conversely, if $J(T,P) = 1$ that means to take T and P as the independent variables.

One of the Jacobian equations for the internal energy $U(S, V, N)$ could be derived from dividing the fundamental equation ($dU = TdS - PdV + \mu dN$) by dx at constant y, where x and y are any suitable variables

$$\left(\frac{\partial U}{\partial x}\right)_y = (T) \bullet \left(\frac{\partial S}{\partial x}\right)_y + (-P) \bullet \left(\frac{\partial V}{\partial x}\right)_y + (\mu) \bullet \left(\frac{\partial N}{\partial x}\right)_y$$

Using Eq. (54), the Jacobian equation for the internal energy is obtained as:

$$J(U, y) = (T) \bullet J(S, y) + (-P) \bullet J(V, y) + (\mu) \bullet J(N, y) \tag{56}$$

Eq. (56) is similar to the fundamental equation for the internal energy. Each potential has

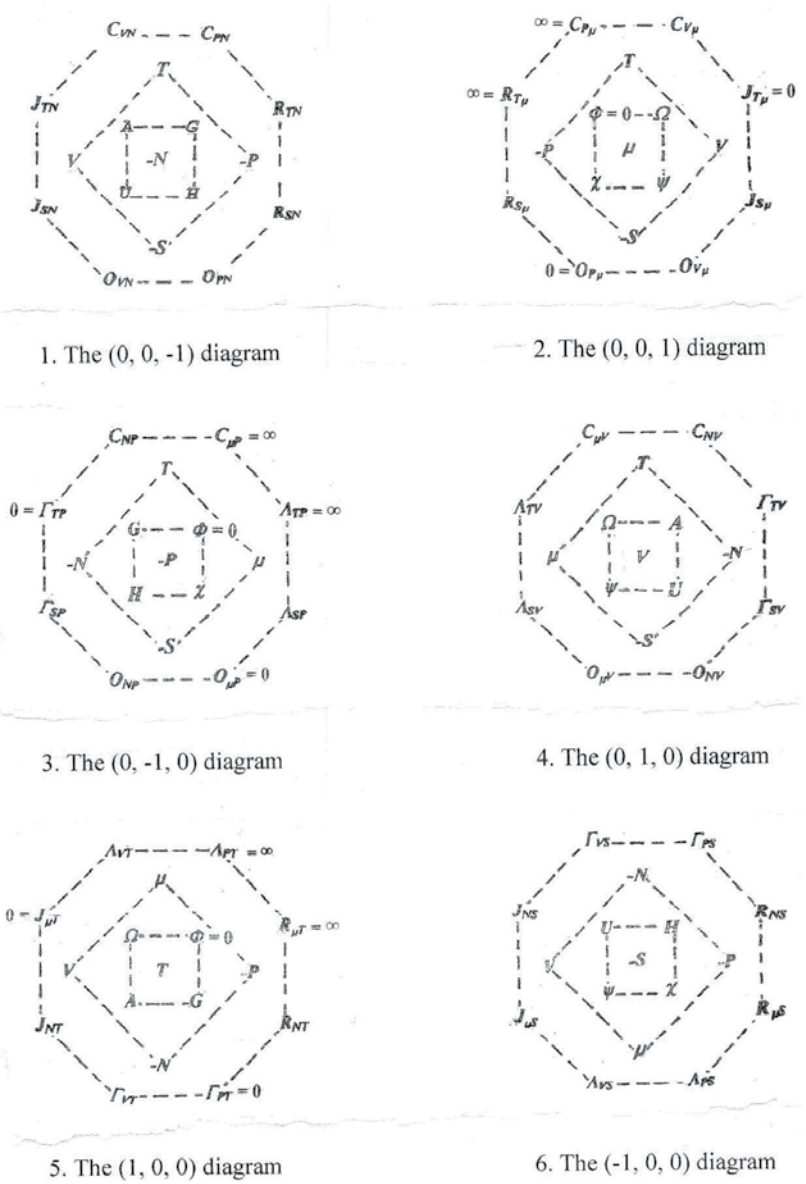

Figure 6. Six {1, 0, 0} projection diagrams.

http://dx.doi.org/10.5772/intechopen.72839

its own total differential and its corresponding Jacobian equation. Thus, total number of the Jacobian equations is same as the total number of the potentials, it is eight.

5.3. To depict thermodynamic equations by an invented graphic method

Based on the equivalence principle of symmetry (reproducibility and predictability) [12], if we knew a sample member of any family we would be able to know all members of the family through symmetric operations [15].

5.3.1. Resolve the 3D diagram into 2D diagrams

Carrying out symmetric operations on the 3D diagram is complicated and quite difficult, whereas doing so on 2D diagrams will be much easier instead. The simplified concentric multi-polyhedron diagram could be resolved into six 2D {1, 0, 0} projection diagrams, which are shown in **Figure 6-**1–6, and each 2D diagram consists of two squares and an octagon and exhibits the fourfold rotation (C_4) and the mirror (σ) symmetries. The "$-N$"-centered (0, 0, −1) diagram (**Figure 6**-1) contains the most common thermodynamic variables (U, H, G, A, T, $-S$, $-P$, V, C_{PN}, C_{VN}, O_{PN}, O_{VN}, J_{TN}, J_{SN}, R_{TN}, and R_{SN}), and it is chosen as first fixed diagram to depict the most familiar basic thermodynamic equations.

5.3.2. Specific notations

5.3.2.1. Graphic patterns for thermodynamic equations

It was mentioned that thermodynamic equations can be grouped into families with "standard forms." Each family with a standard form, or a general formula, can be expressed by a specifically created graphic pattern, which consists of a series of mixed special symbols arranged in a writing order (path) of the formula. Different families are distinguished by different patterns, which display differences in their forms, symbols, and writing orders (paths) graphically.

5.3.2.2. Graphic notations for partial derivatives

A first-order partial derivative of a multi-variable function, $f = f(x,y,z)$, is expressed by $(\partial f/\partial x)_{yz.}$ It consists of two parts in the form: a series of mathematical symbols (∂ and ∂) and a series of variables (f, x, y, and z). Thus, it can be expressed by a specifically created graphic pattern, ∂O → ∂O → O → O or ∂□ → ∂O → O → O, where a series of mathematical symbols (∂ and ∂) and a series of variable's selecting symbols (O and/or □) are alternately mixed together and arranged in a writing order of the partial derivative.

5.3.2.3. Arrows show directions

Arrows show directions of the writing order in a given general formula. For example, arrows (→) in the graphic pattern, ∂O → ∂O → O → O, show directions of the writing order for the partial derivative, $(\partial f/\partial x)_{yz.}$

5.3.2.4. Different symbols for selecting different categories of the variables

A square symbol "□" is used for selecting the potential variables located at four corners of the small square. Both large circle symbol "◯" and small circle symbol "O" are used for selecting the opposite sign conjugate variables located at four corners of the large square. The difference between the large and the small circles is only significant for those three variables ($-S$, $-P$, and $-N$). The large circle symbol ("◯") keeps negative sign in front of those variables, whereas the small circle symbol ("O") cancels the negative sign instead. They are equivalent to a pair of the opposite treatment symbols, { } and [ ], mentioned before. A special symbol "☼" is used for selecting the C_P type variables located at eight corners of the octagon.

5.3.2.5. Symbols for some common mathematical operations

A line segment linking two selected variables, "O --- ◯" or "☼ --- ☼", represents a product "●" of the two selected variables. A slash between two symbols, "☼/◯", stands for a ratio of the variable selected by the special symbol ("☼") to the variable selected by the large circle symbol ("◯"). Symbols including =, d, ∂, ∂^2, and J stand for equal, differential, first-order partial derivative, second-order partial derivative, and Jacobian, respectively, as usual. Sometimes the equal symbol ("=") is omitted. Symbol for addition (positive sign, "+", or plus) is always omitted. Symbol for subtraction (negative sign, "−", or minus) is never shown in the graphic patterns, but it is kept from those selected conjugate variables with the negative sign ($-S$, $-P$, and $-N$) in the fixed diagram by the large circle ("◯").

5.4. General procedure of the invented graphic method

A general procedure to depict all members of 12 thermodynamic families comprises four steps as follows.

Step 1: To employ the (0, 0, −1) diagram (**Figure 6-**1) as a fixed foundation, where four categories of common used thermodynamic variables being arranged at four kinds of locations including unchangeable natural variable (N) at center, four thermodynamic potentials (U, H, G, and A) at four corners of a small square, four first-order partial derivatives of the thermodynamic potentials, or two pairs of the opposite sign intensive versus extensive conjugate variables, i.e., temperature versus entropy and pressure versus volume (T versus $-S$ and $-P$ versus V) at two ends of two diagonals of a large square, and eight C_P type second-order partial derivatives of the thermodynamic potentials (the isobaric thermal capacity, C_{PN}, the isochoric thermal capacity, C_{VN}, and six other C_P type variables (O_{PN}, O_{VN}, J_{TN}, J_{SN}, R_{TN}, and R_{SN}) at eight vertices of an octagon.

Step 2: To create a graphic pattern (or a general formula) for depicting each family on the fixed diagram. It includes choosing a familiar equation in the family as a sample equation of the family, identifying categories of all involved variables in the sample equation, determining a writing order of the sample equation, and resolving the sample equation into two parts: a series of symbols of mathematical expressions and a series of involved variables in the sample equation in the writing order, using a set of specific symbols correctly and individually for each mathematical expression and each category of the involved variables in the sample equation individually, alternately, and gradually, and combining a series of

mathematical symbols with a series of variable selecting symbols together in the writing order of the sample equation.

Step 3: To overlap each family's specific, rigid, movable graphic pattern (Patterns 1–12) on! the fixed diagram for depicting other members of the family. It includes picking up a series of involved variables on the diagram by a series of variable selecting symbols in the graphic pattern, and combining a series of the mathematical symbols with a series of selected variables together in the writing order correspondingly and alternately to depict other member of the family through σ and/or C_4 symmetric operation individually and gradually.

Step 4: To substitute the fixed foundation diagram from one to another gradually (from **Figure 6-**1–6), and continuously to depict more members of each family in a same way above until having all members of the 12 families done.

5.5. Graphic patterns for 12 families

5.5.1. The Legendre transforms

$$-P \rightarrow V;\ H(-S,\ -P,\ -N) \rightarrow U(-S, V,\ -N) : U = H + V \bullet (-P) \tag{57}$$

Pattern 1: □ = □ O --- ◯ parallel

where an uncertain sign (positive or negative) of the product term depends on sign of the converting (starting) conjugate variable without or with a negative sign ("-"), which is selected by a large circle symbol ("◯") located at end. In terms of the order of writing right equations on the spot, it is always true to select the converted (ended) potential first for any equations of this family and to select the converted (ended) conjugate variable using a small circle symbol ("O") first for the product term.

5.5.2. The first-order partial derivative variables

$$\left(\frac{\partial A}{\partial T}\right)_V = (-S) \tag{58}$$

Pattern 2: ∂□ → ∂O → O = ◯

5.5.3. The Maxwell equations

$$\left(\frac{\partial(V)}{\partial T}\right)_P = \left(\frac{\partial(-S)}{\partial P}\right)_T \tag{59}$$

Pattern 3: Two "∂◯ → ∂O → O" equal each other

Both paths go around the large square reversely.

5.5.4. The Maxwell-II equations (or the inverted Maxwell equations)

$$\left(\frac{\partial(-S)}{\partial P}\right)_V = \left(\frac{\partial(V)}{\partial T}\right)_S \tag{60}$$

Pattern 4: Two "∂◯ → ∂O → O" equal each other

Both paths pass through the center like a shape of "8" or "∞."

5.5.5. The fundamental thermodynamic equations

$$\boldsymbol{dU} = (\boldsymbol{T})\cdot\boldsymbol{dS} + (-\boldsymbol{P})\cdot\boldsymbol{dV} \tag{61}$$

Pattern 5: *d*□ = ◯---*d*O ◯---*d*O

5.5.6. The Gibbs-Helmholtz equation's family

$$\left(\frac{\partial(G/T)}{\partial(1/T)}\right)_P = H \tag{62}$$

Pattern 6: ∂(□/O) → ∂(*1*/O) → O = □

5.5.7. The C_P type variables

$$C_P = \left(\frac{\partial H}{\partial T}\right)_P \tag{63}$$

Pattern 7: ☼ = ∂ □ → ∂O → O

5.5.8. The relations between Maxwell-III and C_P type variables

$$\left(\frac{\partial V}{\partial P}\right)_S = \frac{R_S}{(-P)} \tag{64}$$

Pattern 8: ∂O → ∂O → O = ☼/◯

5.5.9. The closest neighbor relations like C_V and C_P

$$C_{PN}(T,\,-P,\,-N) \to C_{VN}(T,V,\,-N) : C_V = C_P + \left(\frac{\partial V}{\partial T}\right)_P \bullet T \bullet \left(\frac{\partial(-P)}{\partial T}\right)_V \tag{65}$$

Pattern 9: ☼ = ☼ $\left(\frac{\partial O}{\partial O}\right)_O$ • O • $\left(\frac{\partial(\bigcirc)}{\partial O}\right)_O$

where a product term consists of three parts (two Maxwell-I partial derivatives and a mid variable, *T* in this case), the two Maxwell-I partial derivatives are symmetric each other with

http://dx.doi.org/10.5772/intechopen.72839

respect to a mirror, which is perpendicular to a line segment of a pair of the opposite sign conjugate variables ($-P \rightarrow V$) and passes through the mid variable (T), an uncertain sign (positive or negative) of the product term in the Pattern 9 depends on sign of the converting (starting), rather than the converted (ended), conjugate variable without or with a negative sign ("-"), and the converting (starting) conjugate variable ($-P$) is selected by a large circle symbol ("◯"), which is located at numerator of the second Maxwell-I partial derivative. In terms of the order of writing right equations on the spot, it is always true to select the converted (ended) C_P type variable first for any equations of this family and to select the converted (ended) conjugate variable using a small circle symbol ("O") first for the product term.

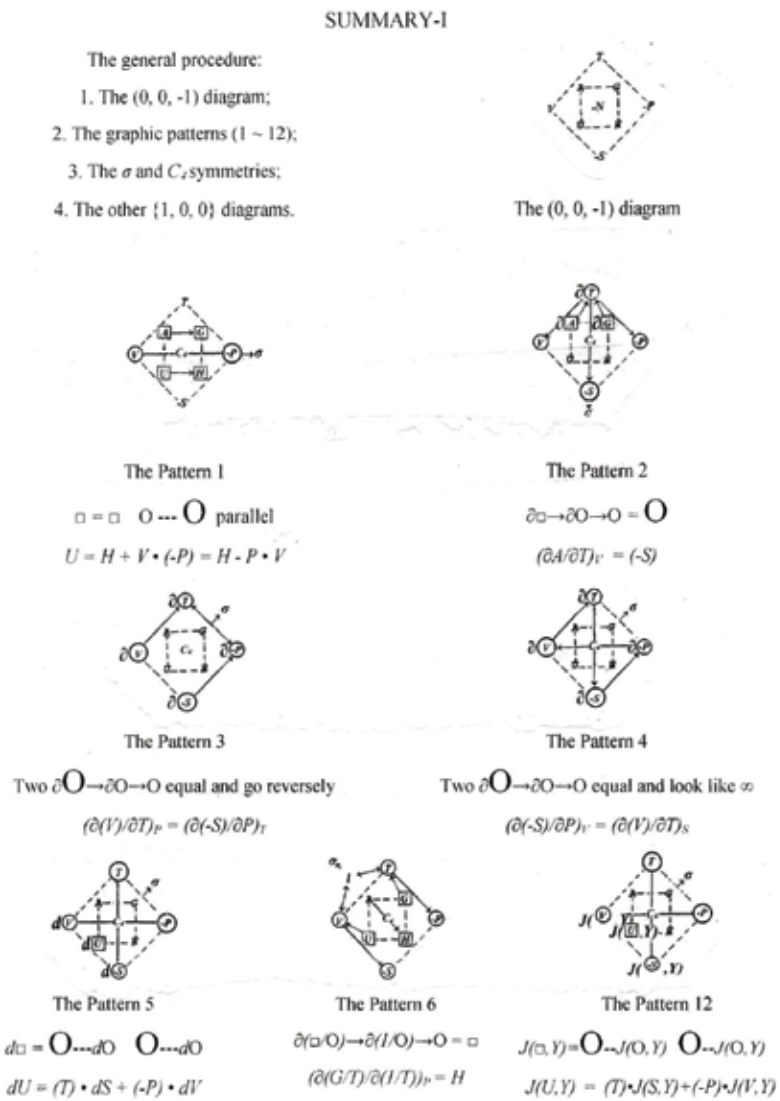

Figure 7. Summary-I of the Patterns (1–6 and 12) on the (0, 0, −1) diagram.

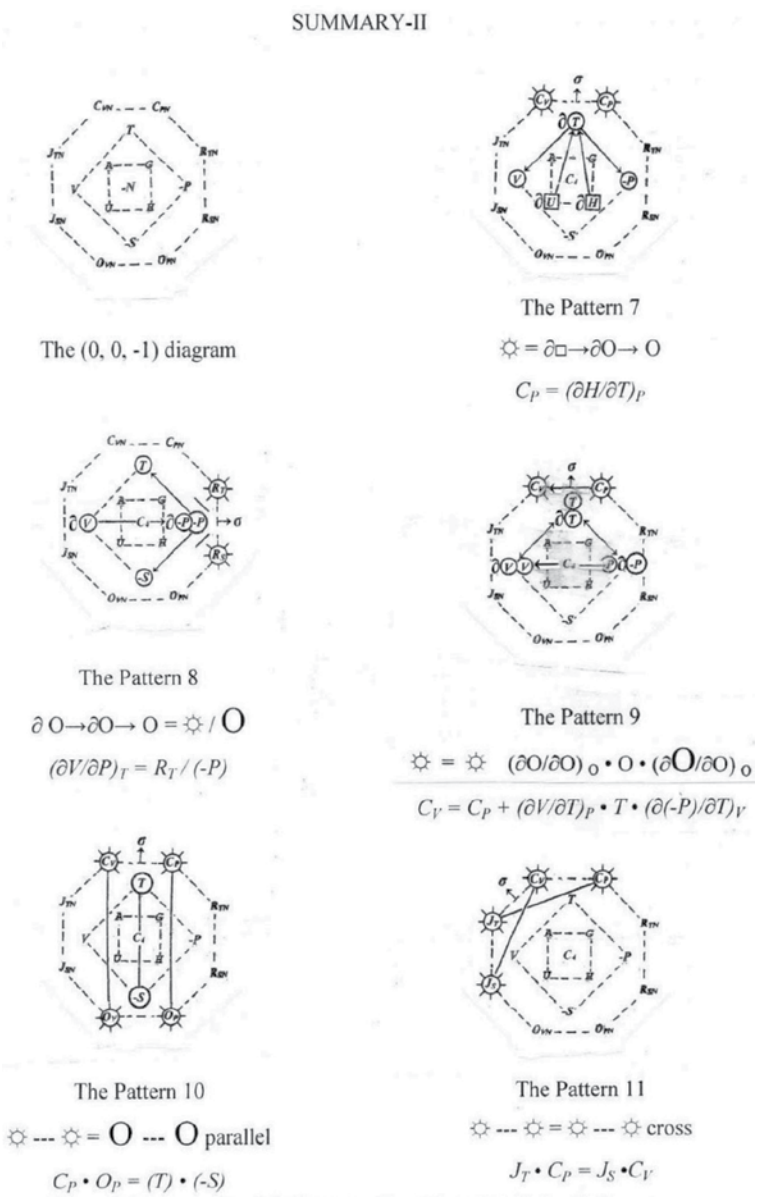

Figure 8. Summary-II of the Patterns (7–11) on the (0, 0, −1) diagram.

5.5.10. The parallel relations

$$C_P \bullet O_P = (T) \bullet (-S) = -T\,S \tag{66}$$

Pattern 10: ☼ --- ☼ = ◯ --- ◯

5.5.11. The cross relations

$$J_T \bullet C_P = J_S \bullet C_V \tag{67}$$

Pattern 11: ☼ --- ☼ = ☼ --- ☼

5.5.12. The Jacobian equations

$$\boldsymbol{J}(U,Y) = (T)\cdot\boldsymbol{J}(S,Y) + (-P)\cdot\boldsymbol{J}(V,Y) \tag{68}$$

Pattern 12: $\boldsymbol{J}(\square,Y)$ = ◯---$\boldsymbol{J}$(O,Y) ◯ --- $\boldsymbol{J}$(O,Y)

This Pattern 12 is similar to Pattern 5: $d\square$ = ◯ ---dO ◯---dO.

All the above 12 graphic patterns are summarized in **Figures 7** and **8**.

5.6. To derive any desired partial derivatives in terms of T, S, P, V, μ, N, C_P, α, κ_T, and ω

If we want to know the total differential of a multi-variable function, we need to know what its partial derivatives are. Often, there is no convenient experimental method to evaluate the partial derivatives needed for the numerical solution of a problem. In this case, we must calculate the partial derivatives and relate them to other quantities that are readily available, such as T, S, P, V, μ, N, C_P, α, κ_T, and ω (the molar grand canonical potential of the system, $\omega = (\partial\Omega/\partial N)_{VT}$).

5.6.1. Results of C_P type variables

Results of the 24 C_P-type variables are derived and given as follows:

$$C_{PN} = C_P \tag{69}$$

$$C_{VN} = C_{PN} + \left(\frac{\partial V}{\partial T}\right)_{P,N} \bullet T \bullet \left(\frac{\partial(-P)}{\partial T}\right)_{V,N} = C_P - \frac{\alpha^2 VT}{\kappa_T} \tag{70}$$

$$J_{TN} = \left(\frac{\partial G}{\partial V}\right)_{TN} = V\left(\frac{\partial P}{\partial V}\right)_{TN} = \frac{-1}{\kappa_T} \tag{71}$$

$$J_{SN} = \frac{J_{TN} \bullet C_{PN}}{C_{VN}} == \frac{-C_{PN}}{\kappa_T C_{VN}} = \frac{C_{PN}}{\alpha^2 VT - \kappa_T C_{PN}} \tag{72}$$

$$O_{PN} == \frac{T \bullet (-S)}{C_{PN}} = \frac{-TS}{C_{PN}} \tag{73}$$

$$O_{VN} = \frac{T \bullet (-S)}{C_{VN}} = \frac{\kappa_T ST}{\alpha^2 VT - \kappa_T C_{PN}} \tag{74}$$

$$R_{TN} = \frac{V \bullet (-P)}{J_{TN}} = \kappa_T PV \tag{75}$$

$$R_{SN} = \frac{V \bullet (-P)}{J_{SN}} = \kappa_T PV - \frac{\alpha^2 V^2 PT}{C_{PN}} \tag{76}$$

$$O_{P\mu} = \left(\frac{\partial \Phi}{\partial S}\right)_{P\mu} = -S\left(\frac{\partial T}{\partial S}\right)_{P\mu} = -S\left(\frac{\partial^2 \chi}{\partial S^2}\right)_{P\mu} = 0 \tag{77}$$

$$J_{T\mu} = \left(\frac{\partial \Phi}{\partial V}\right)_{T\mu} = V\left(\frac{\partial P}{\partial V}\right)_{T\mu} = -V\left(\frac{\partial^2 \Omega}{\partial V^2}\right)_{T\mu} = 0 \tag{78}$$

$$\Gamma_{PT} = \left(\frac{\partial \Phi}{\partial N}\right)_{PT} = N\left(\frac{\partial \mu}{\partial N}\right)_{PT} = -N\left(\frac{\partial^2 G}{\partial N^2}\right)_{PT} = 0 \tag{79}$$

$$C_{P\mu} = \left(\frac{\partial \chi}{\partial T}\right)_{P\mu} = T\left(\frac{\partial S}{\partial T}\right)_{P\mu} = -T\left(\frac{\partial^2 \Phi}{\partial T^2}\right)_{P\mu} = \infty \tag{80}$$

$$R_{T\mu} = \left(\frac{\partial \Omega}{\partial P}\right)_{T\mu} = -P\left(\frac{\partial V}{\partial P}\right)_{T\mu} = -P\left(\frac{\partial^2 \Phi}{\partial P^2}\right)_{T\mu} = \infty \tag{81}$$

$$\Lambda_{PT} = \left(\frac{\partial G}{\partial \mu}\right)_{PT} = \mu\left(\frac{\partial N}{\partial \mu}\right)_{PT} = -\mu\left(\frac{\partial^2 \Phi}{\partial \mu^2}\right)_{PT} = \infty \tag{82}$$

$$\begin{aligned} C_{V\mu} &= \left(\tfrac{\partial \Psi}{\partial T}\right)_{V\mu} = T\left(\tfrac{\partial S}{\partial T}\right)_{V\mu} = -T\left(\tfrac{\partial^2 \Omega}{\partial T^2}\right)_{V\mu} \\ &= C_{VN} + \left(\tfrac{\partial \mu}{\partial T}\right)_{NV} \bullet T \bullet \left(\tfrac{\partial(-N)}{\partial T}\right)_{\mu V} \\ &= C_{PN} - \frac{\alpha^2 VT}{\kappa_T} + \left(\frac{\partial \mu}{\partial T}\right)_{NV} \bullet T \bullet \left(\frac{\partial(-N)}{\partial T}\right)_{\mu V} \end{aligned} \tag{83}$$

$$\begin{aligned} J_{S\mu} &= \left(\tfrac{\partial \chi}{\partial V}\right)_{S\mu} = V\left(\tfrac{\partial P}{\partial V}\right)_{S\mu} = -V\left(\tfrac{\partial^2 \Psi}{\partial V^2}\right)_{S\mu} \\ &= J_{SN} + \left(\tfrac{\partial \mu}{\partial V}\right)_{NS} \bullet V \bullet \left(\tfrac{\partial(-N)}{\partial V}\right)_{\mu S} \\ &= \frac{C_{PN}}{\alpha^2 VT - \kappa_T C_{PN}} + \left(\frac{\partial \mu}{\partial V}\right)_{NS} \bullet V \bullet \left(\frac{\partial(-N)}{\partial V}\right)_{\mu S} \end{aligned} \tag{84}$$

$$\begin{aligned} O_{V\mu} &= \left(\tfrac{\partial \Omega}{\partial S}\right)_{V\mu} = -S\left(\tfrac{\partial T}{\partial S}\right)_{V\mu} = -S\left(\tfrac{\partial^2 \Psi}{\partial S^2}\right)_{V\mu} \\ &= O_{VN} + \left(\tfrac{\partial \mu}{\partial S}\right)_{NV} \bullet S \bullet \left(\tfrac{\partial(-N)}{\partial S}\right)_{\mu V} \\ &= \frac{\kappa_T ST}{\alpha^2 VT - \kappa_T C_{PN}} + \left(\frac{\partial \mu}{\partial S}\right)_{NV} \bullet S \bullet \left(\frac{\partial(-N)}{\partial S}\right)_{\mu V} \end{aligned} \tag{85}$$

$$\begin{aligned} R_{S\mu} &= \left(\frac{\partial \Psi}{\partial P}\right)_{S\mu} = -P\left(\frac{\partial S}{\partial P}\right)_{S\mu} = -P\left(\frac{\partial^2 \chi}{\partial P^2}\right)_{S\mu} \\ &= R_{SN} + \left(\frac{\partial \mu}{\partial P}\right)_{NS} \bullet P \bullet \left(\frac{\partial(-N)}{\partial P}\right)_{\mu S} \\ &= \kappa_T PV - \frac{\alpha^2 V^2 PT}{C_{PN}} + \left(\frac{\partial \mu}{\partial P}\right)_{NS} \bullet P \bullet \left(\frac{\partial(-N)}{\partial P}\right)_{\mu S} \end{aligned} \tag{86}$$

$$\begin{aligned} \Gamma_{VT} &= \left(\frac{\partial \Omega}{\partial N}\right)_{VT} = N\left(\frac{\partial \mu}{\partial N}\right)_{VT} = -N\left(\frac{\partial^2 A}{\partial N^2}\right)_{VT} = \omega \\ \Lambda_{VT} &= \left(\frac{\partial A}{\partial \mu}\right)_{VT} = \mu\left(\frac{\partial N}{\partial \mu}\right)_{VT} = -\mu\left(\frac{\partial^2 \Omega}{\partial \mu^2}\right)_{VT} \end{aligned} \tag{87}$$

$$= \frac{\mu \bullet (-N)}{\Gamma_{VT}} = \frac{-\mu N}{\omega} \tag{88}$$

$$\begin{aligned} \Gamma_{VS} &= \left(\frac{\partial \Psi}{\partial N}\right)_{VS} = N\left(\frac{\partial \mu}{\partial N}\right)_{VS} = -N\left(\frac{\partial^2 U}{\partial N^2}\right)_{VS} \\ &= \Gamma_{VT} + \left(\frac{\partial S}{\partial N}\right)_{TV} \bullet N \bullet \left(\frac{\partial T}{\partial N}\right)_{SV} \\ &= \omega + \left(\frac{\partial S}{\partial N}\right)_{TV} \bullet N \bullet \left(\frac{\partial T}{\partial N}\right)_{SV} \end{aligned} \tag{89}$$

$$\begin{aligned} \Gamma_{PS} &= \left(\frac{\partial \chi}{\partial N}\right)_{PS} = N\left(\frac{\partial \mu}{\partial N}\right)_{PS} = -N\left(\frac{\partial^2 H}{\partial N^2}\right)_{PS} \\ &= \Gamma_{VS} + \left(\frac{\partial P}{\partial N}\right)_{VS} \bullet N \bullet \left(\frac{\partial V}{\partial N}\right)_{PS} \\ &= \omega + \left(\frac{\partial S}{\partial N}\right)_{TV} \bullet N \bullet \left(\frac{\partial T}{\partial N}\right)_{SV} + \left(\frac{\partial P}{\partial N}\right)_{VS} \bullet N \bullet \left(\frac{\partial V}{\partial N}\right)_{PS} \end{aligned} \tag{90}$$

$$\begin{aligned} \Lambda_{VS} &= \left(\frac{\partial U}{\partial \mu}\right)_{VS} = \mu\left(\frac{\partial N}{\partial \mu}\right)_{VS} = -\mu\left(\frac{\partial^2 \Psi}{\partial \mu^2}\right)_{VS} \\ &= \frac{\mu \bullet (-N)}{\Gamma_{VS}} = \frac{-\mu N}{\omega + \left(\frac{\partial S}{\partial N}\right)_{TV} \bullet N \bullet \left(\frac{\partial T}{\partial N}\right)_{SV}} \end{aligned} \tag{91}$$

$$\begin{aligned} \Lambda_{PS} &= \left(\frac{\partial H}{\partial \mu}\right)_{PS} = \mu\left(\frac{\partial N}{\partial \mu}\right)_{PS} = -\mu\left(\frac{\partial^2 \chi}{\partial \mu^2}\right)_{PS} = \frac{\mu \bullet (-N)}{\Gamma_{PS}} \\ &= \frac{-\mu N}{\omega + \left(\frac{\partial S}{\partial N}\right)_{TV} \bullet N \bullet \left(\frac{\partial T}{\partial N}\right)_{SV} + \left(\frac{\partial P}{\partial N}\right)_{VS} \bullet N \bullet \left(\frac{\partial V}{\partial N}\right)_{PS}} \end{aligned} \tag{92}$$

The above 24 results of the C_P type variables are useful for deriving other partial derivatives. It can also be seen on (1, −1, 1) projection diagram (**Figure 3**-2) that locations of three zero-value ($O_{P\mu}$, $J_{T\mu}$, Γ_{PT}) and three infinite-value ($C_{P\mu}$, $R_{T\mu}$, Λ_{PT}) C_P type variables display the C_3 (three-fold rotation) symmetry about the $U \sim \Phi$ pair at the center of the diagram.

5.6.2. To derive any desired partial derivatives

Any desired partial derivatives, $\left(\frac{\partial X}{\partial Y}\right)_{ZW}$, can be derived in terms of T, S, P, V, μ, N, C_P, α, κ_T, and ω by using the graphic patterns (Patterns 1–12) and the results of C_P type variables. Two examples are shown below:

Example 1 $(\partial G/\partial S)_V = ?$

$$\left(\frac{\partial G}{\partial S}\right)_V = \left(\frac{\partial(A + P \bullet (V))}{\partial S}\right)_V \qquad \text{(Pattern 1)}$$

$$= \left(\frac{\partial(U + T \bullet (-S) + P \bullet (V))}{\partial S}\right)_V \qquad \text{(Pattern 1)}$$

$$= \left(\frac{\partial U}{\partial S}\right)_V - T - S\left(\frac{\partial T}{\partial S}\right)_V + V\left(\frac{\partial P}{\partial S}\right)_V$$

$$= T - T - S\left(\frac{O_V}{(-S)}\right) - V\left(\frac{\partial T}{\partial V}\right)_S \qquad \text{(Patterns 2, 8 \& 3)}$$

$$= O_V - V\left(\frac{-(\partial S/\partial V)_T}{(\partial S/\partial T)_V}\right) \qquad \text{(chain eq.)}$$

$$= \frac{T \bullet (-S)}{C_V} - V\left\{\frac{-(\partial P/\partial T)_V}{C_V/T}\right\} \qquad \text{(Patterns 10, 3 \& 8)}$$

$$= \frac{T \bullet (-S)}{C_V} + V\left\{\frac{-\frac{(\partial V/\partial T)_P}{(\partial V/\partial P)_T}}{C_V/T}\right\} \qquad \text{(chain eq.)}$$

$$= \frac{T \bullet (-S)}{C_V} + \frac{V(\alpha/\kappa_T)}{C_V/T} \qquad (\alpha \text{ \& } \kappa_T\text{'s def.})$$

$$= \frac{-TS}{C_V} + \frac{\alpha VT}{\kappa_T C_V} = \frac{\alpha VT - \kappa_T TS}{\kappa_T C_V}$$

$$= \frac{\alpha VT - \kappa_T TS}{\kappa_T(C_P - \alpha^2 VT/\kappa_T)} = \frac{\alpha VT - \kappa_T TS}{\kappa_T C_P - \alpha^2 VT} \qquad (C_V\text{'s result})$$

Example 2 $(\partial A)_H = ?$

This is a question chosen from Bridgman's thermodynamic equations [16], where the symbol of the question stands for the Jacobian of two functions (A and H) with respect to two independent variables (T and P), i.e. $J(T, P) = 1$.

$$(\partial A)_H = \partial(A, H) = J(A, H)$$

$$= (-S) \bullet J(T, H) + (-P) \bullet J(V, H) \text{ (Pattern 12)}$$

$$= (S) \bullet J(H, T) + (P) \bullet J(H, V) \text{ (Eq. (54))}$$

where, $J(H, T) = (V) \bullet J(P, T) + (T) \bullet J(S, T)$ (Pattern 12)

$$= (V) \bullet \frac{J(P, T)}{J(T, P)} + (T) \bullet \frac{J(S, T)}{J(T, P)} \; (J(T,\ P)\ =\ 1)$$

$$= -(V) - (T) \bullet \frac{\partial(S, T)}{\partial(P, T)} \quad \text{(Eq. (54))}$$

$$= -(V) - (T) \bullet \left(\frac{\partial S}{\partial P}\right)_T = -V + T \bullet \left(\frac{\partial V}{\partial T}\right)_P \text{ (Eq. (54) \& Pattern 3)}$$

$$= -V + T \bullet (\alpha V) = \alpha VT - V = (\alpha T - 1)V \text{ (α's definition)}$$

and

$$J(H,V) = (V) \bullet J(P,V) + (T) \bullet J(S,V) \text{ (Pattern 12)}$$

$$= (V) \bullet \frac{J(P,V)}{J(T,P)} + (T) \bullet \frac{J(S,V)}{J(T,V)}\frac{J(T,V)}{J(T,P)} \text{ ($J(T,\ P) = 1$ \& Eq. (55))}$$

$$= -(V) \bullet \left(\frac{\partial V}{\partial T}\right)_P + (T) \bullet \left(\frac{\partial S}{\partial T}\right)_V \left(\frac{\partial V}{\partial P}\right)_T \text{ (Eq. (54))}$$

$$= -(V) \bullet (\alpha V) + (T) \bullet \left(\frac{C_V}{T}\right)(-\kappa_T V) \text{ (α, κ_T's def. \& Pattern 8)}$$

$$= -\alpha V^2 + \left(C_P - \frac{\alpha^2 VT}{\kappa_T}\right)(-\kappa_T V) \text{ (C_V's result)}$$

$$= -\alpha V^2 - C_P \kappa_T V + \alpha^2 V^2 T = \alpha V^2(\alpha T - 1) - C_P \kappa_T V$$

Finally, substitute the results of $J(H,T)$ and $J(H,V)$ into the above equation and yield

$$(\partial A)_H = J(A,H) = S \bullet J(H,T) + P \bullet J(H,V)$$

$$= S \bullet \{(\alpha T - 1)V\} + P \bullet \{\alpha V^2(\alpha T - 1) - C_P \kappa_T V\}$$

$$= V\{(\alpha T - 1) \bullet (S + \alpha PV) - C_P \kappa_T P\}$$

6. Discussion

There are not generally accepted symbols and names for all thermodynamic potentials; however, based on the fact that sum of any pair of the diagonal potentials in the cube is same and equals the internal energy of the system, i.e., $\square + \square^* = TS - PV + \mu N = U(S, V, N)$, it is suggested that three unnamed thermodynamic potentials $\Phi(T, P, \mu)$, $\psi(S, V, \mu)$, and $\chi(S, P, \mu)$ may be meaningfully named to be conjugate internal energy, conjugate Gibbs free energy, and conjugate Helmholtz free energy, respectively, with respect to $U(S, V, N)$, $G(T, P, N)$, and $A(T, V, N)$.

There are not generally accepted symbols and names for all 24 C_P type variables; however, it is clearly found out that an integration of the entire structure of a variety of thermodynamic variables is complete and highly coherent with symmetry. For example, a complete set of the 24 C_P type variables (C_{PN}, C_{VN} O_{PN}, O_{VN}, J_{TN}, J_{SN}, R_{TN}, R_{SN}, $C_{P\mu}$, $C_{V\mu}$, $O_{P\mu}$, $O_{V\mu}$, $J_{T\mu}$, $J_{S\mu}$, $R_{T\mu}$, $R_{S\mu}$, Λ_{PT}, Λ_{VT}, Γ_{PT}, Γ_{VT}, Λ_{PS}, Λ_{VS}, Γ_{PS}, and Γ_{VS}) were initially defined for a completion based on the equivalence principle of symmetry, and they are finally proven to relate each other with three concise (closest neighbor, parallel, and cross) relations symmetrically and consistently.

Based on the fact that the scheme to build up the extended concentric multi-polyhedron corresponds to Ehrenfest's scheme to classify phase transitions, it is reasonable for us to predict that the coherent and complete structure of thermodynamics may further be extended along with novel research results about higher order phase transitions in future.

Based on the fact that symmetry plays an important role to integrate the entire structure of the thermodynamic variables into a coherent and complete exposition of thermodynamics, it is reasonable for us to consider the symmetry as one of foundations (or axioms) of the subject and therefore to believe thermodynamics being a science of symmetry.

7. Conclusions

1. A variety of four categories of total 44 thermodynamic variables are properly arranged at the vertices of the extended concentric multi-polyhedron diagram based on their physical meanings.

2. A symmetric function with "patterned self-similarity" is precisely be defined as the function of a general formula for each family in thermodynamics, which is unchanged not only in function form but also in variable's nature and neighbor relationship under symmetric operations.

3. Although the reversible Legendre transforms ($E \leftrightarrow R$) are asymmetric under a pair of the same sign conjugate variables (w and z), however, the asymmetric ($E \leftrightarrow R$) can become symmetric ($E^* \leftrightarrow R^*$) under two required conditions: a pair of the opposite sign conjugate variables (z and $-w$ or $-z$ and w) and a pair of the opposite conjugate variable treatments (canceling and keeping the negative sign) are involved in the symmetric ($E^* \leftrightarrow R^*$).

4. Thermodynamic symmetry roots in the symmetric reversible Legendre transforms of the potentials under the opposite sign conjugate natural variable pairs ($T \sim -S$, $-P \sim V$, and $\mu \sim -N$). The specific thermodynamic symmetries revealed by the extended concentric multi-polyhedron diagram are only one C_3 (threefold rotation) symmetry about the $U \sim \Phi$ diagonal direction and C_4 (fourfold rotation) and σ (mirror) symmetries on three U-containing squares, where the square including U, H, G, and A is the most important and useful one.

5. Based on the equivalence principle of symmetry (reproducibility and predictability), numerous (more than 300) equations of 12 families can concisely be depicted by overlapping 12 specifically created rigid, movable graphic patterns on the fixed {1, 0, 0} diagrams through σ and/or C_4 symmetric operations. Any desired partial derivatives can be derived in terms of several available quantities by the foolproof graphic method.

6. It is the symmetry that made possible to build up the diagram as an elegant model to exhibit an integration of the entire structure of the thermodynamic variables into a coherent and complete exposition of thermodynamics. The model has much common with the Periodic Table of the Elements in chemistry.

Author details

Zhen-Chuan Li

Address all correspondence to: zhenchuanli@yahoo.com

Department of Physics and Chemistry, Stuyvesant (Specialized in Mathematics and Science) HS, New York, USA

References

[1] Callen H. Thermodynamics as a science of symmetry. Foundations of Physics. 1974;**4**(4): 423-443

[2] Callen HB. Thermodynamics and an Introduction to Thermostatistics. 2nd ed. New York: Wiley; 1985:131, 458

[3] Koenig FO. Families of thermodynamic equations. I—The method of transformations by the characteristic group. The Journal of Chemical Physics. 1935;**3**:29

[4] Koenig FO. Families of thermodynamic equations. II—The case of eight characteristic functions. The Journal of Chemical Physics. 1972;**56**:4556

[5] Prins JA. On the thermodynamic substitution group and its representation by the rotation of a square. The Journal of Chemical Physics. 1948;**16**:65

[6] Fox RF. The thermodynamic cuboctahedron. Journal of Chemical Education. 1976;**53**:441

[7] Li Z. (李震川) A study of graphic representation of thermodynamic state function relations. Huaxue Tongbao (Chemistry). 1982;**1982**(1):48-55. (in Chinese) & Chemical Abstract, 96, 488. 96: 188159t (1982)

[8] Pate SF. The thermodynamic cube: A mnemonic and learning device for students of classic thermodynamics. American Journal of Physics. 1999;**67**(12):1111

[9] Kerr WC, Macosko JC. Thermodynamic Venn diagram: Sorting out force, fluxes, and Legendre transforms. American Journal of Physics. 2011;**79**(9):950-953

[10] Alberty RA. Use of Legendre transforms in chemical thermodynamics. Pure and Applied Chemistry. 2001;**73**(8):1350

[11] Zia RKP, Redish EF, McKay SR. Making sense of the Legendre transform. American Journal of Physics. 2009;**77**:614-622

[12] Rosen J. Symmetry in Science. New York: Springer; 1995. p. 97

[13] Crawford FH. Jacobian methods in thermodynamics. American Journal of Physics. 1949;**17**(1):1

[14] Reid CE. Principles of Chemical Thermodynamics. New York: Reinhold; 1960 p. 36 & 249

[15] Li Z-C. Symmetry Graphical Method in Thermodynamics. US 2017-0242936 A9. Available from: http://www.uspto.gov/patft/ [Accessed: 24 August 2017]

[16] Bridgman PW. Physical Review, 2nd Series. 1914;**3**:273

Chapter 7

Approximate Spin Projection for Broken-Symmetry Method and Its Application

Yasutaka Kitagawa, Toru Saito and
Kizashi Yamaguchi

Additional information is available at the end of the chapter

http://dx.doi.org/10.5772/intechopen.75726

Abstract

A broken-(spin) symmetry (BS) method is now widely used for systems that involve (quasi) degenerated frontier orbitals because of their lower cost of computation. The BS method splits up-spin and down-spin electrons into two different special orbitals, so that a singlet spin state of the degenerate system is expressed as a singlet biradical. In the BS solution, therefore, the spin symmetry is no longer retained. Due to such spin-symmetry breaking, the BS method often suffers from a serious problem called a spin contamination error, so that one must eliminate the error by some kind of projection method. An approximate spin projection (AP) method, which is one of the spin projection procedures, can eliminate the error from the BS solutions by assuming the Heisenberg model and can recover the spin symmetry. In this chapter, we illustrate a theoretical background of the BS and AP methods, followed by some examples of their applications, especially for calculations of the exchange interaction and for the geometry optimizations.

Keywords: quantum chemistry, ab initio calculation, orbital degeneracy, electron correlation, broken-(spin) symmetry (BS) method, approximate spin projection (AP) method, spin polarization, spin contamination error, effective exchange integral (J_{ab}) values

1. Introduction

For the past few decades, many reports about "polynuclear metal complexes" have been presented actively in the field of the coordination chemistry [1–19]. Those systems usually have complicated electronic structures that are constructed by metal–metal (d-d) and metal–ligand (d-p) interactions. Those electronic structures caused by their unique molecular

structures often bring many interesting and noble physical functionalities such as a magnetism [8–17], a nonlinear optics [18], an electron conductivity [19], as well as their chemical functionalities, e.g., a catalyst and so on. For example, some three-dimensional (3D) metal complexes show interesting magnetic behaviors and are expected to be possible candidates for a single molecule magnet, a quantum dot, and so on [11–16]. On the other hand, one-dimensional (1D) metal complexes are studied for the smallest electric wire, i.e., the nanowire [3–7, 17, 19]. In addition, it has been elucidated that the polynuclear metal complexes play an important role in the biosystems [20–24], e.g., Mn cluster [25, 26] in photosystem II and 4Fe-4S cluster [27–30] in electron transfer proteins. In this way, the polynuclear metal complexes are widely noticed from a viewpoint of fundamental studies on their peculiar characters and of applications to materials. From those reasons, an elucidation of a relation among electronic structures, molecular structures, and physical properties is a quite important current subject.

Physical properties of molecules are sometimes discussed by using several parameters such as an exchange integrals (J_{ab}), on-site Coulomb repulsion, and transfer integrals of Heisenberg and Hubbard Hamiltonians, respectively, in material physics [31–35]. In recent years, on the other hand, direct predictions of such electronic structures, molecular structure, and physical properties of those metal complexes are fairly realized by the recent progress in computers and computational methods. In this sense, theoretical calculations are now one of the powerful tools for understanding of such systems. However, those systems are, in a sense, still challenging subjects because they are usually large and orbitally degenerated systems with localized electron spins (localized orbitals). The localized spins are caused by an electron correlation effect called a static (or a non-dynamical) correlation [36]. In addition, a dynamical correlation effect of core electrons also must be treated together with the static correlation in the case of the metal complexes. A treatment of both the static correlation and the dynamical correlation in large molecules is still a difficult task and a serious problem in this field. For those systems, a standard method for the static and dynamical correlation corrections is a complete active space (CAS) method [37–38] or a multi-reference (MR) method [39] that considers all configuration interaction in active valence orbitals, together with the second-order perturbation correction, e.g., CASPT2 or MPMP2 methods. In addition to these methods, recently, other multi-configuration methods such as DDCI [40–42], CASDFT [43–45], MRCC [46–48], and DMRG-CT [49–51] methods are also proposed for the same purpose. These newer methods are developing and seem to be promising tools in terms of accuracy; however, real molecules such as polynuclear metal complexes are still too large to treat computationally with those methods at this state. An alternative way is a broken-symmetry (BS) method, which approximates the static correlation with a lower cost of computation [52–55]. The BS method (or commonly known as an unrestricted (U) method) splits up and down spins (electrons) into two different spatial orbitals (it is sometimes called as different orbitals for different spins; DODS), so a singlet spin state of the orbitally degenerated system is expressed as a singlet biradical, namely, the BS singlet [55]. The BS method such as the unrestricted Hartree-Fock (UHF) and the unrestricted DFT (UDFT) methods are now widely used for the first principle calculations of such large degenerate systems. In this sense, the BS method seems to be the most possible quantum chemical approach for the polynuclear metal complexes, although it has a serious problem called the spin contamination error [56–65]. Therefore one must eliminate the error by

some kind of projection method. An approximate spin projection (AP) method, which is one of the spin projection procedures, can eliminate the error from the BS solutions and can recover the spin symmetry. In this chapter, we illustrate a theoretical background of the BS and AP methods, followed by some examples of their applications.

2. Theoretical background of AP method

In this section, the theoretical background of the BS and AP methods for the biradical systems is explained with the simplest two-spin model (e.g., a dissociated H_2) as illustrated in **Figure 1(a)**.

2.1. Broken-symmetry (BS) solution and approximate spin projection (AP) methods for the (two-spin) biradical state

In the BS method, the spin-polarized orbitals are obtained from HOMO-LUMO mixing [55–56]. For example, HOMO orbitals for up-spin (ψ_{HOMO}) and down-spin ($\overline{\psi}_{\mathrm{HOMO}}$) electrons of the simple H_2 molecule are expressed as follows (**Figure 1(b)**):

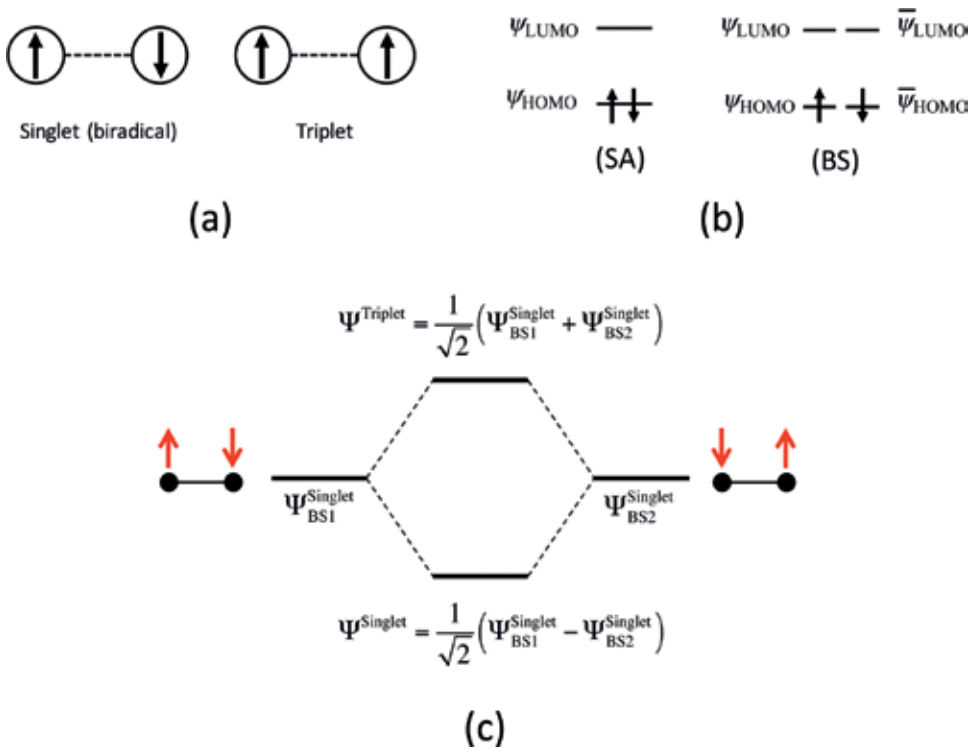

Figure 1. (a) Illustration of the two-spin states of the simplest two-spin model. (b) HOMO and LUMO of spin-adapted (SA) and BS methods. (c) Illustration of spin-symmetry recovery of BS method by AP method.

$$\psi_{\mathrm{HOMO}}^{\mathrm{BS}} = \cos\theta\psi_{\mathrm{HOMO}} + \sin\theta\psi_{\mathrm{LUMO}}, \tag{1}$$

$$\overline{\psi}_{\mathrm{HOMO}}^{\mathrm{BS}} = \cos\theta\psi_{\mathrm{HOMO}} - \sin\theta\psi_{\mathrm{LUMO}}, \tag{2}$$

where $0 \le \theta \le 45^\circ$ and ψ_{HOMO} and ψ_{LUMO} express HOMO and LUMO orbitals of spin-adapted (SA) (or spin-restricted (R)) calculations, respectively, as illustrated in **Figure 1(b)**. And the wavefunction of the BS singlet (e.g., unrestricted Hartree-Fock (UHF)) becomes

$$\left|\Psi_{\mathrm{BS}}^{\mathrm{Singlet}}\right\rangle = \cos^2\theta\left|\psi_{\mathrm{HOMO}}\overline{\psi}_{\mathrm{HOMO}}\right\rangle + \sin^2\theta\left|\psi_{\mathrm{LUMO}}\overline{\psi}_{\mathrm{LUMO}}\right\rangle - \sqrt{2}\cos\theta\sin\theta\left|\Psi^{\mathrm{Triplet}}\right\rangle, \tag{3}$$

where ψ_{HOMO} and $\overline{\psi}_{HOMO}$ express up- and down-spin electrons in orbital ψ_{HOMO}, respectively. If $\theta = 0$, the BS wavefunction corresponds to the closed shell, i.e., SA wavefunctions, while if θ is not zero, one can have spin-polarized, i.e., BS wavefunctions. In the BS solution, $\psi_{HOMO} \neq \overline{\psi}_{HOMO}$ (**Figure 1(b)**), so that a spin symmetry is broken. In addition, it gives nonzero $\left\langle \hat{s}^2 \right\rangle_{\mathrm{BS}}^{\mathrm{Singlet}}$ value, and as described later, up- and down-spin densities appeared on the hydrogen atoms.

We often regard such spin densities as an existence of localized spins. An interaction between localized spins can be expressed by using Heisenberg Hamiltonian:

$$\widehat{\boldsymbol{H}} = -2J_{\mathrm{ab}}\widehat{\boldsymbol{S}}_{\mathbf{a}} \cdot \widehat{\boldsymbol{S}}_{\mathbf{b}}, \tag{4}$$

where $\widehat{\boldsymbol{S}}_{\mathrm{a}}$ and $\widehat{\boldsymbol{S}}_{\mathrm{b}}$ are spin operators for spin sites a and b, respectively, and J_{ab} is an effective exchange integral. Using a total spin operator of the system $\widehat{\boldsymbol{S}} = \widehat{\boldsymbol{S}}_{\mathrm{a}} + \widehat{\boldsymbol{S}}_{\mathrm{b}}$, Eq. (4) becomes

$$\widehat{\boldsymbol{H}} = -2J_{\mathrm{ab}}\left(-\widehat{\boldsymbol{S}}^2 + \widehat{\boldsymbol{S}}_{\mathbf{a}}^2 + \widehat{\boldsymbol{S}}_{\mathbf{b}}^2\right). \tag{5}$$

Operating Eq. (5) to Eq. (3), the singlet state energy in Heisenberg Hamiltonian ($E_{\mathrm{HH}}^{\mathrm{Singlet}}$) is expressed as

$$E_{\mathrm{HH}}^{\mathrm{Singlet}} = J_{\mathrm{ab}}\left(-\left\langle\widehat{\boldsymbol{S}}^2\right\rangle^{\mathrm{Singlet}} + \left\langle\widehat{\boldsymbol{S}}_{\mathbf{a}}^2\right\rangle^{\mathrm{Singlet}} + \left\langle\widehat{\boldsymbol{S}}_{\mathbf{b}}^2\right\rangle^{\mathrm{Singlet}}\right). \tag{6}$$

Similarly, for triplet state

$$E_{\mathrm{HH}}^{\mathrm{Triplet}} = J_{\mathrm{ab}}\left(-\left\langle\widehat{\boldsymbol{S}}^2\right\rangle^{\mathrm{Triplet}} + \left\langle\widehat{\boldsymbol{S}}_{\mathbf{a}}^2\right\rangle^{\mathrm{Triplet}} + \left\langle\widehat{\boldsymbol{S}}_{\mathbf{b}}^2\right\rangle^{\mathrm{Triplet}}\right). \tag{7}$$

The energy difference between singlet ($E_{\mathrm{HH}}^{\mathrm{Singlet}}$) and triplet ($E_{\mathrm{HH}}^{\mathrm{Triplet}}$) states (S-T gap) within Heisenberg Hamiltonian should be equal to the S-T gap calculated by the difference in total energies of ab initio calculations (here we denote $E_{\mathrm{BS}}^{\mathrm{Singlet}}$ and E^{Triplet} for the BS singlet and triplet states, respectively). And if we can assume that spin densities of the BS singlet state on spin site i (i = a or b) are almost equal to ones of the triplet state, i.e., $\left\langle\widehat{s}_i^2\right\rangle^{\mathrm{Triplet}} \cong \left\langle\widehat{s}_i^2\right\rangle^{\mathrm{Singlet}}$, then J_{ab} can be derived as

$$J_{ab} = \frac{E_{HH}^{Singlet} - E_{HH}^{Triplet}}{\left\langle \hat{S}^2 \right\rangle^{Triplet} - \left\langle \hat{S}^2 \right\rangle^{Singlet}} = \frac{E_{BS}^{Singlet} - E^{Triplet}}{\left\langle \hat{S}^2 \right\rangle^{Triplet} - \left\langle \hat{S}^2 \right\rangle_{BS}^{Singlet}}. \quad (8)$$

If the method is exact and the spin contamination error is not found in both singlet and triplet states (i.e., $\left\langle \hat{s}^2 \right\rangle_{Exact}^{Singlet} = 0$ and $\left\langle \hat{s}^2 \right\rangle_{Exact}^{Triplet} = 2$), the S-T gap between those states can be expressed as

$$E_{Exact}^{Singlet} - E_{Exact}^{Triplet} = 2J_{ab}. \quad (9)$$

The spin contamination in the triplet state is usually negligible (i.e., $\left\langle \hat{s}^2 \right\rangle_{Exact}^{Triplet} \cong \left\langle \hat{s}^2 \right\rangle^{Triplet} \cong 2$), and one must consider the error only in the BS singlet state, so the S-T gap becomes

$$E_{BS}^{Singlet} - E^{Triplet} = 2J_{ab} - J_{ab}\left\langle \hat{S}^2 \right\rangle_{BS}^{Singlet}. \quad (10)$$

A second term in a right side of Eq. (10) indicates the spin contamination error in the S-T gap, and consequently, a second term in a denominator of Eq. (8) eliminates the spin contamination in the BS singlet solution. In this way, Eq. (8) gives approximately spin-projected (AP) J_{ab} values. Eq. (8) can be easily expanded into any spin dimers, namely, the lowest spin (LS) state and the highest spin (HS) state, e.g., singlet-quintet for $S_a = S_b = 2/2$ pairs, singlet-sextet for $S_a = S_b = 3/2$ pairs, and so on, as follows:

$$J_{ab} = \frac{E_{BS}^{LS} - E^{HS}}{\left\langle \hat{S}^2 \right\rangle^{HS} - \left\langle \hat{S}^2 \right\rangle_{BS}^{LS}}. \quad (11)$$

Eq. (11) is the so-called Yamaguchi equation to calculate J_{ab} values with the AP procedure, which is simply denoted by J_{ab} here. The calculated J_{ab} value can explain an interaction between two spins. If a sign of calculated J_{ab} value is positive, the HS, i.e., ferromagnetic coupling state, is stable, while if it is negative, the LS, i.e., antiferromagnetic coupling state is stable. Therefore, one can discuss the magnetic interactions in a given system.

2.2. Approximate spin projection for BS energy and energy derivatives

Because J_{ab} calculated by Eq. (11) is a value that the spin contamination error is approximately eliminated, it should be equal to J_{ab} value calculated by the approximately spin-projected LS energy (E_{AP}^{LS}) as

$$J_{ab} = \frac{E_{BS}^{LS} - E^{HS}}{\left\langle \hat{S}^2 \right\rangle^{HS} - \left\langle \hat{S}^2 \right\rangle_{BS}^{LS}} = \frac{E_{AP}^{LS} - E^{HS}}{\left\langle \hat{S}^2 \right\rangle_{exact}^{HS} - \left\langle \hat{S}^2 \right\rangle_{ecact}^{LS}}. \quad (12)$$

Here, we assume $\left\langle \hat{s}^2 \right\rangle_{Exact}^{HS} \cong \left\langle \hat{s}^2 \right\rangle^{HS}$; then one can obtain a spin-projected energy of the singlet state without the spin contamination error as follows [62–65]:

$$E_{\mathrm{AP}}^{\mathrm{LS}} = \alpha E_{\mathrm{BS}}^{\mathrm{LS}} - \beta E^{\mathrm{HS}}, \tag{13}$$

where

$$\alpha = \frac{\left\langle \widehat{S}^2 \right\rangle^{\mathrm{HS}} - \left\langle \widehat{S}^2 \right\rangle_{\mathrm{exact}}^{\mathrm{LS}}}{\left\langle \widehat{S}^2 \right\rangle^{\mathrm{HS}} - \left\langle \widehat{S}^2 \right\rangle_{\mathrm{BS}}^{\mathrm{LS}}} \tag{14}$$

and

$$\beta = \alpha - 1 \tag{14}$$

Then, we explain about derivatives of this spin-projected energy ($E_{\mathrm{AP}}^{\mathrm{LS}}$). In order to carry out the geometry optimization using the AP method, an energy gradient of $E_{\mathrm{AP}}^{\mathrm{LS}}$ is necessary. $E_{\mathrm{AP}}^{\mathrm{LS}}$ can be expanded by using Taylor expansion:

$$E_{\mathrm{AP}}^{\mathrm{LS}}\left(\boldsymbol{R}_{\boldsymbol{AP}}^{\boldsymbol{LS}}\right) = E_{\mathrm{AP}}^{\mathrm{LS}}(\boldsymbol{R}) + \boldsymbol{X}^T \boldsymbol{G}_{\mathrm{AP}}^{\mathrm{LS}}(\boldsymbol{R}) + \frac{1}{2}\boldsymbol{X}^T \boldsymbol{F}_{\mathrm{AP}}^{\mathrm{LS}}(\boldsymbol{R})\boldsymbol{X}, \tag{15}$$

where $\boldsymbol{G}_{\mathrm{AP}}^{\mathrm{LS}}(\boldsymbol{R})$ and $\boldsymbol{F}_{\mathrm{AP}}^{\mathrm{LS}}(\boldsymbol{R})$ are the first and second derivatives (i.e., gradient and Hessian) of $E_{\mathrm{AP}}^{\mathrm{LS}}(\boldsymbol{R})$, respectively [62–65]; $\boldsymbol{R}_{\mathrm{AP}}^{\mathrm{LS}}$ and $\boldsymbol{R}$ are a stationary point of $E_{\mathrm{AP}}^{\mathrm{LS}}(\boldsymbol{R})$ and a present position, respectively; and $\boldsymbol{X}$ is a position vector ($\boldsymbol{X} = \boldsymbol{R}_{\mathrm{AP}}^{\mathrm{LS}} - \boldsymbol{R}$). The stationary point $\boldsymbol{R}_{\mathrm{AP}}^{\mathrm{LS}}$ is a position where $\boldsymbol{G}_{\mathrm{AP}}^{\mathrm{LS}}(\boldsymbol{R}) = 0$; therefore one can obtain $\boldsymbol{R}_{\mathrm{AP}}^{\mathrm{LS}}$ if $\boldsymbol{G}_{\mathrm{AP}}^{\mathrm{LS}}(\boldsymbol{R})$ can be calculated. By differentiating $E_{\mathrm{AP}}^{\mathrm{LS}}(\boldsymbol{R})$ in Eq. (13), we obtain

$$\boldsymbol{G}_{\mathrm{AP}}^{\mathrm{LS}}(\boldsymbol{R}) = \frac{\partial E_{\mathrm{AP}}^{\mathrm{LS}}(\boldsymbol{R})}{\partial \boldsymbol{R}} = \left\{\alpha(\boldsymbol{R})\boldsymbol{G}_{\mathrm{BS}}^{\mathrm{LS}}(\boldsymbol{R}) - \beta(\boldsymbol{R})\boldsymbol{G}^{\mathrm{HS}}(\boldsymbol{R})\right\} + \frac{\partial \alpha(\boldsymbol{R})}{\partial \boldsymbol{R}}\left\{E_{\mathrm{BS}}^{\mathrm{LS}}(\boldsymbol{R}) - E^{\mathrm{HS}}(\boldsymbol{R})\right\}, \tag{16}$$

where $\boldsymbol{G}_{\mathrm{BS}}^{\mathrm{LS}}$ and $\boldsymbol{G}^{\mathrm{HS}}$ are the first energy derivatives (energy gradients) of the BS and the HS states, respectively. As mentioned above, the spin contamination in the HS state is negligible, so that $\left\langle \hat{s}^2 \right\rangle^{\mathrm{HS}}$ is usually a constant. Then $\partial\alpha(\boldsymbol{R})/\partial\boldsymbol{R}$ can be written as

$$\frac{\partial \alpha(\boldsymbol{R})}{\partial \boldsymbol{R}} = \frac{\left\langle \widehat{S}^2 \right\rangle^{\mathrm{HS}} - \left\langle \widehat{S}^2 \right\rangle_{\mathrm{exact}}^{\mathrm{LS}}}{\left(\left\langle \widehat{S}^2 \right\rangle^{\mathrm{HS}} - \left\langle \widehat{S}^2 \right\rangle_{\mathrm{BS}}^{\mathrm{LS}}\right)^2} \frac{\partial \left\langle \widehat{S}^2 \right\rangle_{\mathrm{BS}}^{\mathrm{LS}}}{\partial \boldsymbol{R}}. \tag{17}$$

By using Eqs. (16) and (17), the AP optimization can be carried out. In addition, one can also calculate the spin-projected Hessian (AP Hessian; $\boldsymbol{F}_{\mathrm{AP}}^{\mathrm{LS}}(\boldsymbol{R})$ in Eq. (15)) as follows:

$$\boldsymbol{F}_{\mathrm{AP}}^{\mathrm{LS}}(\boldsymbol{R}) = \frac{\partial^2 E_{\mathrm{AP}}^{\mathrm{LS}}(\boldsymbol{R})}{\partial^2 \boldsymbol{R}} = \left\{\alpha(\boldsymbol{R})\boldsymbol{F}_{\mathrm{BS}}^{\mathrm{LS}}(\boldsymbol{R}) - \beta(\boldsymbol{R})\boldsymbol{F}^{\mathrm{HS}}(\boldsymbol{R})\right\},$$

$$+2\frac{\partial \alpha(\boldsymbol{R})}{\partial \boldsymbol{R}}\left\{\boldsymbol{G}_{\mathrm{BS}}^{\mathrm{LS}}(\boldsymbol{R}) - \boldsymbol{G}^{\mathrm{HS}}(\boldsymbol{R})\right\} + \frac{\partial^2 \alpha(\boldsymbol{R})}{\partial^2 \boldsymbol{R}}\left\{E_{\mathrm{BS}}^{\mathrm{LS}}(\boldsymbol{R}) - E^{\mathrm{HS}}(\boldsymbol{R})\right\}, \tag{18}$$

where $\boldsymbol{F}_{\mathrm{BS}}^{\mathrm{LS}}$ and $\boldsymbol{F}^{\mathrm{HS}}$ are the Hessians calculated by the BS and the HS states, respectively. And a second derivative of α can be expressed by

$$\frac{\partial^2\alpha(\boldsymbol{R})}{\partial\boldsymbol{R}^2}=\frac{2\left(\left\langle\widehat{S}^2\right\rangle^{\mathrm{HS}}-\left\langle\widehat{S}^2\right\rangle_{\mathrm{exact}}^{\mathrm{LS}}\right)}{\left(\left\langle\widehat{S}^2\right\rangle^{\mathrm{HS}}-\left\langle\widehat{S}^2\right\rangle_{\mathrm{BS}}^{\mathrm{LS}}\right)^3}\left(\frac{\partial\left\langle\widehat{S}^2\right\rangle_{\mathrm{BS}}^{\mathrm{LS}}}{\partial\boldsymbol{R}}\right)^2+\frac{\left\langle\widehat{S}^2\right\rangle^{\mathrm{HS}}-\left\langle\widehat{S}^2\right\rangle_{\mathrm{exact}}^{\mathrm{LS}}}{\left(\left\langle\widehat{S}^2\right\rangle^{\mathrm{HS}}-\left\langle\widehat{S}^2\right\rangle_{\mathrm{BS}}^{\mathrm{LS}}\right)^2}\frac{\partial\left\langle\widehat{S}^2\right\rangle_{\mathrm{BS}}^{\mathrm{LS}}}{\partial\boldsymbol{R}}. \tag{19}$$

By using Eqs. (18) and (19), the spin-projected vibrational frequencies are also calculated. The AP optimization can be carried out based on Eq. (16) with $\partial\left\langle\hat{S}^2\right\rangle_{\mathrm{BS}}^{\mathrm{LS}}/\partial\boldsymbol{R}$ obtained by numerical fitting or analytical ways.

2.3. Relationship between the BS and projected wavefunctions

As well as a calculated energy and its derivatives, the BS wavefunction itself has also vital information. Here let us go back to Eq. (3). From the equation, an overlap between up-spin (so-called alpha) and down-spin (so-called beta) orbitals (T) becomes

$$T=\left\langle\psi_{\mathrm{HOMO}}^{\mathrm{BS}}|\overline{\psi}_{\mathrm{HOMO}}^{\mathrm{BS}}\right\rangle=\cos^2\theta-\sin^2\theta=\cos2\theta. \tag{20}$$

And because occupation number (n) of natural orbital (NO) for the corresponding orbital is expressed as $n=2\cos^2\theta$, we get the relation:

$$T=\cos2\theta=n-1 \tag{21}$$

On the other hand, we can define projected wavefunction (PUHF) by eliminating triplet species from BS singlet wavefunction from Eq. (3) as follows:

$$\begin{aligned}\left|\Psi_{\mathrm{PUHF}}^{\mathrm{Singlet}}\right\rangle&=\sqrt{\frac{2}{1+(\cos2\theta)^2}}\left(\frac{1+\cos2\theta}{2}\left|\psi_{\mathrm{HOMO}}\overline{\psi}_{\mathrm{HOMO}}\right\rangle-\frac{1-\cos2\theta}{2}\left|\psi_{\mathrm{LUMO}}\overline{\psi}_{\mathrm{LUMO}}\right\rangle\right)\\&=\sqrt{\frac{2}{1+T^2}}\left(\frac{1+T}{2}\left|\psi_{\mathrm{HOMO}}\overline{\psi}_{\mathrm{HOMO}}\right\rangle-\frac{1-T}{2}\left|\psi_{\mathrm{LUMO}}\overline{\psi}_{\mathrm{LUMO}}\right\rangle\right).\end{aligned} \tag{22}$$

If we focus on the second term, which is related to double (two-electron) excitation, its weight (W_{D}) can be obtained from Eqs. (21) and (22) as follows:

$$W_D=\left\{\sqrt{\frac{2}{1+T^2}}\frac{1-T}{2}\right\}^2=\frac{1}{2}\left\{1-\frac{2T}{1+T^2}\right\} \tag{23}$$

This is the weight of double excitation calculated by the BS wavefunction. By applying Eq. (21)–Eq. (23), the W_{D} is related to the occupation number of the corresponding NO as follows:

$$y = 2W_D = \frac{n^2 - 4n + 4}{n^2 - 2n + 2}. \tag{24}$$

This y value is called an instability value of a chemical bond (or diradical character). In the case of the spin-restricted (or spin-adapted (SA)) calculations, the y value is zero. However if a couple of electrons tends to be separated and to be localized on each hydrogen atom, in other words the chemical bond becomes unstable with the strong static correlation effect, the y value becomes larger and finally becomes 1.0. So, the y value can be applied for the analyses of di- or polyradical species, and it is often useful to discuss the stability (or instability) of chemical bonds. The idea is also described by an effective bond order (b), which is defined by the difference in occupation numbers of occupied NO (n) and unoccupied NO (n^*):

$$b = \frac{n - n^*}{2} \tag{25}$$

Different from the y value, the b value becomes smaller when the chemical bond becomes unstable. If we define the effective bond order with the spin projection b(AP), it is related to the y value:

$$b(\mathrm{AP}) = 1\text{–}y \tag{26}$$

Those indices show how the BS and AP wavefunctions are connected. In addition, one can utilize the indices to estimate the contribution of double excitation for very large systems that CAS and MR methods cannot be applied.

Finally, a relationship between the BS wavefunction and $\langle \hat{s}^2 \rangle$ values are briefly explained. The $\langle \hat{s}^2 \rangle$ values of the BS singlet states do not show the exact value by the spin contamination error. $\langle \hat{s}^2 \rangle$ value of the SA calculation is.

$$\left\langle \widehat{S}^2 \right\rangle_{\mathrm{SA}} = S(S+1), \text{where } \mathrm{S} = \mathrm{S_a} + \mathrm{S_b} \tag{27}$$

However, in the case of the BS singlet state of H_2 molecule, it becomes

$$\left\langle \widehat{S}^2 \right\rangle_{BS} = \left\langle \widehat{S}^2 \right\rangle_{exact} + N^{down} - \sum_{ij} T_{ij} \cong 1 - T \tag{28}$$

where N^{down} and T are number of down electrons and the overlap between spin-polarized up-spin and down-spin orbitals in Eq. (21). Therefore $\left\langle \widehat{S}^2 \right\rangle$ is also closely related to a degree of spin polarization. For the BS singlet state of the hydrogen molecule model, by substituting Eq. (21) into Eq. (28), we can obtain

$$\left\langle \widehat{S}^2 \right\rangle_{BS} \cong 2 - n \tag{29}$$

Here we explain another aspect of the spin projection method. As depicted in **Figure 1(c)**, the BS wavefunction indicates only one spin-polarized configuration, e.g., BS1 in the figure.

However, in order to obtain a pure singlet wavefunction, which satisfies the spin symmetry, the opposite spin-polarized state (BS2) must be included. The projection method can give a linear combination of the both BS states, and therefore it can give an appropriate quantum state for the singlet state.

3. Application of BS and AP methods to several biradical systems

3.1. Hydrogen molecule: comparison among SA, BS, and AP methods by simple biradical system

In this section, we briefly illustrate how the BS and AP methods approximate a dissociation of a hydrogen molecule. **Figure 2(a)** shows potential energy curves of Hartree-Fock and full CI methods. In the case of the spin-adapted (SA) HF, i.e., the spin-restricted (R) HF method, the curve does not converge to the dissociation limit. On the other hand, the BS HF, i.e., spin-unrestricted (U) HF calculation, successfully reproduces the dissociation limit of full CI method. This result indicates that the static correlation is included in the BS procedure. Around 1.2 Å, there is a bifurcation point between RHF and UHF methods. Within the closed shell (i.e., SA) region, where $r_{H\text{-}H} < 1.2$ Å, the UHF solution does not appear, and the singlet state is described by RHF (single slater determinant). In this region, the energy gap between full CI and RHF that is known as correlation energy indicates a necessity of the dynamical correlation correction as discussed later.

In order to elucidate how the double-excitation state is included in the BS solution, the occupation numbers of the highest occupied natural orbital (HONO) are plotted along the H-H distance in **Figure 2(b)**. The figure indicates that the occupation number is 2.0 in the closed shell region, while it suddenly decreases at the bifurcation point. And it finally closes to 1.0 at the dissociation limit. In **Figure 2(c)**, calculated $y/2$ values from the occupation numbers are compared with the weight of the double excitation (W_D) of CI double (CID) method. The figure indicates that the BS method approximates the bond dissociation by taking the double excitation into account. As frequently mentioned above, the BS wavefunction is not pure singlet state by the contamination of the triplet wavefunction. In **Figure 2(b)**, $\langle \hat{s}^2 \rangle$ values of the BS states are plotted. It suddenly increases at the bifurcation point and finally closes to the 1.0, which corresponds to occupation number n at the dissociation limit. And as mentioned above, $\langle \hat{s}^2 \rangle$ and 2-n values are closely related.

Next, we illustrate results of calculated effective exchange integral (J_{ab}) values of the hydrogen molecule by Eq. (11). The calculated J values are shown in **Figure 2(d)**. In a longer-distance region ($r_{H\text{-}H} > 2.0$ Å), the AP-UHF method reproduces the full CI result, indicating that the inclusion of double excitation state and elimination of the triplet state work well within the BS and AP framework. On the other hand, in a shorter-region ($r_{H\text{-}H} < 1.2$ Å), a hybrid DFT (B3LYP) method reproduces the full CI curve. In the region, the dynamical correlation that the RHF method cannot include is a dominant. Therefore the dynamical correlation must be

compensated by other approaches, such as MP, CC, and DFT methods. The hybrid DFT methods are effective way in terms of the computational costs; however, one must be careful in a ratio of the HF exchange. It is reported that a larger HF exchange ratio is preferable in the intermediate region as well as the dissociation limit [69, 70].

3.2. Dichromium (II) complex: effectiveness of hybrid DFT method for calculation of *J* value

Next, the BS and AP methods are applied for $Cr_2(O_2CCH_3)_4(OH_2)_2$ (**1**) complex [1] as illustrated in **Figure 3(a)**. This complex involves a quadruple Cr(II)-Cr(II) bond (σ, $\pi_{//}$, $\pi_{\perp}$, and δ

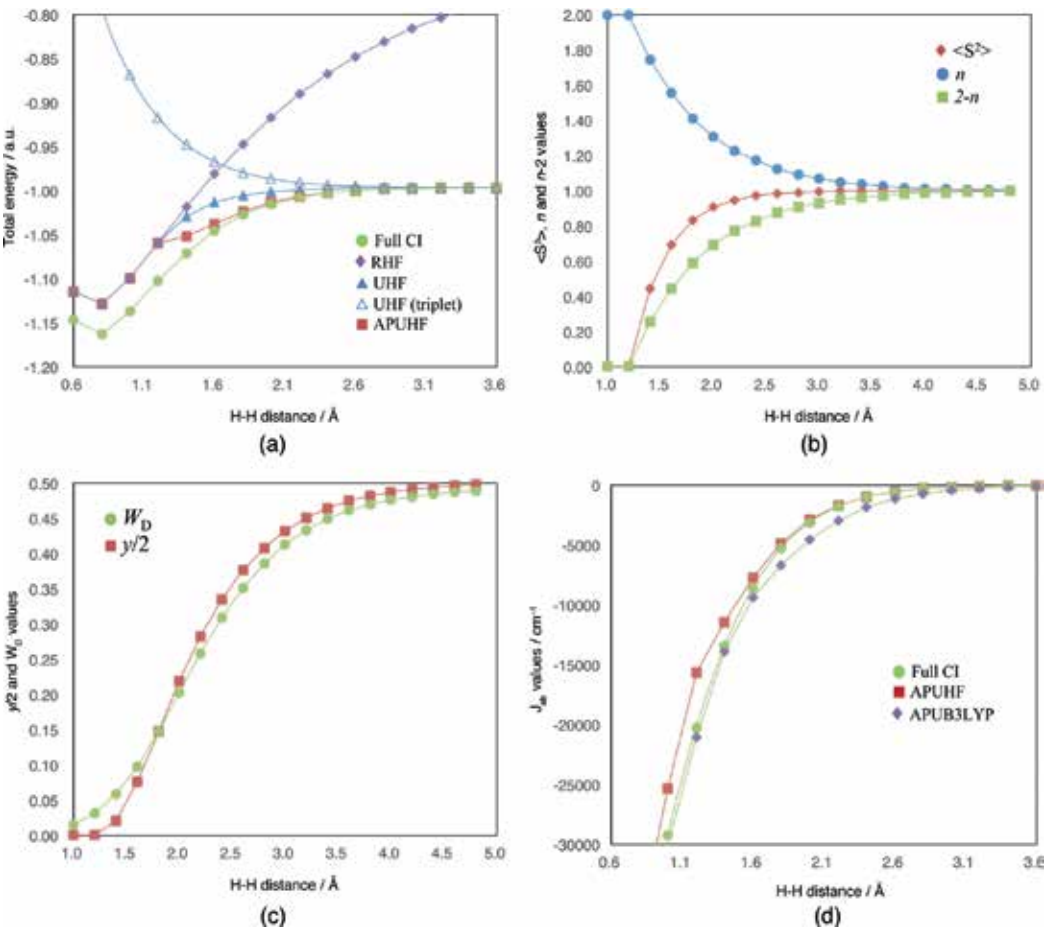

Figure 2. (a) Calculated potential energy surface of H_2 molecule by spin-restricted (R), spin-unrestricted (U), and approximate spin-projected HF methods as well as full CI method. (b) Calculated $\langle \hat{S}^2 \rangle$, occupation number ($n$), and 2–$n$ values of H_2 molecule by UHF calculation. (c) a weight of double (two-electron) excitation (W_D) by double CI (CID) calculation and $y/2$ values in Eq. 24. (d) Calculated effective exchange integral (J) values of H_2 molecule with several H-H distances. For all calculations, 6-31G** basis set was used.

orbitals). Due to the strong static correlation effect, it requires the multi-reference approach. Within the BS procedure, as a consequence, the electronic structure of the complex is expressed by the spin localization on each Cr(II) ions. First, let us examine the nature of the metal–metal bond between Cr(II) ions. For the purpose, natural orbitals and their occupation numbers are obtained from the BS wavefunctions using an experimental geometry.

As depicted in **Figure 3(b)**, there are eight magnetic orbitals, i.e., bonding and antibonding σ, $\pi_{//}$, $\pi_{\perp}$, and δ orbitals that concern about the direct bond between Cr(II) ions. The NO analysis clarifies the nature of the Cr-Cr bond. If d-orbitals of two Cr(II) ions have sufficient overlap to form the stable covalent bond, the occupation numbers of each occupied orbital will be almost 2.0 (i.e., T is close to 1.0). As summarized in **Table 1**, however, those bonds show much smaller values. The occupation numbers of all of occupied σ, π, and δ orbitals are close to 1.0, indicating that electronic structure of the complex **1** is described by a spin-polarized spin structure like the biradical singlet state.

By substituting the obtained energies and $\langle \hat{s}^2 \rangle$ values into Eq. (11), J_{ab} values of the complex **1** are calculated as summarized in **Table 2**. In comparison with the experimental value, HF method underestimates the effective exchange interaction, while B3LYP method overestimates it. This result is quite similar to a tendency of the J_{ab} curve of H_2 molecule at the intermediation region in **Figure 2(d)**. In that region, BH and HLYP method, which involves 50% HF exchange, gives better value in comparison with B3LYP. The results also suggest an importance of the effect on the ratio of the HF/DFT exchange for estimation of the effective exchange interaction [71, 72].

3.3. Singlet methylene molecule: Spin contamination error in optimized geometry by BS method and its elimination by AP method

Finally, we examine the spin contamination error in the optimized structure. Here we focus on a singlet methylene (CH_2). As illustrated in **Figure 4(a)**, the methylene molecule has two valence

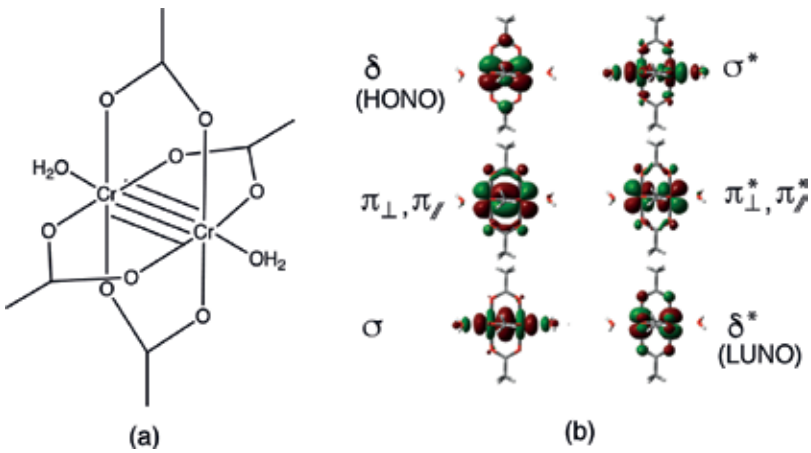

Figure 3. (a) Illustration of $Cr_2(O_2CCH_3)_4(OH_2)_2$ (**1**) complex. (b) Calculated natural orbitals of complex **1** by UB3LYP/basis set **I** (basis set **I**: Cr, MIDI+p; others, 6-31G*).

Orbital	Occupation number (*n*)	Overlap (*T*)
δ	1.148	0.148
π_{ave}[2]	1.242	0.242
σ	1.625	0.625

[1]Cr, MIDI+p, and others, 6-31G*
[2]Averaged value of $\pi_{\perp}$ and $\pi_{//}$

Table 1. *n* and *T* values of complex **1** calculated by UB3LYP/basis set **I**[1].

Method	J_{ab} values
B3LYP	−734
BH and HLYP	−520
HF	−264
Expt	−490

[1]In cm^{-1}
[2]Basis set **I** was used.

Table 2. Calculated J_{ab} values[1] of complex **1** by several functional sets[2].

orbitals (ψ_1 and ψ_2) and two spins in those orbitals. Those two orbitals are orthogonal and energetically quasi-degenerate each other. The ground state of the molecule is $^3B_1$ (triplet) state, and $^1A_1$ (singlet) state is the first excited state. Components of the wavefunction of $^1A_1$ state obtained by BS method as illustrated in **Figure 4(b)** have been graphically explained [36]. The spin-restricted method such as RHF considers only single component (the first term of **Figure 4(b)**) although the BS wavefunction involves three components as illustrated in **Figure 4(b)**. The existence of the triplet component is the origin of the spin contamination error in this system.

Both $^1A_1$ and $^3B_1$ methylene molecules have bent structures, but the experimental data indicates a large structural difference between them. For example, as summarized in **Table 3**, experimental HCH angles (θ_{HCH}) of $^1A_1$ and $^3B_1$ states are 102.4° and 134.0°, respectively [66, 67]. There have also been many reports of the SA results as summarized in Ref. [68]. On the other hand, the BS method is a convenient substitute for CI and CAS method, so here we examined the optimized geometry of the $^1A_1$ methylene by SA and BS methods. In order to elucidate a dependency of the spin contamination error on the calculation methods, HF, configuration interaction method with all double substitutions (CID), coupled-cluster method with double substitutions (CCD), several levels of Møller-Plesset energy correction methods (MP2, MP3, and MP4(SDQ)), and a hybrid DFT (B3LYP) method are also examined. In the case of $^1A_1$ state, all SA results are in good agreement with the experimental values; however, it is reported that energy gap between the singlet and triplet (S-T gap) value is too much underestimated [65]. On the other hand, all BS results overestimate the HCH angle. The difference in HCH angle between the BS values and experimental one is about 10–20°. The HCH angles of UCI and UCC methods are especially larger than MP and DFT methods,

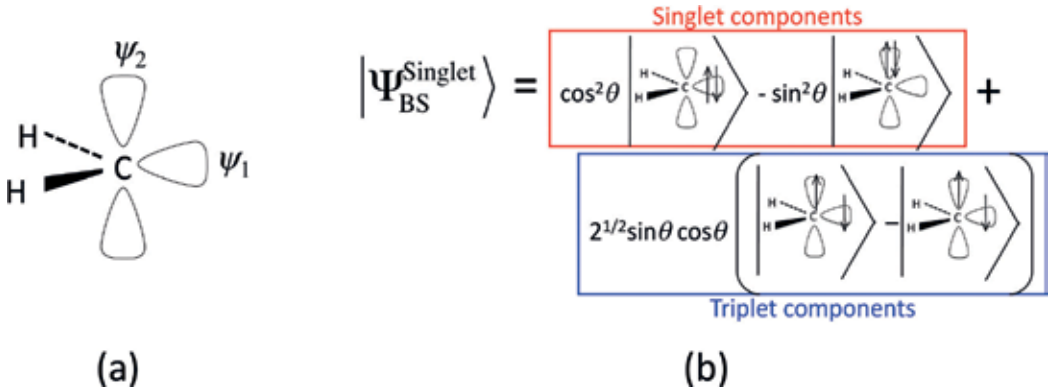

Figure 4. Illustrations of (a) a methylene molecule and (b) components of BS wavefunctions.

indicating that the post-HF methods even require some correction for such systems if the BS procedure is utilized. Therefore it is difficult to use the BS solution for $^1A_1$ state without some corrections. On the other hand, by applying the AP method to the BS solution, the error is drastically improved, and the optimized structural parameters became in good agreement with experimental ones. The difference in the optimized θ_{HCH} values between the BS and the AP method, i.e., the spin contamination error in the optimized geometry, is about 10–20°.

Method	r_{CH}[a]				θ_{HCH}[b]			
	SA	BS	AP	($^3B_1$)	SA	BS	AP	($^3B_1$)
HF	1.097	1.083	1.098	1.071	103.1	115.5	102.9	130.7
CID	1.114	1.091	1.112	1.081	101.6	119.7	101.9	131.8
CCD	1.116	1.087	1.113	1.082	101.7	125.1	102.4	132.0
MP2	1.109	1.091	1.109	1.077	102.0	114.7	100.9	131.6
MP3	1.109	1.094	1.112	1.080	102.0	114.9	101.0	131.8
MP4(SDQ)	1.117	1.096	1.114	1.081	101.2	115.0	101.0	131.9
B3LYP	1.120	1.100	1.113	1.082	100.3	112.9	103.2	133.1
CASSCF(2,2)	1.097				102.9			
CASSCF(6,6)	1.124				100.9			
MRMP2(2,2)	1.109				102.0			
MRMP2(6,6)	1.122				101.1			
Expt.[d]	1.107			1.077	102.4			134.0

[a]In Å
[b]In degree
[c]6-31G* basis set was used
[d]In Refs. [66, 67] for singlet and triplet states, respectively

Table 3. Optimized C-H bond lengths (r_{CH})[a] and H-C-H angle (θ_{HCH})[b] by SA, BS, and AP approaches with several methods[c].

Method	θ_{HCH} °	Mode		
		Symmetry	Bent	Antisymmetry
BS	114.1	3008	1069	3152
AP	104.5	2959	1252	3054
Expt.[c] ($^1A_1$)	102.4	2806	1353	2865
($^3B_1$)	134.0	2992	963	3190

[a]In cm^{-1}
[b]B3LYP/6–31++G(2d,2p) was used
[c]In Refs. [66, 67] for singlet and triplet states, respectively.

Table 4. Calculated vibrational frequencies[a] of singlet methylene by SA, BS, and AP approaches with several methods[b].

Those results strongly indicate that the spin contamination sometimes becomes a serious problem in the structural optimization of spin-polarized systems and the AP method can work well for its elimination. On the other hand, the optimized structure with the AP-UHF method almost corresponds to CASSCF(2,2) result. This means that the AP method approximates two-electron excitation in the (2,2) active space well. The θ_{HCH} values become smaller by including higher electron correlation with the larger CAS space such as CASSCF(6,6) or with the dynamical correlation correction such as MRMP2(2,2) and MRMP2(6,6). The result of the spin-projected MP4 (AP MP4(SDQ)) successfully reproduced the MRMP2(6,6) result, indicating that the AP method plus dynamical correlation correction is a promising approach.

By calculating Hessian, one can also obtain frequencies of the normal modes. In **Table 4**, the calculated frequencies of the normal mode singlet methylene are summarized. The significant difference between the BS and AP methods can be found in a bending mode. The BS result underestimates the binding mode frequency by the contamination of the triplet state. On the other hand, the AP result gives close to the experimental result of $^1A_1$ species. In this way, the AP method is also effective for the normal mode analysis as well as the geometry optimization.

4. Summary

In this chapter, we explain how the BS method breaks the spin symmetry and AP method recover it. In addition, we also demonstrate how those methods work the biradical systems. The theoretical studies of the large biradical and polyradical systems such as polynuclear metal complexes have been fairly realized by the BS HDFT methods in this decade. The BS method is quite powerful for the large degenerate systems, but one must be careful about the spin contamination error. Therefore the AP method would be important for those studies. For example, it is suggested that the spin contamination error misleads a reaction path that involves biradical transition states (TS) or intermediate state (IM) [73]. In addition, in the case of the more larger systems, e.g., metalloproteins, some kind of semiempirical approach combined with the AP hybrid DFT method by ONIOM method will be effective [74]. By using the method, the mechanisms of the long-distance electron transfers and so on will be elucidated. In

such cases, one also must be careful about the parameter of the semiempirical approach to fit the spin-polarized systems. Recently, some improvements for PM6 method have been proposed [75, 76]. Because the PM6 calculation can be utilized for the outer region in ONIOM approach, therefore the AP method is also the effective method for the larger systems. In addition, the BS wavefunction can be applied for other molecular properties by combining with other theoretical procedures. For example, it was reported that the electron conductivity of spin-polarized systems could be simulated by using the BS wavefunction together with elastic Green's function method [77], and some applications for one-dimensional complexes have reported [78, 79]. The results indicate that the BS wavefunctions can be applied for calculations of the physical properties of the strong electron correlation systems as well as their electronic structures. The spin-projected wavefunctions seem to be effective for such simulations of the physical properties. From those points of view, the BS and AP methods have a great potential to clarify chemical and physical phenomena that are still open questions.

Author details

Yasutaka Kitagawa[1,2]*, Toru Saito[3] and Kizashi Yamaguchi[4]

*Address all correspondence to: kitagawa@cheng.es.osaka-u.ac.jp

1 Graduate School of Engineering Science, Osaka University, Toyonaka, Osaka, Japan

2 Center for Spintronics Research Network (CSRN), Graduate School of Engineering Science, Osaka University, Toyonaka, Osaka, Japan

3 Department of Biomedical Information Sciences, Graduate School of Information Sciences, Hiroshima City University, Hiroshima, Japan

4 Graduate School of Science, Osaka University, Toyonaka, Osaka, Japan

References

[1] Cotton FA, Walton RA. Multiple Bonds Between Metal Atoms. Oxford: Clarrendon Press; 1993

[2] Bera JK, Dunbar KR. Angewandte Chemie, International Edition. 2002;**41**:23

[3] Mashima K, Tanaka M, Tani T, Nakamura A, Takeda S, Mori W, Yamaguchi WK. Journal of the American Chemical Society. 1997;**119**:4307

[4] Mashima K. Bulletin of the Chemical Society of Japan. 2010;**83**:299

[5] Murahashi T, Mochizuki E, Kai Y, Kurosawa H. Journal of the American Chemical Society. 1999;**121**:10660

[6] Wang C-C, Lo W-C, Chou C-C, Lee G-H, Chen J-M, Peng S-M. Inorganic Chemistry. 1998; **37**:4059

[7] Lai S-Y, Lin T-W, Chen Y-H, Wang C-C, Lee G-H, Yang M-H, Leung M-K, Peng S-M. Journal of the American Chemical Society. 1999;**121**:250

[8] Gatteschi D, Kahn O, Miller JS, Palacio F, editors. Magnetic Molecular Materials. Dordrecht: Kluwer Academic Publishers; 1991

[9] Kahn O, editor. Magnetism: A Supermolecular Function; NATO ASI Series C. Vol. 484. Dordrecht: Kluwer Academic Publishers; 1996

[10] Coronado E, Dekhais P, Gatteschi D, Miller JS, editors. Molecular Magnetism: From Molecular Assemblies to the Devices, NATO ASI Series E. Vol. 321. Dordrecht: Kluwer Academic Publishers; 1996

[11] Müller A, Kögerler P, Dress AWM. Coordination Chemistry Reviews. 2001;**222**:193

[12] Sessoli R, Gatteschi D, Aneschi A, Novak MA. Nature. 1993;**365**:141

[13] Taft KL, Delfs CD, Papaefthymiou GC, Foner S, Gatteschi D, Lippard SJ. Journal of the American Chemical Society. 1994;**116**:823

[14] Oshio H, Hoshino N, Ito T, Nakano M. Journal of the American Chemical Society. 2004; **126**:8805

[15] Hoshino N, Nakano M, Nojiri H, Wernsdorfer W, Oshio H. Journal of the American Chemical Society. 2009;**131**:15100

[16] Clerac R, Miyasaka H, Yamashita M, Coulon C. Journal of the American Chemical Society. 2002;**124**:12837

[17] Peng S-M, Wang C-C, Jang Y-L, Chen Y-H, Li F-Y, Mou C-Y, Leung M-K. Journal of Magnetism and Magnetic Materials. 2000;**209**:80

[18] Kisida H, Matsuzaki H, Okamoto H, Manabe T, Yamashita M, Taguchi Y, Tokura Y. Nature. 2000;**405**:929

[19] S-Y Lin, Chen I-WP, Chen C-H, Hsieh M-H, Yeh C-Y, Lin T-W, Chen Y-H, Peng S-M. Journal of Physical Chemistry B. 2004;**108**:959

[20] Messerschmidt A, Huber R, Poulos T, Wieghardt K, editors. Handbook of Metalloproteins. West Sussex, England: John Wiley & Sons, Ltd; 2001

[21] Siegbahn PEM. Chemical Reviews. 2000;**100**:4211

[22] Inoue T, Shiota Y, Yoshizawa K. Journal of the American Chemical Society. 2008;**130**:16890

[23] Nakatani N, Nakao Y, Sato H, Sakaki S. The Journal of Physical Chemistry. B;**113**:4826

[24] Noodleman L, Lovell T, Han W-G, Li J, Himo F. Chemical Reviews. 2004;**104**:459

[25] Siegbahn PEM. Inorganic Chemistry. 2000;**39**:2923

[26] Yamanaka S, Takeda R, Yamaguchi K. Polyhedron. 2003;**22**:2013

[27] Torres RA, Lovell T, Noodleman L, Case DA. Journal of the American Chemical Society. 2003;**125**:1923

[28] Day A, Jenney J FE, Adams MWW, Babini E, Takahashi Y, Fukuyama K, Hodgson KO, Hedman B, Solomon EI. Science. 2007;**318**:1464

[29] Shoji M, Koizumi K, Kitagawa Y, Kawakami T, Yamanaka S, Okumura M, Yamaguchi K. Lecture Series on Computer and Computational Sciences. 2006;**7**:499

[30] Kitagawa Y, Shoji M, Saito T, Nakanishi Y, Koizumi K, Kawakami T, Okumura M, Yamaguchi K. International Journal of Quantum Chemistry. 2008;**108**:2881

[31] Carbo R, Klobukowski Ed M. Self-Consistent Field Theory and Applications. Amsterdam: Elsevier; 1990. p. 727

[32] Yamaguchi K, Kawakami T, Takano Y, Kitagawa Y, Yamashita Y, Fujita H. International Journal of Quantum Chemistry. 2002;**90**:370

[33] Yamaguchi K, Yamanaka S, Kitagawa Y. The nature of effective exchange interactions. In: Palacio F et al., editors. Carbon Magnet. Elsevier; 2006. pp. 201-228

[34] Yamaguchi K, Kitagawa Y, Yamanaka S, Yamaki D, Kawakami T, Okumura M, Nagao H, Kruchinin SK. In: Scharnburg K, editor. First Principle Calculations of Effective Exchange Integrals for Copper Oxides and Isoelectronic Species, in NATO Series. Elsevier; 2006

[35] Caneschi A, Gatteschi D, Sangregorio C, Sessoli R, Sorace L, Cornia A, Novak MA, Paulsen C, Wernsdorfer W. Journal of Magnetism and Magnetic Materials. 1999;**200**:182

[36] Cremer D. Molecular Physics. 2001;**99**:1899

[37] Roos BO, Taylor PR, Siegbahn PEM. Chemical Physics. 1980;**48**:157

[38] Andersson K, Malmqvist P-Å, Roos BO, Sadlej SJ, Wolinski K. The Journal of Chemical Physics. 1990;**94**:5483

[39] Hirao K. Chemical Physics Letters. 1992;**190**:374

[40] Miralles J, Castell O, Cabollol R, Malrieu JP. Chemical Physics. 1993;**172**:33

[41] Calzado CJ, Cabrero J, Malrieu JP, Caballol R. The Journal of Chemical Physics. 2002;**116**: 2728

[42] Calzado CJ, Cabrero J, Malrieu JP, Caballol R. The Journal of Chemical Physics. 2002;**116**: 3985

[43] Miehlich B, Stoll H, Savin A. Molecular Physics. 1997;**91**:527

[44] Grafenstein J, Cremer D. Chemical Physics Letters. 2000;**316**:569

[45] Takeda R, Yamanaka S, Yamaguchi K. Chemical Physics Letters. 2002;**366**:321

[46] Laidig WD, Bartlett RJ. Chemical Physics Letters. 1983;**104**:424

[47] Jeziorski B, Paldus JJ. Chemical Physics. 1988;**88**:5673

[48] Mahapatra US, Datta B, Mukherjee D. The Journal of Physical Chemistry. A. 1999;**103**: 1822

[49] Yanai T, Chan GK-L. The Journal of Chemical Physics. 2006;**124**:19416

[50] Kurashige Y, Yanai T. The Journal of Chemical Physics. 2009;**130**:234114

[51] Yanai T, Kurashige Y, Neuscamman E, Chan GK-L. The Journal of Chemical Physics. 2010;**132**:024105

[52] Löwdin P-O. Physics Review. 1955;**97**:1509

[53] Lykos P, Pratt GW. Reviews of Modern Physics. 1963;**35**:496

[54] Yamaguchi K, Yamanaka S, Nishino M, Takano Y, Kitagawa Y, Nagao H, Yoshioka Y. Theoretical Chemistry Accounts. 1999;**102**:328

[55] Szabo A, Ostlund NS. Modern Quantum Chemistry. New York: Dover Publications, Inc; 1996. ch. 3. pp. 205-230

[56] Sonnenberg JL, Schlegel HB, Hratchian HP. In: Solomon IE, Scott RA, King RB, editors. Computational Inorganic and Bioinorganic Chemistry (EIC Books). UK: John Wiley & Sons Ltd; 2009. p. 173

[57] Mayer I. In: Löwdin P-O, editor. Advances in Quantum Chemistry. Vol. vol. 12. New York: Academic Press, Inc; 1980. p. 189

[58] Löwdin P-O. Reviews of Modern Physics. 1964;**36**:966

[59] (a) Yamaguchi K, Takahara Y, Fueno T, Houk KN. Theoretica Chimica Acta. 1988;**73**:337; (b) Takahara Y, Yamaguchi, K, Fueno T, Chemical Physics. Letters. 1989;**157**:211; (c) Yamaguchi K, Toyoda Y, Fueno T. Chemical Physics. Letters. 1989;**159**:459

[60] Yamaguchi K, Okumura M, Mori W. Chemical Physics Letters. 1993;**210**:201

[61] Yamanaka S, Okumura M, Nakano M, Yamaguchi K. Journal of Molecular Structure: THEOCHEM. 1994;**310**:205

[62] Kitagawa Y, Saito T, Ito M, Shoji M, Koizumi K, Yamanaka S, Kawakami T, Okumura M, Yamaguchi K. Chemical Physics Letters. 2007;**442**:445

[63] Saito T, Nishihara S, Kataoka Y, Nakanishi Y, Matsui T, Kitagawa Y, Kawakami T, Okumura M, Yamaguchi K. Chemical Physics Letters. 2009;**483**:168

[64] Kitagawa Y, Saito T, Nakanishi Y, Kataoka Y, Shoji M, Koizumi K, Kawakami T, Okumura M, Yamaguchi K. International Journal of Quantum Chemistry. 2009;**109**:3641

[65] Kitagawa Y, Saito T, Nakanishi Y, Kataoka Y, Matsui T, Kawakami T, Okumura M, Yamaguchi K. The Journal of Physical Chemistry. A. 2009;**113**:15041

[66] Petek H, Nesbitt DJ, Darwin DC, Ogilby PR, Moore CB, Ramsay DA. The Journal of Chemical Physics. 1989;**91**:6566

[67] Bunker PR, Jensen P, Kraemer WP, Beardsworth R. The Journal of Chemical Physics. 1986;**85**:3724

[68] Hargittai M, Schults G, Hargittai I. Russian Chemical Bulletin, International Edition. 2001;**50**:1903

[69] Kitagawa Y, Soda T, Shigeta Y, Yamanaka S, Yoshioka Y, Yamaguchi K. International Journal of Quantum Chemistry. 2001;**84**:592

[70] Kitagawa Y, Kawakami T, Yamaguchi K. Molecular Physics. 2002;**100**:1829

[71] Kitagawa Y, Kawakami T, Yoshioka Y, Yamaguchi K. Polyhedron. 2001;**20**:1189

[72] Kitagawa Y, Yasuda N, Hatake H, Saito T, Kataoka Y, Matsui T, Kawakami T, Yamanaka S, Okumura M, Yamaguchi K. International Journal of Quantum Chemistry. 2013;**113**:290

[73] Saito T, Nishihara S, Kataoka Y, Nakanishi Y, Kitagawa Y, Kawakami T, Yamanaka S, Okumura M, Yamaguchi K. The Journal of Physical Chemistry. A. 2010;**114**:12116

[74] Kitagawa Y, Yasuda N, Hatake H, Saito T, Kataoka Y, Matsui T, Kawakami T, Yamanaka S, Okumura M, Yamaguchi K. International Journal of Quantum Chemistry. 2013;**113**:290

[75] Saito T, Kitagawa Y, Takano Y. The Journal of Physical Chemistry. A. 2016;**120**:8750

[76] Saito T, Kitagawa Y, Kawakami T, Yamanaka S, Okumura M, Takano Y. Polyedeon. 2017; **136**:52

[77] Nakanishi Y, Matsui T, Kitagawa Y, Shigeta Y, Saito T, Kataoka Y, Kawakami T, Okumura M, Yamaguchi K. Bulletin of the Chemical Society of Japan. 2011;**84**:366

[78] Kitagawa Y, Matsui T, Nakanishi Y, Shigeta Y, Kawakami T, Okumura M, Yamaguchi K. Dalton Transactions. 2013;**42**:16200

[79] Kitagawa Y, Asaoka M, Natori Y, Miyagi K, Teramoto R, Matsui T, Shigeta Y, Okumura M, Nakano M. Polyhedron. 2017;**136**:125

Chapter 8

A Computational Chemistry Approach for the Catalytic Cycle of AHAS

Eduardo J. Delgado

Additional information is available at the end of the chapter

http://dx.doi.org/10.5772/intechopen.73705

Abstract

Acetohydroxy acid synthase (AHAS) is a thiamin diphosphate (ThDP)-dependent enzyme involved in the biosynthesis of branched-chain amino acids (valine, leucine, and isoleucine) in plants, bacteria, and fungi. This makes AHAS an attractive target for herbicides and bactericides, which act by interrupting the catalytic cycle and preventing the synthesis of acetolactate and 2-keto-hydroxybutyrate intermediates, in the biosynthetic pathway toward the synthesis of branched amino acids, causing the death of the organism. Several articles on the catalytic cycle of AHAS have been published in the literature; however, there are certain aspects, which continue being controversial or unknown. This lack of information at the molecular level makes difficult the rational development of novel herbicides and bactericides, which act inhibiting this enzyme. In this chapter, we review the results from our group for the different stages of the catalytic cycle of AHAS, using both quantum chemical cluster and Quantum Mechanics/Molecular Mechanics approaches.

Keywords: AHAS, catalytic cycle, DFT, QM/MM

1. Introduction

Computational chemistry is a branch of chemistry in which quantum mechanics and/or molecular mechanics methods are implemented on computers for understanding and predicting the behavior of chemical systems from molecular information. It plays a key role in the rational design of drugs, biomolecules, organic and inorganic molecules, catalysts, and so on.

Amino acids are organic compounds containing amine ($–NH_2$) and carboxyl (–COOH) functional groups, along with a side chain (R group) specific to each amino acid. An essential amino acid is an amino acid that cannot be synthetized by the organism and consequently

must be supplied by the food. Unlike animals, plants and microorganisms have the biosynthetic machinery to synthesize all the essential metabolites required for their survival. These differences in the metabolic paths between plants and animals are the basis for the rational development of herbicides and bactericides, chemicals that interrupt the biosynthetic route to branched chain amino acids causing the death of the plant or bacteria. To achieve this goal, detailed knowledge of the mechanisms at the molecular level is essential.

Plants and bacteria utilize several enzymes for the biosynthesis of branched chain amino acids such as valine, leucine, and isoleucine, being acetohydroxy acid synthase (AHAS), the one which catalyzes the first common step, followed by the participation of other enzymes which finally lead to the formation of these essential amino acids [1–5].

AHAS requires for its catalytic role the cofactor thiamin diphosphate, ThDP, in addition to flavin-adenine dinucleotide (FAD) and a divalent metal ion, Mg^{2+}. FAD has no catalytic function, and Mg^{2+} is required to anchor the diphosphate moiety of ThDP in the active site. During catalysis by ThDP-dependent enzymes, the 4-mino-pyrimidine moiety can interconvert among four ionization/tautomeric states: the 4′-aminopyrimidine (AP), the N1′-protonated 4′-aminopyrimidium ion (APH^+), the 1′,4′-iminopyrimidine (IP), and the C_2-ionized ylide (Y), whose formation is believed to activate ThDP to initiate the catalytic cycle in thiamin-dependent enzymes [6–10], **Figure 1**.

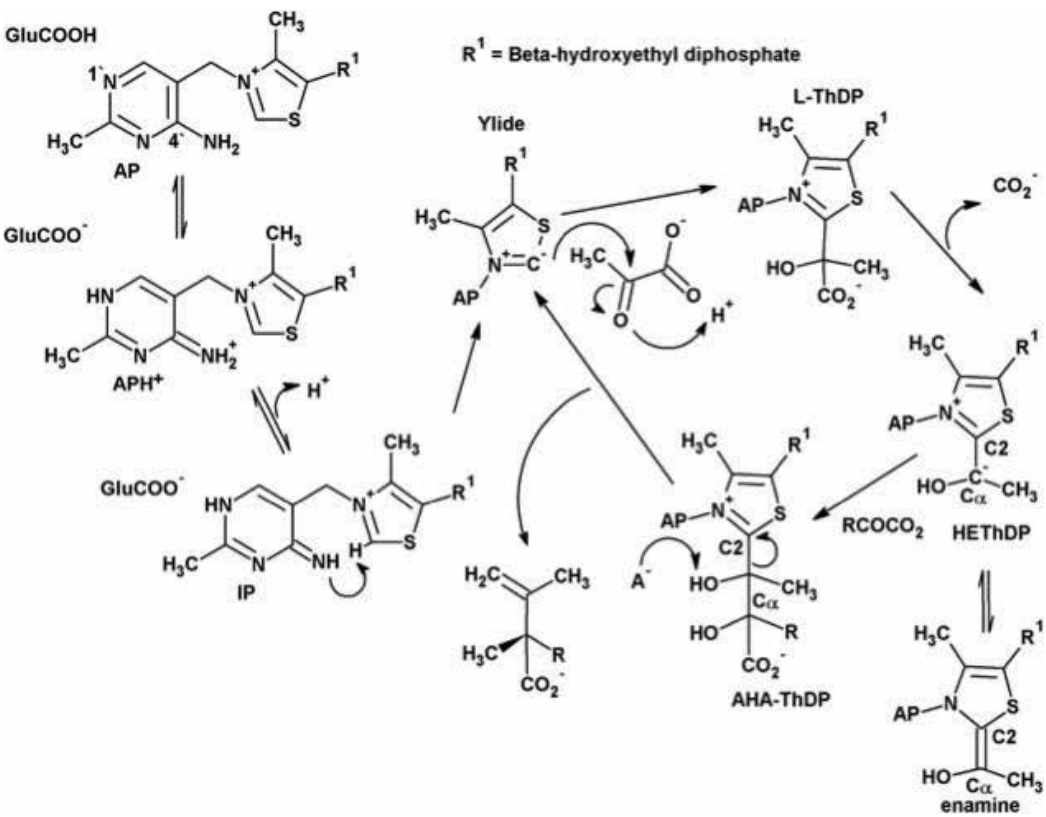

Figure 1. Activation of ThDP and catalytic cycle of AHAS.

In this chapter, we review the results from our group for the different stages of the catalytic cycle of AHAS from a theoretical point of view, using both quantum chemical cluster and Quantum Mechanics/Molecular Mechanics approaches.

2. Activation of thiamin diphosphate (ThDP)

The cofactor ThDP is involved in the sugar metabolism by catalyzing carbon–carbon bond breaking, as well as bond forming [7–9]. During catalysis, the 4′-aminopyrimidine ring can interconvert among four ionization/tautomeric states: AP, APH^+, IP, and the ylide Y (**Figure 2**). In this section, the equilibria among the various ionization and tautomeric states involved in the activation of ThDP and the electron density reactivity indexes of the tautomeric/ionization forms of thiamin diphosphate are addressed using high-level density functional theory calculations.

2.1. Thermodynamics

We have studied the equilibria among the various ionization and tautomeric states involved in the activation of ThDP by using density functional theory calculations at the X3LYP/6-311++G(d,p)//X3LYP(PB)/6-31++G(d,p) level of theory [11, 12]. Briefly, the procedure consists of geometry optimization in solution without any constraint. Solvation effects were modeled using the Poisson-Boltzmann model as implemented in Jaguar. The solvents chosen were water and cyclohexane, as paradigms of polar and apolar media, respectively. All computations were

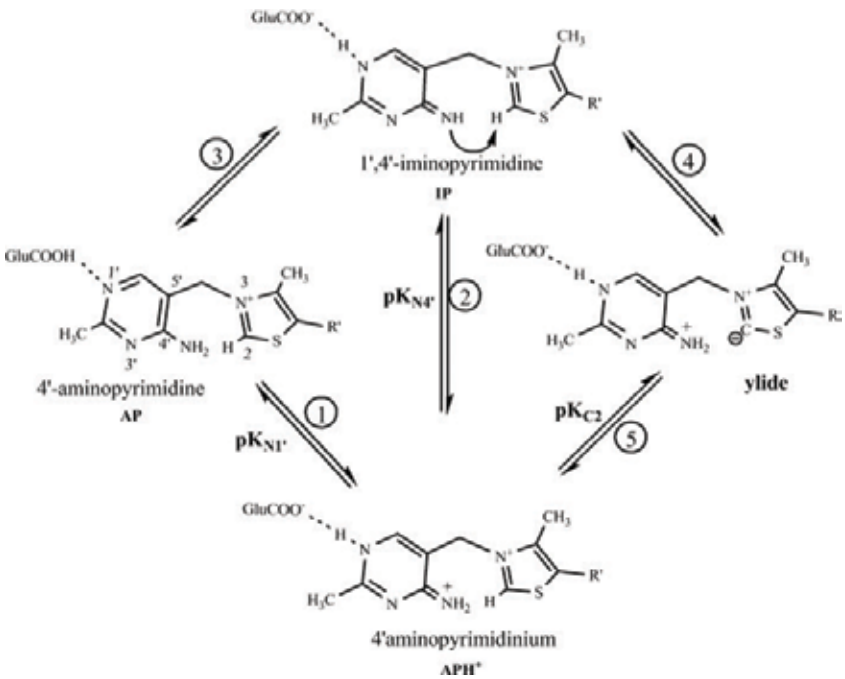

Figure 2. Equilibria among the different tautomeric/ionization forms of thiamin diphosphate.

done considering the highly conserved glutamic residue interacting with the N1′ atom of the 4-aminopyrimidine ring, as a simple way of considering the apoenzymatic environment.

The first equilibrium involves the proton transfer from the glutamic acid side chain to the N1′ atom. In order to evaluate the acidity constant of the N1′ atom, it is necessary to determine the free energy change corresponding to the protonation of the N1′ atom solely. This can be performed applying the Hess's Law considering the following two equations:

$$AP + GluCOOH \leftrightarrow APH^+ + GluCOOH \quad (1)$$

$$GluCOO^- + H^+ \leftrightarrow GluCOOH \quad (2)$$

whose sum gives the desired equation:

$$AP + H^+ \leftrightarrow APH^+ \quad (3)$$

The calculated standard free energy changes for the first equation are −1.1 and +3.0 kcal/mol, in the solvents cyclohexane and water, respectively. While for the second equation, the free energy changes are those that correspond to pKa's values of 4.5 in aqueous solution, and 7 in the enzymatic environment, as predicted by the Propka software. Using these figures, the resulting values of ΔG^0 for Eq. (3) are −3.2 and −10.7 (kcal/mol), in water and cyclohexane, respectively. The results show that the protonation of the N1′ atom is thermodynamically favored in both solvents. The resulting values of pK_{N1}′ are 2.32 and 7.81, in water and cyclohexane, respectively. The low value obtained in water is in the characteristic range of a weak acid and do not reflect the well-known basicity of amines. The obtained value in cyclohexane, however, is in the typical range of amines, on the one hand; and it is in agreement with the accepted value of about 7 for glutamates in the proteic ambient, on the other hand.

The second equilibrium involves the transfer of a proton from the N4′ atom to an amino acid side chain, for instance, Glu473 in pyruvate decarboxylase (PDC). Its respective value of the standard free energy change includes the values corresponding to the deprotonation of the N1′ atom and the protonation of glutamate. In order to determine $pK_{N4'}$ we follow an analog procedure to that considered for the first equilibrium. We consider the following chemical equations:

$$APH^+ + GluCOO^- \leftrightarrow IP + GluCOOH \quad (4)$$

$$GluCOOH \leftrightarrow GluCOO^- + H^+ \quad (5)$$

to give the desired equation:

$$APH^+ \leftrightarrow IP + H^+ \quad (6)$$

The resulting values of ΔG^0 for the reaction (6) are +6.0 and +10.6 kcal/mol in water and cyclohexane, respectively. These values imply that this reaction does not proceed spontaneously

under standard conditions. However, at temperature and pressure constant, the spontaneity of a process is given by ΔG and not by ΔG^0. They are related by the well-known relation $\Delta G = \Delta G^0 + RT \ln Q$, where Q is the ratio of the activities of the products to the activities of the reactants. Considering that the concentrations of the different forms of ThDP in the enzyme are quite low, their activity coefficients must not be very different from unity, and consequently, the activities could be replaced by the concentrations. Under this assumption, Q takes the form $[IP][H^+]/[APH^+]$, where the concentration of hydrogen ions is about 10^{-7} mol/L. In consequence under physiological conditions, the reaction becomes thermodynamically favored because of the cancelation of the positive value of ΔG^0 by the contribution of $[H^+]$ to ΔG. The corresponding calculated values of pK_{N4}' are 4.35 and 7.72 in water and cyclohexane, respectively.

The standard free energy change for the third equilibrium, tautomeric equilibrium between AP and IP, can be calculated by combining the chemical Eqs. (3) and (6). The calculated values are +2.8 and -8.3×10^{-2} kcal/mol, for water and cyclohexane, respectively. The corresponding equilibrium constants are 8×10^{-3} and 1.1, respectively. These values imply that in aqueous solution, the formation of IP from AP is thermodynamically forbidden, while the value in cyclohexane is in agreement with the suggested values of about 1 for the equilibrium constant [13].

The fourth equilibrium involves the transformation of IP into the ylide. The calculated values of ΔG^0 are +0.1 and +1.0 kcal/mol, in water and cyclohexane, respectively. The corresponding equilibrium constants are 0.85 and 0.18, respectively. The calculated values are in agreement with the value suggested in the literature of 1–10 for the ratio [IP]/[ylide] [13].

The fifth equilibrium involves the deprotonation of the C_2 atom of APH^+ to form the ylide. The standard free energy change for this reaction can be obtained by combination of the following equations, whose ΔG^0 are known:

$$IP \leftrightarrow \text{ylide} \tag{7}$$

$$\text{GluCOOH} \leftrightarrow \text{GluCOO}^- + H^+ \tag{8}$$

$$APH^+ + \text{GluCOO}^- \leftrightarrow IP + \text{GluCOOH} \tag{9}$$

Resulting in the desired equation:

$$APH^+ \leftrightarrow \text{ylide} + H^+ \tag{10}$$

The calculated values of ΔG^0 are +6.1 and +11.6 kcal/mol, in water and cyclohexane, respectively. These values imply that the ylide is not formed by the direct transformation of APH^+, but via the IP species through via the following sequence: $APH^+ \rightarrow IP \rightarrow$ ylide, as suggested in the literature. On the other hand, the value of ΔG^0 in aqueous solution does not correspond with weakly acidic nature of the thiazolium C_2H group, while its value in cyclohexane is in agreement with the value reported in the literature in the range of 8–9 for the deprotonation of the C_2 atom [13]. **Table 1** summarizes the calculated values of ΔG^0 for the possible equilibria for the diverse tautomeric/ionization forms of ThDP.

Equilibrium	Solvent	Reaction	ΔG^0 (kcal/mol)
1	Cyclohexane	GluCOOH + AP ↔ $GluCOO^-$ + APH^+	−1.1
	Water		+3.0
2	Cyclohexane	APH^+ + $GluCOO^-$ ↔ IP + GluCOOH	+1.0
	Water		−0.2
3	Cyclohexane	AP ↔ IP	−0.083
	Water		+2.8
4	Cyclohexane	IP ↔ ylide	+1.0
	Water		+0.1
5	Cyclohexane	APH^+ ↔ ylide + H^+	+11.6
	Water		+6.1

Table 1. Standard free energy for the possible equilibria of ThDP.

2.2. Electron density reactivity indexes

In order to complement the thermodynamic results described above, the electron density reactivity indexes of the diverse tautomeric/ionization forms of ThDP were calculated using density functional theory (DFT) calculations at the X3LYP/6-31++G(d,p) level of theory. The study includes the calculation of Fukui functions and condensed-to-tom Fukui indices as a means to assess the electrophilic and nucleophilic character of key atoms in the pathway leading to the formation of the ylide [12].

The quantum chemical calculations were performed considering a clusterized model consisting only of ThDP and the conserved chain of glutamic acid interacting with the N1′ atom of the pyrimidyl ring, and the rest of residues were ignored. In order to simplify the calculations, the diphosphate group of ThDP was replaced by a hydroxyl group, having in mind that the primary function of the diphosphate group is to anchor the cofactor, and it is not involved in the catalysis. The geometries of all structures were optimized in gas phase using the same level of theory X3LYP/6-31++G(d,p). All the quantum chemical calculations of the study were performed using Jaguar 7.0 suite of programs.

The generation of the ylide requires the proton abstraction from the C_2 atom by the N4′ atom of the IP form. Therefore, the nucleophilicity of the N4′ atom is essential for the formation of the ylide. Therefore, the Fukui function and the atomic Fukui indices on this atom were calculated for two alternative forms of IP, those having the N1′ atom protonated and deprotonated, respectively. The nucleophilic character of the N4′ atom as expressed by f^-_{N4} f^- Fukui functions is shown in **Figures 3** and **4**. **Figure 3** shows that the isosurface is negligible in the structure having the N1′ atom protonated. On the other hand, **Figure 4** shows that for the N1′ atom deprotonated form, there is an important nucleophilicity on the N4′ atom as required for the proton abstraction from de C_2 atom. In line with the above finding, the respective condensed-to-atom Fukui indices are 0.00 and 0.41, respectively. These results suggest that the imino form should be with the N1′ atom deprotonated in order to favor the proton abstraction. The

http://dx.doi.org/10.5772/intechopen.73705

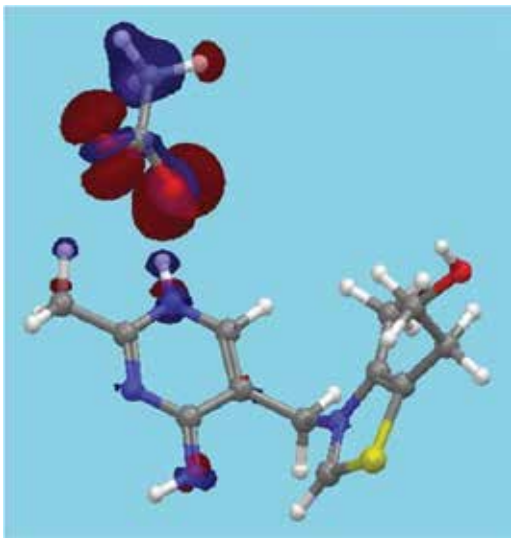

Figure 3. Nucleophilic character of the N1′-protonated IP form as expressed by the *f* − Fukui function.

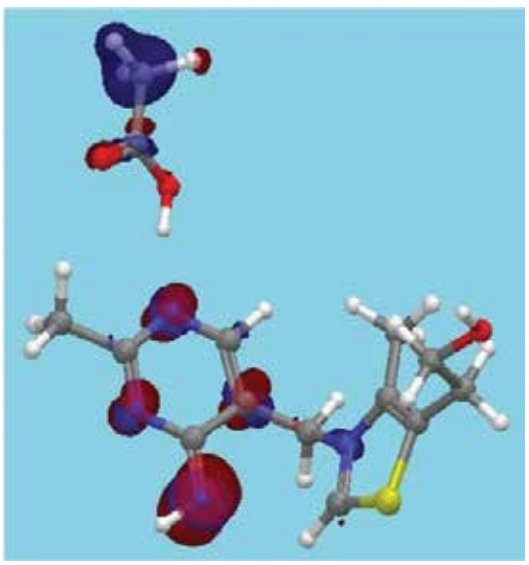

Figure 4. Nucleophilic character of the N1′-deprotonated IP form as expressed by the *f* − Fukui function.

optimization of the structures of both forms of IP shows that the N4′ atom and the proton attached to the C_2 atom are at close distance, 2.39 Å. The transition state associated to this proton transference, **Figure 5**, is characterized with one and only one imaginary frequency, 893.2 cm^{-1}, corresponding to the stretching of the H ↔ C2 bond. The dihedral angles ϕ_t and ϕ_p reach values 67.1^0 and -70.4^0, respectively. In this distorted V–type structure, the N4′atom is only at 1.45 Å from the proton as compared to the rather long C_2-H bond of 1.25 Å. These

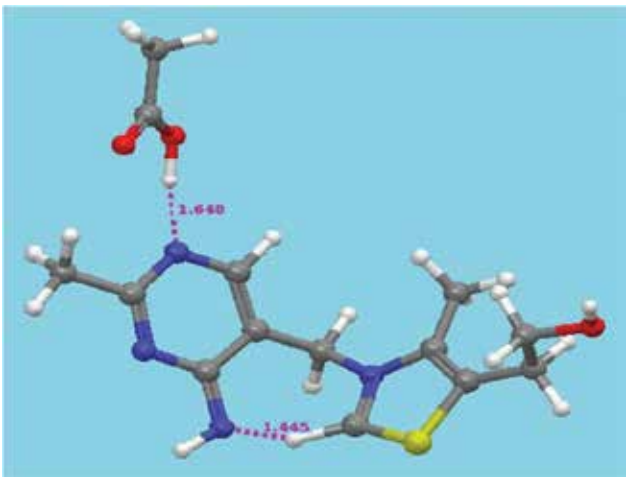

Figure 5. Optimized structure of the transition state for the proton abstraction from the C2 atom.

bond lengths accounts for the proton transfer in progress. The observed activation barrier is just 0.7 kcal/mol, as expected for rapid proton transference. On the other hand, the results show that the reaction of formation of the ylide is exergonic with a standard free energy change of −35.19 kcal/mol.

In ThDP-dependent enzymes, the ylide so formed has the role of to initiate the catalytic cycle with the nucleophilic attack on the C_α atom of the pyruvate molecule to form the intermediate lactyl-ThDP. Consequently, the reaction is strongly dependent on the nucleophilic character of the C_2 atom. In order to address this issue, the f_{C2} Fukui functions were calculated and shown in **Figures 6** and **7**. The results show that only the ylide form having the N1′ atom deprotonated

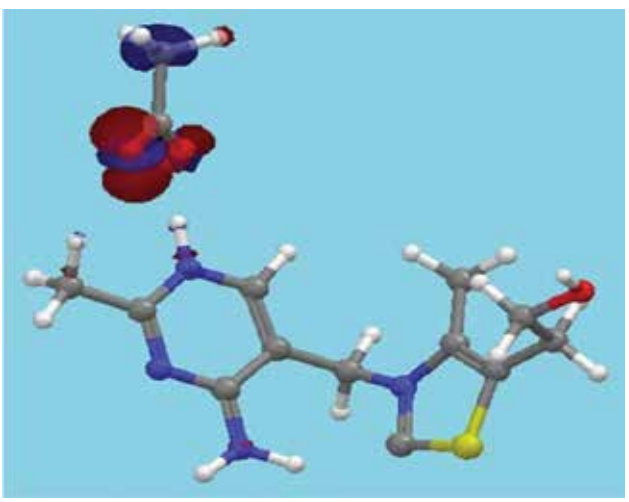

Figure 6. Nucleophilic character of the N1′-protonated ylide form as expressed by the $f-$ Fukui function.

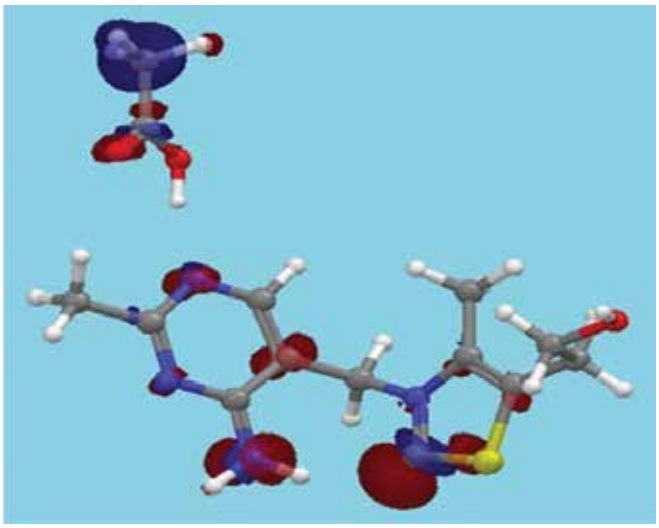

Figure 7. Nucleophilic character of the N1′-deprotonated ylide form as expressed *f* − Fukui function.

shows an important nucleophilicity on the C_2 atom, as required to initiate the catalytic cycle. On the other hand, the other form of the ylide in which the N1′ atom is protonated the C_2 atom does not show any tendency to carry out a nucleophilic attack. Instead, the most important nucleophilic reactivity is lying on the carboxylic oxygen atoms, evidencing the stronger Lewis basicity of these atoms compared to the N1′ atom, and suggesting in turn that the N1′ atom should be deprotonated. The respective atomic Fukui indices on the C_2 atom are 0.00 and 0.34 for the protonated and deprotonated N1′ atom forms, respectively.

2.3. Conclusions

The obtained results in aqueous solution do not correlate with the experimental results; moreover, they cannot be supported from a chemical point of view. Instead, when the enzymatic environment is modeled with a solvent of low dielectric constant, like cyclohexane, the results correlate well both qualitatively and quantitatively to the empirical evidence. In addition, the results show that thermodynamically all ionization/tautomeric forms of ThDP are accessible. The ylide is formed from the IP species as a result of a concerted event in which the increase in the negative partial charge, basicity on the N4′ atom, occurs in conjunction with a decrease in the basicity of the C_2 atom, allowing its deprotonation. The calculated values of pK_a's for the key stages are 7.8, 7.7, and 8.5 for $pK_{N1'}$, $pK_{N4'}$,and pK_{C2}, respectively. These findings support the suggestion given in the literature [14] concerning that the deprotonation and protonation of the C_2 atom are accomplished by a fast proton shuttle enabled by a closely matched pK_a values. The calculated equilibrium constants for the remaining two equilibria are: [IP]/[AP] = 1.2, and [IP]/[ylide] = 5.6. These values are in agreement with those given in the literature [13], of about 1 for equilibrium 3, and values in the range 1–10 for equilibrium 4. In addition, the results allow to conclude that the highly conserved glutamic residue does not protonate the N1′atom of the pyrimidyl ring, but it participates in a strong

hydrogen bonding, stabilizing the eventual negative charge on the nitrogen. This condition provides the necessary reactivity on key atoms, N4′ and C_2, to carry out the formation of the ylide required to initiate the catalytic cycle of ThDP-dependent enzymes.

3. Formation of Lactyl-THDP intermediate

The intermediate Lactyl-ThDP (L-ThDP) is formed in the first stage of the catalytic cycle of AHAS as product of the attack of the ylide on the C_α atom of pyruvate. Despite the number of articles published on the topic, there are still some aspects that remain unknown or controversial, specifically, the manner in which the reaction occurs (i.e., via a stepwise or concerted mechanism) and the protonation states of the N1′ and N4′ atoms during the attack.

In this chapter, we investigate the formation of the L-ThDP intermediate by postulating that the ylide intermediate itself can act as the proton donor, avoiding in this way the involvement of any additional acid-base ionizable group, **Figure 8**. The issue is addressed from a theoretical point of view, considering the total proteic ambient. This chapter includes molecular dynamics simulations, exploration of the potential energy surface (PES) by means of QM/MM calculations, and reactivity analysis on key centers of the reacting species. The PESs are explored for both forms of the ylide, namely, that having the N1′ deprotonated and that having the N1′ atom protonated (henceforth called the Y_1 and Y_2 forms, respectively). The exploration of the PES is carried out in terms of two reaction coordinates accounting for the carboligation and proton transfer. The methodology used has been described earlier in the literature [15].

3.1. Results

The PESs obtained for the two forms of the ylide, Y_1 and Y_2, show very similar topologies, having three critical points that are associated to reactants (R), transition state (TS), and product (P), **Figures 9** and **10**. The topology shows a clear reaction path in which both reaction coordinates vary nearly symmetrically, suggesting a concerted mechanism in which the carboligation and proton transfer occur simultaneously, that is, while the C_2 atom attacks the carbonyl oxygen of pyruvate, the proton of the N4′ amine group is gradually transferred to the carbonyl oxygen of pyruvate as a consequence of the increasing nucleophilic character on the

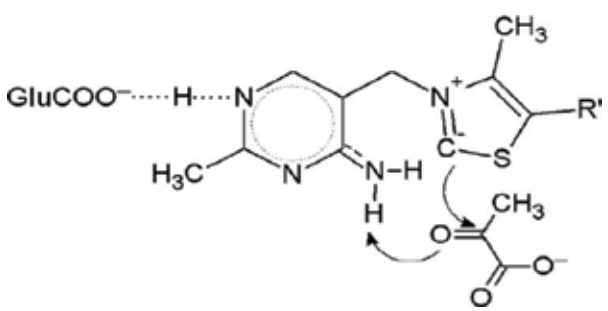

Figure 8. Proposed mechanism for the formation of L-ThDP.

http://dx.doi.org/10.5772/intechopen.73705

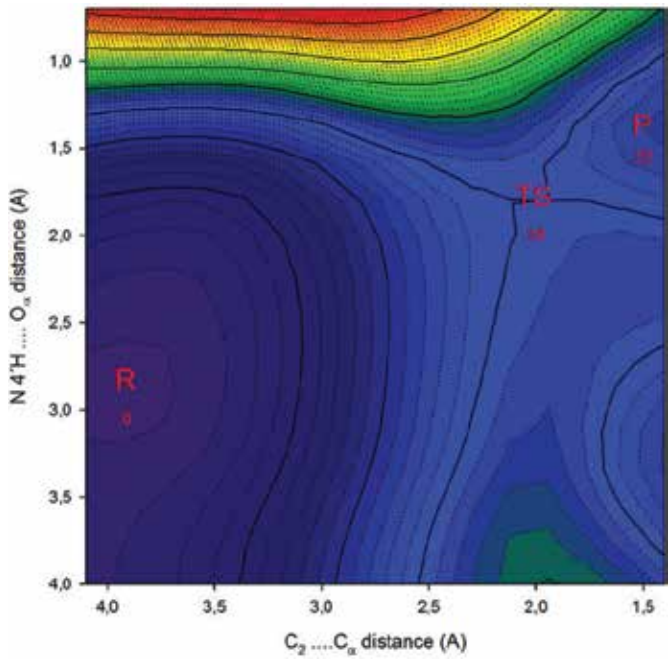

Figure 9. Potential energy surface for the Y_1 form of the ylide.

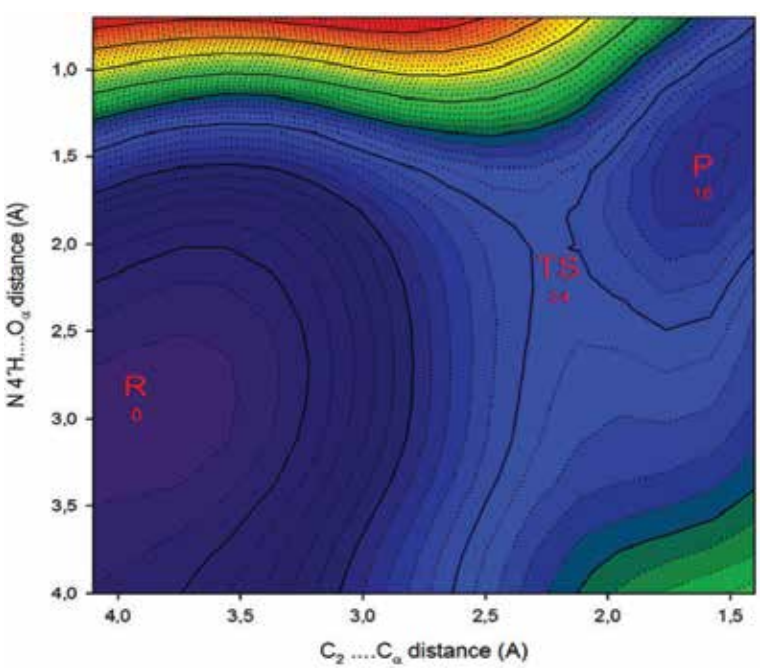

Figure 10. Potential energy surface for the Y_2 form of the ylide.

oxygen atom. On the other hand, the TS of the Y_2 form of the ylide is stabilized in 4 kcal/mol with respect to the TS of the Y_1 form. The respective activation barriers are 28 and 24 kcal/mol. The product, L-ThDP, under the Y_2 form, is stabilized in 6 kcal/mol with respect to the Y_1 form.

The relative stability of the forms Y_1 and Y_2 was assessed by means of the study of the proton transfer from the carboxylic group of Glu139 to the N1′ atom of ThDP. It is found that the Y_2 form (N1′ atom protonated) is energetically lower in about 4 kcal/mol than the Y_1 form. The calculated activation barrier for this proton transference is about 4.5 kcal/mol. These results are summarized in the energy diagram, **Figure 11**. The calculated energy barriers are 28 and 24 kcal/mol for the Y_1 and Y_2 forms, respectively. In consequence, the reaction leading to the formation of L-ThDP should occur under Y_2 form of the ylide. However, the reactivity analysis using the condensed to atom Fukui índices show that at long C_2-C_α distance (reactant state), the nucleophilic character of the C_2 atom is null for the Y_2 form, **Table 2**. On the other hand, an important nucleophilic character on the carboxylic oxygens of Glu139 is observed, strong enough to detach the proton from the N1′ atom located at close distance, about 1.8 Å. These findings suggest that reaction cannot be initiated under the Y_2 form. Unlike, the Y_1 form shows non-null nucleophilic character on the C_2 atom at early stages of the reaction suggesting that the reaction should be initiated under this form.

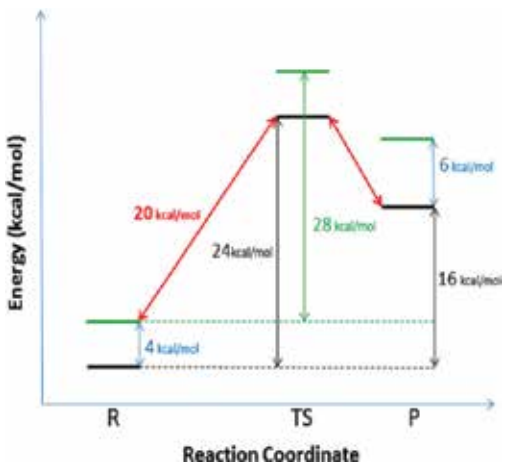

Figure 11. Schematic energy profile for the reaction (red: minimum-energy path; green: Y_1 form of the ylide; black: Y_2 form of the ylide).

	Y_1			Y_2	
C_2–C_α distance (Å)	C_2	O_α	$GluCOO^-$	C_2	O_α
4.0	0.02	0.00	0.50	0.00	0.00
3.5	0.29	0.02	0.50	0.00	0.00
3.0	0.57	0.04	0.00	0.51	0.07
2.5	0.49	0.11	0.00	0.50	0.12

Table 2. Nucleophilic character on selected atoms as expressed by the f^- Fukui index.

Having in mind the energetics and reactivity results, it is possible to postulate the following reaction path of minimum energy: the reaction is initiated with the attack of the ylide, in its Y_1 form, on the carbonylic carbon of pyruvate to reach a transition state in which the N1′ atom is protonated. This postulated mechanism allows to reduce the activation barrier to 20 kcal/mol, in agreement with the experimental evidence [15].

4. Formation of 2-aceto-2-hydroxybutyrate

The second stage of the catalytic cycle of AHAS involves the decarboxylation of the L-ThDP intermediate to form the 2-hydroxyethyl-ThDP carbanion/enamine ($HEThDP^-$) intermediate. Then, HEThDP reacts with 2-ketobutyrate (2 KB) to form the 2-aceto-2-hydroxybutyrate (AHA-ThDP) intermediate. In this chapter, the formation of the 2-aceto-2-hydroxybutyrate (AHA-ThDP) intermediate is addressed from a theoretical point of view by means of hybrid quantum/molecular (QM/MM) mechanical calculations [18]. The QM region includes one molecule of 2-KB, the $HEThDP^-$ intermediate, and the residues Arg380 and Glu139, whereas the MM region includes the rest of the protein. This chapter includes potential energy surface (PES) scans to identify and characterize critical points on it, transition state search and activation energy calculations.

The initial structure of AHAS-HEThDP-2 KB for the exploration of the PES was obtained from the solvated and equilibrated structure of AHAS in complex with pyruvate and HEThDP after 15 ns molecular dynamics (MD) simulation, according to the methodology elsewhere [18–20]. Along the simulation, significant displacements of the residues were not observed. In consequence, to model the reaction mechanism, we took the final MD structure as a single representative configuration. This structure was trimmed to a sphere of radius of 30 Å with center at the C_α atom of the $HEThDP^-$ intermediate. Then, the 2 KB structure was superimposed on the structure of pyruvate, and this was deleted.

The reaction mechanism was described on a single PES as a function of two asymmetric reactions coordinates. The reaction coordinate R_1 is defined as the bond length difference between C_α–C_2 and C_α–C_B bonds; the reaction coordinate R_2 is defined as the bond length difference between O_α–H_α and O_B–H_α.

4.1. Results

The PES obtained shows five critical points that are associated to reactants (R), transition states (TS_1 and TS_2), intermediate (I), and product (P), **Figures 12** and **13**. The PESs suggest that the reaction is initiated with the nucleophilic attack of the carbanion on the carbonylic carbon of 2 KB, reaching a transition state TS_1 located at $R_1 \sim -1.0$ and $R_2 \sim -0.6$, evidencing that the nucleophilic attack is in progress while the hydroxyl proton of $HEThDP^-$ remains at constant distance of about 1.7 Å., from the carbonyl oxygen of ketobutyrate, **Figure 14**.

Once the transition state is reached, the PES shows a concerted asynchronous mechanism, namely, the nucleophilic attack continues until R_1 reaches the values of about −0.3; afterward, the proton transfer from the hydroxyl of $HEThDP^-$ to the carbonyl oxygen of ketobutyrate

occurs, leading to the intermediate located at $R_1 \sim -0.25$ and $R_2 \sim 0.75$, indicating that at this point the proton transfer has been completed, **Figure 15**.

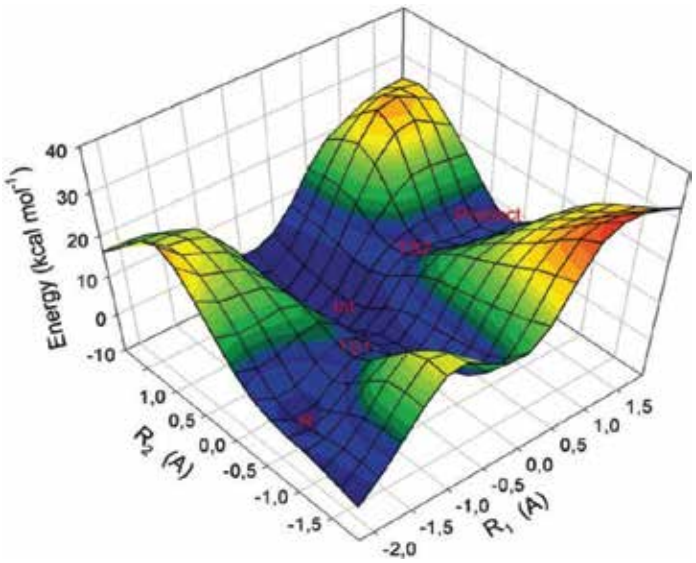

Figure 12. 3-D view of the DFT corrected PES.

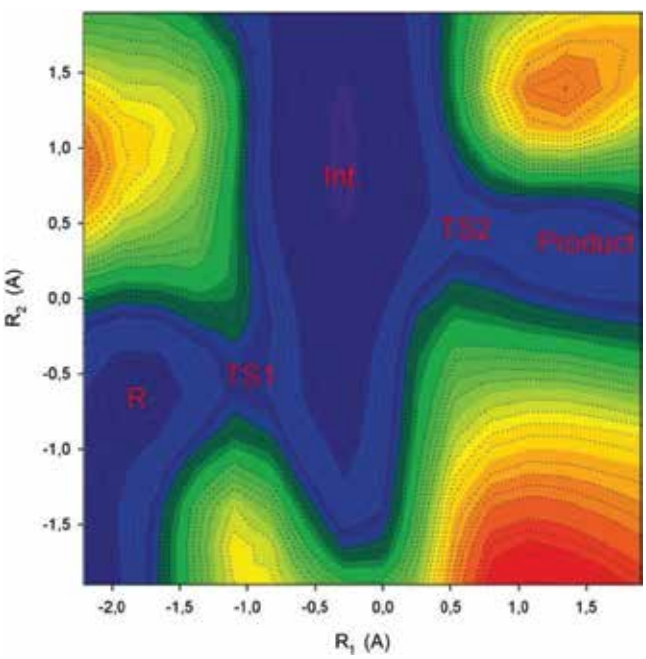

Figure 13. 2-D view of the DFT corrected PES.

http://dx.doi.org/10.5772/intechopen.73705

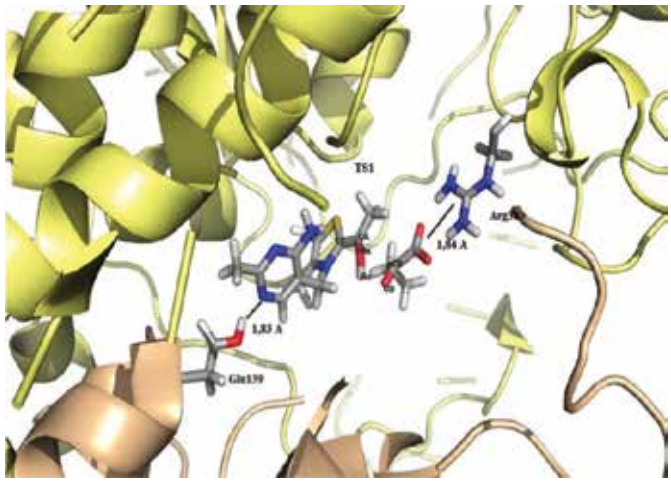

Figure 14. Optimized geometry of the transition state TS1.

The reaction continues with the increase of the reaction coordinate R_1 reaching the second transition state TS2 located at coordinates $R_1 \sim 0.5$ and $R_2 \sim 0.5$, **Figure 16**. The reaction path for this event is clearly observed on the PES; in this step, the reaction proceeds at R_2 constant, while the coordinate R_1 changes systematically toward positive values indicating the separation of the product from the C_2 atom of the thiazolium ring of ThDP, and the consequent ylide regeneration is in progress, **Figure 17**. The relevant distances and relative energies of the critical points observed in the PES are summarized in **Table 3**. It is observed the gradual shortening of the distance C_α–C_B and lengthening of the distance C_α–C_2 when going from reactant to product, accounting for the nucleophilic attack and product release. Similar trend for the distances

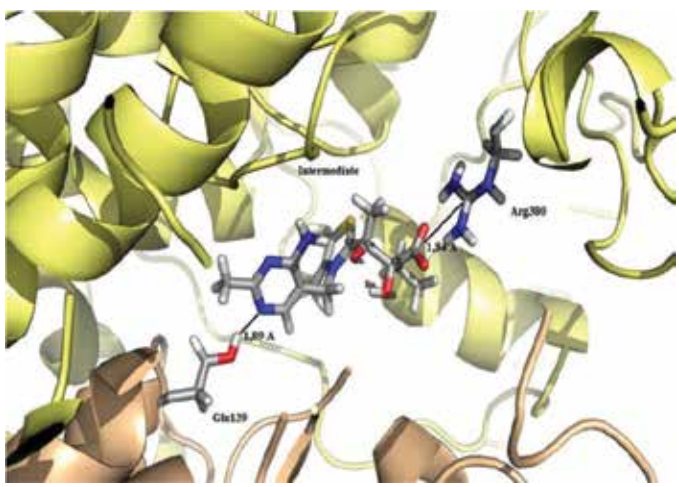

Figure 15. Optimized geometry of the intermediate.

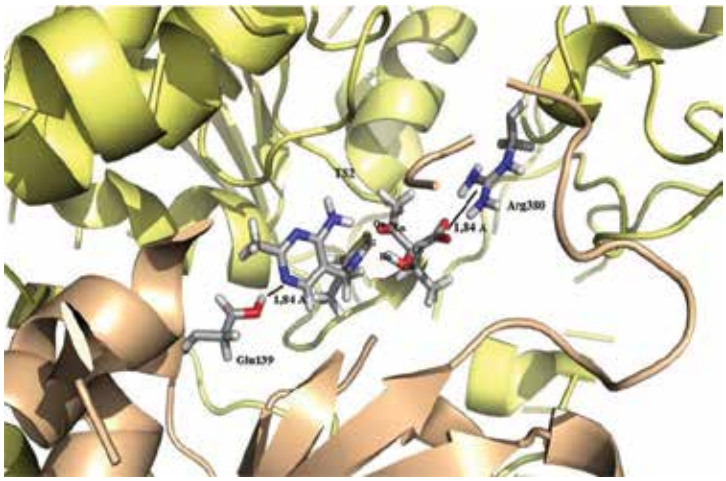

Figure 16. Optimized geometry of the transition state TS2.

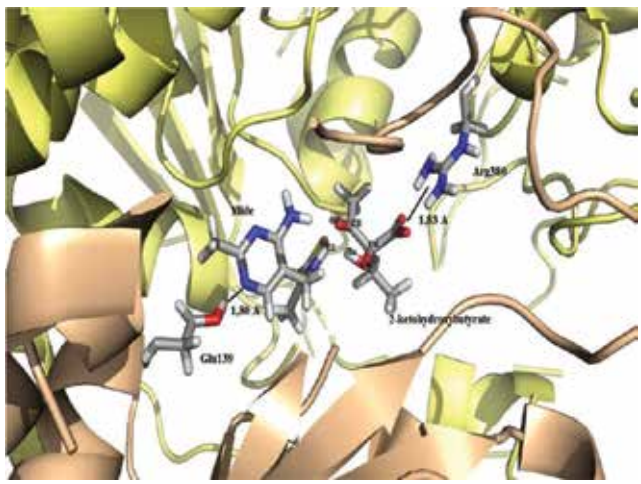

Figure 17. Optimized geometry of the product.

	Reactant	TS1	Intermediate	TS2	Product
C_{α}–C_2 (Å)	1.37	1.43	1.51	2.30	3.48
C_{α}–C_{β} (Å)	3.28	2.35	1.80	1.60	1.56
O_{α}–H_{α} (Å)	1.02	0.98	1.94	1.60	1.71
O_{β}–H_{α} (Å)	1.55	1.69	0.95	1.02	1.00
Relative energy (kcal/mol)	0.0	11.0	−9.0	6.10	3.00

Table 3. Interatomic distances and relative energies of the critical points on the PES.

O_α–H_α and O_B–H_α is observed as long as the reaction proceeds. The respective activation barriers are 11 and 15 kcal/mol, evidencing that the second stage is the rate controlling step, in agreement with the empirical evidence.

4.2. Conclusions

The main conclusions can be summarized as follows: (1) the reaction between the intermediate HEThDP$^-$ and 2-ketobutyrate occurs via a stepwise mechanism consisting of two steps; (2) the first reaction step corresponds to the nucleophilic attack of the carbanion on the carbonylic carbon of 2-KB; this stage occurs via a concerted asynchronous mechanism, that is, the proton transfer follows the carboligation event; (3) the second reaction stage involves the product release and ylide recovery, allowing in this way to reinitiate the catalytic cycle once more; (4) two transition states are observed on the PES, the first one, TS1 corresponding to the first reaction step, has an activation barrier of about 11 kcal/mol, while the second one, TS2 corresponding to the product liberation, has an activation barrier of about 15 kcal/mol. (5) The results are in agreement with literature values [16, 17] which states that the next step to the formation of the adduct is the rate controlling step among the last two stages of the AHAS catalytic cycle.

Acknowledgements

The author acknowledges financial support from FONDECYT grants 1130082 and 1170091.

Author details

Eduardo J. Delgado

Address all correspondence to: edelgado@udec.cl

Computational Chemistry Group, Faculty of Chemical Sciences, Universidad de Concepción, Concepción, Chile

References

[1] Duggleby RG, Pang SS. Acetohydroxyacid synthase. Journal of Biochemistry and Molecular Biology. 2000;**33**:1-36

[2] Pang S, Duggleby RG, Guddat LW. Crystal structure of yeast acrtohydroxyacid synthase: A target for herbicidal inhibitors. Journal of Molecular Biology. 2002;**317**:249-262

[3] Chipman DM, Duggleby RG, Tittmann K. Mechanisms of acetohydroxyacid synthases. Current Opinion in Chemical Biology. 2005;**9**:475-481

[4] McCourt JA, Duggleby RG. Acetohydroxyacid synthase and its role in the biosynthetic pathway for branched-chain amino acids. Amino Acids. 2006;**31**:173-210

[5] Gedi V, Yoon MY. Bacterial acetohydroxyacid synthase and its inhibitors – A summary of their structure, biological activity and current status. The FEBS Journal. 2012;**279**:946-963

[6] Kluger R, Tittmann K. Thiamin diphosphate catalysis: Enzymatic and nonenzymic covalent intermediates. Chemical Reviews. 2008;**108**:1797-1833

[7] Jordan F, Nemeria NS. Experimental observation of thiamin diphosphate-bound intermediates on enzymes and mechanistic information derived from these observations. Bioorganic Chemistry. 2005;**33**:190-215

[8] Agyei-Owusu K, Leeper FJ. Thiamin diphosphate in biological chemistry: Analogues of thiamin diphosphate in studies of enzymes and riboswitches. The FEBS Journal. 2009;**276**:2906-2916

[9] Kern D, Kern G, Neef Holger TK, Killenberg-Jabs M, Wikner C, Schneider G, Hübner G. How thiamine diphosphate is activated in enzymes. Science. 1997;**275**:67-70

[10] Nemeria NS, Chakraborty S, Balakrishnan A, Jordan F. Reaction mechanisms of thiamin diphosphate enzymes: Defining states of ionization and tautomerization of the cofactor at individual steps. The FEBS Journal. 2009;**276**:2432-2446

[11] Delgado EJ, Alderete JB, Jaña GA. Density-functional study on the equilibria in in the ThDP activation. Journal of Molecular Modeling. 2011;**17**:2735-2739

[12] Jaña GA, Delgado EJ. Electron density reactivity indexes of the tautomeric/ionization forms of thiamin diphosphate. Journal of Molecular Modeling. 2013;**19**:3799-3803

[13] Nemeria N, Korotchkina L, McLeish MJ, Kenyon GL, Patel MS, Jordan F. Elucidation of the chemistry of enzyme-bound thiamin diphosphate prior to substrate binding: Defining internal equilibria among tautomeric and ionization states. Biochemistry US. 2007;**46**:10739-10744

[14] Tittmann K, Neef H, Golbik R, Hubner G, Kern D. Kinetic control of thiamin diphosphate activation in enzymes studied by proton-nitrogen correlated NMR spectroscopy. Biochemistry US. 2005;**44**:8697-8700

[15] Lizana I, Delgado EJ. New insights on the reaction pathway leading to lactyl-ThDP: A theoretical approach. Journal of Chemical Information and Modeling. 2015;**55**:1640-1644

[16] Friedemann R, Titmann K, Golbik R, Hübner G. DFT and MP2 stdies on the C_2–$C_{2\alpha}$ bond cleavage in thiamin catalysis. Journal of Molecular Catalysis B: Enzymatic. 2009;**61**:36-38

[17] Alvarado O, Jaña G, Delgado EJ. Computer-assisted study on the reaction between pyruvate and ylide in the pathway leading to lactyl-ThDP. Journal of Computer-Aided Molecular Design. 2012;**26**:977-982

[18] Sanchez L, Jaña GA, Delgado EJ. A QM/MM study on the reaction pathway leading to 2-aceto-2-hydroxybutyrate in the catalytic cycle of AHAS. Journal of Computational Chemistry. 2014;**35**:488-494

[19] Jaña G, Jimenez V, Villa-Freixa J, Prat-Resina X, Delgado E, Alderete J. Computational study on the carboligation reaction of acetohydroxyacid synthase: New approach on the role of the HEThDP intermediate. Proteins. 2010;**78**:1774-1788

[20] Jaña G, Jimenez V, Villa-Freixa J, Prat- Resina X, Delgado E, Alderete JB. A QM/MM study on the last two steps of the catalytic cycle of acetohydroxyacid synthase. Computational & Theoretical Chemistry. 2011;**966**:159-166

Chapter 9

Molecular Descriptors and Properties of Organic Molecules

Amalia Stefaniu and Lucia Pintilie

Additional information is available at the end of the chapter

http://dx.doi.org/10.5772/intechopen.72840

Abstract

The main goal of this chapter is to reveal the importance of molecular structure analysis with specific computational tools using quantum chemistry methods based on density functional theory (DFT) with focus on pharmaceutical compounds. A wide series of molecular properties and descriptors related with chemical reactivity is discussed and compared for small organic molecules (e.g., quinolones, oxazolidinones). Structural and physicochemical information, important for quantitative structure-property relationships (QSPR) and quantitative structure-activity relationships (QSAR) modeling analysis, obtained using Spartan 14 software Wavefunction, are reported. Thus, by a computational procedure including energy minimization and predictive calculations, values of quantum chemical parameters and molecular properties related with electronic charge distribution are reported and discussed. Frontier molecular orbitals energy diagram and their bandgap provide indications about chemical reactivity and kinetic stability of the molecules. Derived parameters (ionization potential (I), electron affinity (A), electronegativity (χ), global hardness (η), softness (σ), chemical potential (μ) and global electrophilicity index (ω)) are given. Also, graphic quantities are reported: electrostatic potential maps, local ionization potential maps and LUMO maps, as visual representation of the chemically active sites and comparative reactivity of different constitutive atoms.

Keywords: quantum chemical parameters, linezolid, cadazolid, ciprofloxacin, molecular docking

1. Introduction

In recent years, prediction of chemical properties by computed tools becomes a useful and suitable way to analyze and compare wide libraries of compounds aiming to design and develop new molecules with higher biological activity and/or better and controlled chemical

behavior. Molecular design and prediction of molecular parameters using *ab initio* methods and mathematical modeling of physical and chemical properties are imperative steps in new scientific approaches for developing new drugs or advanced materials.

Due to the evolution of computing data storage and processor performance, molecular modeling rapidly integrates into the study of therapeutic molecules, due to the opportunities, it offers to solve relevant issues in a considerably short time without doing rebate from the accuracy of the predicted data.

The prediction of chemical properties and the assessment of chemical behavior in pseudo-physiological media by computational methods has become a necessary and fast tool to analyze and compare wide libraries of compounds in order to design and develop new molecules with important biological activity or to potentiate them or conduct their chemical behavior. Computed structural analysis and chemical parameters prediction using *ab initio* methods and mathematical modeling of physicochemical properties are imperative steps in these new approaches in developing drugs or advanced new materials.

Mathematical models are used to predict the strength of intermolecular interactions between drug candidates and their biological protein/enzyme target, allowing to identify the most probable binding mode and affinity and, finally, to explore the molecular mechanism or biochemical pathways.

Recent studies have been focused on the development of noncleavable dual-action molecules with antimicrobial activity. One of the noncleavable antibiotic hybrids is cadazolid, composed of a fluoroquinolone and an oxazolidinone core via a stable linker [1]. Regarding the mode of action, it was reported that cadazolid is acting as an oxazolidinone molecule but fails to demonstrate a substantial contribution from the fluoroquinolone function. Cadazolid behaves like a potent linezolid with a low systemic exposure and a high local concentration in the gastrointestinal tract [1]. Our theoretical studies focus on the characteristics, molecular properties and molecular docking simulations to identify and visualize the most likely interactions between ligands such as cadazolid, linezolid, quinolone and the receptor protein (***Staphylococcus aureus*** ribosomal subunit, PDB ID: 4WFA).

2. Materials and methods

2.1. Prediction properties computation procedure

The properties calculations were carried out using Spartan 14 software Wavefunction, Inc. Irvine, CA, USA [2] on a PC with Intel(R) Core i5 at 3.2 GHz CPU. First, the 3D CPK models of the studied compounds were generated. Then, a systematic conformational search and analysis were performed to establish the more stable conformers of the three pharmacological compounds, presenting the energy minima. The lowest energy conformer was obtained using MMFF molecular mechanics model by refining the geometry for each studied molecule. On these structures, a series of calculations of molecular properties and topological descriptors were performed using density functional method [3], software algorithm hybrid B3LYP model (Becke's three

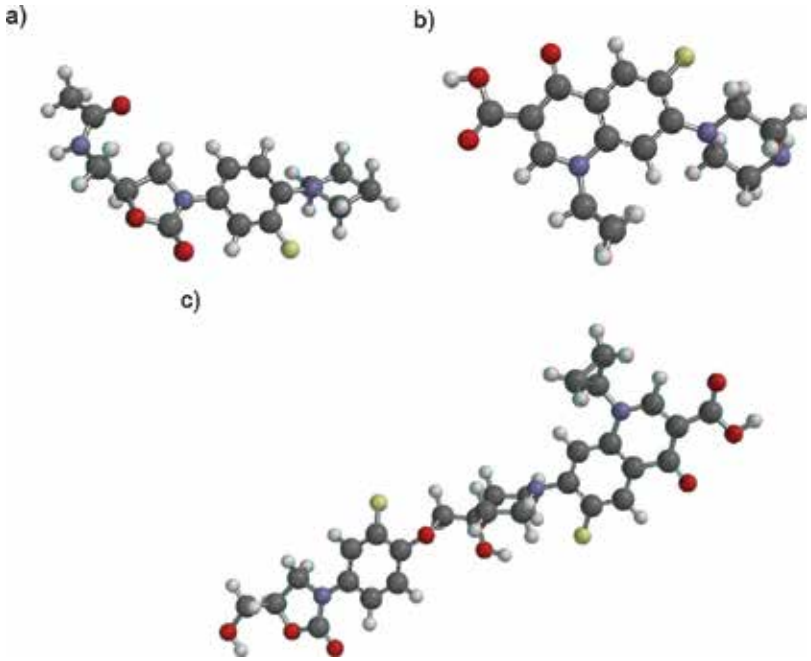

Figure 1. The optimized geometry of the pharmaceutical compounds: linezolid (a), ciprofloxacin (b) and cadazolid (c), ball and spoke representation.

parameter hybrid exchange functional with the Lee-Yang-Parr correlation functional) [3–5] and polarization basis set 6-31G* [2, 6] in vacuum, for equilibrium geometry at ground state.

2.2. Molecular docking simulations

The docking studies have been carried out using CLC Drug Discovery Workbench Software in order to predict the most possible type of interactions, the binding affinities and the orientation of the docked ligand (cadazolid, linezolid or quinolone) at the active site of ***Staphylococcus aureus*** ribosomal subunit [7]. The protein-ligand complex has been realized based on the X-ray structure of crystal structure of the large ribosomal subunit of ***Staphylococcus aureus*** in complex with linezolid, which was downloaded from the Protein Data Bank (PDB ID: 4WFA) [7]. Co-crystallized ligand linezolid (ZLD) was extracted and redocked into 4WFA fragment to validate the docking protocol. The docked ligands and their optimized geometry are illustrated in **Figure 1**, as ball and spoke representation.

3. Results and discussion

3.1. Molecular properties

Structural and physicochemical information, important for *quantitative structure-**p**roperty relationships* (QSPR) and *quantitative structure-activity relationships* (QSAR) modeling analysis,

obtained using Spartan 14 software Wavefunction, are reported in **Table 1**. Thus, by a computational procedure, including energy minimization to obtain the most stable conformer for each studied structure and predictive calculations, values of quantum chemical parameters and molecular properties related with electronic charge distribution are obtained. Using the Calculate Molecular Properties Tool of Spartan 14 software, relevant properties of small molecules have been calculated, related with Lipinski's rule of five [8]. To be efficient drug candidates, the compounds must respect the following conditions: maximum five hydrogen bond donors (as total number of nitrogen-hydrogen and oxygen-hydrogen bonds); maximum 10 hydrogen bond acceptors (as total number of nitrogen and oxygen atoms); maximum molecular weight of 500 Da; the octanol-water partition coefficient (log P) value less than 5. In our study, the prediction log P coefficient is based on the XLOGP3-AA method [9]. These properties are important when several drug candidate compounds need to be analyzed, before their chemical synthesis, in order to evaluate their drug-likeness. In **Table 1** are listed the calculated molecular properties from CPK and from Wavefunction models for the three studied

	Linezolid	**Ciprofloxacin**	**Cadazolid**
Molecular properties			
Formula	$C_{16}H_{20}FN_3O_4$	$C_{17}H_{18}FN_3O_3$	$C_{29}H_{29}F_2N_3O$
Weight (amu)	337.351	331.347	585.560
Energy (au)	–1186.74569	–1148.36687	–2088.23350
Energy (aq) (au)	–1186.76351	–1148.36687	–2088.26194
Solvation E (kJ/mol)	–46.79	–57.23	–74.66
Dipole moment (Debye)	7.28	6.42	8.39
E HOMO (eV)	–5.28	–5.72	–5.88
E LUMO (eV)	–0.19	–1.33	–1.52
QSAR properties from CPK model			
Area (Å^2)	346.66	330.26	557.72
Volume (Å^3)	324.83	318.18	541.53
PSA (Å^2)	55.071	62.218	114.809
Ovality	1.52	1.47	1.74
QSAR properties from computed wavefunction			
Log P	0.58	1.32	2.37
HBD count	1	1	2
HBA count	6	5	9
Polarizability (10^{-30} m^3)	66.52	66.15	84.27

Table 1. Predicted molecular properties for linezolid, ciprofloxacin and cadazolid, using DFT method, B3LYP model, 6-31G* basis set, in vacuum, for equilibrium geometry at ground state.

molecules obtained for the most stable conformer of each after geometry minimization: dipole moment, ovality, polarizability, the octanol-water partition coefficient (log P), the number of hydrogen bond donors (HBDs) and acceptors (HBAs) and acceptor sites (HBAs), area, volume, polar surface area (PSA) and energies of frontier molecular orbitals (FMOs).

Area, volume and polar surface area have the same variation as the molecular weight, increasing in the following order: ciprofloxacin < linezolid < cadazolid.

The ovality index represents the deviation from the spherical form, considering its value 1 for spherical shape. From our calculations, we found the following variation of this parameter: 1.47 (ciprofloxacin) < 1.52 (linezolid) < 1.74 (cadazolid). Ovality index is related with molecular surface area and van der Waals volume, and it increases with the increase of structural linearity. The polarizability provides information about induction (polarization) interactions resulting from an ion or a dipole inducing a temporary dipole in an adjacent molecule. The same variation is observed for both polarizability and for the dipole moment.

The octanol-water partition coefficient (log P) is related with the lipophilicity of compounds and is useful to predict the absorption of drugs across the intestinal epithelium.

Log P values are calculated according to Ghose, Pritchett and Crippen method [10]. The criteria of Lipinski's rule of five [11], log P must be smaller than 5 for a good drug candidate, are based on the observation that the most orally absorbed compounds have log P < 5. Log P can be correlated with PSA when the potential drugs are evaluated according to Hughes et al. [12] who proposed the criteria as log P < 4 and PSA > 75 $Å^2$.

Molecular orbitals energy diagrams and gap (ΔE) are obtained from the energetic level values (eV) of frontier molecular energy orbitals (FMNOs): HOMO— the *highest occupied molecular orbital* and LUMO—the *lowest unoccupied molecular orbital*.

The molecular frontier orbitals are important descriptors related to the reactivity of molecules. Thus the higher value refers to chemically stable molecules. The HOMO energy is linked to the tendency of a molecule to donate electrons to empty molecular orbitals with low energy of convenient molecules. The LUMO energy indicates the ability to accept electrons. The frontier molecular orbital density distribution of the studied therapeutic compounds is shown in **Figure 2** (for linezolid (a), ciprofloxacin (b) and cadazolid (c): HOMO (top) and LUMO (bottom). Black and dark gray regions correspond to positive and negative values of the orbital.

The frontier orbital gap helps to characterize chemical reactivity and kinetic stability [13, 14] of the molecules. HOMO and LUMO determine the way in which it interacts with other species.

The obtained energy gap increases in the order: cadazolid < ciprofloxacin < linezolid (4.36 < 4.39 < 5.09). Consequently, among the three analyzed therapeutical compounds, linezolid presents the lowest reactivity (the most chemically stable) followed by ciprofloxacin and cadazolid (the most reactive).

Other derived quantum chemical parameters for the most stable conformers of linezolid, ciprofloxacin and cadazolid, such as ionization potential (*I*), electron affinity (*A*), electronegativity

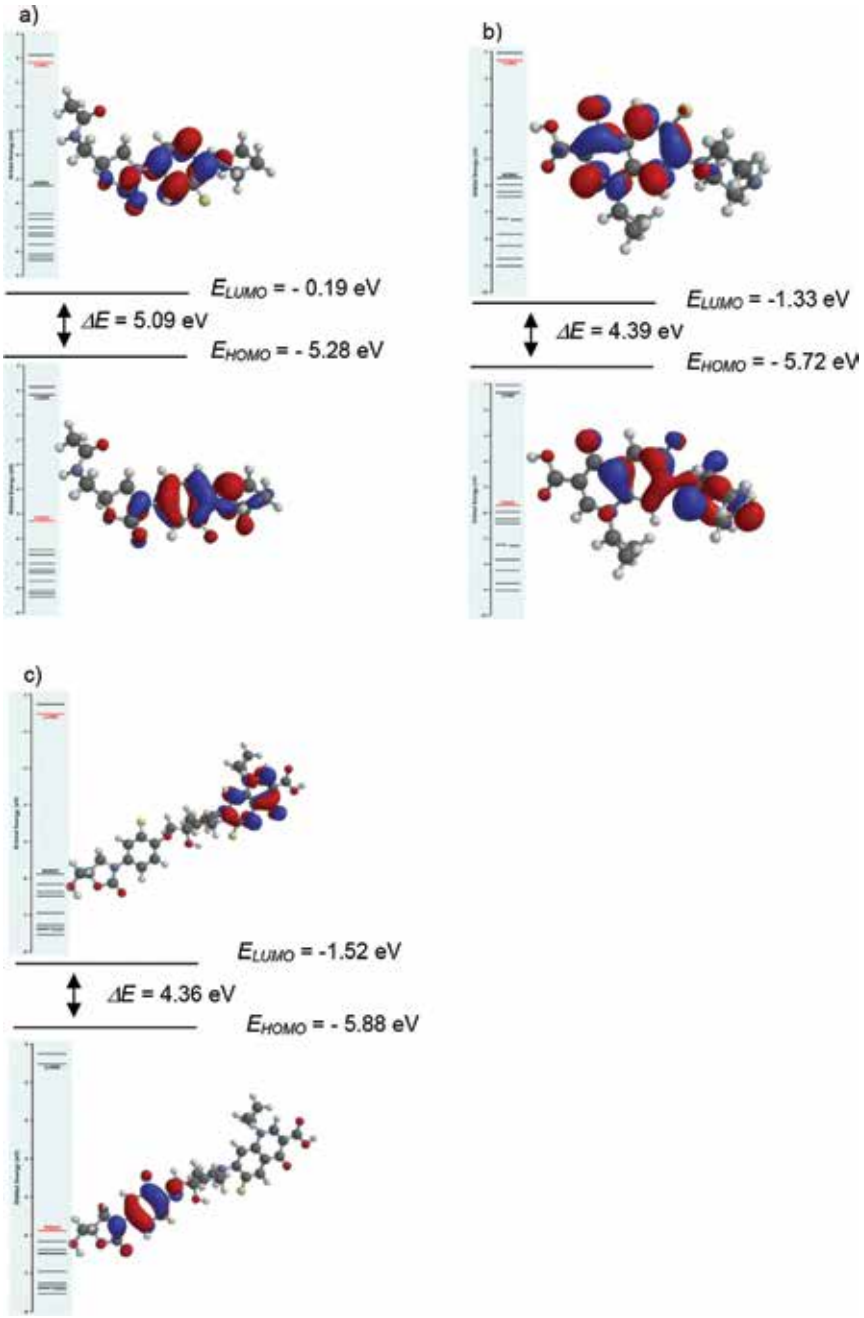

Figure 2. HOMO-LUMO plots (ground state) and energy diagram. HOMO-LUMO plots of (a) linezolid, (b) ciprofloxacin and (c) cadazolid.

(χ), global hardness (η), softness (σ), chemical potential (μ) and global electrophilicity index (ω), are obtained and listed in **Table 2**. Their values were derived from HOMO and LUMO energy diagram [15, 16], according to Koopmans' theorem [17, 18]. The ionization potential is defined as $I = -E_{HOMO}$ and the electron affinity as $A = -E_{LUMO}$.

Quantum parameters	Linezolid	Ciprofloxacin	Cadazolid
E_{HOMO} (eV)	−5.2763	−5.7170	−5.8839
E_{LUMO} (eV)	−0.1856	−1.3262	−1.5517
ΔE (E_{HOMO}–E_{LUMO}) (eV)	5.0907	4.3908	4.3670
$I = -E_{HOMO}$ (eV)	5.2763	5.7170	5.8839
$A = -E_{LUMO}$ (eV)	0.1856	1.3262	1.5517
$\chi = (I + A)/2$ (eV)	2.7309	3.5216	3.7178
$\eta = (I - A)/2$ (eV)	2.5453	2.1954	2.1661
$\sigma = 1/\eta$	2.0829	2.6041	2.7163
$\mu = (E_{HOMO} + E_{LUMO})/2$	−2.7309	−3.5216	−3.7178
$\omega = \mu^2/2\eta$	−1.4650	2.4362	3.1905

Table 2. Calculated quantum chemical parameters of the studied compounds.

3.1.1. Graphical quantities: electrostatic potential, local ionization potential and |LUMO| maps

These graphical quantities provide a visual representation of the chemically active sites and comparative local reactivity of analyzed structures.

***Molecular electrostatic potential* (*MEP*)** is used to investigate the chemical reactivity of a molecule. The MEP is especially important for the identification of the reactive sites of nucleophilic or electrophilic attack in hydrogen bonding interactions and for the understanding of the process of biological recognition. The electrostatic potential map for all three compounds shows hydrophilic regions (negative and positive potentials) and hydrophobic regions (neutral). Their variations and local values are illustrated in **Figure 3**. For linezolid (**Figure 3a**), the negative potentials are localized over oxygen atoms, presenting values: −154, −156 and −160 kJ/mol. The positive electrostatic potential presents a maximum value of 234 kJ/mol. For ciprofloxacin (**Figure 3b**), the negative values vary between −209 and −166 kJ/mol, while positive values are lower than those found for linezolid (194 kJ/mol). For cadazolid (**Figure 3c**), the negative regions present values between −219 and −159 kJ/mol, and positive regions vary between 190 and 214 kJ/mol.

Local ionization potential map (LIPM) is represented in **Figure 4** for linezolid (a), ciprofloxacin (b) and cadazolid (c). The ionization potential represents an overlay of the energy of electron removal (ionization) on the electron density, being particularly useful to assess chemical reactivity and selectivity, in terms of electrophilic reactions.

|LUMO| map is an indicator of nucleophilic addition and it is provided by an overlay of the absolute value of the lowest unoccupied molecular orbital (LUMO) on the electron density.

Figure 5 illustrates the graphical representation for ***|LUMO|*** maps for linezolid (a), ciprofloxacin (b) and cadazolid (c).

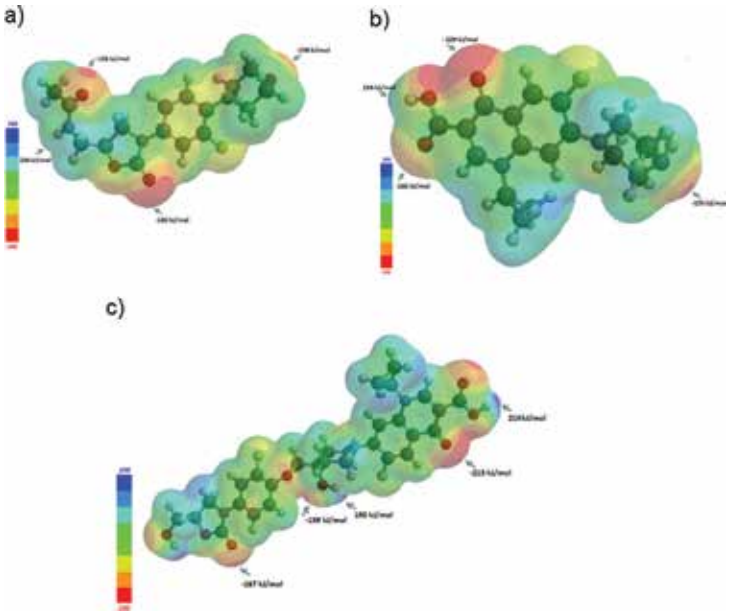

Figure 3. Electrostatic potential map (EPM) of linezolid (a), ciprofloxacin (b) and cadazolid (c), ball and spoke representation.

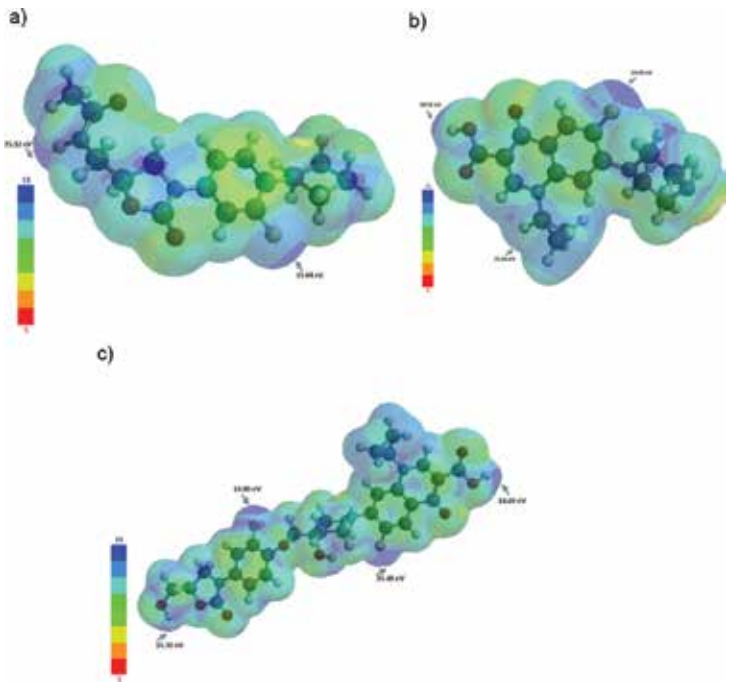

Figure 4. Local ionization potential map (LIPM) of (a) linezolid, (b) ciprofloxacin and (c) cadazolid.

http://dx.doi.org/10.5772/intechopen.72840

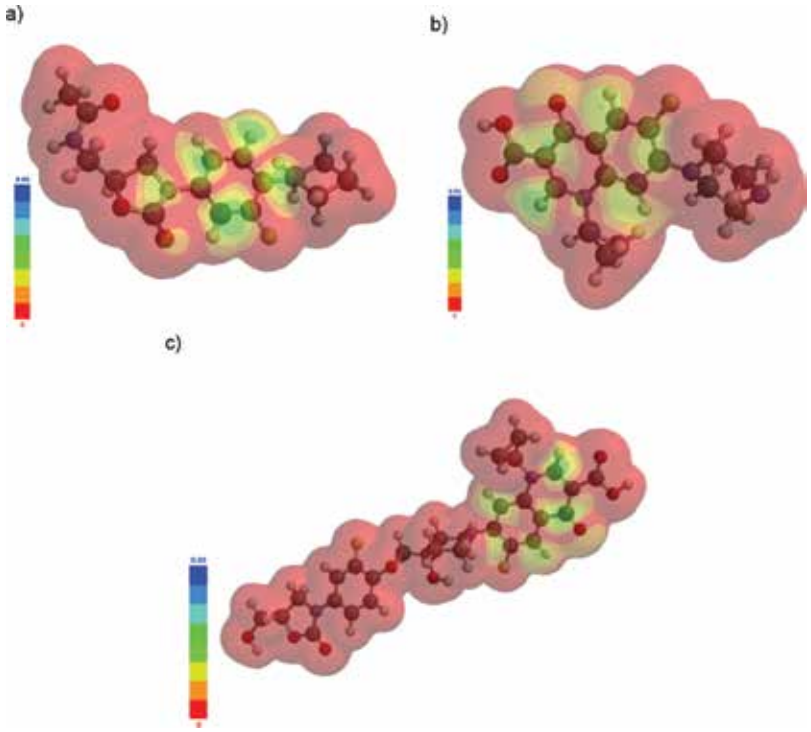

Figure 5. |*LUMO*| map (a) linezolid, (b) ciprofloxacin and (c) cadazolid.

The values of energetic intermediary levels of HOMO and LUMO orbitals for the studied compounds, predicted with B3LYP, 6-31G* algorithm are listed in **Table 3**.

Contribution of other occupied (HOMO{−1}–HOMO{−9}) and unoccupied molecular orbitals (LUMO{+1}) at UV VIS allowed transitions are presented in **Table 4** for linezolid, **Table 5** for ciprofloxacin and **Table 6** for cadazolid.

3.2. Molecular docking simulations

The docking score is a measure of the antimicrobial activity of the studied molecules. The 4WFA fragment, imported from PDB, was chosen for docking study because of the presence in its crystallographic structure of co-crystallized linezolid (ZLD). The crystal structure validated by X-ray diffraction contains a large ribosomal subunit of *Staphylococcus aureus* in complex with linezolid (ZLD). The polymeric chains also include 36 unique types of molecules: RNA chain 23S rRNA; RNA chain 5S rRNA, 50S ribosomal proteins L2–L6, 50S ribosomal proteins L13–L36, molecule N-{[(5S)-3-(3-fluoro-4-morpholin-4-ylphenyl)-2-oxo-1,3-oxazolidin-5-yl]methyl}acetamide (ZLD-linezolid), molecule (4S)-2-methyl-2,4-pentanediol (MPD), magnesium ion, manganese(ii) ion, sodium ion, molecule 4-(2-hydroxyethyl)-1-piperazine ethanesulfonic acid (EPE), spermidine (SPD) and ethanol, as deposited in PDB on 2014-09-14, with the ID 4WFA [19].

Orbital	Linezolid	Ciprofloxacin	Cadazolid
HOMO	**−5.3**	**−5.7**	**−5.9**
HOMO{−1}	−6.5	−6.0	−6.2
HOMO{−2}	−6.6	−6.3	−6.4
HOMO{−3}	−7.0	−6.4	−6.5
HOMO{−4}	−7.3	−7.2	−7.0
HOMO{−5}	−7.4	−7.3	−7.3
HOMO{−6}	−7.7	−7.8	−7.4
HOMO{−7}	−8.1	−8.3	−7.4
HOMO{−8}	−8.2	−8.8	−7.4
HOMO{−9}	−8.4	−9.0	−7.5
LUMO	**−0.2**	**−1.3**	**−1.5**
LUMO{+1}	0.1	−1.0	−1.3

HOMO and LUMO orbitals and their values are in bold characters to highlight that they are the frontier molecular orbitals, and their values occur in the calculus of the energy gap (ΔE) and other quantum molecular parameters related with the global chemical reactivity of molecules.

Table 3. Linezolid, ciprofloxacin and cadazolid energetic levels (eV) of intermediary molecular orbitals (MO).

Wavelength (nm)	Strength	MO component	Contribution
211.68	0.1076	HOMO−1 → LUMO+1	43%
		HOMO−1 → LUMO	38%
		HOMO−2 → LUMO	13%
223.10	0.0605	HOMO−1 → LUMO	51%
		HOMO−1 → LUMO+1	25%
255.34	0.3172	HOMO → LUMO+1	65%
		HOMO → LUMO	20%
274.49	0.1237	HOMO → LUMO	70%
		HOMO → LUMO+1	18%

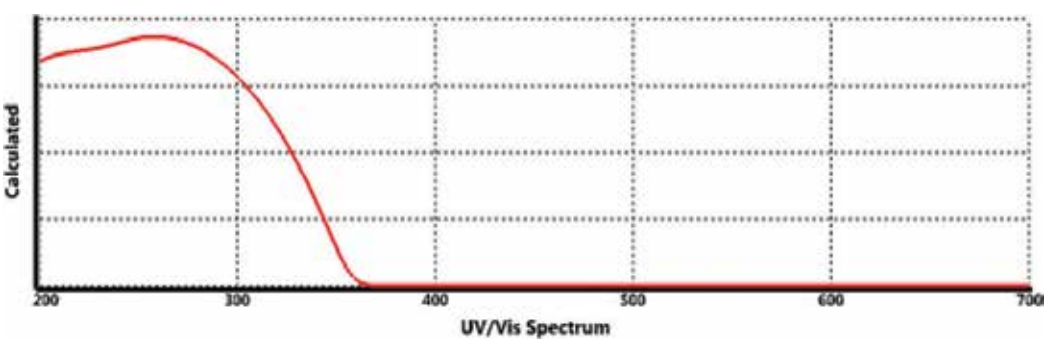

Table 4. Linezolid UV/Vis allowed transitions.

http://dx.doi.org/10.5772/intechopen.72840

Wavelength (nm)	Strength	MO component	Contribution
277.36	0.3043	HOMO–1 → LUMO+1	33%
		HOMO–3 → LUMO	19%
		HOMO–1 → LUMO	16%
		HOMO → LUMO+1	16%
279.79	0.0653	HOMO–1 → LUMO+1	36%
		HOMO → LUMO+1	33%
		HOMO–1 → LUMO	14%
292.77	0.0014	HOMO–2 → LUMO+1	92%
300.49	0.0204	HOMO–1 → LUMO	51%
		HOMO → LUMO+1	43%
318.08	0.0927	HOMO → LUMO	84%
334.30	0.0023	HOMO–2 → LUMO	88%

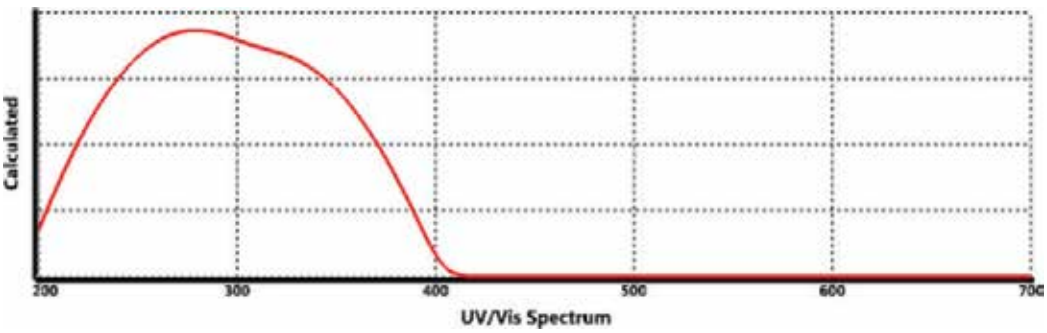

Table 5. Ciprofloxacin UV/Vis allowed transitions.

Wavelength (nm)	Strength	MO component	Contribution
286.51	286.51	HOMO-1 → LUMO	82%

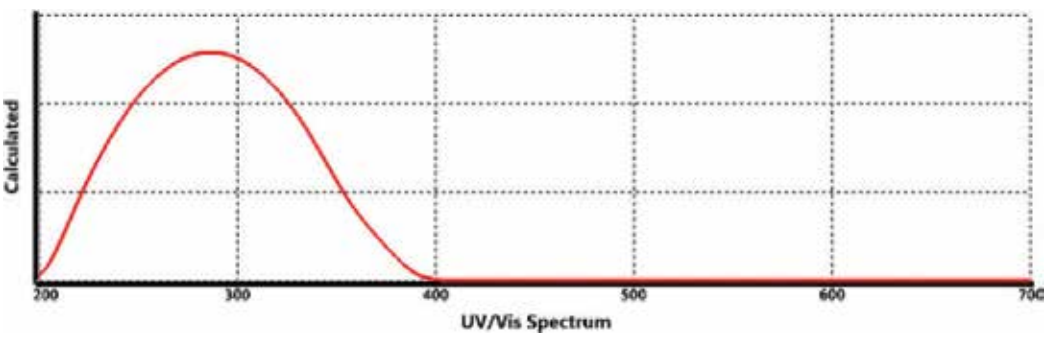

Table 6. Cadazolid UV/Vis allowed transitions.

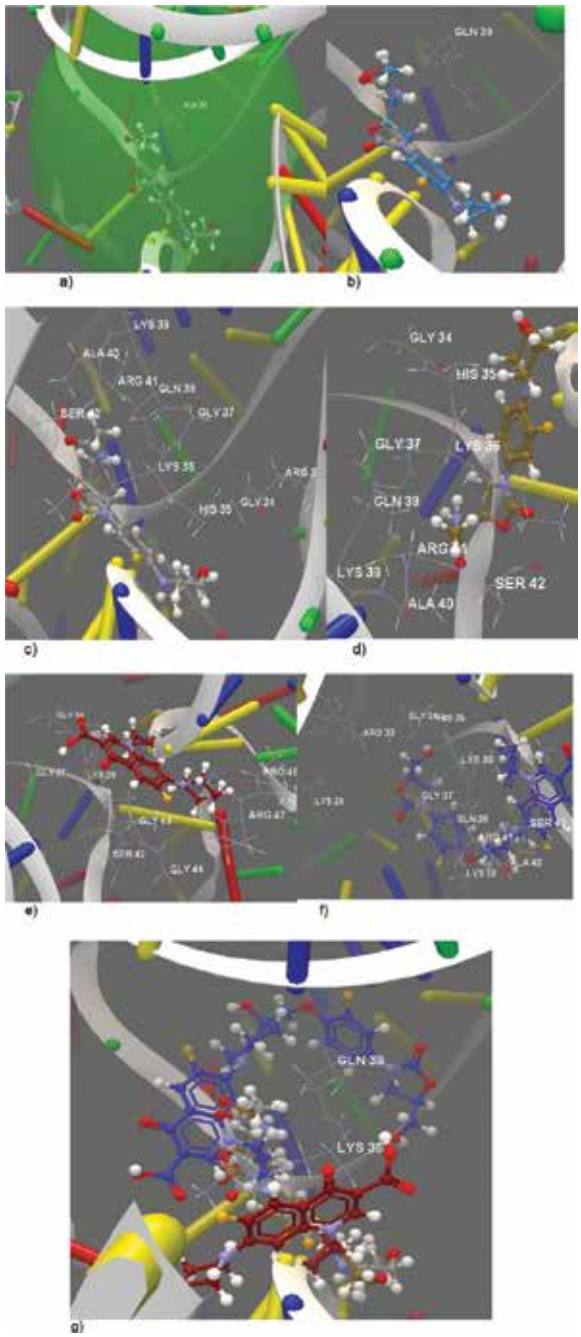

Figure 6. Molecular docking results on linezolid, ciprofloxacin and cadazolid with 4WFA receptor. (a) Active binding site of 4WFA. (b) Docking validation of co-crystallized ZLD. (c) Interacting group and hydrogen bonds between the residues of the GLN 38 and the co-crystallized ZLD. (d) Interacting group of linezolid and hydrogen bonds between the residues of the GLN 38 and the linezolid. (e) Interacting group of ciprofloxacin and hydrogen bonds between the residues of LYS 36 and ciprofloxacin. (f) Interacting group of cadazolid and hydrogen bonds between the residues of LYS 36 and GLN 38 and cadazolid. (g) Docking pose of the four ligands: co-crystallized ZLD (light gray), linezolid (gray), ciprofloxacin (black) and cadazolid (dark gray) with 4WFA.

The docking simulations comprise the following steps: ligands preparation and calculate molecular properties, setup the binding site of the receptor protein, dock ligands, validation of docking, analyze and measure the interactions of the ligand with the amino acid group, analyze docking results in terms of docking score and root-mean-square deviation (RMSD). The docking studies aim to predict the binding modes, the binding affinities and the orientation of the docked ligands. In **Figure 6,** the docking results are illustrated; the active binding site of 4WFA (a), docking validation of co-crystallized ZLD (b), interacting group and hydrogen bonds between the residues of GLN 38 and co-crystallized ZLD (c), interacting group of linezolid and hydrogen bonds between the residues of GLN 38 and linezolid (d), interacting group of ciprofloxacin and hydrogen bonds between the residues of LYS 36 and ciprofloxacin (e), *the* interacting group of cadazolid and hydrogen bonds between the residues of LYS 36 and GLN 38 and cadazolid (f), docking pose of the four ligands: co-crystallized ZLD (gray), linezolid (brown), ciprofloxacin (red) and cadazolid (blue) with 4WFA (g).

The results of molecular docking studies reveal the docking score −49.75 (RMSD: 2.65 Å) for cadazolid and shows the occurrence of two hydrogen bonds with GLN 38 (2.930 Å) and LYS 36 (3.020 Å). Cadazolid forms a hydrogen bond with the same amino acid as linezolid (the first oxazolidinone introduced into therapeutics) and a hydrogen bond with the same amino acid as ciprofloxacin (second-generation fluoroquinolone) (**Table 7**). The obtained docking score resulted from the contributions of hydrogen bond score, metal interaction score and steric interaction score.

3.2.1. Drug-likeness of the studied therapeutical compounds

As seen from the analysis of docked ligands, from **Table 8**, cadazolid presents two violations of the parameters involved in Lipinski's rule of five: the mass and the number of hydrogen acceptors (11), although the docking score is better, yet the RMSD has the higher value. These results can be correlated with cadazolid behavior, acting more likely as an oxazolidinone. Also, cadazolid presents the higher values of the water-octanol coefficient, from calculations made not only with CLC Drug Discovery Workbench software but also with Spartan software,

Compound	Score/RMSD	Interacting group	Hydrogen bond	Bond length (Å)
Linezolid-co-crystallized (ZLD)	−34.55/1.66	ARG 33(I), GLY 34(I), HIS 35(I), LYS 36(I), GLY 37(I), GLN 38(I), LYS 39(I), ARG 41(I), ALA 40(I), SER 42(I)	N sp^2(N14) – O sp^2 from GLN 38(I)	2.917
Linezolid	−37.97/0.22	GLY 34(I), HIS 35(I), LYS 36(I), GLY 37(I), GLN 38(I), LYS 39(I), ARG 41(I), ALA 40(I), SER 42(I)	N sp^2(N14) – O sp^2 from GLN 38(I)	2.989
Ciprofloxacin	−36.79/0.19	GLY 34(I0, GLY 37(I), LYS 36(I), SER 42(I), HIS 35(I), GLY 43(I), PRO 48(I), GLY 49(I)	O sp^3 (O2) – O sp^2 from LYS 36(I)	2.996
Cadazolid	−49.75/2.65	LYS 29(I), ARG 33(I), GLY 34(I), HIS 35(I), LYS 36(I), GLY 37(I), GLN 38(I), ARG 41(I), LYS(39(I), ALA 40(I), SER 42(I).	O sp^2(O9) – Nsp^2 from LYS 36(I)	3.020
			O sp^3(O8) – N sp^2 from GLN 38(I)	2.930

Table 7. The list of intermolecular interactions between the ligands docked with 4WFA using CLC Drug Discovery Workbench software.

Compound	Atoms	Weight [Da]	Flexible bonds	Lipinski violations	Hydrogen donors	Hydrogen acceptors	Log P
Linezolid-co-crystallized (ZLD)	44	337.35	4	0	1	7	1.29
Linezolid	44	337.35	4	0	1	7	1.29
Ciprofloxacin	42	331.34	3	0	2	6	0.84
Cadazolid	71	585.55	8	2	3	11	4.14

Table 8. Ligands properties, computed with CLC Drug Discovery Workbench software.

both using different methods for the calculation of this parameter. Also, the differences in predicted values of log P can be attributed to the fact that Spartan software considers a rigorous conformational analysis before calculating the molecular properties. The calculated values with Spartan software are obtained only for the conformer with the lower energy.

4. Conclusions

Ab initio computation to molecular properties prediction and *in silico* molecular docking simulations help to evaluate the biological activity of several compounds and to assess their therapeutical potential.

Ciprofloxacin and linezolid can be used as reference compounds for their antimicrobial activity in order to analyze several derivatives of their class as drug candidates. Ciprofloxacin and linezolid fulfill both Lipinski and Hughes et al. rules about drug likeness, confirmed also by their use in therapeutics. Spartan 14 and CLC Drug Discovery Workbench Software offer the possibility of a deep conformational analysis and to obtain accurate predictive property data.

Acknowledgements

This study has been financed through the NUCLEU Program, which is implemented with the support of ANCSI, project no. PN 16-27 01 01 of the National Institute of Chemical-Pharmaceutical Research & Development—Bucharest, Romania.

Author details

Amalia Stefaniu* and Lucia Pintilie

*Address all correspondence to: astefaniu@gmail.com

National Institute of Chemical - Pharmaceutical Research and Development, ICCF Bucharest, Romania

References

[1] Ma Z, Lynch AS. Development of a dual-acting antibacterial agent (TNP-2092) for the treatment of persistent bacterial infections. Journal of Medicinal Chemistry. 2016;**59**: 6645-6657

[2] Shao Y, Molnar LF, Jung Y, Kussmann J, Ochsenfeld C, Brown ST, Gilbert ATB, Slipchenko LV, Levchenko SV, O'Neill DP, DiStasio RA, Lochan RC, Wang T, Beran GJO, Besley NA, Herbert JM, Lin CY, Van Voorhis T, Chien SH, Sodt A, Steele RP, Rassolov VA, Maslen PE, Korambath PP, Adamson RD, Austin B, Baker J, Byrd EFC, Dachsel H, Doerksen RJ, Dreuw A, Dunietz BD, Dutoi D, Furlani TR, Gwaltney SR, Heyden A, Hirata S, Hsu CP, Kedziora G, Khalliulin RZ, Klunzinger P, Lee AM, Lee MS, Liang WZ, Lotan I, Nair N, Peters B, Proynov EI, Pieniazek PA, Rhee YM, Ritchie J, Rosta E, Sherrill CD, Simmonett AC, Subotnik JE, Woodcock HL, Zhang W, Bell AT, Chakraborty AK, Chipman DM, Keil FJ, Warshel A, Hehre WJ, Schaefer HF, Kong J, Krylov AI, PMW G, Head-Gordon M. Advances in methods and algorithms in a modern quantum chemistry program package. Physical Chemistry Chemical Physics. 2006;**8**(27):3172-3191

[3] Parr RG, Yang W. Density Functional Theory of Atoms and Molecules. Oxford: Oxford University Press; 1989

[4] Lee C, Yang W, Parr RG. Development of the Colle-Salvetti correlation-energy formula into a functional of the electron density. Physical Review B. 1988;**37**:785-789

[5] Becke AD. Density functional thermochemistry. III. The role of exact exchange. The Journal of Chemical Physics. 1993;**98**:5648-5652

[6] Hehre WJ. A Guide to Molecular Mechanics and Quantum Chemical Calculations. Irvine, CA: Wavefunction Inc.; 2003

[7] Eyal Z, Matzov D, Krupkin M, Wekselman I, Paukner S, Zimmerman E, Rozenberg H, Bashan A, Yonath A. Structural insights into species-specific features of the ribosome from the pathogen *Staphylococcus aureus*. Proceedings of the National Academy of Sciences of the United States of America. 2015;**112**:E5805-E5814. DOI: 10.1073/pnas.1517952112

[8] Lipinski CA, Lombardo F, Dominy BW, Feeney PJ. Experimental and computational approaches to estimate solubility and permeability in drug discovery and development settings. Advanced Drug Delivery Reviews. 2001;**46**:3-26. DOI: 10.1016/S0169-409X(00)00129-0

[9] Cheng T, Zhao Y, Li X, Lin F, Xu Y, Zhang X, Li Y, Wang R. Computation of octanol-water partition coefficients by guiding an additive model with knowledge. Journal of Chemical Information and Modeling. 2007;**47**:2140-2148. DOI: 10.1021/ci700257y

[10] Arup K, Ghose AK, Pritchett A, Crippen GM. Atomic physicochemical parameters for three-dimensional structure directed quantitative structure-activity relationships. III: Modeling hydrophobic interactions. Journal of Computational Chemistry. 1988; **9**:80-90

[11] Lipinski CA, Lombardo F, Dominy BW, Feeney PJ. Experimental and computational approaches to estimate solubility and permeability in drug discovery and development settings. Advanced Drug Delivery Reviews. 1997;**23**:3-25

[12] Hughes JD, Blagg J, Price DA, Bailey S, Decrescenzo GA, Devraj RV, et al. Physicochemical drug properties associated with in vivo toxicological outcomes. Bioorganic & Medicinal Chemistry Letters. 2008;**18**(17):4872-4875

[13] Alam MJ, Ahmad S. Anharmonic vibrational studies of L-aspartic acid using HF and DFT calculations. Spectrochimica Acta A: Molecular and Biomolecular Spectroscopy. 2012; **96**:992-1004

[14] Demir P, Akman F. Molecular structure, spectroscopic characterization, HOMO and LUMO analysis of PU and PCL grafted onto PEMA-co-PHEMA with DFT quantum chemical calculations. Journal of Molecular Structures. 2017;**1134**:404-415

[15] Zarrouk A, Zarrok H, Salghi R, Hammouti B, Al-Dey Ab SS, Touzani R, Bouachrine M, Warad I, Hadda TB. A theoretical investigation on the corrosion inhibition of copper by quinoxaline derivatives in nitric acid solution. International Journal of Electrochemical Science. 2012;**7**:6353-6364

[16] Wang H, Wang X, Wang H, Wang L, Liu A. DFT study of new bipyrazole derivatives and their potential activity as corrosion inhibitors. Journal of Molecular Modeling. 2007; **13**(1):147-153

[17] Sastri VS, Perumareddi JR. Molecular orbital theoretical studies of some organic corrosion inhibitors. Corrosion Science. 1997;**53**(8):617-622

[18] Yankova R, Genieva S, Halachev N, Dimitrova G. Molecular structure, vibrational spectra, MEP, HOMO-LUMO and NBO analysis of $Hf(SeO_3)(SeO_4)(H_2O)_4$. Journal of Molecular Structure. 2016;**1106**:82-88

[19] Eyal Z, Matzov D, Krupkin M, Wekselman I, Zimmerman E, Rozenberg H, Bashan A, Yonath AE. The crystal structure of the large ribosomal subunit of *Staphylococcus aureus* in complex with linezolid-deposited PDB as 4WFA. 2014

Edited by Takashiro Akitsu

The aim of this book *Symmetry (Group Theory) and Mathematical Treatment in Chemistry* is to be a graduate school-level text about introducing recent research examples associated with symmetry (group theory) and mathematical treatment in inorganic or organic chemistry, physical chemistry or chemical physics, and theoretical chemistry. Chapters contained can be classified into mini-review, tutorial review, or original research chapters of mathematical treatment in chemistry with brief explanation of related mathematical theories. Keywords are symmetry, group theory, crystallography, solid state, topology, molecular structure, electronic state, quantum chemistry, theoretical chemistry, and DFT calculations.

Published in London, UK

IntechOpen

ISBN 978-1-83881-324-6